

# **Chemorheology of Thermosetting Polymers**



# Chemorheology of Thermosetting Polymers

**Clayton A. May, EDITOR**

*Lockheed Missiles & Space Company, Inc.*

Based on a symposium  
sponsored by the ACS Division  
of Organic Coatings  
and Plastics Chemistry  
at the 184th Meeting  
of the American Chemical Society,  
Kansas City, Missouri,  
September 12–17, 1982

A C S   S Y M P O S I U M   S E R I E S

**227**

**AMERICAN CHEMICAL SOCIETY**  
**WASHINGTON, D.C.      1983**



**Library of Congress Cataloging in Publication Data**

**Chemorheology of thermosetting polymers.**

(ACS symposium series, ISSN 0097-6156; 227)

“Based on a symposium sponsored by the ACS Division of Organic Coatings and Plastics Chemistry at the 184th Meeting of the American Chemical Society, Kansas City, Missouri, September 12–17, 1982.”

Includes bibliographies and index.

1. Thermosetting plastics—Congresses. 2. Rheology—Congresses.

I. May, Clayton A. II. American Chemical Society. Division of Organic Coatings and Plastics Chemistry. III. American Chemical Society. Meeting (184th: 1982: Kansas City, Mo.) IV. Series.

TPI180.T55C46 1983      668.4'22      83-12280  
ISBN 0-8412-0794-1

Copyright © 1983

American Chemical Society

All Rights Reserved. The appearance of the code at the bottom of the first page of each article in this volume indicates the copyright owner's consent that reprographic copies of the article may be made for personal or internal use or for the personal or internal use of specific clients. This consent is given on the condition, however, that the copier pay the stated per copy fee through the Copyright Clearance Center, Inc. for copying beyond that permitted by Sections 107 or 108 of the U.S. Copyright Law. This consent does not extend to copying or transmission by any means—graphic or electronic—for any other purpose, such as for general distribution, for advertising or promotional purposes, for creating new collective work, for resale, or for information storage and retrieval systems. The copying fee for each chapter is indicated in the code at the bottom of the first page of the chapter.

The citation of trade names and/or names of manufacturers in this publication is not to be construed as an endorsement or as approval by ACS of the commercial products or services referenced herein; nor should the mere reference herein to any drawing, specification, chemical process, or other data be regarded as a license or as a conveyance of any right or permission, to the holder, reader, or any other person or corporation, to manufacture, reproduce, use, or sell any patented invention or copyrighted work that may in any way be related thereto.

PRINTED IN THE UNITED STATES OF AMERICA

**American Chemical  
Society Library  
1155 16th St. N. W.**

In Chemorheology of Thermosetting Polymers, May, C.;  
ACS Symposium Series; American Chemical Society: Washington, DC, 1982.

# ACS Symposium Series

**M. Joan Comstock, *Series Editor***

## *Advisory Board*

David L. Allara

Robert Baker

Donald D. Dollberg

Brian M. Harney

W. Jeffrey Howe

Herbert D. Kaesz

Marvin Margoshes

Donald E. Moreland

Robert Ory

Geoffrey D. Parfitt

Theodore Provder

Charles N. Satterfield

Dennis Schuetzle

Davis L. Temple, Jr.

Charles S. Tuesday

C. Grant Willson

## FOREWORD

The ACS SYMPOSIUM SERIES was founded in 1974 to provide a medium for publishing symposia quickly in book form. The format of the Series parallels that of the continuing ADVANCES IN CHEMISTRY SERIES except that in order to save time the papers are not typeset but are reproduced as they are submitted by the authors in camera-ready form. Papers are reviewed under the supervision of the Editors with the assistance of the Series Advisory Board and are selected to maintain the integrity of the symposia; however, verbatim reproductions of previously published papers are not accepted. Both reviews and reports of research are acceptable since symposia may embrace both types of presentation.

## PREFACE

**T**O OBTAIN A SOUND SCIENTIFIC UNDERSTANDING of the processes by which thermosetting polymers cure is a difficult task because of the insoluble, cross-linked nature of these polymers as the cure reaches completion. Advances in instrumentation over the past 10 years now permit a greater comprehension of the complex character of these materials. Thermosetting polymers are rapidly gaining acceptance in areas that affect our lives on a daily basis: The automotive, aerospace, electronics, housing, and sporting goods industries are good examples. Increasing numbers of scientists are being attracted to thermoset resin studies that use nonempirical, scientific approaches.

The term chemorheology arises from the two areas of concern being studied. The first concern comes early in the cure. The processability or flow (rheology) of the polymer system is of primary importance because process changes such as heating rates, hold temperatures, or pressures normally are made during this early period. The other area of concern is the chemistry of the process: the rate of reaction, the mechanisms, the kinetics, and the cessation of the chemical reaction or the end of the cure. The interactions between these two concerns are obvious because the rate of rheological change in either the liquid or solid state and the development of the optimum glass transition temperatures cannot be separated from the chemical contribution to these effects.

In this all too brief volume the reader will find how advances in liquid chromatography, differential scanning calorimetry, IR spectroscopy, and particularly liquid and solid state rheology have contributed to a better understanding of the curing of thermosetting polymers. Also discussed are the mathematical models being developed to describe and predict the chemical and physical events occurring during thermoset cure. The use of dielectric measurements to follow the chemical and rheological changes is also considered. Since this volume was compiled, there appears to be a new wave of interest developing in this area.

The field of research on the chemorheology of thermosetting polymers is new and exciting. As our knowledge of the curing processes expands, new materials will come into focus. These too, must be understood. The reader should also look beyond the application of these methodologies to the thermoset materials discussed herein, and use the information to develop further

the techniques as they apply to his or her own problems. Because the area of thermoset polymers is complex, no particular technological skill dominates. Through cooperative efforts that knit these individual skills together, we can make rapid advances toward the evaluation of materials that afford the properties necessary to meet the needs of future generations.

CLAYTON A. MAY  
Lockheed Missiles and Space Company, Inc.  
Sunnyvale, CA

May 1983



## Process Automation

### A Rheological and Chemical Overview of Thermoset Curing

C. A. MAY, M. R. DUSI, J. S. FRITZEN, D. K. HADAD,  
M. G. MAXIMOVICH, K. G. THRASHER, and A. WERETA, JR.

Lockheed Missiles and Space Company, Inc., Sunnyvale, CA 94086

As little as ten years ago the processing of thermosetting polymers was more a skilled craft than a scientifically sound procedure. Whereas scientists in laboratories throughout the world had synthesized and formulated many remarkably useful thermoset products, the processing was, for the most part, dependent on the judgement of the operator. Beginning in the early 70's, instrumentation started becoming available which permitted accurate analysis of complex formulations and various means of monitoring and studying the chemistry and rheology of their cure. Thus, a methodology was evolving whereby thermoset curing could be controlled in a manner similar to other chemical processes - precise raw material control and monitoring process chemistry to the proper end point.

In the chapters which follow this introductory dissertation, you will find many examples of how contemporary instrumentation and methodology can be used to understand and control the production of useful artifacts from thermoset materials. Obviously, the various materials themselves cannot be overlooked. However, the reader should think beyond how a particular chemical structure is studied or analyzed to the techniques and instrumentation involved and how they may be used or modified to solve a problem of his or her interest. Herein will be found a heavy emphasis on chemical kinetics and rheology the interaction between the two goals achieved by analytical techniques, application of chemorheological techniques to surface coatings, often the final step in manufacturing, and finally the use of mathematics and computers in the processing of thermoset polymers. It is the purpose of this chapter to offer an introduction to the instrumental methods of thermoset material and process control as they evolved from adhesive and composite studies in the Lockheed Laboratories. The results have brought us to the threshold of scientifically automated processing based on quantitative understanding.

The development of a scientifically controlled hardware fabrication process is not an easy task. A multi-disciplined scientific approach is required. The study team members must be skilled in analytical, physical and polymer chemistry, spectros-

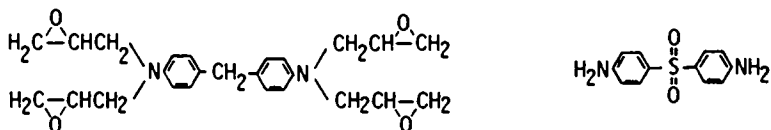
0097-6156/83/0227-0001\$07.00/0

© 1983 American Chemical Society

copy, chemical, electrical and manufacturing engineering, and computer sciences. A total understanding of the chemical and rheological events is prerequisite. By monitoring these events it is possible to use the information to control the process heat history and the timing of other special events such as application of pressure during a lamination or bonding process. Physical restrictions, such as presses or autoclaves, generally preclude rapid and direct measurement of these events during hardware fabrication. However, in our work (1-5) and that of others (6-12) it has been shown that changes in the dielectric properties of a curing resin can be related to the chemical and rheological events of the process. This can be illustrated by the data in Figure 1, a plot of the changes in vector voltage (V) and phase angle ( $\phi$ ), in an alternating current electrical field of 1000 Hz, as a function of a simple cure cycle (T).

As the cure proceeds, two peaks separated by a valley are observed. The first peak is associated with the melting of the matrix material, debulking of the hardware and the wetting of fibers, fillers, or substrates as in the case of adhesive bonding. The valley in the dielectric curves is a region of high dipole mobility when the matrix viscosity is low. It is the part of the process where consolidation pressure is normally applied during bonding or lamination. The final peak represents a rapid viscosity increase as the resin gels and then hardens and the dipole movement becomes more restricted. In shop practice dielectric properties are obtained by building a small capacitor into the hardware which has a minimal effect on hardware mechanical properties.

The work described herein relates primarily to lamination and bonding processes. However, the techniques are generic to most forms of thermoset resin processing. In the discussion which follows many of the resin systems contain glycidyl amines. The bulk of the epoxy formulations used in the aerospace industry today are based on tetraglycidylmethylenedianiline, I (TGMDA) and with diaminodiphenylsulfone, II (DDS). Systems based on



Tetraglycidylmethylenedianiline, I      Diaminodiphenylsulfone, II

these products cure by two mechanisms, the conventional amine/epoxide addition (A) and homopolymerization of the epoxide (B).

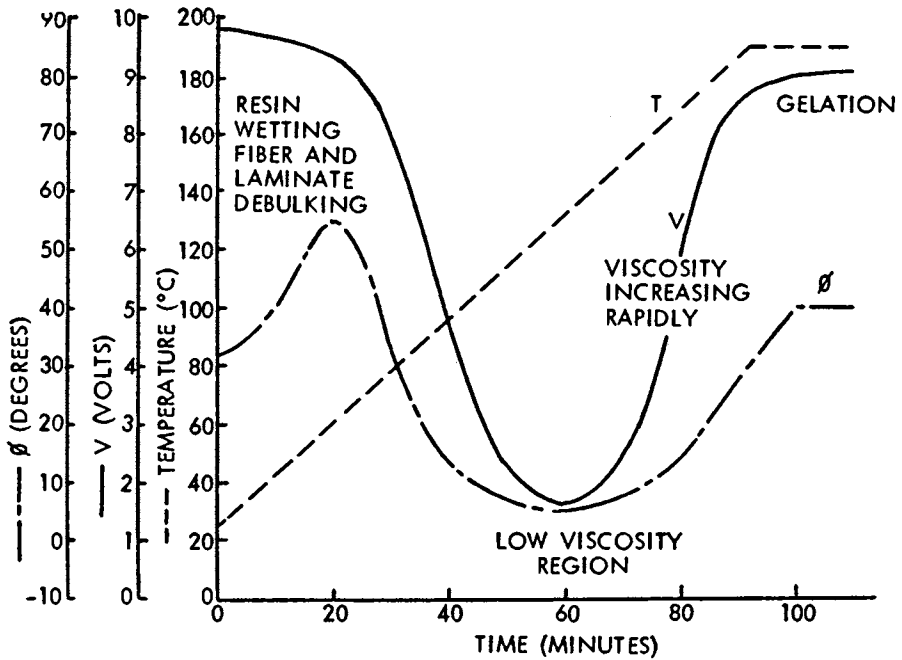
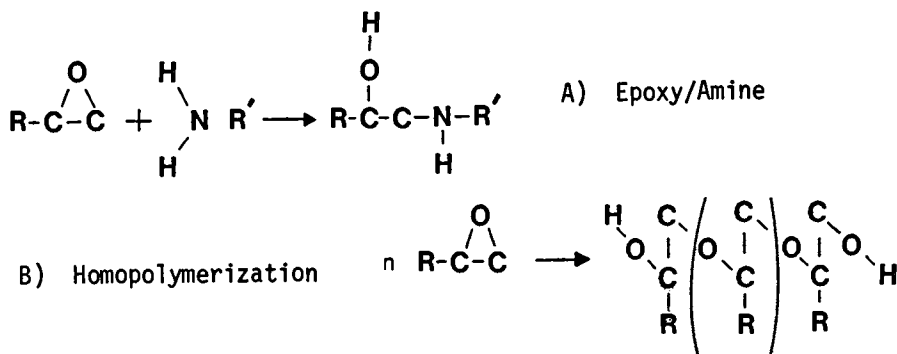


Figure 1. Influence of Physical Changes on Dielectric Properties.



Exact definition of the cure chemistry is difficult since formulations of this type may also contain auxiliary catalysts (Lewis Acids) which enhance the homopolymerization reaction.

We have demonstrated that formulative changes, even minor ones, (13) can measurably alter the cure rate and the subsequent dielectric response. Shown in Table 1 are three epoxy prepreg

Table 1 Prepreg Formulations

Formula No.	1	2	3
TGMDA	100	100	100
DDS	32	32	32
BF <sub>3</sub> ·400	-	1	-
RC-2	-	-	1.43

formulations. Each contains the same TGMDA/DDS resin system. However, one resin has no accelerator (1) another (2) has a widely used BF<sub>3</sub> monoethylamine salt and the third (3) contains a proprietary Lewis Acid with the electron acceptor concentration equal to that of the BF<sub>3</sub>·400 system. Shown in Figures 2 and 3 are differential calorimetry (DSC) and dielectric scans obtained from a simple 177°C (350°F) cure cycle. The DSC data shows that the uncatalyzed system (1) definitely reacts at a slower rate than the other two formulations. Note also that this system displays only one peak in the DSC while the accelerated combinations show two. The left hand peaks in these latter two formulations are caused by the accelerators, a point which will be discussed momentarily.

The dielectric scans (Figure 3) also show differences in the rates of reaction indicating sensitivity to chemical change. From these data it can also be concluded that the proprietary accelerator causes the most rapid cure.

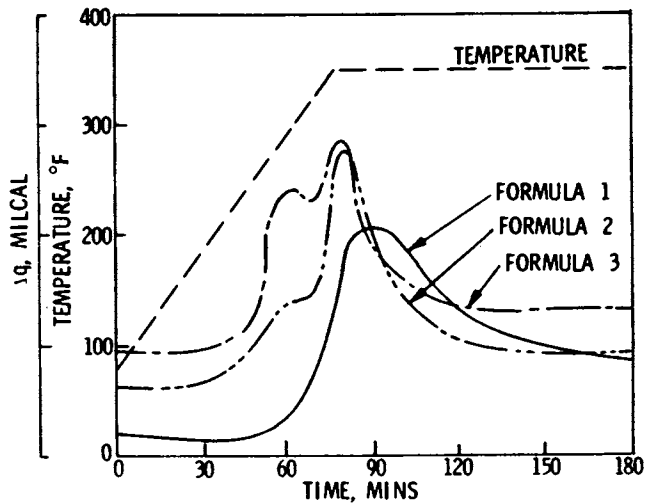


Figure 2. Calorimetric Analysis.

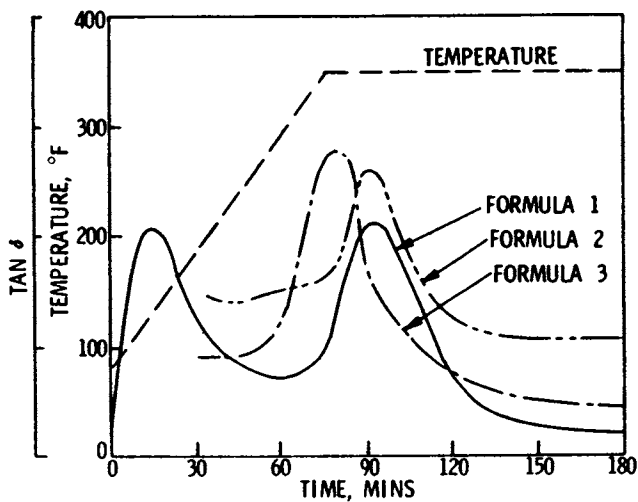


Figure 3. Dielectric Analysis.

An obvious prerequisite to good process control of thermoset curing is a consistent, well defined starting material. The laboratory methods suggested for this purpose are DSC, high performance liquid chromatography (HPLC), infrared spectroscopy (IR), wet chemistry, dielectric analysis and rheology.

DSC not only gives information on the chemistry and quality of thermoset formulations, but can also be used in the design of cure cycles. It is highly sensitive to changes in catalyst concentration as illustrated by the data in Figure 4. As the catalyst concentration is increased, the accelerator or initial DSC peak increases and the main reaction peak decreases while the total areas under the curves (heats of reaction) remain essentially unchanged.

Although the changes in the DSC data are relatively small, the impact on processing of these systems can be significant. Shown in Figure 5 is a plot of viscosity of the three resins as a function of time at 135°C (275°F). If the critical viscosity were, for example, 1000 poises for some critical process change, such as pressure application during lamination, it can be seen that the proper timing of this event would vary by about 20 minutes.

HPLC is probably the most useful tool in the chemical characterization of thermosetting resin formulations. Highly complex mixtures can be separated by this technique. A case in point are the three chromatographs shown in Figure 6. This is a staging study on the polymerization of a monomeric reactants (PMR) type of polyimide called LARC-160 14). It is a complex mixture of the ethyl half esters of Nadic and 3,3',4,4' benzophenone tetracarboxylic acid dianhydride blended with an oligomeric amine precursor of methylene dianiline. The components of the starting mixture are clearly defined. As the material stages a reaction, product peak appears between peaks 2 and 3 and grows as the staging proceeds while the peaks representative of the reactants diminish.

In addition to fingerprinting matrix systems, IR can also be used to quantitatively assess certain formulative components. Dicyandiamide and DDS, two important curing agents in today's technology, can be measured quantitatively with this technique. As Fourier transform IR (FTIR) technology continues to develop, it too should prove valuable in chemical characterization technology. In Figure 7 the use of subtractive FTIR is demonstrated. In the upper left hand corner is the IR spectrum of an epoxy resin/curing agent mixture. If the spectrum of the resin (upper right) is subtracted from that of the mixture the spectrum of the curing agent results (lower left). The curing agent spectrum compares favorably with that of the original material (lower right) suggesting quantitative application of the method.

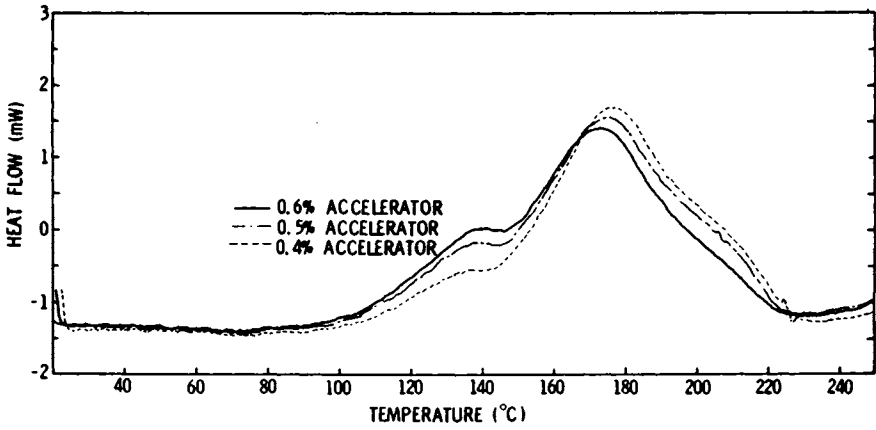


Figure 4. Effect of Accelerator Level on DSC.

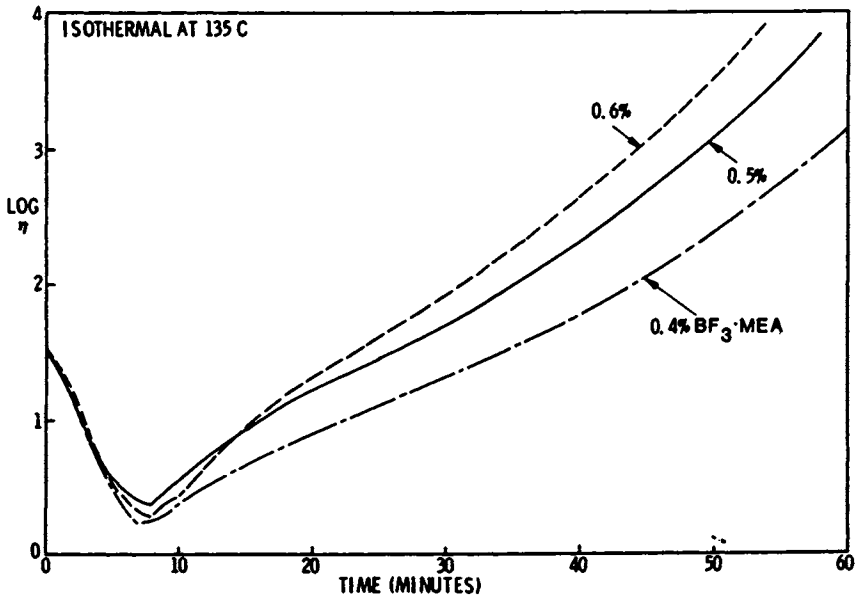


Figure 5. Effect of Accelerator Concentration on Viscosity.

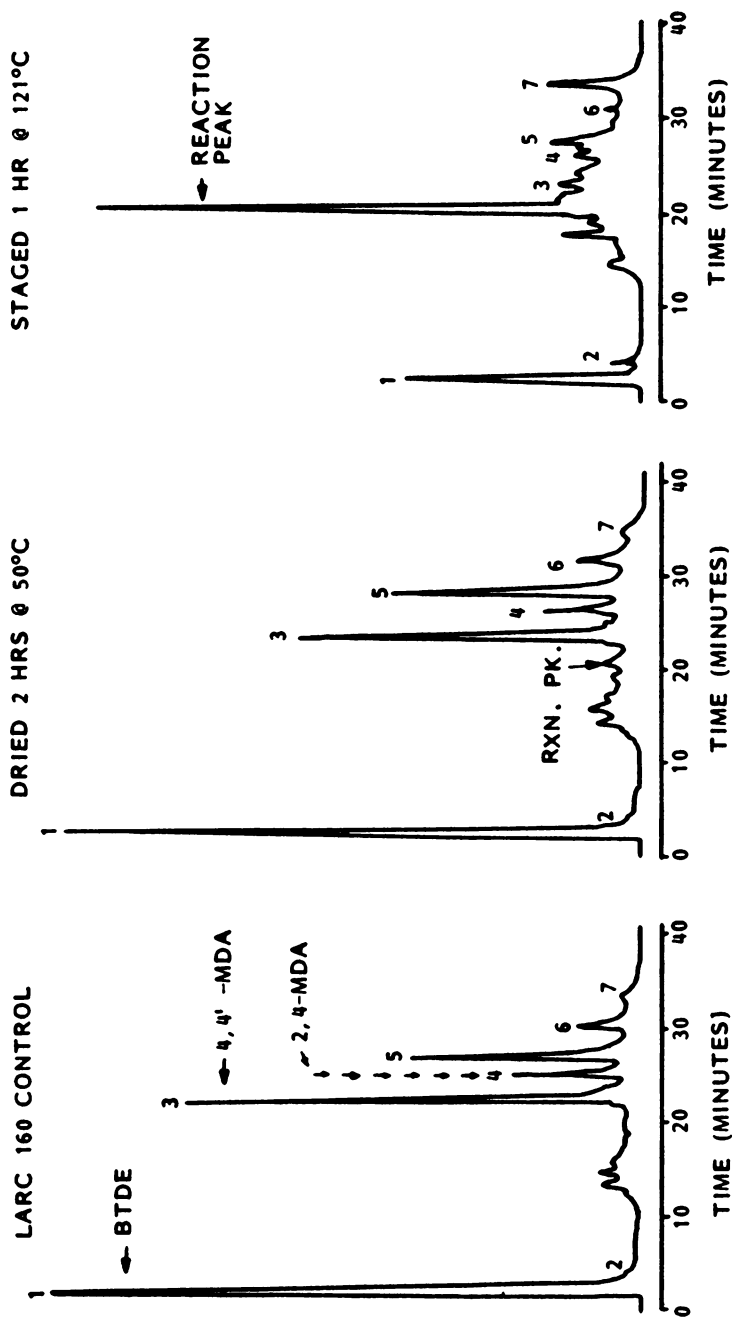


Figure 6. Effects of Staging on HPLC Chromatograms.



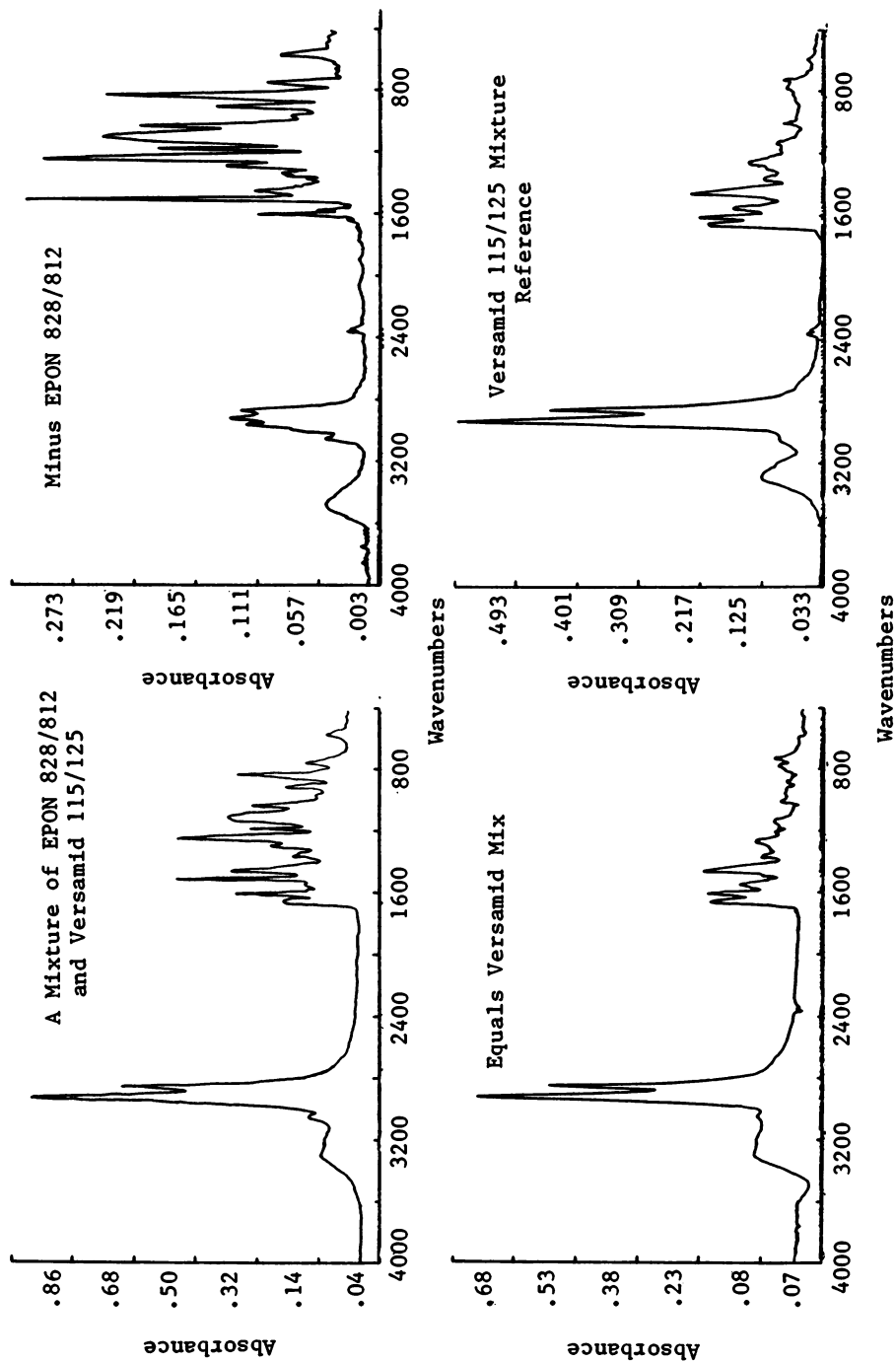


Figure 7. Subtractive FTIR Analysis.

Some twenty years ago Cheng<sup>15)</sup>, in his book on analysis of linear systems, pointed out that electrical and physical measurements were analogous since they are governed by similar mathematical relationships. This permits the construction of the force-voltage analogy shown in Table 2. One could thus speculate that

Table 2 Force-Voltage Analogy

<u>Mechanical System</u>	<u>Electrical System</u>
Force	Voltage
Velocity	Current
Displacement	Charge
Mass	Inductance
Damping Coefficient	Resistance
Compliance	Capacitance
Mechanical Loss	Loss Tangent

measurement of the electrical properties of a curing thermoset resin system should reflect the physical and chemical changes in a curing resin mass. An excellent correlation of this type is given in Figure 8 which shows how the viscosity ( $\eta^*$ ) and dielectric dissipation factor (D) change with time during a simple cure cycle (T) of the PMR type polyimide. Even though the peaks and valleys occur at slightly different times due to different measurement frequencies, the data correlates extremely well. It should also be noted that the viscosity-time-temperature plot is a measure of the behavioral characteristics of the resin for the particular cure cycle shown. This type of information is quite useful for incoming material inspection to assure that each lot of material will behave in a similar manner during cure.

To demonstrate the practical utility of the aforementioned procedures let us consider the results of a room temperature aging study on a typical TGMDA/DDS prepreg. A summary of the chromatographic analysis of the aging process is given in Table 3. As the

Table 3 HPLC Analysis of Aged Prepregs

<u>Days Aging</u>	<u>% DDS</u>	<u>% Diluent</u>	<u>% TGMDA</u>	<u>% B-Stage</u>
0	30.3	13.0	51.0	5.7
2	30.1	12.8	50.3	6.8
7	29.1	12.9	46.2	11.8
14	27.4	11.6	44.9	16.1
30	25.3	10.3	43.1	21.2
63	22.4	9.9	42.7	24.0

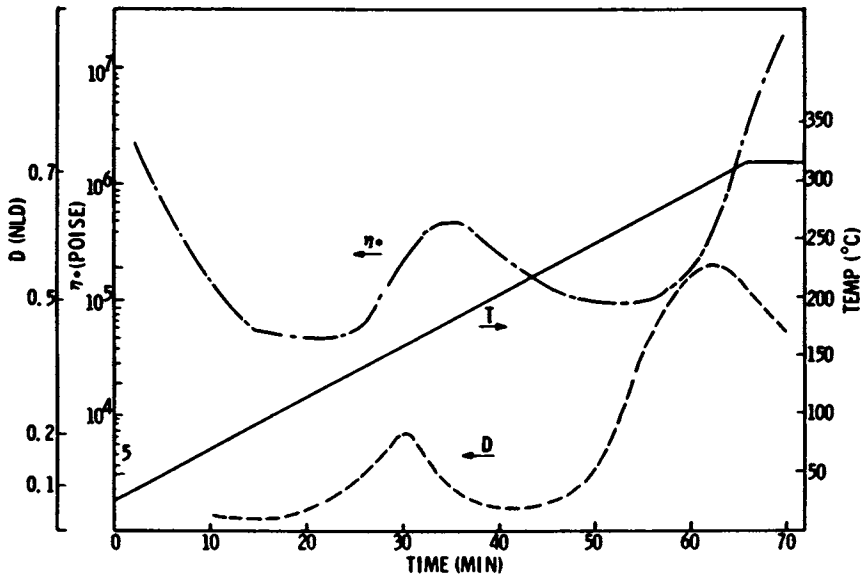


Figure 8. Dielectric Rheological Response of a Curing Polyimide.

material ages the curing agent, diluent and major resin content all decline and the concentration of reacted or B-staged components increases. As a prepreg of this type is stored under these conditions it changes from a highly viscous liquid to a glass. The data clearly shows that as the glassy state is approached, the rate of the aging process slows considerably.

In the case of DSC measurements, Figure 9, as the prepreg becomes older, the peak associated with the catalyst gradually disappears and the height of the major exotherm peak increases. This seemingly indicates that a change in the chemical nature of the Lewis Acid catalyst has occurred. However, this should not be taken as an indication that aging proceeds via homopolymerization (B) only. Undoubtedly, the Lewis Acid catalysis of the amine/epoxide reaction (A) involves association between the catalyst and the oxirane ring.

Shown in Figure 10 are the rheological properties of the prepreg and the neat matrix resin after aging for 21 and 60 days at room temperature. The viscosity determinations, run at 1.5 Hz, were made using a process cycle typical of a production shop. The application of pressure to consolidate the laminate would normally be made at the end of the 122°C hold cycle. Within limits, it is important to apply consolidation pressure in the proper viscosity range to insure adequate compaction of the laminate and the desired resin to fiber ratio.

The neat resin data indicate that after aging for 21 days there is little difference between it and the original sample. It also indicates that it should be possible to process the resin after a 60 day aging period by shortening the hold period to around 20 minutes. But note what happens when a similar study is made on the prepreg (upper three curves). The data clearly indicates that the hold period for the 21 day old sample should be shortened to around 30 minutes and that the 60 day old prepreg may not be processible at all! This is a clear indication of the importance of proper material selection and testing when doing process studies.

The influence of prepreg aging on the dielectric properties of the matrix is shown in Figure 11. The effects of the aging are clearly evident after only 5 days. The initial drop in both vector voltage (VV) and phase angle ( $\phi$ ) show a definite shift to the right. Thus, our work indicates that vector voltage correlates well with viscosity. The data also suggest that the hold cycle at 121°C could be shortened by as much as 15 minutes.

Time, temperature, viscosity models are another useful element in understanding the science of thermoset resin processing. They perform a number of valuable functions such as defining the proper point for consolidation pressure application in FRP lamin-

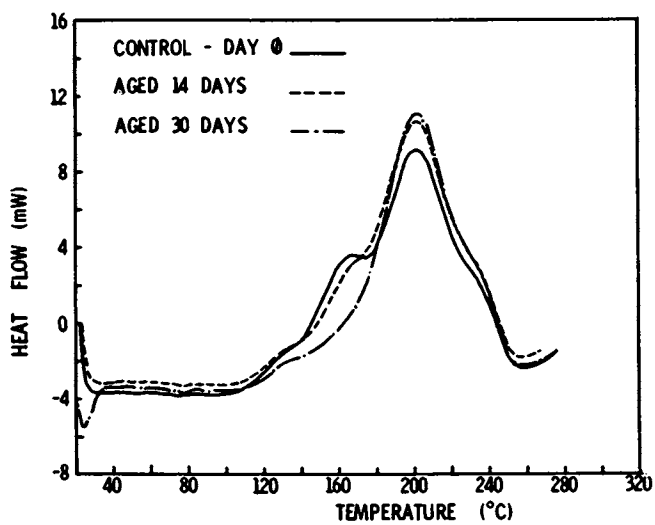


Figure 9. DSC Analysis of the Aging Process.

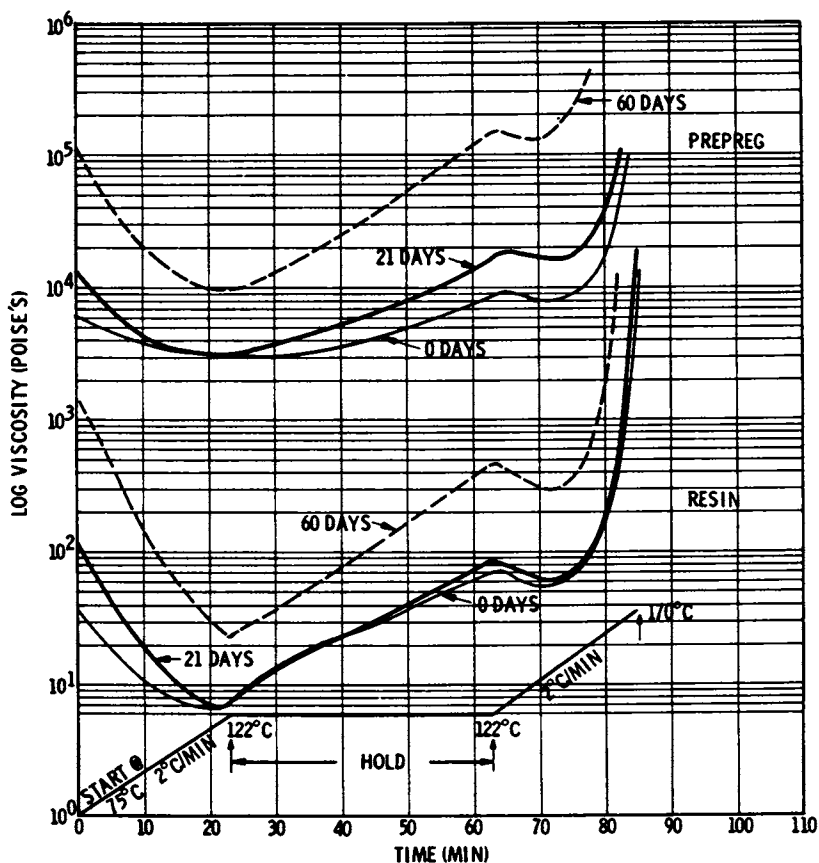


Figure 10. Effect of Ambient Aging on Prepreg and Resin Viscosity.

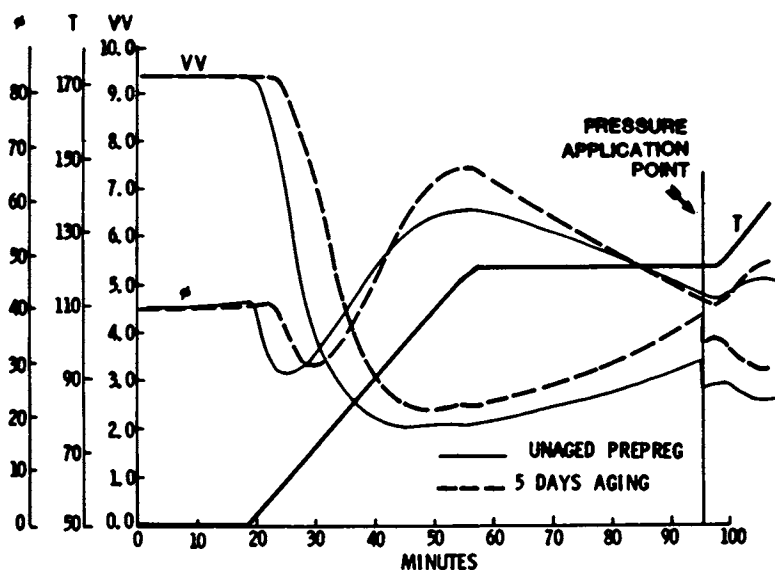


Figure 11. Dielectric Analysis of Aged Prepreg.

ation cycles, an aid in tool design and more effective quality control. During our earlier work the following four parameter model was developed based on the rheology and kinetics of the curing matrix:

$$\ln \eta(T, t) = \ln \eta_x + E_\eta/RT + k_x \int_0^t \frac{-E_k}{RT} dt$$

The diagram illustrates the four terms of the equation above. Each term is enclosed in a circle or oval and connected by a plus sign. Below each term, a line points to a label:
 

- $\ln \eta(T, t)$  is labeled "PREDICTED VISCOSITY".
- $\ln \eta_x$  is labeled "DERIVED FLOW TERMS".
- $E_\eta/RT$  is labeled "RHEOLOGICAL FLOW TERMS".
- $k_x \int \frac{-E_k}{RT} dt$  is labeled "DERIVED KINETIC TERMS".

The model parameters were derived from isothermal rheological data and when applied to a production cure cycle gave a reasonably good correlation with observed data as demonstrated in Figure 12. However, as seen in Figure 13, the fit was not considered satisfactory under isothermal conditions particularly in the latter stages of the heating. This is the area where important process decisions, such as application of laminate consolidation pressure, are often made. As a result a 6-parameter model was derived which includes terms for chain entanglement and overall reaction order. This subject is discussed in detail in Chapter 18.

As mentioned earlier, dielectric signals appear to offer the best means for process control and documentation. They are responsive to material changes and correlate with physical changes in a curing matrix. Current thinking has progressed to the point where it would appear that the physical changes which occur in the matrix during the fluid state correlate well with dielectric measurements such as vector voltage, resistance and capacitance. Later in the cure, as the resin system gels, these quantities at first change inversely with the physical changes and then show very marginal response. During the final stages of cure, as the resin matrix becomes increasingly rigid, the only dielectric changes of significance are logically, those associated with segmental or dipolar activity in an AC field. Thus measurements such as loss tangent or dissipation factor should be used to assess the extent of cure at the temperature in question. Once molecular motion ceases, as evidenced by no further changes in these measurements, the cure should be terminated.

Dielectric monitoring can be accomplished in a variety of ways as illustrated in Figure 14. Here, phase angle (phase meter),  $\tan \delta$  (dielectrometer) and DC resistivity (ionographing) are plotted as a function of a simple cure cycle, a fixed rate of heating



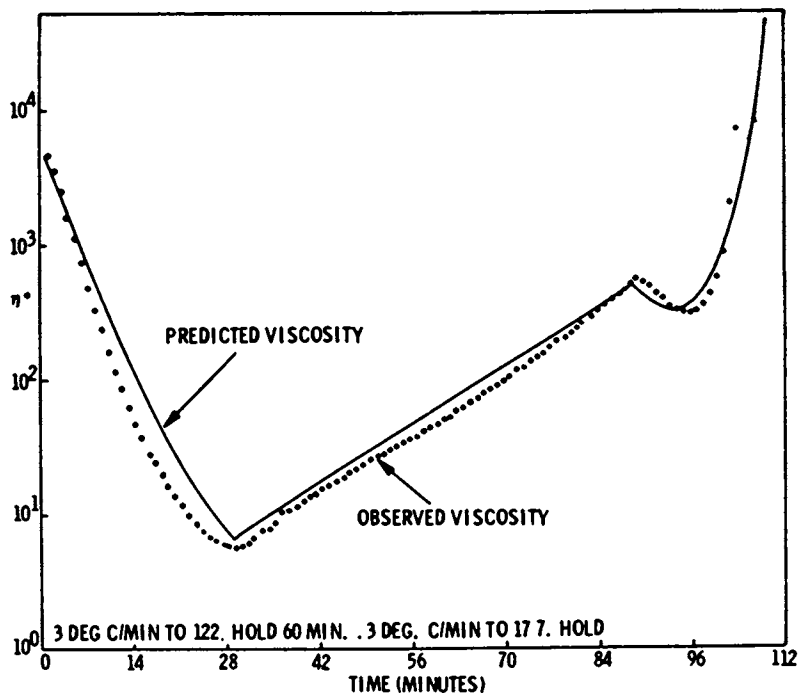


Figure 12. Four Parameter Model Fit - Production Cycle.

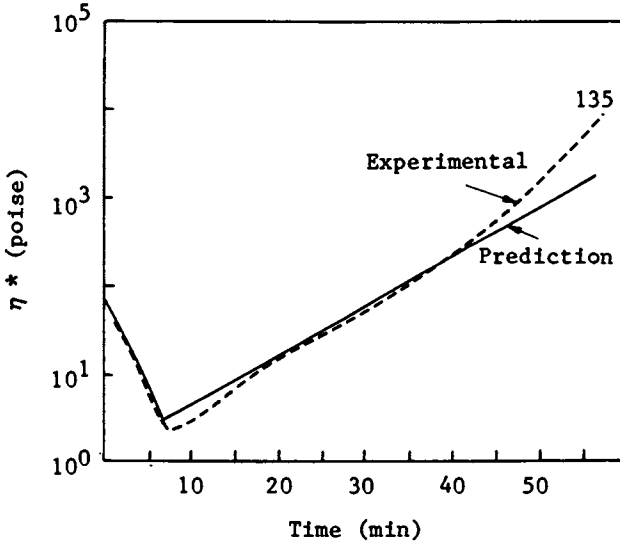


Figure 13. Four Parameter Model Fit - Isothermal Cure.

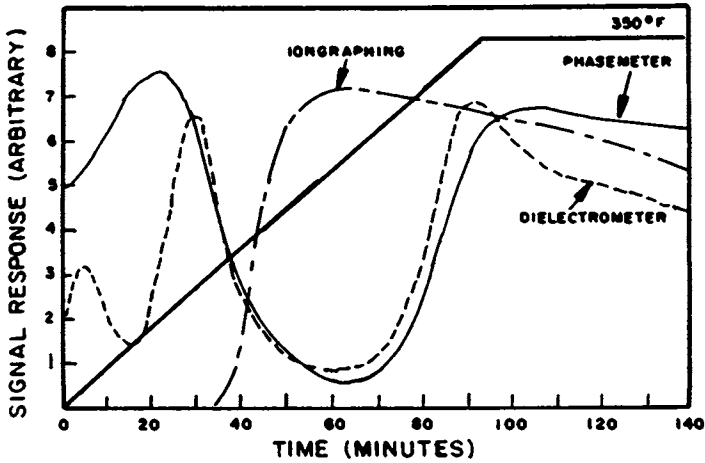


Figure 14. Comparison of Dielectric Monitoring Traces.

to a cure temperature of 177°C (350°F). The data which follows is based on the phasemeter measurements for a variety of reasons. The ionographing lacks definition in a process critical (low viscosity) region. The dielectrometer, while giving excellent definition of significant cure events, is a commercial instrument with an internal ground which complicates work in cure media such as an autoclave. The phase meter approach has the added advantage of being useful over a broad range of voltage and frequency. Thus, low signal to noise ratios are readily attainable.

There is little question that dielectric monitoring is a production practical monitoring procedure. Shown in Figure 15 are the phase meter responses from an actual hardware part during fabrication in a production mold. The inverse  $\tan \delta$  response was calculated by a microprocessor during the cure using equations based on earlier work<sup>16</sup>). By careful control of the prepreg material the dielectric signal was repeatable and the mechanical properties of the part were well within the hardware specifications.

The feasibility of using dielectric signals to control a cure cycle is demonstrated in Figure 16. A mathematical algorithm was developed which predicted what the cure cycle temperature should be at the next reading following the current one. Although not entirely compatible with our current thinking as expressed above, it was a linear regression based on vector voltage, phase angle and heat history. Using this calculation, the microprocessor sent a signal to a laboratory press which activated the platen heaters in a manner which should achieve the desired temperature at the next data collection point.

Shown in the figure are the vector voltage (VV) phase angle ( $\phi$ ) and cure cycle (T) used to develop the algorithm and the subsequent temperature response (dashed line T). Although the cure cycles are not exactly the same, the similarity is evident. Both cycles gave laminates with satisfactory mechanical properties. Thus the only question is which cycle is "best" bearing in mind that the algorithm based closed-loop cycle was dictated by responses related to chemical and physical changes occurring in the composite matrix as it cured.

It is obvious that this phase of total process control is not complete and work remains to be done. The mathematical algorithm requires further refinement. There is little question that the starting matrix and the B-stage resulting from its manufacture can be accurately defined. However, two further material changes can take place prior to actual part fabrication. First, the degree of B-staging can increase as a result of the required handling prior to the actual cure. Second, most polar thermoset resins are hygroscopic and moisture will alter both the dielectric response and the viscosity changes during the process-

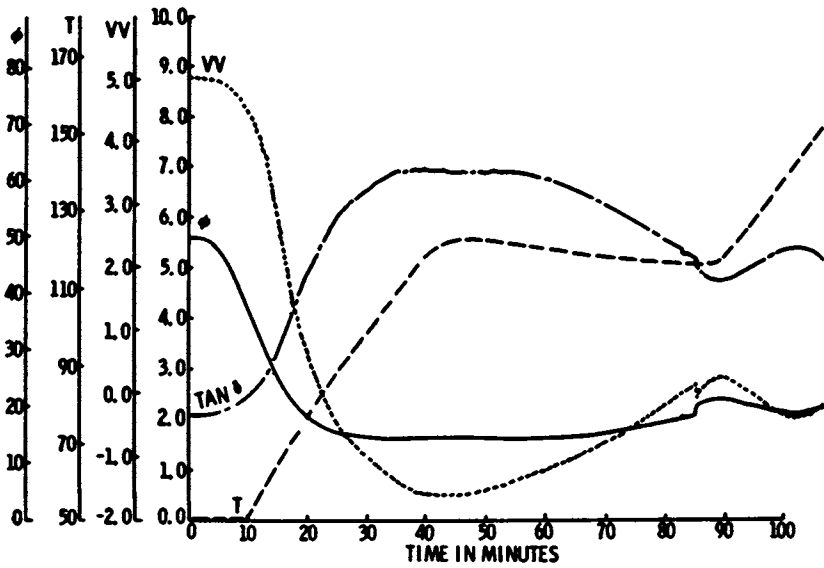


Figure 15. Dielectric Response from Production Mold.

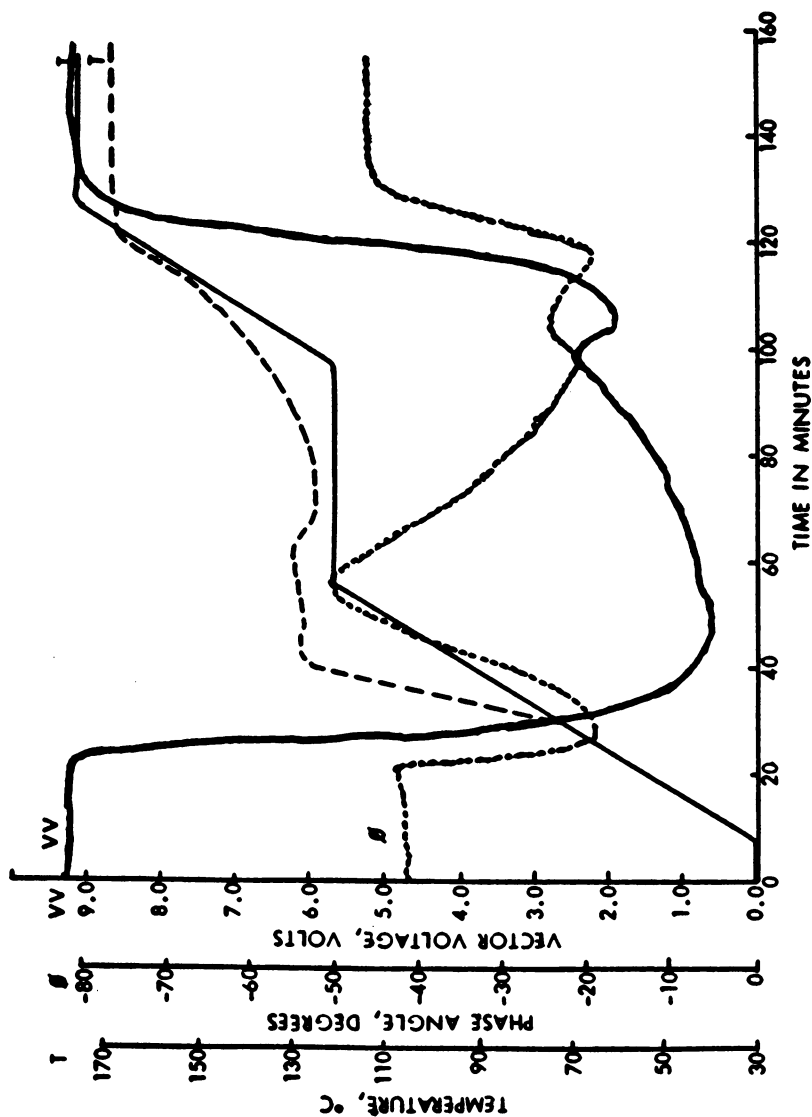


Figure 16. Normal Cure Cycle vs Preliminary Closed-Loop Cure Cycle.

ing. Since both of these changes are measurable by dielectric response, total automation of the thermoset resin process should be achievable in the near future. It is evident that different formulations will require different algorithms, however, once one material is controlled, control of the others should be readily simple.

Using chemical and physical characterization methods to assure consistent starting materials and dielectric measurements to control and verify the proper cure, a totally controlled process concept is possible. All decision points, from prepreg acceptance through part layup and cure control to non-destructive hardware evaluation (NDE), are freed from the errors possible by human decision. One concept of this type is illustrated in Figure 17 for the fabrication of fiber reinforced composite hardware. The coded incoming material is first subjected to a series of laboratory (chemical characterization) tests. If these meet specifications, mechanical characterizations are run which determine acceptable fiber and interfacial bonding strengths. Since the latter is the more expensive acceptance procedure, it should be run after the starting prepreg meets the chemical and physical standards. Simultaneously, with receipt of the prepreg, computer documentation of storage life should begin.

This data becomes a traceable entity for each hardware item made from the material by linking it through a central computer active data file. As the next step the fabricator is identified and his actions are controlled by means such as CRT video displays, voice data entry, etc. The hardware is then cured using a closed-loop microprocessor controlled cycle involving dielectric signals which also verify that the hardware was properly processed. If non-destructive evaluation shows the part is below an acceptable void level and thus mechanically sound, hardware quality is assured with a high degree of confidence. Further, should a failure occur at some point during its useful life, every step of the fabrication is traceable. Through a data analysis each part with the same production history can be located and corrective action can be taken. In all probability with better scientific understanding of materials and processes this will not happen. However, with human lives dependent on thermoset products in the future, this type of control is worthwhile insurance.

Current hardware acceptance procedures are based on either mechanical testing of tag ends or destruct testing of actual parts based on statistical selection. Procedures of this type only verify the quality of the test specimen. They say nothing about the quality of the hardware being used. However, by using fabrication processes based on sound scientific principles and documenting that these events have occurred, we can have a high degree of confidence that reliable thermoset products have been produced. On

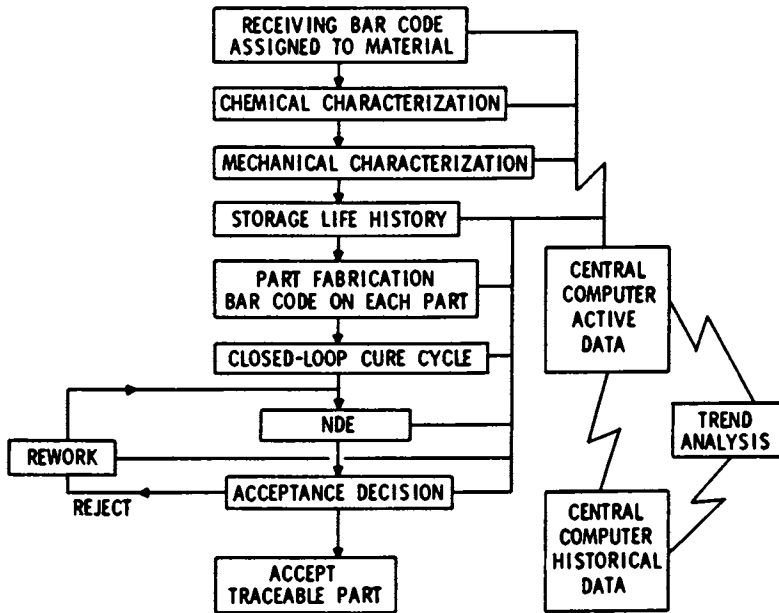


Figure 17. Composite Hardware Control Concept.

the basis of what has been discussed herein and in the chapters which follow, it is evident that this time is close at hand.

#### Literature Cited

- 1) May, C.A., Fritzen, J.S. and Brown, G.R., International Conference on Composite Materials, Proceedings, 264-84, Boston/Geneva (1975).
- 2) May, C.A., SAMPE Series 20; 108-16, San Diego (April 1975).
- 3) Wereta, A., Jr., and May, C.A., Org. Coatings and Plastics Chem., ACS Preprints 38, 679-84, Anaheim (March 1978).
- 4) Wereta, A., Jr., and May, C.A., J. Adhesion 12, 317-331 (1981).
- 5) Fritzen, J.S., Wereta, A., Jr., and Arvay, E.A., SAMPE Series 22, 430-34, San Diego (April 1977).
- 6) von Hippel, A., Dielectric Properties of Materials, MIT Press, Cambridge, MA. (1954)
- 7) Turner, A. Jr., Mechanical Behavior of High Polymers, Interscience Publishers, New York (1948).
- 8) Smyth, C.P., Dielectric Behavior and Structure, McGraw-Hill, New York (1955).
- 9) McCrum, N.G., Reed, B.E. and Williams, G., Anelastic and Dielectric Effects in Polymeric Solids, John Wiley and Sons, New York (1967).
- 10) Wrasidlo, W.J., Motions in Poly-Pyromellitimide, Boeing Scientific Research Laboratories, Rpt. No. D1-82-1061.
- 11) Yaloff, S.A. and Wrasidlo, W.J., J. Appl. Polymer Sci 16, 2159, (1972).
- 12) Hedvig, P., Dielectric Spectroscopy of Polymers, John Wiley and Sons, New York (1975).
- 13) May, C.A., Whearty, D.K. and Fritzen, J.S., SAMPE Series 21, 803-18, Los Angeles (April 1976).
- 14) St. Clair, T.L. and Jewell, R. A., National SAMPE Tech. Conf. Series, 8, 82-93 Seattle (Oct. 1976).
- 15) Cheng, D.K., Analysis of Linear Systems, Addison-Wesly Publishing Co., Inc., Reading, MA. (1961).
- 16) May, C.A., Wereta, A., Jr., Fritzen, J.S. and Keck, F.L., AFWAL-TR-80-4171 (Nov. 1980).

RECEIVED March 31, 1983



# Cure Kinetics and Mechanical Properties of a Resin Matrix

## Effects of Impurities and Stoichiometry

GARY L. HAGNAUER, PETER J. PEARCE, BERNARD R. LALIBERTE,  
and MARGARET E. ROYLANCE

Army Materials and Mechanics Research Center, Organic Materials Laboratory,  
Watertown, MA 02172

The effects of impurities, or synthesis by-products, and stoichiometry on the cure kinetics of N,N'-tetraglycidyl methylene dianiline (TGMDA) resins formulated with diaminodiphenyl sulfone (DDS) are evaluated using gel permeation chromatography and differential scanning calorimetry. During the early stages of cure (177°C), the predominant reaction is amine-epoxy addition represented by a third-order rate expression. Impurities increase the rate of reaction and lead to higher extents of reaction. Increasing the epoxy/amine equivalent ratio decreases the rate of reaction and leads to higher extents of cross-linking and reaction. The mechanical properties of a series of resin specimens cured from TGMDA/DDS formulations with varying stoichiometry and different impurity levels are evaluated using standard ASTM test methods. Impurities in commercial TGMDA resins cured with DDS and changes in the epoxy/amine ratio (1.46-1.95) are found to have no significant effects on the mechanical properties of the cured resin matrix. Post-curing improves the tensile and compressive strength and decreases the stiffness of the resin matrix.

Epoxy resins containing N,N'-tetraglycidyl methylene dianiline (TGMDA) are widely used in the manufacture of fiber-reinforced structural composites for aerospace applications. The monomer TGMDA is the principle component (ca. 60-80%) in Ciba-Geigy Corporation's Araldite MY720 and in FIC Corporation's Glyamine G-120. Synthesis by-products occurring in these resins include chlorohydrins, glycols, dimers, trimers and higher

This chapter not subject to U.S. copyright.  
Published 1983, American Chemical Society

oligomers. Additionally, water, organic solvents and inorganic salts may be present as impurities. It has been shown that the synthesis by-products and impurities have a significant effect on the physical properties, hydrolytic stability and reactivity of TGMDA (1). At 50°C the viscosity of relatively pure (96%) TGMDA is about one-tenth that of the commercial resins. Impurities (synthesis by-products) accelerate the rate of hydrolysis of TGMDA and lower the curing temperature for the reaction of TGMDA with diaminodiphenyl sulfone (DDS).

In this paper the effects of impurities and stoichiometry on the TGMDA-DDS polymerization reaction are investigated. Preliminary data showing the effects of impurities and post-cure treatment on the mechanical properties and moisture up-take of the TGMDA/DDS resin matrix are presented. The purified TGMDA monomer, the commercial resins G-120 and MY720, and a sample consisting primarily of TGMDA oligomers are used for this study. Gel permeation chromatography (GPC) and differential scanning calorimetry (DSC) techniques are applied to evaluate the TGMDA-DDS cure kinetics at 177°C. Mechanical test specimens are prepared and conditioned for tension, compression, flexure, Izod impact and torsion pendulum analyses. Conclusions are made regarding the effects of impurities, stoichiometry and post-cure treatment on the cure behavior, structure, strength, stiffness, impact energy, glass-transition temperature and moisture absorption properties of the TGMDA/DDS resin matrix.

## Experimental

**Samples.** The TGMDA resins Araldite MY720 (batch No. 5093) and Glyamine G-120 (Lot No. 1003) were obtained from Ciba Geigy Corp. and FIC Corp., respectively, and were stored in closed containers at -13°C. The samples designated "TGMDA" and "Residue" were isolated from the G-120 resin using preparative liquid chromatography (1). Sample TGMDA is essentially pure monomer; whereas the Residue consists primarily of higher molecular weight oligomers and relatively polar resin components.

Data characterizing the TGMDA resins are shown in Table I. Epoxy equivalent weights (EEW) were obtained by the standard nonaqueous titration method (2) using chloroform as the solvent. The % epoxy values are based upon the theoretical EEW value 105.5 g/eq for the TGMDA monomer. The GPC and high performance liquid chromatography (HPLC) techniques for determining weight-% TGMDA monomer have already been described (1). Viscosity measurements were made at 50°C using a Rheometrics Mechanical Spectrometer Model RMS-7200 in steady shear mode with cone and plate geometry.

To prepare formulations of the TGMDA samples with DDS for GPC and DSC studies, the components were first weighed (ca. 30g total), then heated to about 90°C and mixed until a homogeneous solution was formed at 80-90°C. HPLC and GPC analyses of the formulations showed that no apparent reaction occurred during mixing. The resin formulations were stored in sealed containers

Table I. Characteristics of the TGMDA Resins

Sample	Non-Aqueous Titration EEM(g/eq.)	% Epoxy	% TGMDA Monomer GPC	HPLC	n <sub>D</sub> 50°C (cp)	Description (21°C)
TGMDA (theoretical)	108 (105.5)	98 (100)	98.5	97.7	1270-1590	clear-pale yellow liquid
G-120	118	89	76.2	77.7	5000-15,000	amber liquid
MY720	127	83	61.5	69.2	17,600	amber liquid
Residue	168	63	-	9.0	50,400-54,700	dark amber liquid- solid

at  $-13^{\circ}\text{C}$  and removed only for sampling. The curing agent DDS was highly pure (ca. 99%) as received from Aldrich Chemical Co. The compositions of the formulations are indicated in parenthesis as weight percentage of DDS.

**GPC Study.** GPC is used to analyze changes in the chemical compositions of the TGMDA/DDS formulations cured for differing periods of time at  $177^{\circ}\text{C}$ . Molecular weights and the weight percentages of TGMDA monomer, DDS, reaction products and gel are determined as a function of cure time.

Samples (5-10mg) were weighed on a microbalance and partially cured on the heating stage of a Perkin-Elmer DSC 1B instrument in a nitrogen atmosphere. Cures were terminated by transferring the sample pans to 25ml volumetric flasks and adding tetrahydrofuran (THF). To facilitate dissolution the flasks were aggitated and the samples allowed to soak for 1-4 days. Except for highly cross-linked gel, all the components were soluble. The sample solutions were diluted to 25ml and filtered through a  $0.2\mu\text{M}$  Millipore membrane filter prior to GPC analysis. Only soluble components were analyzed by GPC.

A Waters Associates ALC/GPC-244 instrument with M6000A solvent delivery system, M720 system controller, M730 data module, 710B WISP auto-injector and M440 UV detector was used for the GPC analyses and operated under the following conditions:

Column Set:  $\mu\text{Styragel}$  ( $2 \times 500\text{\AA}$ ,  $3 \times 100\text{\AA}$ )  
 Concentration:  $0.2-0.5\mu\text{g}/\mu\text{l}$   
 Injection Volume:  $20-60\mu\text{l}$   
 Mobile Phase: THF (UV grade, Burdick & Jackson, Labs).  
 Flow Rate:  $1\text{ ml}/\text{min}$   
 Detector: UV  $254\text{nm}$   
 Run Time:  $45\text{ min}$ .

Typical GPC chromatograms are shown in Figure 1. The chromatograms are displaced along the ordinate to illustrate compositional changes. Reaction products elute with retention times between 28 and 34 minutes. The indicated products were isolated by preparative GPC for purposes of identification and calibration. Areas under the GPC peaks and peak segments are directly proportional to the concentrations of the components. Therefore, the weight-% of each component or set of components designated  $C_i$  may be calculated

$$\%C_i = \frac{A_i \cdot K_i}{m \cdot V} \cdot 100\% \quad (1)$$

where  $K_i = \frac{(m_i)_s \cdot V_s}{(A_i)_s}$  is the calibration constant,  $A_i$  is the peak area of component  $i$  and  $m$  and  $V$  represent the sample

concentration ( $\mu\text{g}/\mu\text{l}$ ) and injection volume ( $\mu\text{l}$ ). The subscript "s" denotes the respective parameters for the calibration standard(s). It is noted that the calibration constants for TGMDA and DDS are quite similar and that the 1:1 product has a different constant which is essentially identical to those of the higher molecular weight products.

The calibration curve for determining molecular weights (MW) is shown in Figure 2. Discrete MWs obtained by averaging the MWs

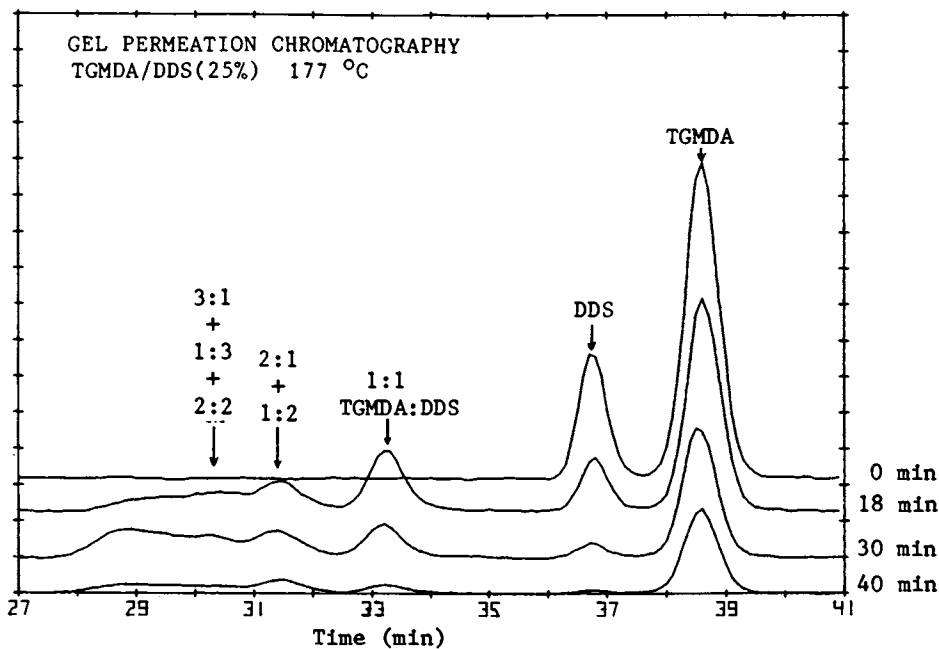


Figure 1. GPC Analysis of the TGMDA/DDS (25%) Reaction (177°C).

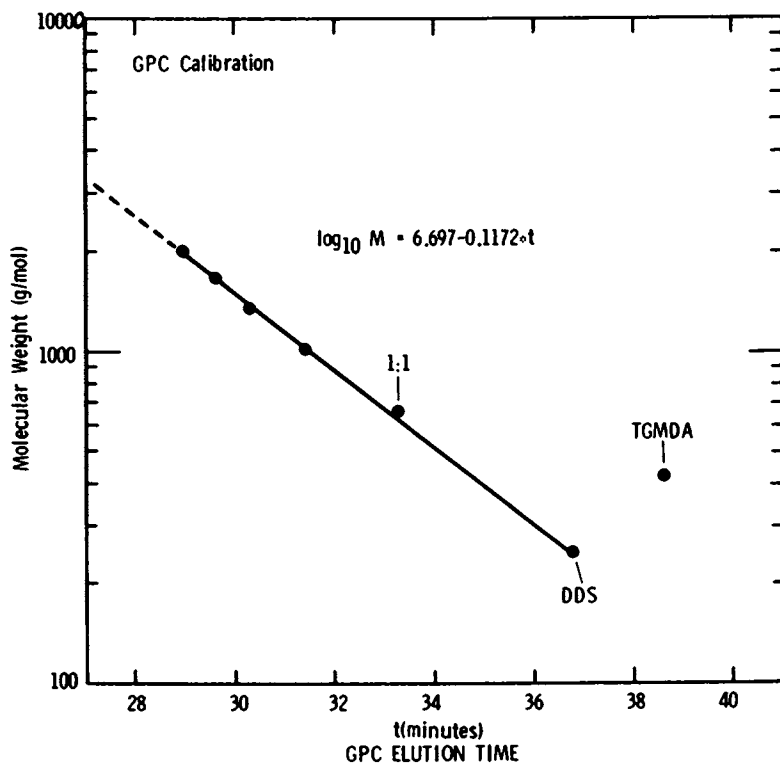


Figure 2. GPC Calibration Plot for TGMDA-DDS Reaction Products.

of components eluting at the same times are indicated as data points and extrapolated to account for higher MW components. Standard equations are applied to calculate number-, weight- and z-average MWs -

$$M_n = \frac{\sum A_i}{\sum A_i/M_i} \quad (2)$$

$$M_w = \frac{\sum A_i \cdot M_i}{\sum A_i} \quad (3)$$

$$M_z = \frac{\sum A_i \cdot M_i^2}{\sum A_i \cdot M_i} \quad (4)$$

where  $A_i$  is the peak area for component(s)  $i$  of average molecular weight  $M_i$  and the area segment for component(s) eluting in the extrapolated region at time  $t_i$  over the interval  $t_i - t_{i-1}$  with  $M_i$  defined by

$$\log M_i = 6.697 - 0.1172 \cdot t_i \quad (5)$$

Gel content is determined indirectly according to the equation

$$\% \text{gel} = \frac{m \cdot V - \sum A_i \cdot K_i}{m \cdot V} \cdot 100\% \quad (6)$$

**DSC Study.** DSC is used to determine the extent  $\alpha$  and rate  $\dot{\alpha}$  of reaction during the isothermal cure of the TGMDA/DDS formulations. These parameters are then related to compositional changes determined by GPC. Measurements were made using a DuPont 990 thermal analyzer with 920 DSC module. Procedures described in the instrument operating manual were used for temperature and calorimetric calibration. Samples were weighed (ca. 20-30mg) in open aluminum pans and run in a nitrogen atmosphere. An initial baseline was established by equilibrating the instrument at the curing temperature with empty sample pans and a run was initiated by inserting a filled sample pan. Thermal equilibrium was regained within 2 minutes after sample insertion and the exothermic reaction was considered complete when the recorder signal levelled off to a baseline. The final baseline was extrapolated to determine the total area under the exotherm curve and hence the isothermal heat of cure  $\Delta H_{iso}$ . Each isothermally cured sample was then analyzed using dynamic DSC at a heating rate of 2°C/min to obtain the residual heat of reaction  $\Delta H_{res}$ . Sample weight losses were negligible. Data from the isothermal analyses were digitized and evaluated using a Hewlett Packard 9830 computer.

The total heat of reaction  $\Delta H_{tot}$  was calculated from the sum of the isothermal and residual heats,  $\Delta H_{iso} + \Delta H_{res}$ , for each sample. For isothermal cures the extent of reaction  $\alpha_i$  at time  $t_i$  is defined

$$\alpha_i = \frac{\sum_{j=1}^i \Delta H_j}{\Delta H_{tot}} \quad (7)$$

where  $\sum_{j=1}^i \Delta H_j$  is the cumulative heat generated or area integrated

under the DSC exotherm curve over the time interval  $t_1=0$  to  $t_i$  and  $\Delta H_{tot}$  is the total heat or the sum of the total integrated areas. The extent of reaction is assumed to be proportional to the heat evolved during cure. The rate of reaction is defined

$$\dot{\alpha}_i = \left( \frac{d\alpha}{dt} \right)_i \quad (8)$$

at  $\alpha_i$  or  $t_i$ .

**Mechanical Testing.** A series of resin plates (ca. 0.1 inch thickness) and cylindrical specimens (0.5 inch diameter) were prepared from TGMDA/DDS formulations with varying stoichiometry and different impurity levels for mechanical testing. The TGMDA resin, curing agent DDS, mixing implements and molds were preheated to 120°C and the appropriate amount of DDS was mixed into the resin until all visible traces of DDS disappeared. Maintaining the temperature at 120°C, the resin formulation was degassed in vacuo until a marked decrease in the outgassing rate was noted (ca. 10 min) and then carefully poured into the preheated vertical Teflon molds to prevent entrapment of air. The cure cycle consisted of heating the samples from 120°C to 135°C (1°C/min), holding at 135°C for 4 hours, heating to 177°C (1°C/min), holding at 177°C for 2 hours and cooling slowly overnight to room temperature. Using this technique essentially void free castings were achieved.

ASTM standard specimens and procedures were used for flexure (D-690), compression (D-695), Izod impact and torsional pendulum analysis (TPA). For tension, D1822 tensile impact specimens were substituted for D638 specimens to conserve material. Test specimens were machined from the plates and cylinders using a water cooled diamond wheel. All the specimens were dried in vacuo at 100°C for three weeks before testing or subsequent post-cure treatment. Half the specimens were post-cured for 2 hours at 225°C in vacuo before testing. Selected specimens were immersed in distilled water at 80°C for 6 weeks for moisture uptake determinations.



Results and Discussion

GPC Studies. Figure 3(a) and (b) illustrates how the composition of the purified TGMDA resin formulated with DDS (25%) changes during cure at 177°C. The formation of gel corresponds to a marked decrease in the concentration of the higher MW products occurring between 30 and 40 minutes (also see Figure 1). Focusing on the early stage of cure prior to the onset of gelation, isolation and identification of the reaction products shows that simple amine-to-epoxy addition is the predominant reaction. Indeed Fourier transform infrared spectroscopic analysis of the reaction mixture at various stages of cure supports the conclusion that there is a one-to-one correlation between epoxide concentration and TGMDA concentration and that no significant side reactions occur during the early stages of cure. Hence, GPC may be applied to investigate the kinetics of the TGMDA/DDS reaction.

Experimental data are plotted in Figure 4 and show that the concentrations C (mol/kg) of TGMDA and DDS decrease in parallel as the reaction time increases; i.e.,

$$-\frac{d[\text{TGMDA}]}{dt} = \frac{-d[\text{DDS}]}{dt} \quad (9)$$

over nearly 20% of the total theoretical extent of reaction. Stoichiometric studies show that the reaction is first-order with respect to the concentration of TGMDA and second-order with respect to DDS

$$-\frac{d[\text{TGMDA}]}{dt} = k_3 [\text{TGMDA}] [\text{DDS}]^2 \quad (10)$$

The rate constants  $k_3$  in Table II are calculated from both the rate of reaction of TGMDA and of DDS.  $C_0$  represents the initial reactant concentrations.

Table II. GPC Rate Constants for the TGMDA/DDS Reaction at 177°C

Sample	$C_0$ (mol/kg)		$k_3$ ( $\text{kg}^2 \text{mol}^{-2} \text{min}^{-1}$ )	
	TGMDA	DDS	TGMDA	DDS
TGMDA/DDS (15%)	2.01	0.605	0.0179	0.0179
TGMDA/DDS (25%)	1.78	1.01	0.0184	0.0182
TGMDA/DDS (37%)	1.49	1.49	0.0224	0.0224

Molecular weight parameters for the TGMDA/DDS (25%) reaction at 177°C are plotted in Figure 5. The rate of change and values of the parameters provide information relating to the formation of the gel network. Parameters  $M_w$  and  $M_z$  are most sensitive to the formation of high MW products<sup>w</sup> and approach infinity as the reaction nears the onset of gelation. The finite values of these

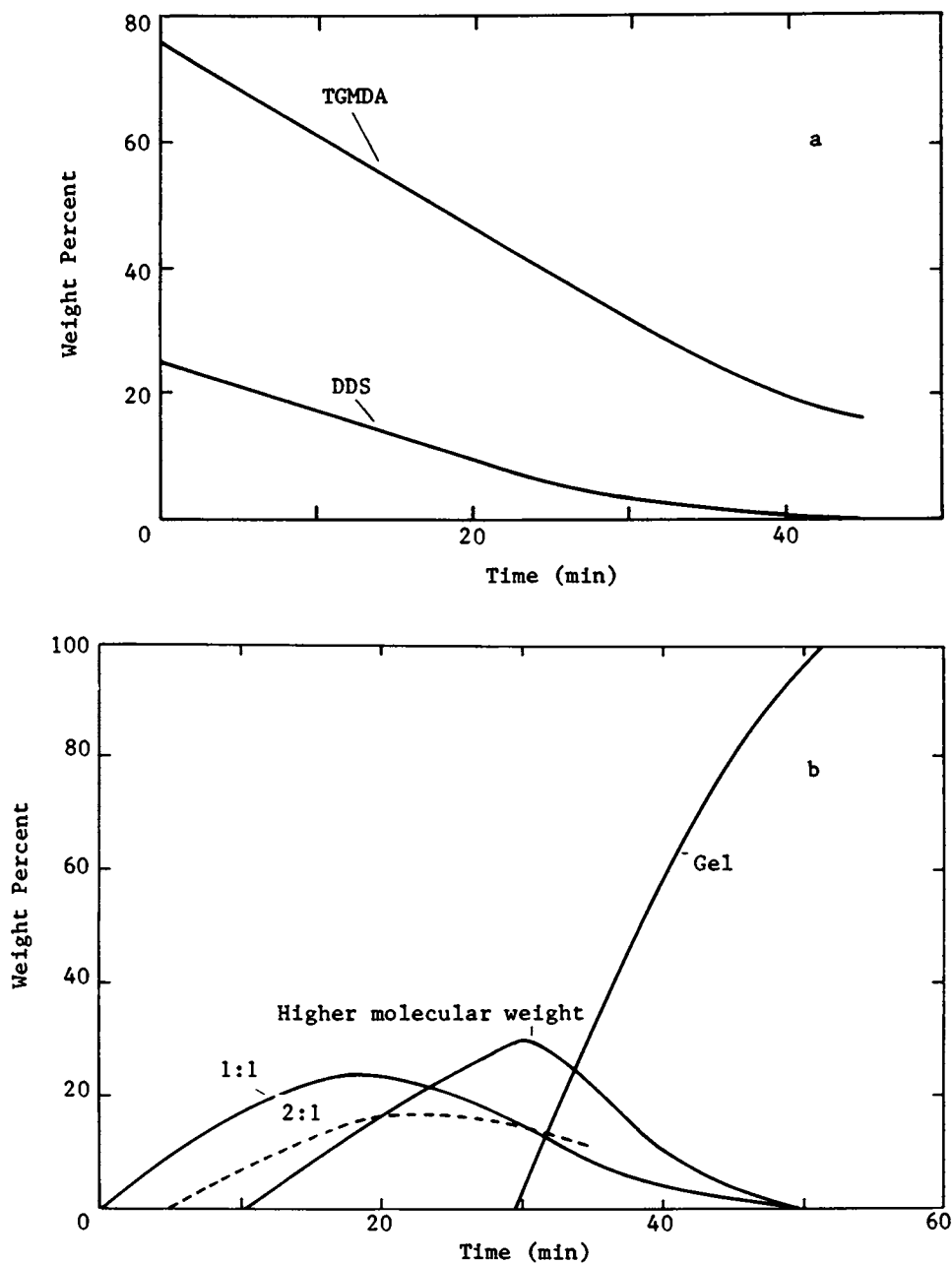


Figure 3. Changes in the TGMDA/DDS (25%) (a) Reactant and (b) Reaction Product Concentrations (Weight %) with Cure Time ( $t$ ) at 177°C.

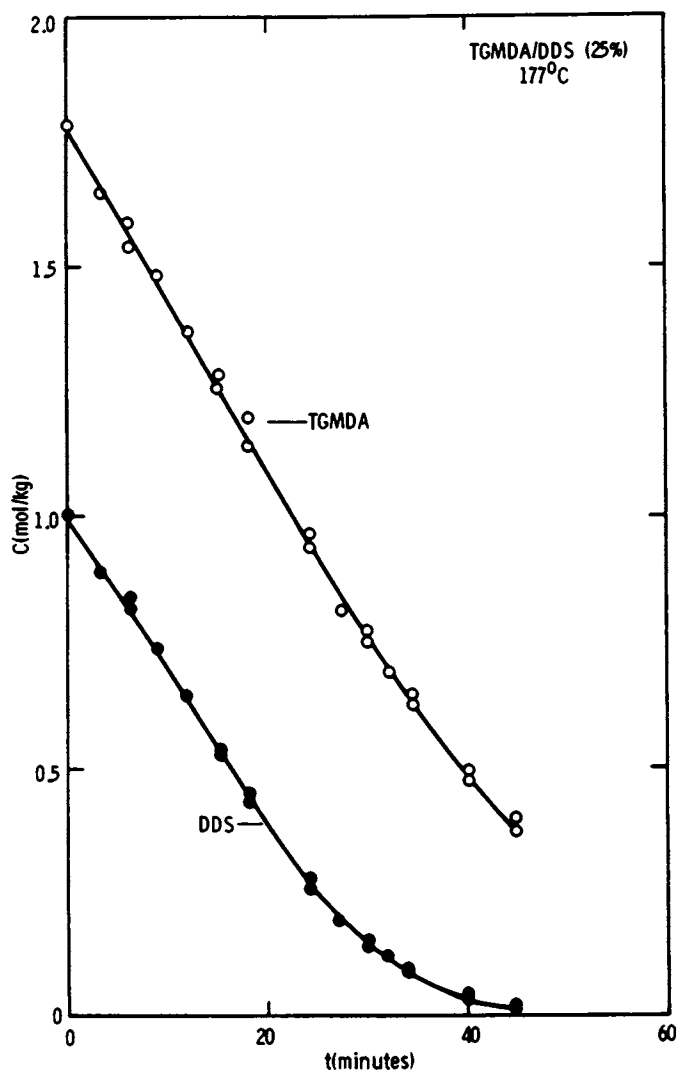


Figure 4. TGMDA and DDS Concentrations Versus Cure Time for TGMDA/DDS (25%) at 177°C.

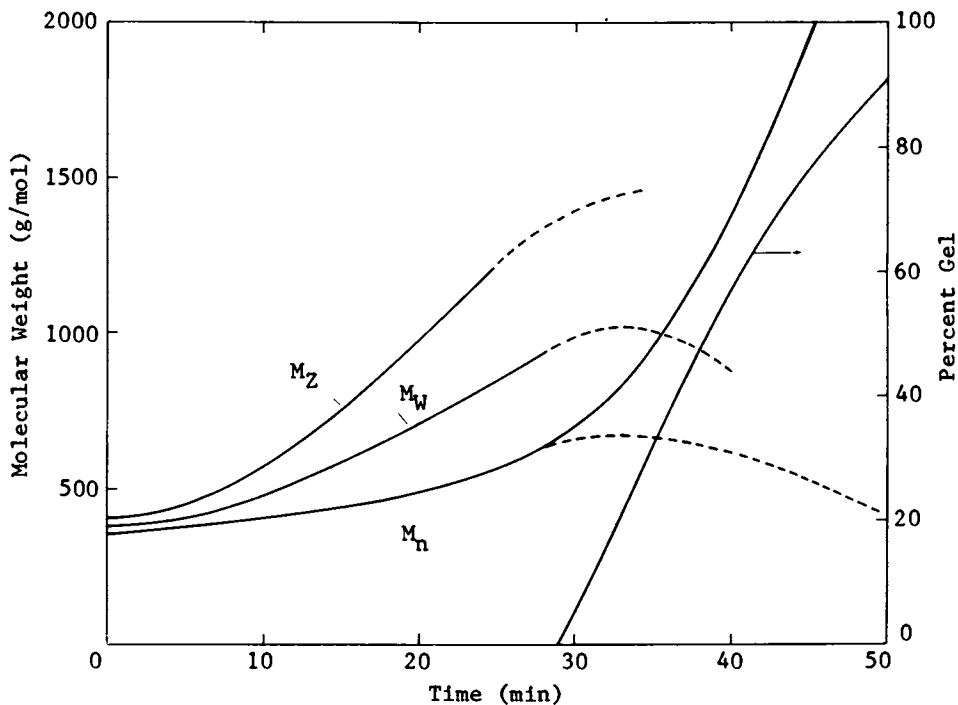


Figure 5. Molecular Weight Parameters and % Gel Versus Cure Time for TGMDA/DDS (25%) at 177°C.

parameters beyond the onset of gelation and the downward curvature of the plots are a consequence of the fact that only soluble components can be analyzed by GPC and that the highest MW products tend to be incorporated into the gel network first. Most likely,  $M_z$  curves downward early because the GPC calibration is no longer applicable at relatively high extents of reaction where a variety of highly branched products are formed. Only  $M_n$  can be interpreted beyond the onset of gelation (solid line) by<sup>n</sup> including the weight fraction of gel in the equation

$$M_n = \frac{\sum C_i}{\sum C_i / M_i} \quad (11)$$

where  $C_i$  is the weight fraction of components define by Eqs. 1 and 6.

DSC Study. From the analysis of the total heats of reaction of the commercial and fractionated TGMDA resin/DDS formulations over a broad stoichiometric range, it is concluded that the total heat of reaction divided by the epoxy concentration has a constant value

$$\frac{\Delta H_{\text{tot}}}{(\text{eq. epoxy}/100\text{g})} = \text{constant} \quad (12)$$

and that the exotherm for the epoxy-amine reaction is essentially identical to that of the epoxy-epoxy polymerization reaction

$$\Delta H (\text{epoxy-amine}) = \Delta H (\text{epoxy}) \quad (13)$$

Thus the assumption that the DSC parameter  $\alpha$  represents the overall extent of reaction is valid, and comparisons of quite different resin formulations and correlations between DSC and GPC data may be made.

The effect of stoichiometry on the rate of reaction as measured by DSC is shown in Figure 6. As the %DDS increases, the extrapolated rate of reaction  $K_1$  at  $\alpha=0$  increases and the extent of reaction  $\alpha_p$  for the maximum (peak) rate of reaction  $\dot{\alpha}$  shifts to higher values (Table III). It is also noted that as the % DDS increases the reaction time  $t_p$  to reach  $\alpha$  decreases and the extent of reaction at the onset of gelation  $\alpha_{\text{gel}}$  increases slightly. Finally, the extent of reaction  $\alpha_{\text{final}}$  as  $t \rightarrow \infty$  and  $\dot{\alpha} \rightarrow 0$  is observed to decrease with increasing % DDS.

The rate constant for the initial TGMDA-DDS reaction may be calculated from the extrapolated DSC rate of reaction defined

$$K_1 = \left( \frac{d\alpha}{dt} \right)_{\alpha \rightarrow 0} \quad (14)$$

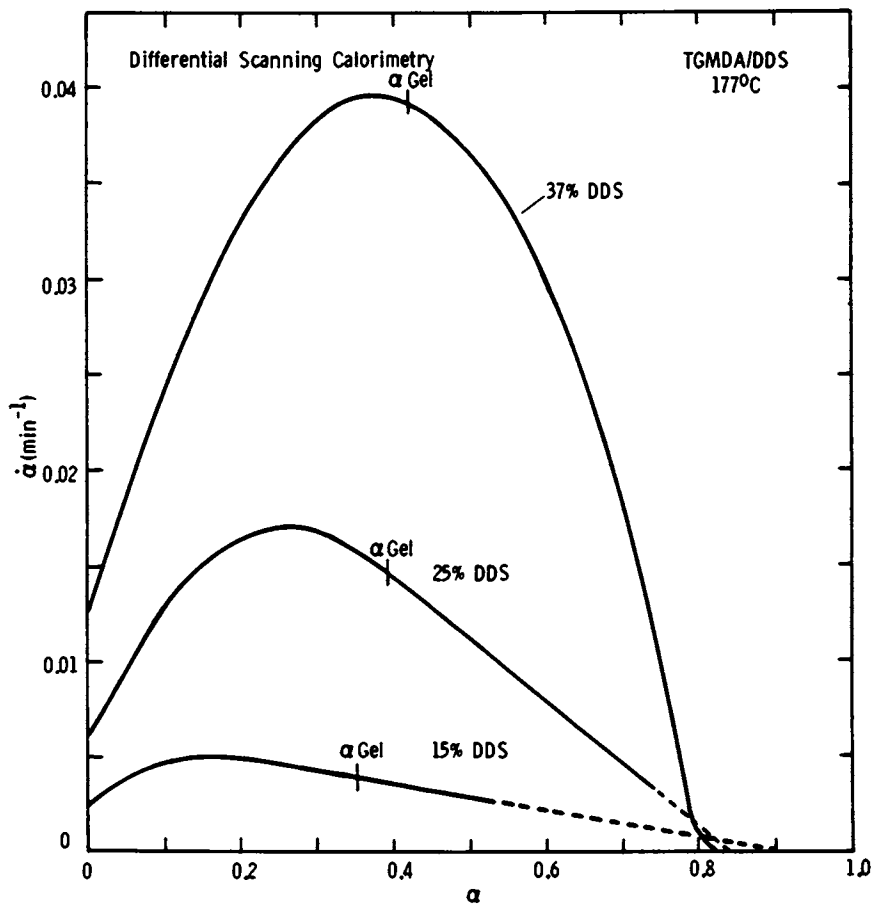


Figure 6. DSC Analysis of the Rate  $\dot{\alpha}$  Versus the Extent  $\alpha$  of Reaction of Different TGMDA/DDS Formulations at 177°C.

Table III. DSC Parameters for the TGMDA/DDS Reaction at 177°C

Sample	$\frac{\text{eq. epoxy}}{\text{eq. amine}}$	$K_1$ ( $\text{min}^{-1}$ )	$\dot{\alpha}_p$ ( $\text{min}^{-1}$ )	$\alpha_p$	$t_p$ ( $\text{min}$ )	$\alpha_{\text{gel}}$	$\alpha_{\text{final}}$	$k_3$ ( $\frac{\text{kg}^2}{\text{mol}^2 \text{min}^{-1}}$ )
TGMDA/DDS (15%)	3.25	0.00235	0.00486	0.16	41.8	0.35	0.92	0.0166
TGMDA/DDS (25%)	1.72	.00582	.0170	.25	20.6	0.39	0.86	0.0180
TGMDA/DDS (37%)	0.98	.0126	.0396	.39	13.8	0.42	0.82	0.0228

Assuming that both TGMDA and DDS have effective functionalities of 4 and that only the 1:1 product forms in the earliest stage of the reaction, the extent and rate of reaction are defined as

$$\alpha = \frac{2[1:1]}{[\text{epoxy}]_0 + [\text{amine}]_0} = \frac{2[1:1]}{4[\text{TGMDA}]_0 + 4[\text{DDS}]_0} \quad (15)$$

and

$$\frac{d\alpha}{dt} = \frac{0.5}{[\text{TGMDA}]_0 + [\text{DDS}]_0} \frac{d[1:1]}{dt} \quad (16)$$

$$\frac{d[1:1]}{dt} = - \frac{d[\text{TGMDA}]}{dt} \quad \text{near } \alpha=0,$$

upon substitution of Eq. 10 and rearrangement the relation for the rate constant is

$$k_3 = \frac{2 K_1 ([\text{TGMDA}]_0 + [\text{DDS}]_0)}{[\text{TGMDA}]_0 [\text{DDS}]_0^2} \quad (17)$$

at  $\alpha=0$ . Rate constants  $k_3$  calculated using Eq. 17 are reported in Table III and are found to be remarkably similar to those determined by GPC (Table II).

A number of interesting correlations may be made between data obtained by DSC and GPC. Relating compositional data to the overall extent or rate of reaction is a sensitive approach for obtaining information about the reaction mechanism and resin network structure. For example,  $M_n$  increases exponentially with  $\alpha$  and reaches an infinite value at 100% gelation. Correlations between  $M_n$  and  $\alpha$  show the effects of stoichiometry on the structure of the reaction mixture (Figure 7). At constant  $\alpha$ ,  $M_n$  increases with decreasing % DDS primarily because the MW of TGMDA is greater than that of DDS. However, the effects of reactant functionality and changes in reaction mechanism are apparent, especially as  $\alpha$  increases. The decrease in the extent of reaction at the onset of gelation  $\alpha_{gel}$  with increasing % DDS may be the consequence of a net decrease in the average functionality of the reactants. A. Gupta (3) has found that the secondary amine formed in TGMDA-DDS reaction products is relatively non-reactive and proposes that the effective functionality of DDS is nearer 2 than 4.

Both GPC and DSC show that impurities or reaction by-products in commercial TGMDA resins increase the rate of reaction. This effect is illustrated in Figures 8 and 9 where the epoxy/amine equivalent ratios are held constant. Impurities also tend to lower  $\alpha_p$ , reduce the gelation time, increase  $M_n$  at  $\alpha_{gel}$  and increase  $\alpha_{final}$ . The magnitude of these effects are particularly notable upon comparing the DSC parameters of the TGMDA and Residue formulations (Table IV).



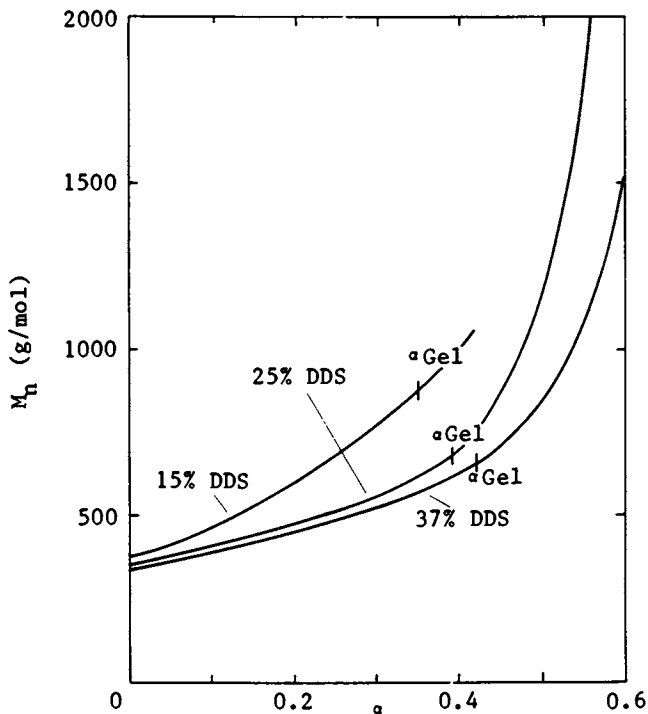


Figure 7. Number-Average Molecular Weight  $M_n$  Versus the Extent of Reaction  $\alpha$  of Different TGMDA/DDS Formulations at 177°C.

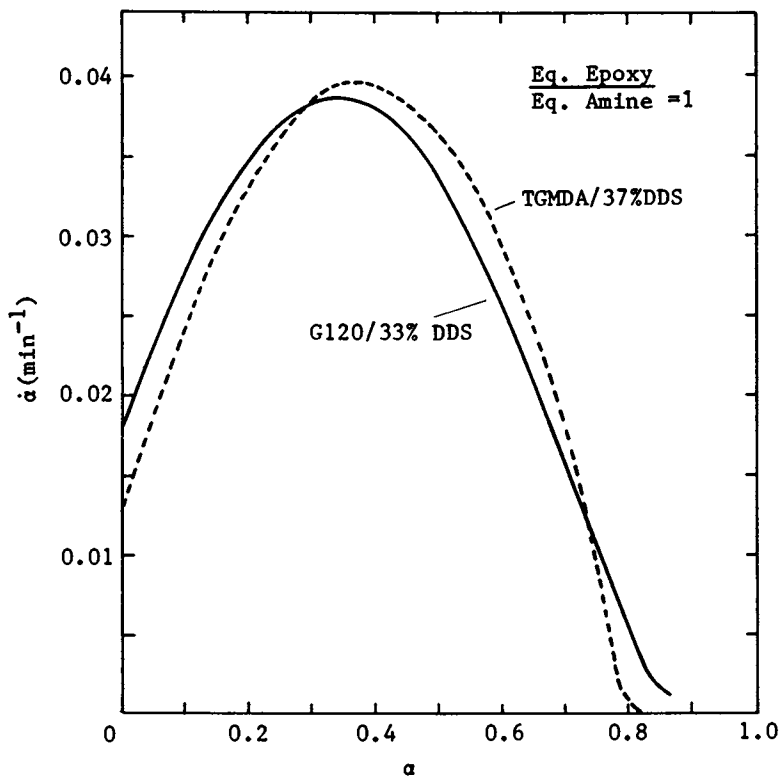


Figure 8. DSC Analysis of the G-120/DDS (33%) and TGMDA/DDS (37%) Reactions at 177°C.

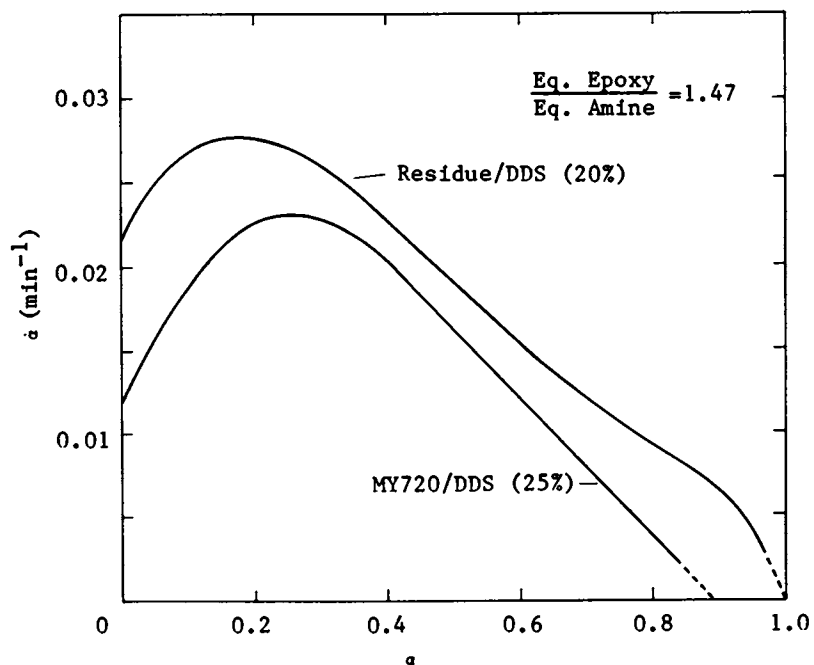


Figure 9. DSC Analysis of the MY720/DDS (25%) and Residue/DDS (20%) Reactions at 177°C.

Table IV. DSC Parameters for the Isothermal Cure of TGMDA Resin/DDS Formulations ( $\frac{\text{eq. epoxy}}{\text{eq. amine}} = 1.47$ ) at 177°C

Sample	$K_1$ ( $\text{min}^{-1}$ )	$\alpha_p$ ( $\text{min}^{-1}$ )	$\alpha_p$	$\alpha_{\text{final}}$
TGMDA/DDS (28.1%)	0.0075	0.0224	0.28	0.85
MY720/DDS (25%)	.0121	0.0233	0.25	0.89
Residue/DDS (20%)	.0218	0.0276	0.17	1.0

**Mechanical Testing.** Mechanical strength and stiffness parameters of the dried specimens before and after the post-cure treatment are compared in Table V. Variations in stoichiometry and impurity levels are achieved using different TGMDA resins and by varying the %DDS. Before post-curing, the extent of reaction  $\alpha$  of the TGMDA and MY720 specimens was determined by DSC to be approximately 0.75. The Residue specimen was found to be fully cured and therefore was not post-cured. Post-curing the TGMDA and MY720 specimens raised their  $\alpha$  values to ca. 0.95.

The variations in resin composition and the post-cure treatment do not affect the flexural strength. Except for the Residue specimen which has significantly enhanced tensile strength and flexure stiffness values, resin composition does not appear to have an effect on mechanical properties. Post-curing tends to improve the tensile and compressive strength and to decrease stiffness. There is a slight tendency for the Izod impact energy to increase as the epoxy/amine ratio is decreased (Table VI). Except for the Residue specimen, the samples are found to have similar glass transition temperatures  $T_g$  as determined by TPA. Post-curing raises the  $T_g$  values by 25–30°C and increases the initial rate at which the specimens absorb moisture. It cannot be ascertained from this data whether an increase in the epoxy/amine ratio or in the impurity level has the greatest effect on moisture uptake.

The increase in strength after post-cure can be attributed to the increase in crosslink density which occurs during the additional chemical reaction. The decrease in stiffness and the increase in moisture uptake rate may reflect the decrease in density which also tends to occur during post-cure. This density decrease is a result of post-cure being performed at a temperature which is above the onset of the glass transition in these materials. Since post-cure shifts the glass transition range to considerably higher temperatures, the coefficient of thermal expansion is greater during heating to the post-cure temperature than during subsequent cooling.

Table V. Comparison of Mechanical Testing Data

Specimen	Eq. Epoxy Eq. Amine	Flexure		Tension		Compression	
		Strength (psi)	Stiffness (ksi)	Strength (psi)	Stiffness (ksi)	Strength (psi)	Stiffness (ksi)
MY720/DDS(20%) dried post-cured	1.95	23,600	695	6120	1950	-	-
		21,000	653	7250	1260	-	-
TGMDA/DDS(25%) dried post-cured	1.72	22,000	667	6400	1480	28,100	287
		19,300	623	7060	1390	33,200	263
MY720/DDS(25%) dried post-cured	1.46	21,300	683	5450	2000	28,700	289
		24,600	650	5320	1690	34,200	269
Residue/DDS(25%) dried	1.11	22,400	810	11,100	1950	-	-

Table VI. Comparison of Izod Impact, TPA and Moisture Uptake Results

<u>Specimen</u>	<u>Eq. Epoxy</u> <u>Eq. Amine</u>	<u>Izod</u> <u>Energy</u> <u>(ft-lb/in)</u>	<u>Tg</u> <u>(°C)</u>	<u>Moisture Uptake 80°C</u> <u>after 6 wks Immer-</u> <u>sion (% increase)</u>
MY720/DDS(20%)	1.95			
dried		0.56	240	-
post cured		.58	270	-
TGMDA/DDS(25%)	1.72			
dried		0.58	250	4.28
post cured		.57	275	6.04
MY720/DDS(25%)	1.46			
dried		0.65	250	4.46
post cured		.61	275	5.82
Residue/DDS(25%)	1.11			
dried		0.65	220	6.86

Conclusions and Comments

Results obtained by the GPC and DSC studies are in excellent agreement. Correlations between GPC and DSC data provide a better understanding of epoxy resin cure behavior and are useful in assessing the effects of stoichiometry and impurities. Simple amine-to-epoxy addition is the predominant reaction between TGMDA and DDS during the early stages of cure. This reaction is adequately described by a third-order rate expression (Eq. 10). An equivalence between the exotherms for the epoxy-amine addition and the epoxy-epoxy polymerization reaction simplifies the interpretation of data and permits the direct comparison of TGMDA resins having quite different compositions. For TGMDA/DDS reactions, increasing the epoxy/amine equivalent ratio -

1. decreases the rate of reaction,
2. lowers  $\alpha_0$  and  $\alpha_{gel}$ ,
3. increases MW and the extent of cross-linking, and
4. leads to higher extents of reaction ( $\alpha_{final}$ ).

Impurities or reaction by-products -

1. increase the rate of reaction,
2. lowers  $\alpha_0$ , and
3. leads to higher extents of reaction ( $\alpha_{final}$ ).

Impurities in commercial TGMDA resins cured with DDS and changes in the epoxy/amine equivalent ratio (1.46-1.95) have no significant effects on the mechanical properties of the cured resin matrix. High impurity levels actually enhance tensile strength and flexural stiffness. Post-curing improves the tensile and compressive strengths and decreases the stiffness of the resin matrix. Additional work is underway to assess the effects of impurities on the mechanical properties of specimens having widely differing impurity levels but constant epoxy/amine ratios and to explore the effects of moisture on the mechanical properties of specimens prepared with purified TGMDA.

Acknowledgment

The authors gratefully acknowledge the assistance of Ms. Judith Brodtkin for helping with the GPC and infrared spectroscopy analyses, Mr. Seth Ghiorse for fabricating the test specimens, and Mr. William Houghton and Mr. Eli Pattie for running the mechanical property and testing experiments.

Literature Cited

1. Hagnauer, G. L. and Pearce, P. J. Org. Coat. & Appl. Polym. Sci. Proc., Am. Chem. Soc., 1982, 46, 580-584.
2. Jay, R. R. Anal. Chem., 1964, 36, 667.
3. Gupta, A. (Jet Propulsion Laboratory, Pasadena, CA), private communication.

RECEIVED May 19, 1983

**American Chemical  
Society Library  
1155 16th St. N. W.  
Washington, D. C. 20036**

## Kinetics of Acetylene-Terminated Resin Cure and Its Effects on Dynamic Mechanical Properties

I. J. GOLDFARB, C. Y-C. LEE, and C. C. KUO<sup>1</sup>

Materials Laboratory (AFWAL/MLBP), Air Force Wright Aeronautical Laboratories, Wright-Patterson Air Force Base, OH 45433

Kinetics of the cure of acetylene terminated resins can be obtained by differential scanning calorimetry (DSC) of the reaction exotherm and by disappearance of the ethynyl band in the infrared spectrum. Multiple scan DSC curves at various heating rates were utilized to obtain kinetic parameters for an acetylene terminated sulfone (ATS) which were compared with isothermal reaction rates. The comparison between scanning and isothermal reaction kinetics illustrated the retarding effect of incipient vitrification of the ATS on the reaction rate. Glass transition temperatures ( $T_g$ ) were determined for partially cured resins as a function of the extent of cure by dynamic mechanical analysis. This allowed the determination of the reduced parameter ( $T-T_g$ ) during cure of the resin under a variety of time-temperature profiles. The dynamic mechanical properties were then estimated as a function of ( $T-T_g$ ). This estimate is compared with the results of torsion impregnated cloth analysis of the curing of the ATS resin.

Recent advances in acetylene terminated resin technology have provided a family of new high performance structural materials (1,2). One member of this family, the acetylene terminated sulfone (ATS) (3) has been made available in sufficient quantities to allow research efforts on characterization and determination of the effects of structure on physical and mechanical properties (4-6). In a companion paper (7) the effects of environment on the cure of ATS was reported. This paper reports

<sup>1</sup> Current address: University of Dayton Research Institute, Dayton, OH 45469

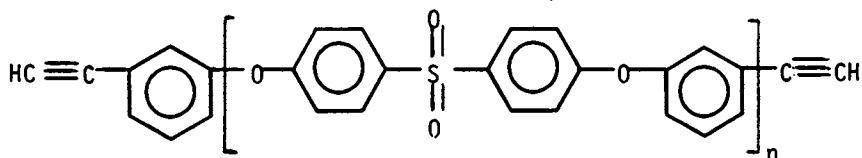


on the effects of the kinetics of the ATS cure and the resultant  $T_g$  on further cure.

## EXPERIMENTAL

### Material

The uncured resin used in this study has the basic structure



where the monomer ( $n=1$ ), 4,4'-bis(3-ethynylphenoxy)diphenyl sulfone, represents  $\sim 77\%$  of the resin. The other components are primarily  $n=0,2,3$  oligomers. An average value of  $n=1.23$  is computed based on heat of reaction compared to pure monomer.

### Extent of Cure

The extents of cure were determined utilizing DSC and FT-IR. DSC experiments were conducted on a Perkin-Elmer DSC-2 instrument. The method for obtaining kinetic parameters from scanning DSC has been described elsewhere (8). Isothermal extents of cure were determined by curing in the DSC for a predetermined time under nitrogen and then scanning at  $10^\circ\text{K}/\text{min}$  to determine the residual exothermic heat of reaction as compared with a scan of uncured resin.

Infrared measurements of extent of cure under conditions similar to the TICA experiments were conducted. ATS was cast from methylene chloride solution onto KBr windows and, after vacuum evaporation of all solvent, the KBr windows were put into the Rheometrics RMS environmental chamber and were subjected to a temperature profile under nitrogen identical to the mechanical measurement experiments ( $2^\circ\text{C}/\text{min}$ ). The windows were removed one at a time at various temperatures and IR spectra were taken at room temperature.

### TICA Experiments

The Torsion Impregnated Cloth Analysis (TICA) measurements utilized here were conducted under nitrogen with a Rheometrics Mechanical Spectrometer (RMS) according to the procedures described in the previous paper (7).

## RESULTS AND DISCUSSION

### Kinetics of ATS Cure

The kinetics of the cure of ATS at 130°C in nitrogen determined by various methods are shown in Figure 1. The dashed curve represents the prediction based on kinetic parameters determined by analysis of scanning DSC data by the method of multiple heating rates described previously (8). This method utilizes a rate equation of the form:

$$\frac{d\alpha}{dt} = Af(\alpha)e^{-E/RT} \quad (1)$$

where  $\alpha$  = degree of conversion and  $f(\alpha)$  is a rate functionality determined by the analysis at least in tabular form. To produce an isothermal curve,

$$g(\alpha) = \int_0^{\alpha} \frac{d\alpha'}{Af(\alpha')} = e^{-E/RT} \cdot t \quad (2)$$

$$\text{or } t = g(\alpha) \cdot e^{E/RT} \quad (3)$$

The function  $g(\alpha)$  of equation (3) is determined by numerically integrating  $1/Af(\alpha)$  vs  $\alpha$  and is tabulated along with  $Af(\alpha)$  during the computer analysis of the DSC data. Because of the scanning rates in the kinetic analysis (5,10,20,40 and 80°K/min) the predicted curve in Figure 1 is seen to effectively proceed to completion ( $\alpha=1$ ) even though 130°C is much below the  $T_g$  of the completely cured resin (366°C). This kinetic analysis is thus insensitive to the vitrification which we shall subsequently show does indeed occur during such a low temperature curing reaction. The solid curve is the actual 130°C isothermal reaction curve. The circles show measurements of  $\alpha$  determined by the disappearance of the acetylene IR band at 941  $\text{cm}^{-1}$  (6). The squares show the DSC residual heat measurements. It should be noted that a problem occurs in the analysis of the DSC data since another exotherm is observed in acetylene terminated sulfones at higher temperatures than the reaction exotherm but sufficiently low so as to overlap with the end of the reaction exotherm. The residual heat data were determined by estimating the contribution of the second exotherm and graphically subtracting it from the total heat evolved. While this approximate method produces considerable scatter in the data, it appears to agree quite well with the infrared data.

With this data the effect of incipient vitrification and subsequent loss of mobility is quite evident. The reaction was carried out for 89 hours to make sure that the reaction had

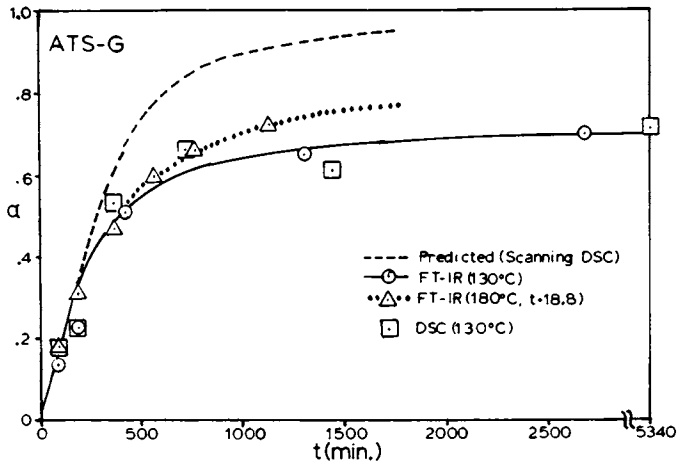


Figure 1. ATS isothermal curing curves at 130 °C in N<sub>2</sub>.

indeed ceased and a final conversion  $\alpha_{\infty}(130^{\circ}) \approx .72$  is observed. A similar isothermal reaction at  $180^{\circ}\text{C}$  can be plotted on the same graph by applying a time shift factor  $e^{-E/R(1/T_1-1/T_2)}$  which in this case equals 18.8 where  $T_1 = 403^{\circ}\text{K}$ ,  $T_2 = 453^{\circ}\text{K}$  and  $E = 21.3$  Kcal/mole. This is shown by the dotted line where the triangles represent the FT-IR conversion data (6). As would be expected the two curves superimpose at low extents of conversion but at higher conversions the  $180^{\circ}$  curve continues to rise beyond the  $130^{\circ}\text{C}$  curve to a final conversion,  $\alpha_{\infty}(180^{\circ}) \approx .80$ .

### Glass Transition Temperatures ( $T_g$ )

$T_g$  of ATS resin as a function of the extent of cure were determined utilizing the criterion of the maximum of the loss modulus in TICA experiments on the RMS at 1.6 Hz (10 rad/sec). Several methods were utilized to identify the  $T_g$  and  $\alpha$  values. The values along with the methods of measurements are given in Table I. Points No. 2,3,4,6, and 7 represent  $T_g$  as described in the previous paper (7) which are at low enough temperatures to be the instantaneous  $T_g$  for the reaction time given in the last column of Table I. By comparison with Figure 1, one obtains the value of  $\alpha$  for each time. Points No. 5 and 8 represent the time to reach a loss modulus maximum at  $130^{\circ}$  and  $180^{\circ}$  respectively. So once again  $\alpha$  can be obtained from the time from Figure 1. Points No. 1, 9, and 10 are from the scanning TICA curve and are the initial uncured  $T_g$ , the vitrification loss maximum and the final completely cured  $T_g$  respectively.

TABLE I  
ATS  $T_g$  as a Function of Conversion

No.	$T_g$ Value	Method of Measurement	Value	$\alpha$ Method of Measurement
1	38	$T_{g0}$ (n.r.)	0	no reaction assumed
2	68	$T_c$ (131 $\pm$ /56min)	.095	$t_{gel}(131^{\circ}\text{C})$ 56min
3	78	$T_c$ (131 $^{\circ}$ /1.5hr)	.160	$t_c=90$ min
4	118	$T_c$ (130 $^{\circ}$ /4.5hr)	.410	$t_c=270$ min
5	131	$b_{max}$ (131 $^{\circ}\text{C}$ )	.446	$t_c=340$ min
6	135	$T_c$ (131 $^{\circ}$ /6.2hr)	.480	$t_b=372$ min
7	158	$T_c$ (130 $^{\circ}$ /12hr)	.603	$t_c=720$ min
8	180	$b_{max}$ (180 $^{\circ}$ )	.674	$t_c=43.8$ min
9	205	$T_g$ (n.r.)	.770	from Fig. (4)
10	366	$T_g^{bmax}$ (n.r.)	1.000	reaction assumed comp.

The results of Table I are plotted in Figure 2. The points up to  $\alpha = 0.6$  fit on a straight line (least squares: slope =  $195.2^\circ$ , intercept =  $43.3^\circ$ , correlation coefficient = 0.996). Above  $\alpha = 0.7$  the  $T_g$  rises rapidly to the fully cured value of  $366^\circ\text{C}$ . This is in agreement with the proposal by Nielsen (9) that the  $T_g$  of crosslinked polymers is composed of two parts: a "copolymer" effect and a crosslinking effect. The "copolymer" effect in this case is just the disappearance of end groups as the reaction proceeds which, since each end group is assumed to contribute the same amount of free volume, should be linear with  $\alpha$ . Nielsen proposed a crosslinking effect that is inversely proportional to the molecular weight between crosslinks. Inasmuch as crosslink density does not build up until the latter stages of the reaction, the observed upswing of the curve in Figure 2 is consistent with Nielsen's proposed relationship.

Utilizing Figure 2, one can predict the final  $T_g$  for the isothermal reactions of Figure 1. Thus for the  $130^\circ\text{C}$  reaction where  $\alpha_\infty = .72$ ,  $T_g = 186^\circ$  and for the  $180^\circ\text{C}$  reaction where  $\alpha_\infty = .80$ ,  $T_g = 200^\circ$ .<sup>9</sup> The values of  $(T_g - T_g^{\text{cure}})$  are  $56^\circ$  and  $42^\circ$  respectively. Thus while it is evident that incipient vitrification does quench the reaction before its completion, the reaction proceeds well into the glassy state.

Having obtained  $T_g$  as a function of conversion and conversion as a function of time for different temperatures, it is possible to construct the time-temperature-transformation (TTT) diagram as described by Enns and Gillham (10). The results are shown in Figure 3. The circled points were obtained by interpolating for conversion for each temperature from Figure 2 and applying equation (3) to calculate the reaction time. The dotted line separating liquid from rubber regions was obtained by utilizing the value of  $\alpha = 0.095$  for the gel point (see Point No. 2 in Table I) and once again using equation (3) to calculate the reaction time. The resulting TTT diagram appears to accurately display all the features of the cure of ATS at least up to the vitrification.

### TICA Experiment

Figure 4 shows a temperature scan TICA of the ATS resin under nitrogen, conducted as described in the previous paper (7) utilizing glass cloth that did not evolve volatile material during the run. Three maxima occur in b, the loss modulus. The first, at  $38^\circ\text{C}$ , corresponds to  $T_g$ , the glass transition temperature of the unreacted oligomer. The second maximum occurs at  $205^\circ\text{C}$  and corresponds to vitrification during the curing reaction and the third maximum is assumed to be  $T_{g\infty}$ , the glass transition temperature of fully cured ATS. It should be noted that the scan down curves show a lower  $T_g$  than the scan up indicating that some degradation probably occurs at  $400^\circ\text{C}$ . Two

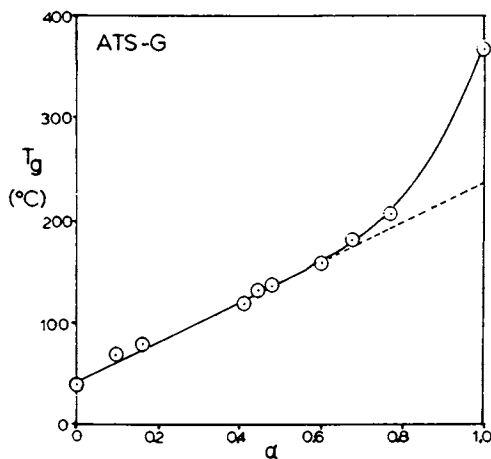


Figure 2. ATS  $T_g$  as a function of cure in  $N_2$ .

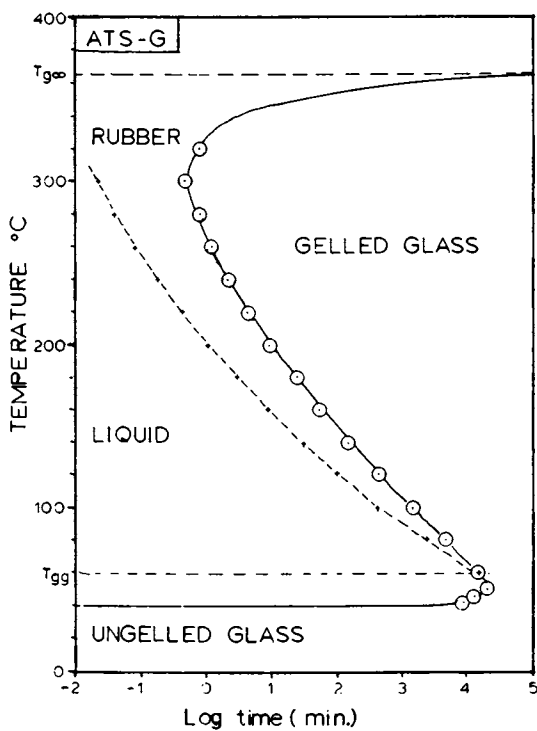


Figure 3. ATS time-temperature-transformation diagram for isothermal cures in  $N_2$ .

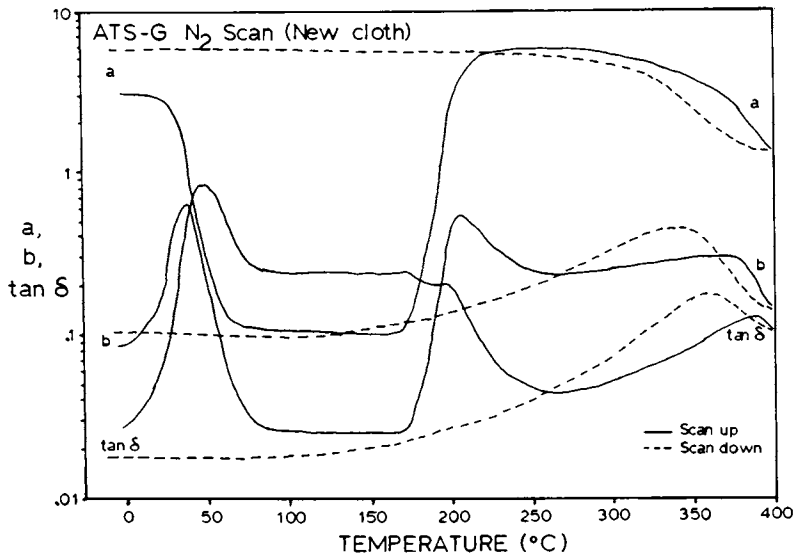


Figure 4. ATS TICA scan in N<sub>2</sub> at 2 °C/min.

other points are of interest in this TICA scan: the minima that occur between the  $T_g$ 's identified above. There is an obvious minimum of all three components at the same temperature indicating an R point where  $dT_g/dt = dT/dt$  as described previously (7). This occurs at  $\approx 285^\circ\text{C}$ . There should be another such minimum in the first part of the scan during the fluid melt phase of the reaction but it cannot be seen on a TICA scan due to its insensitivity at regions of low matrix resin modulus. Parallel plate measurements on the RMS under the same environmental conditions as the TICA scan indicate a minimum occurring at  $142^\circ\text{C}$ .

Figure 5 shows the extent of conversion as a function of time (and temperature) under the same conditions as the TICA scan by the disappearance of the normalized acetylene band at  $3300\text{ cm}^{-1}$ . The curve drawn through the experimental points was utilized to obtain values of  $\alpha$  at regular temperature intervals during the TICA scan. Instantaneous  $T_g$  values for each value of  $\alpha$  were obtained from Figure 2 and are plotted as the reduced parameter  $T - T_g$  in Figure 6. It should be noted that this curve successfully predicts the two R points described above as well as the vitrification, all at approximately the correct temperatures. It is thus apparent that Figure 6 is at least a self-consistent description of the TICA scan results.

In order to test the effects of vitrification upon the reaction rates, three temperatures from the TICA scan were chosen to compare experimental with predicted reaction rates. These results are shown in Table II.

TABLE II  
Predicted vs Experimental Reaction Rates

TEMP C°	$\alpha$	$d\alpha/dt(\text{pred})$ min. <sup>-1</sup>	$d\alpha/dt(\text{exp})$ min. <sup>-1</sup>	ratio
182	0.46	0.0395	0.0293	1.35
200	0.70	0.0732	0.0214	3.42
270	0.95	0.1124	0.0020	56.2

The temperatures 182, 200 and  $270^\circ\text{C}$  represent regions before, during and after vitrification respectively. The values of  $\alpha$  were obtained from Figure 5 as was the experimental reaction rate. The predicted reaction rate was obtained by substituting  $\alpha$  and  $T$  into equation (1). It is interesting that the reaction rate at  $250$ - $270^\circ\text{C}$ , where the temperature remains at more than  $40^\circ$  below the glass transition temperature, is approximately  $0.002\text{ min}^{-1}$ . The rate at this temperature and conversion from the DSC kinetic analysis would be  $0.112\text{ min}^{-1}$  or 56 times the actual rate. This indicates that the reaction rate at  $\approx 40^\circ$  below the  $T_g$  is slowed down by lack of mobility by over 50 times.



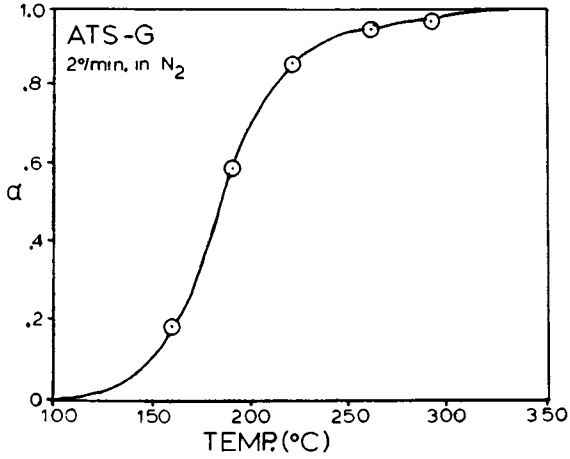


Figure 5. ATS degree of cure as a function of temperature at 2 °C/min in N<sub>2</sub> as determined by FT-IR.

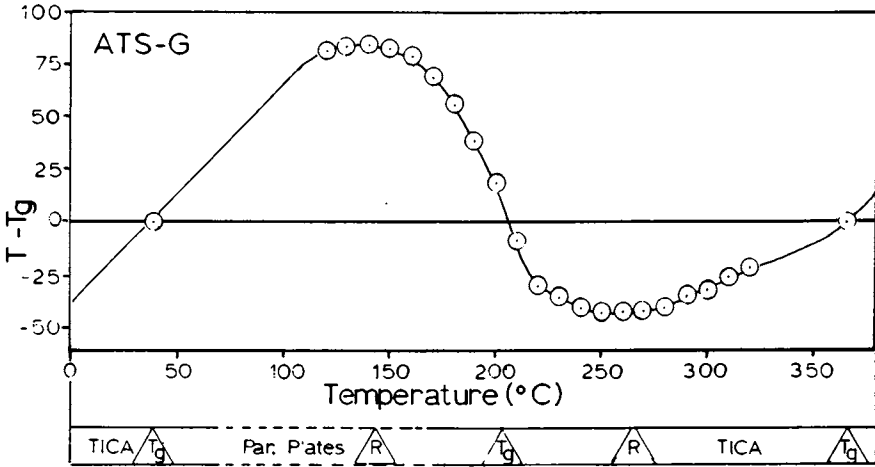


Figure 6. ATS (T-T<sub>g</sub>) as a function of temperature during a 2 °C/min scan in N<sub>2</sub>.

While this is a sizeable reduction, it is not near as severe a retardation as would be predicted by using the WLF equation to predict a retardation time.

#### Acknowledgments

One of us (IJG) gratefully acknowledges the hospitality, facilities and helpful discussion of the faculty and staff of the Polymer Science and Engineering Department, University of Massachusetts, while he was a visiting scientist.

#### Literature Cited

1. Kovar, R.; Ehlers, G. and Arnold, F. E. J. Polym. Sci., Chem. Ed. 1977, 15, 1981.
2. Hedberg, F. L. and Arnold, F. E. J. Appl. Polym. Sci., 1979, 24, 763.
3. Loughran, G. A.; Reinhardt, B. A.; Arnold, F. E. and Soloski, E. J. ACS Org. Coat. Plast. Prepr., 1980, 43, 777.
4. Leung, C. L. ACS Org. Coat. Plast. Chem. Prepr., 1982, 46, 322.
5. Kaelble, D. H. and Leung, C. ACS Org. Coat. Plast. Chem. Prepr., 1982, 45, 328.
6. Levy, R. L. and Lee, C. Y-C. ACS Polym. Prep., 1982, 23, (2), 181.
7. Lee, C. Y-C.; Kuo, C. C. and Goldfarb, I. J. ACS Org. Coat. Plast. Chem. Prepr., 1982, 47, 595.
8. Goldfarb, I. J. and Adams, W. W. ACS Org. Coat. Plast. Chem. Prepr. 1981, 45, 133.
9. Nielson, L. E., "Mechanical Properties of Polymers and Composites. Vol. I," Marcel Dekker, Inc., New York, 1974; p.23.
10. Enns, J. B. and Gillham, J. K. ACS Org. Coat. Plast. Chem. Prepr. 1982, 47, 575.

RECEIVED March 31, 1983

# Acetylene-Terminated Resin Cures

## Air and Nitrogen Effects

C. Y-C. LEE, C. C. KUO<sup>1</sup>, and I. J. GOLDFARB

Materials Laboratory (AFWAL/MLBP), Air Force Wright Aeronautical Laboratories, Wright-Patterson Air Force Base, OH 45433

Acetylene terminated resins exhibited different Torsion Impregnated Cloth Analysis behavior when they were scanned under nitrogen and air environments. A resin with a quinoxaline backbone structure showed good thermal stability under nitrogen environment at high temperature. However, under air environment at high temperature, additional crosslinking occurred, which appeared to further advance the glass transition temperature of the system. Samples that had been precured in air at low temperature showed lower glass transition temperature. Sulfone Resins cured in air and nitrogen showed different partially cured Tg, indicating different cure kinetics.

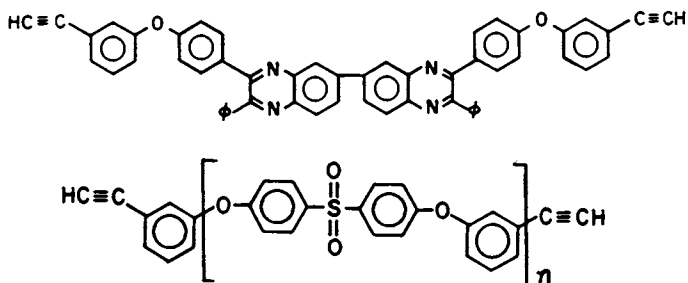
Acetylene terminated (AT) resins are being studied as a new technology to form the matrix of high performance structural composites (1). This class of resin cures by an addition reaction mechanism. Because of the absence of volatile by-product during cure, these resins are easy to process to yield void-free components. These resins also have the advantage over epoxy resins in terms of resistance to deterioration of properties at elevated temperature due to exposure to humid environments (2).

The end use properties of these resins are influenced by the cure cycle. Mechanical properties of the cured specimens showed difference when different curing environments were used (3).

This paper is to describe a series of Torsional Impregnated Cloth Analysis (TICA)(4) experiments where the dynamic mechanical behavior of the resin can be studied during the cure. The resins used in this study are the (3,3'([3-ethynylphenoxy]-phenyl)-2,2' diphenyl-6,6'biquinoxaline) (5,6) and the 4,4'-bis(3-ethynyl-

<sup>1</sup> Current address: University of Dayton Research Institute, Dayton, OH 45469

phenoxydiphenylsulfone) (7,8). These resins will be referred to as the quinoxaline resin and the sulfone resin in this paper; and their respective structures are as shown.



## EXPERIMENTAL

The quinoxaline resin was provided by F. Arnold of Materials Laboratory. The synthesis of this resin has been described elsewhere (5). The sulfone resin was synthesized by Gulf Research and Development Co. (9). This batch of resin is labelled as ATS-G.

The TICA specimen preparation procedure has been described elsewhere (4). The mechanical measurements were made with the Rheometrics Mechanical Spectrometer (RMS) which measures the in-phase and out-of-phase stress response (a and b component respectively) of a specimen being subjected to a sinusoidal shear strain. The instrumental set-up was reported by Lee (6). The frequency of the strain function was kept constant at 1.6 Hz (10 rad/sec). All temperature scan experiments were scanned at 2°C/min rate. The temperature was scanned down at the same rate when the maximum temperature was reached.

The precuring of the specimens were accomplished by using the RMS environmental chamber as the curing oven. Compressed air or vaporized liquid nitrogen was used as the convection medium.

## RESULTS AND DISCUSSION

A modified four-stage scheme (6) has been used to distinguish different rates of change of glass transition temperature during temperature scans of curing resins. These stages are defined as:

- I:  $dT_g/dt = 0$
- II:  $dT/dt > dT_g/dt > 0$
- III:  $dT_g/dt > dT/dt > 0$
- IV:  $dT_g/dt < 0$

R:  $dT_g/dt = dT/dt$ , where  $T_g$  is the glass transition temperature,  $T$  is the experimental temperature and  $t$  is time.

Stage I is when no reaction occurs during the scan. Stage II and III are when the glass transition temperature of the system increases as a result of additional curing. They are distinguished further by comparing with the experimental temperature increase rate. Stage IV is to account for instances where the glass transition temperature has actually decreased. The R point is called the rate conversion point. It is when the two rates are equal and is the transition point between Stage II and Stage III.

When an uncured resin is scanned by increasing temperature, it usually goes through different stages in the sequence I-II-III-II-I. At low temperature, there is no reaction occurring so the experiment starts out in Stage I. Then as the temperature is increased the reaction starts to occur. Initially the rate of glass transition temperature increase due to the reaction is slower than the temperature scanning rate. Therefore, the resin is in Stage II. At even higher temperature, the reaction will proceed at a faster rate and the glass transition temperature increases at a faster rate than the temperature scanning rate. The resin will then be in Stage III. One should notice the increase in viscosity with increasing temperature and eventually the resin will go through gelation and vitrification. As the reaction continues, the reactive groups concentration will eventually decrease and the glass transition temperature increase rate will slow down as a result. The resin will then proceed back to Stage II; and eventually to Stage I when the resin is fully cured.

#### THERMAL SCANS IN AIR/NITROGEN

Figure 1 shows the TICA scan results of the quinoxaline resins from 0°C up to 390°C. Figure 1a shows the scan under nitrogen environment and Figure 1b shows a similar scan in air. It is obvious that different behavior is exhibited by the same resin in the different environments. Similar scans of the sulfone resin are shown in Figure 2.

In all the scans, there is evidence of temporary softening of the TICA samples at around 200°C to 300°C. The softening behavior is the same between the two resins, but the behavior exhibited in air is distinctly different from that in nitrogen. It was later determined that volatiles coming off the glass cloth which was used as the substrate for these TICA experiments were the cause of this softening. This phenomenon is the subject of a current study but is not observed if the cloth is pretreated to remove the volatiles or another cloth is used. However, all the other transitions (b component maxima) are observed to occur at the same temperatures as shown in Figure 2. This means that the volatiles are not affecting the observation of the resin's behavior at other temperature ranges.

Figure 1 shows that the air and nitrogen environments do not change the vitrification temperature of the quinoxaline resin.

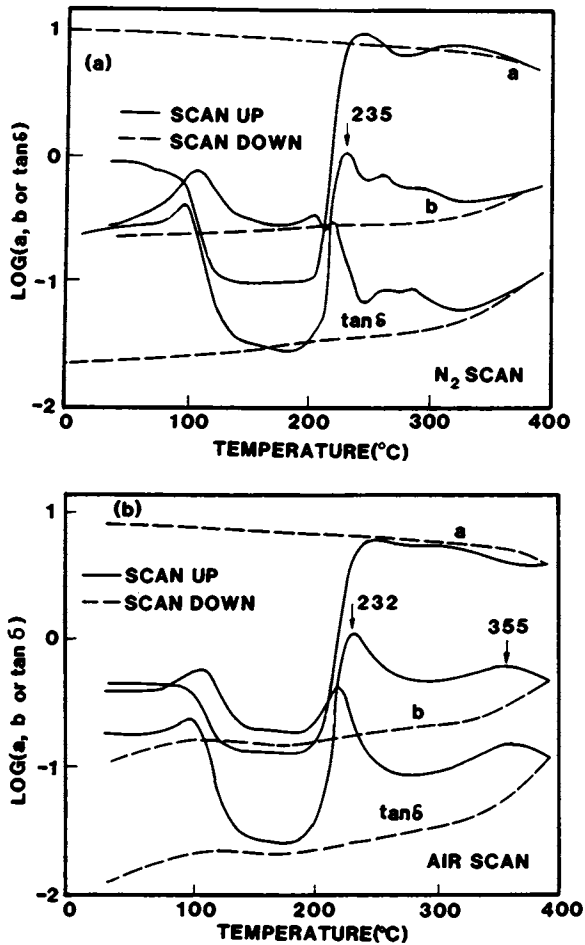


Figure 1. TICA temperature scan of the AT quinoxaline resin in (a) nitrogen environment; and in (b) air. The in-phase component is labelled as curve a, and the out-of-phase component as b.  $\tan \delta$  is the ratio of the two components (b/a).

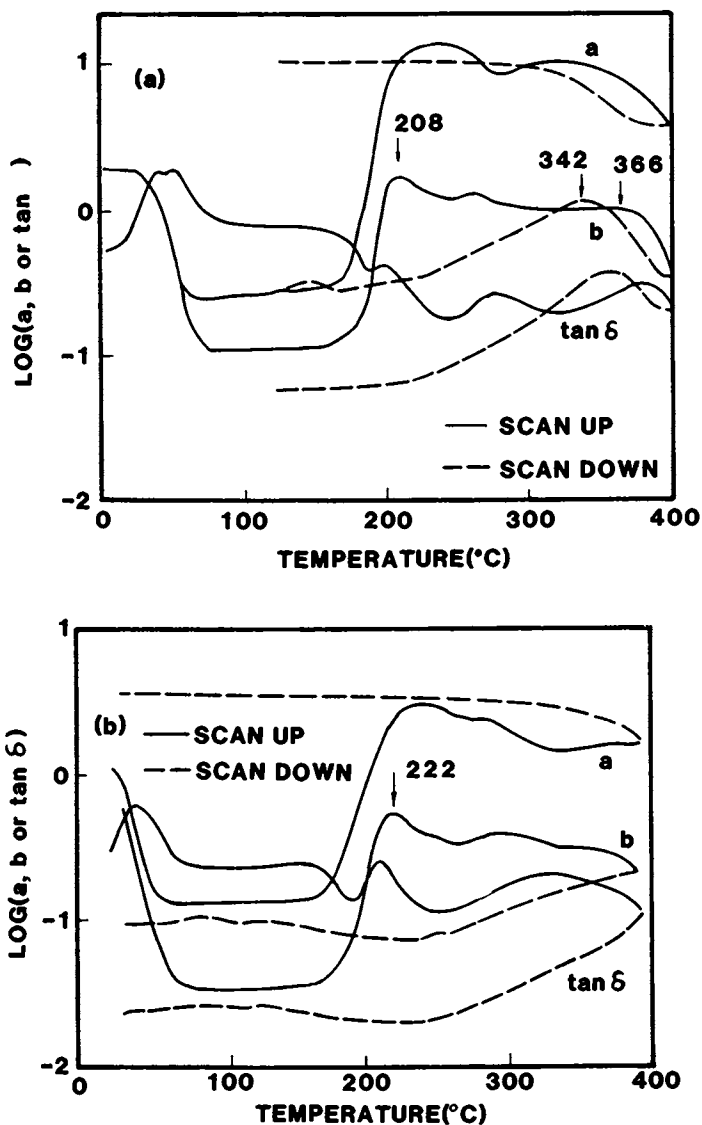


Figure 2. TICA temperature scan of the AT sulfone resin in (a) nitrogen environment; and in (b) air.

The nitrogen scan indicates a vitrification temperature of 235°C. The corresponding air scan yields a vitrification temperature of 232°C, well within the limit of experimental uncertainty. However, the curves in Figure 2 shows that while the nitrogen cure shows a vitrification temperature of the sulfone resin at 208°C; the corresponding air scan vitrification temperature is 222°C.

Because of the lower glass transition temperature of the precured sulfone resin, the viscosity of the reactive resin during the scan was low. This may have helped the diffusion of air through the sample, thus accentuating the difference between the air and nitrogen scan results.

The higher uncured T<sub>g</sub> of the quinoxaline resin requires a lower extent of reaction to reach the vitrification point during the scan. The cumulative effect at vitrification may not be sufficient to show different vitrification temperatures.

At high temperatures, the quinoxaline nitrogen scan indicates that the resin is in Stage II or even Stage I. However, the air scan appears to be in Stage III after about 370°C. This is because the quinoxaline is more stable under nitrogen environment at high temperature than in air. At high temperature under air, however, the quinoxaline resin shows oxidative crosslinking, the result of which is to increase the glass transition temperature, thus, the Stage III appearance. The temperature scan down results indicates that in both instances, the resins have T<sub>g</sub> values higher than the maximum scanning temperature used in the experiments.

The nitrogen scan of the sulfone resin indicates that there is a b maximum at about 366°C. However, on scanning down in temperature after reaching 390°C, this peak has been shifted to 342°C. This may mean that the sulfone resin is not thermally stable at high temperature. The degradation of the cured resin shifts the glass transition to a lower temperature (Stage IV effect). The air scan shows the Stage III effect at high temperature just like the quinoxaline resin. The scan down similarly indicate that the glass transition is above the maximum scanning temperature. This does not necessarily mean that degradation does not occur in air. It may merely indicate that the oxidative crosslinking masks out the degradation.

Another plausible explanation of the Stage IV effect is a high temperature reaction or molecular rearrangement that causes a decrease in glass transition temperature.

#### ISOTHERMAL CURE

Figure 3 shows the result of a TICA experiment during an isothermal cure at 170°C. The rise in the rigidity of the resin (a component) during the cure is accompanied by a peak of the loss component (b component). The time required to reach the b maximum, labelled as t<sub>b</sub> in Figure 3, is the time required for the sample to cure to a T<sub>g</sub> equal to the curing temperature.



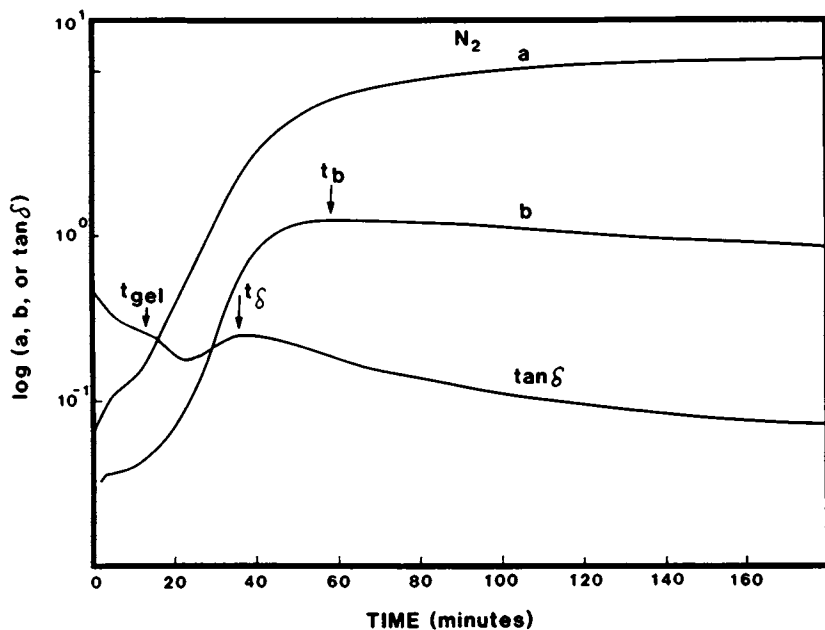


Figure 3. Isothermal cure results of the sulfone resin at 170 °C. The time  $t_b$  is the time where the resin had a glass transition temperature equal to the cure temperature.

Comparison of these vitrification times will show the differences in curing kinetics.

Figure 4 shows the quinoxaline vitrification time as a function of cure temperature. The difference between the air and nitrogen data is small, and can be explained by the different temperature increase profiles to reach the experimental temperature in these two types of experiments (6), where either room temperature compressed air or vaporized liquid nitrogen was used as the convection medium. The insignificant difference observed is because of the short times required to reach these vitrification points; so the cumulative effect is not sufficient to show a substantial air curing effect. Figure 5 shows the results from the sulfone resin. At low temperature, the time required to reach the vitrification point is long. It is clear from Figure 5 that curing in air will require longer time to reach the same  $T_g$ . At higher temperature, however, the same explanation offered for the quinoxaline results can be applied; and the air/nitrogen effect on the vitrification times diminishes.

#### SCANS OF PRECURED SPECIMENS

Precuring the TICA specimens of these resins in either air or nitrogen environments and subsequently scanning these in nitrogen will reveal different behavior. Figure 6 and Figure 7 show the TICA scans in nitrogen of the sulfone specimens that had been cured in nitrogen and air respectively for 4½ hours at 131°C. The nitrogen cured specimen had a glass transition temperature of 119°C. The air cured specimen showed a lower transition temperature at 96°C. The difference in  $T_g$  due to the precuring is in agreement with the observation in the isothermal curing experiments.

The rate conversion point of the nitrogen cured specimen is higher than the air cured specimen (160°C vs 141°C). This is expected since the nitrogen cured specimen had a higher  $T_g$  before the experiment, thereby raising the viscosity level of the specimen at a given temperature, and influencing the rate of additional cure during the scan. Eventually, the cumulative additional cure will cancel the difference in  $T_g$  due to precuring. The results show both specimens to revitrify at 192°C.

When the partially cured glass transition temperature of a specimen is high, the subsequent scan of this specimen may not reveal a glass transition temperature because it will be masked by the additional cure. In such instances, the first b component peak observed during the scan will be the rate conversion point. Such is the case in the data shown in Figures 8 and 9, which are the temperature scan results of the sulfone specimens after they were cured in nitrogen and air environments respectively at 170°C for 4½ hours. The additional cure causes the rate conversion point of these two specimens to occur at the same temperature (around 200°C). Comparing the decrease in magnitude of the a

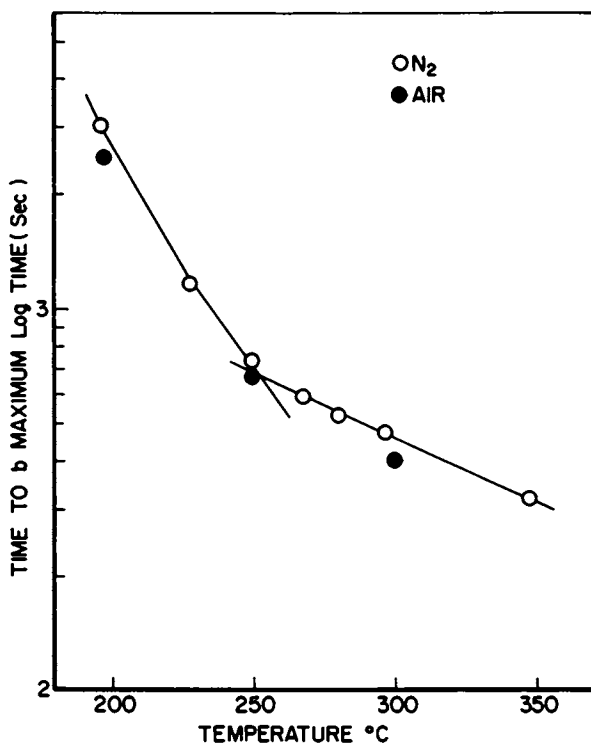


Figure 4. Time to vitrification of the quinoxaline resin as a function of temperature.

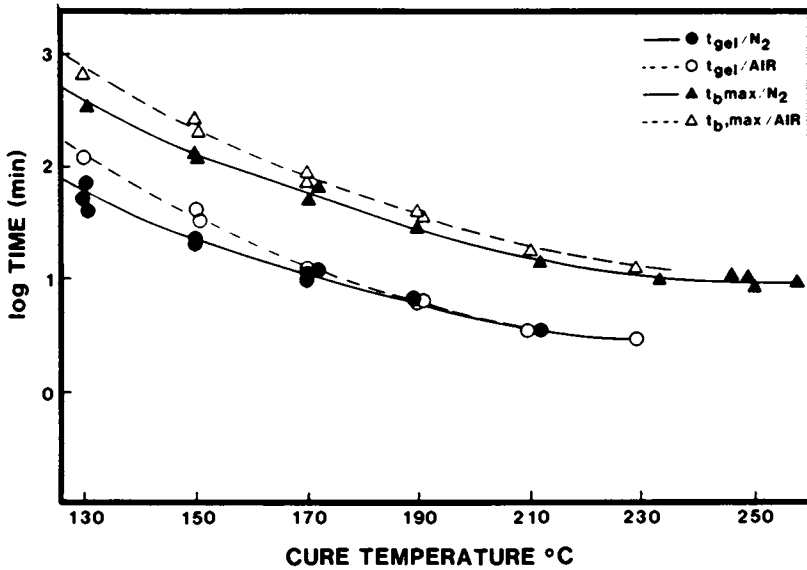


Figure 5. Time to vitrification of the sulfone resin as a function of temperature.

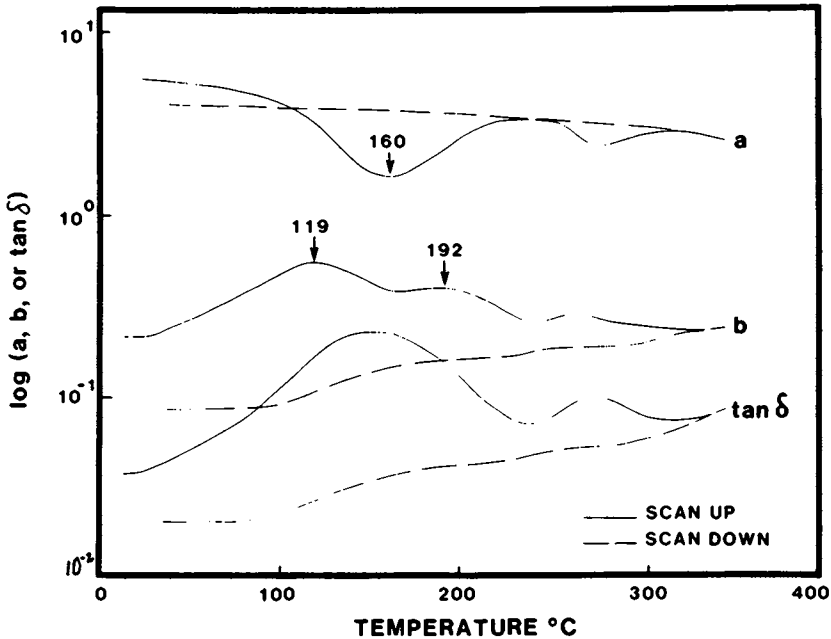


Figure 6. Temperature scan of the sulfone resin after curing in nitrogen at 131 °C for 4½ hours. The temperature was scanned down when a maximum temperature of 350 °C was reached.

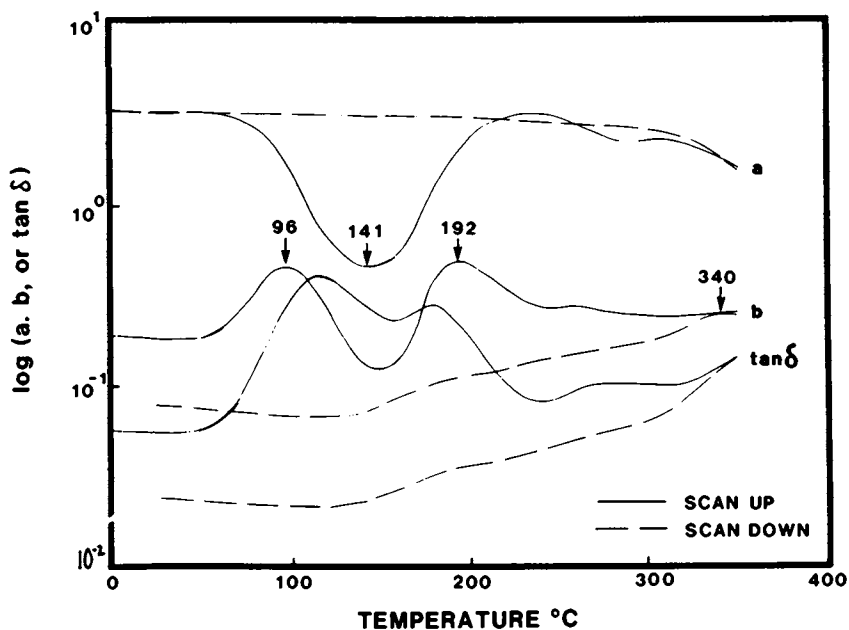


Figure 7. Temperature scan of the sulfone resin after curing at 131 °C in air for 4½ hours. Both the scan-up and scan-down curves are shown.

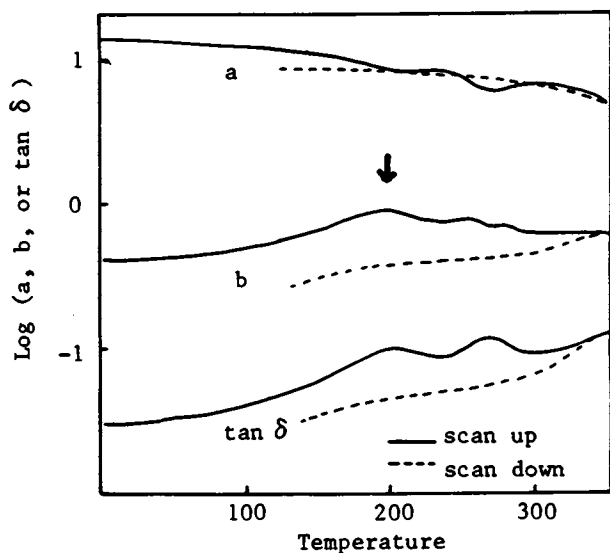


Figure 8. Temperature scan of the sulfone resin after curing in nitrogen at 170 °C for 4½ hours. The arrow indicates the temperature of T<sub>c</sub> due to the precuring.

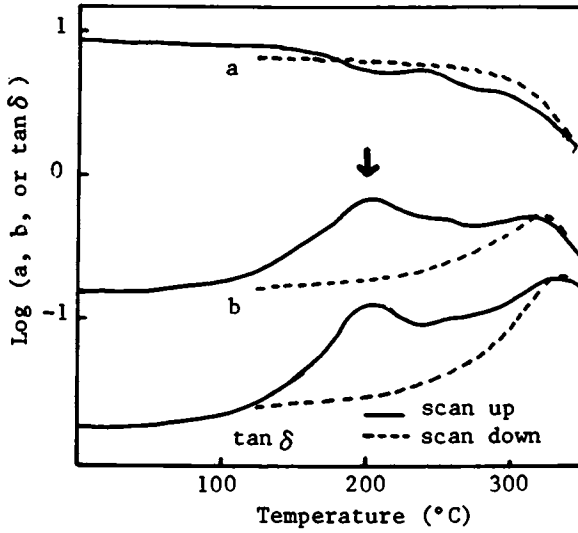


Figure 9. Temperature scan of the sulfone resin after curing in air at 170 °C for 4½ hours. The arrow indicates the temperature of  $T_c$  due to the precuring.

components in these two figures, it is clear that the air cured specimen was closer to the glass transition temperature when the rate conversion point occurred. This indicates that the air cured specimen had a lower glass transition temperature as a result of the precuring.

Since the first b component peak during the subsequent nitrogen scan can either be the glass transition temperature resulting from the precuring condition, or the rate conversion point from the additional cure during the scan, it is arbitrarily labelled as T<sub>c</sub> to cover both possibilities. Because of the higher glass transition temperature of the uncured quinoxaline resin, only the latter type of T<sub>c</sub> has been observed. Figures 10 and 11 show the scan results of the quinoxaline specimens that have been cured in nitrogen and air for 1 hour at 200°C. Again, the temperature of the rate conversion points are very close, but the traces indicated that the air cured specimen has a lower T<sub>g</sub> when the rate conversion occurs.

Two conclusions can be drawn from the air and nitrogen effects on the times to vitrification and the observed T<sub>c</sub>. Firstly, increasing cure time will increase the difference between the air and nitrogen cured specimens. Secondly, when the glass transition temperatures resulting from the cure are high, the difference in the observed T<sub>c</sub> values during the scan will decrease. These conclusions are further illustrated by Figures 12 and 13. Figure 12 shows the plot of T<sub>c</sub> as a function of cure time at 131°C. The difference in T<sub>c</sub> between the air cured and nitrogen cured specimens increases with increasing cure time. Figure 13 shows the T<sub>c</sub> values as a function of the cure temperature. All specimens were cured for a period of 4½ hours. The difference decreases with higher cure temperature.

There is a third factor that can influence the observed T<sub>c</sub> difference, that is, the quenching of the reaction rate due to the vitrification process. This is shown in Figure 14, which shows the T<sub>c</sub> values as a function of cure time at 183°C. At short cure times, the glass transition temperature of the system is lower than the cure temperature; i.e. the specimens have not yet vitrified. Increasing cure times shows an increasing difference in the air and nitrogen cured T<sub>c</sub> values. The nitrogen cured specimen reaches vitrification first; and its reaction rate is quenched as a consequence. The air cured specimen with comparable cure time, however, is still curing above its glass transition temperature. The difference in T<sub>c</sub> begins to decrease. Finally, both specimens' reaction rate is quenched by the vitrification process. It is possible that at the long cure time limit, both types of specimens will reach the same limiting T<sub>c</sub> values.

Figure 10 and Figure 11 also show that, as a result of the precuring in nitrogen and air, the final T<sub>g</sub>s, as indicated by the high temperature b maxima, are different. The scan down result

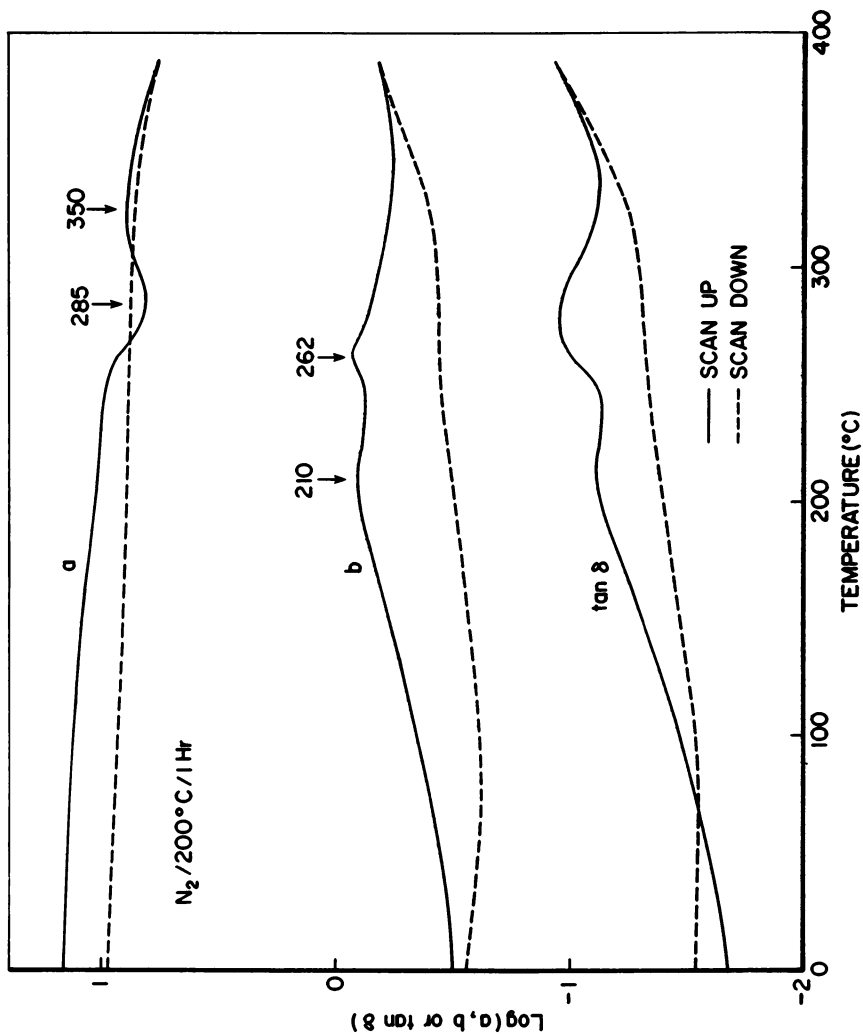


Figure 10. Temperature scan of the quinoxaline resin after curing in nitrogen at 200 °C for 1 hour. The scan down curves show the final  $T_g$  is above the experimental temperature (390 °C).



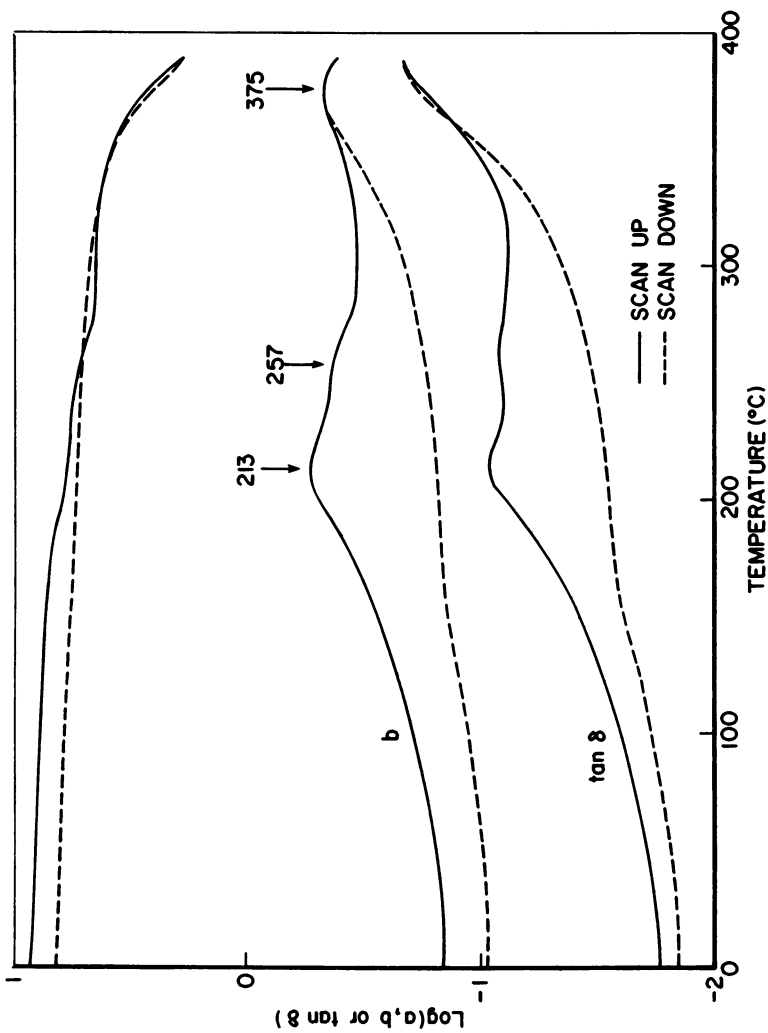


Figure 11. Temperature scan of the quinoxaline resin after curing in air at 200 °C for 1 hour. As a result of the precuring in air, the final  $T_g$  was lowered to 375 °C.

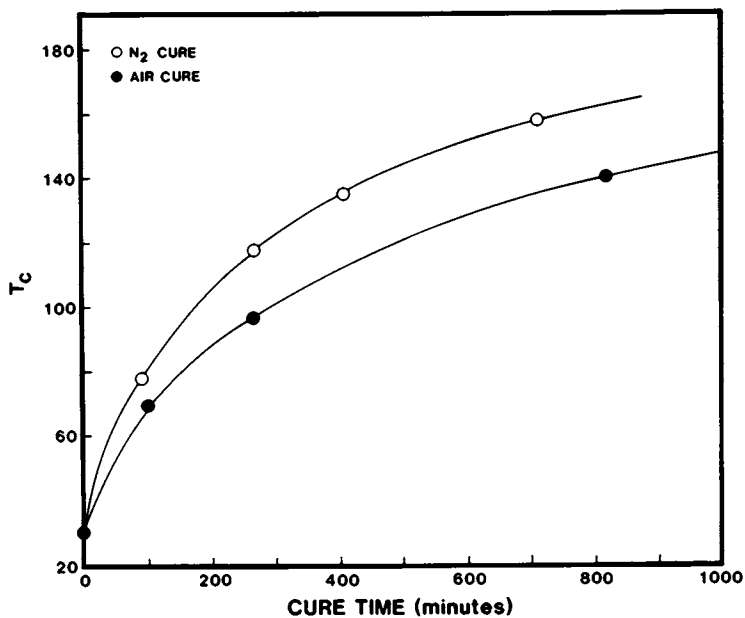


Figure 12. Plot of  $T_c$  vs. cure time of the sulfone resin isothermally cured at 131 °C.

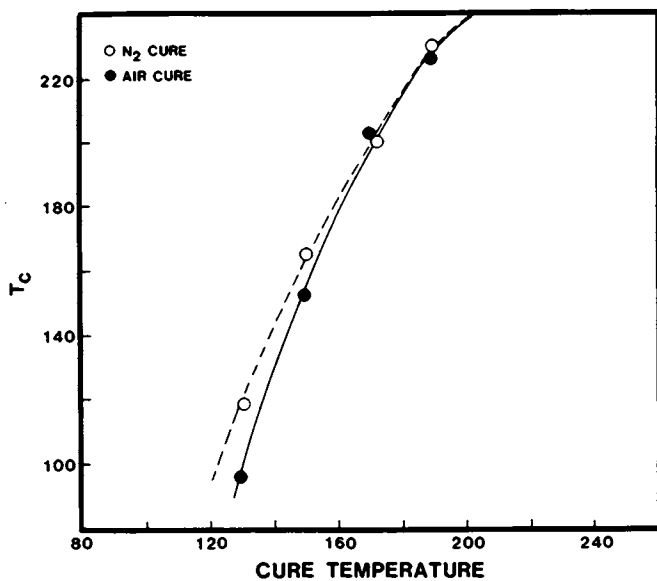


Figure 13. Plot of  $T_c$  of the sulfone resin at different cure temperature. All specimens had been cured for 4½ hours.

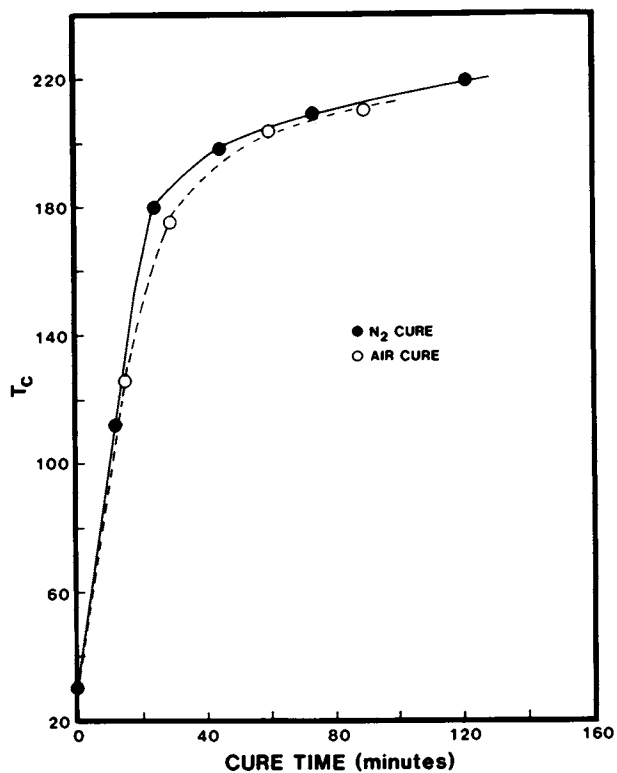


Figure 14.  $T_c$  of the sulfone resin isothermally cured at 183 °C.

of the nitrogen cured specimen (Figure 10) shows the final Tg of this specimen to be above 390°C. The air cured specimen shows a final Tg of 375°C (Figure 11). All quinoxaline specimens that were cured in nitrogen had fully cured Tgs above 390°C. Those that were cured in air resulted in lower Tg's. Figure 15 and Figure 16 show that, with increasing cure time and temperature in air, the final Tg decreases.

#### HIGH TEMPERATURE STABILITY

In the discussion of Figure 1, it was noted that oxidative crosslinking can increase the glass transition temperature of the specimen. This point is illustrated by the results shown in Figure 17. A specimen that had been cured in air and showed a final Tg of 360°C during the subsequent temperature scan in nitrogen was subjected to heat treatment at 380°C under nitrogen. The specimen was then rescanned in nitrogen and the result is shown in Figure 17 as solid lines. The glass transition temperature remains unchanged at 360°C. However, when the same specimen was subjected to the same heat treatment in air, the subsequent temperature scan in nitrogen revealed that the glass transition temperature had been advanced to above 390°C.

#### CONCLUSION

This work has shown that AT resins exhibit different dynamic mechanical behavior when they are cured in air or nitrogen. Curing in air will lower the fully cured Tg of the resins, and also decrease the curing kinetics. It is possible that oxygen inhibits the radical initiated chain propagation step, causing the cure kinetics to decrease and altering the final network topology to give a lower glass transition temperature matrix. FTIR studies of the quinoxaline resin cured in air showed the possible formation of carbonyl groups in the beginning of the cure (10), suggesting that oxygen was incorporated in the reaction.

It was also shown that AT resins under went oxidative crosslinking at high temperature. At this point, however, it is not clear whether the backbone of the resin or the reaction product of the acetylene is responsible for such a reaction.

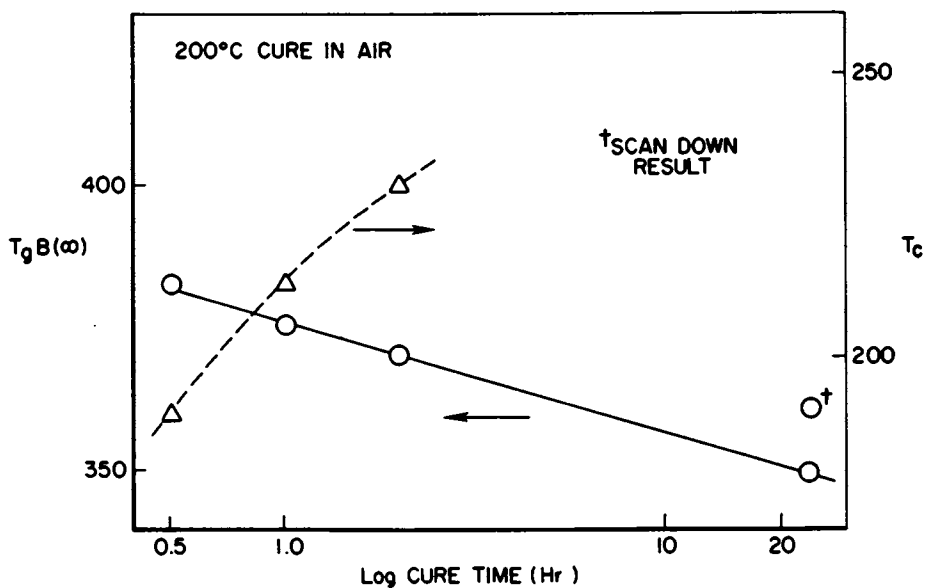


Figure 15. Final  $T_g$  of the quinoxaline resin as a function of cure time (in air).

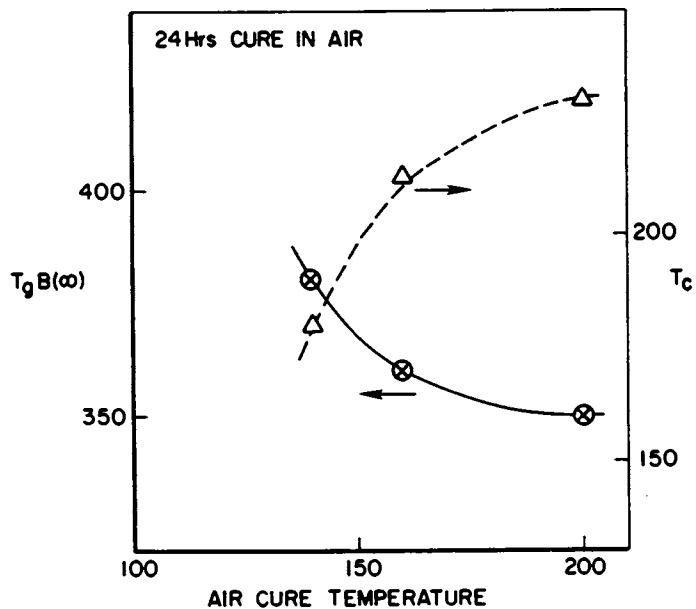


Figure 16. Final  $T_g$  of the quinoxaline resin as a function of cure temperature (in air).

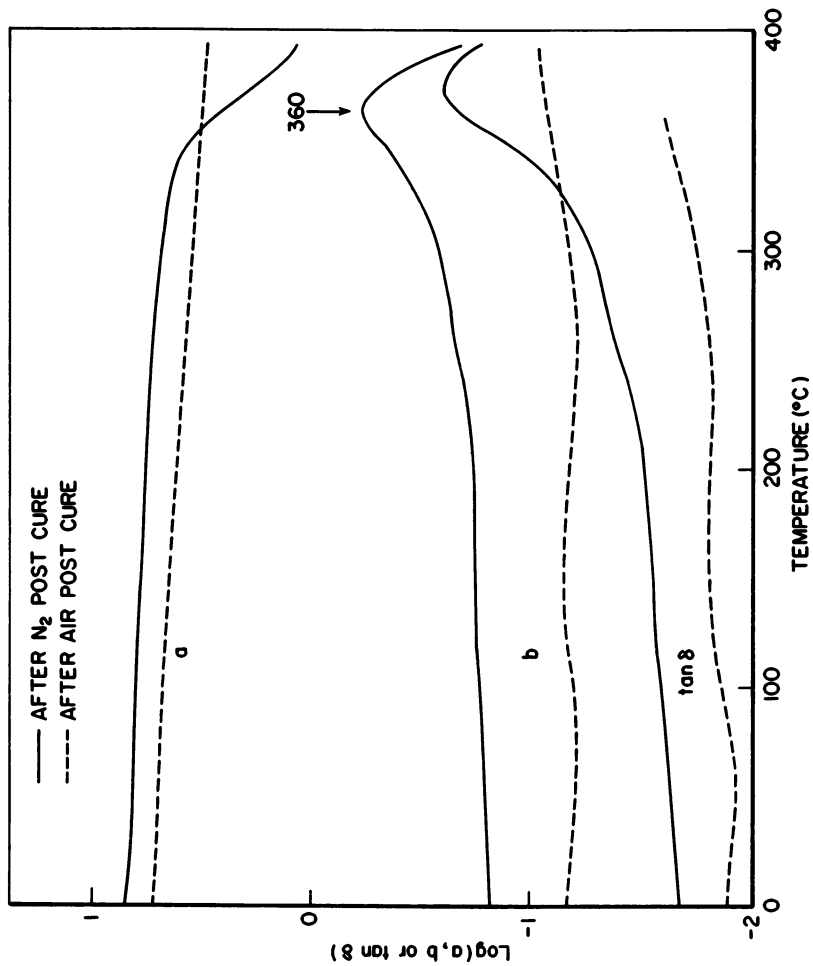


Figure 17. Temperature scan of the quinoxaline resin after exposing to nitrogen and air at 380 °C. After post curing in nitrogen, the glass transition temperature remained unchanged. However, after curing in air, there was no observable  $T_g$ .

Literature Cited

1. Kovar, R.; Ehlers, G.; and Arnold, F. E. J. Polym. Sci., Polym. Chem. Ed. **15**, 1081 (1977).
2. Browning, C. E.; Wereta, A.; Hartness, J. T. and Kovar, R. F. SAMPE Series, **21**, 83 (1976).
3. Lee, C. Y-C.; Kuo, C. C. and Lee, N. C. Air Force Technical Report, AFWAL-TR-4098.
4. Lee, C. Y-C. and Goldfarb, I. J. Polym. Eng. Sci., **21**, 390 (1981).
5. Hedberg, F. L. and Arnold, F. E. J. Appl. Polym. Sci., **24**, 763 (1979).
6. Lee, C. Y-C. J. Appl. Polym. Sci., **27**, 407 (1982).
7. Soloski, E. J.; Loughran, G. A.; Reinhardt, B. A. and Arnold, F. E. ACS ORPL Preprints, **43**, (2), 777 (1980).
8. Kuo, C. C. and Lee, C. Y-C. Air Force Technical Report, AFWAL-TR-82-4037.
9. J. J. Harrison and C. M. Selwitz, AFML-TR-79-4183.
10. Lee, C. Y-C., unpublished results.

RECEIVED May 11, 1983

# Mechanism and Kinetics of the Curing Process in a Resin System

J. MOACANIN, M. CIZMECIOGLU, S. D. HONG, and A. GUPTA

Applied Mechanics Division, Jet Propulsion Laboratory, California Institute of Technology, Pasadena, CA 91109

The starting point in course of development of a network model of a thermoset is the reactivity relationships which control the curing reactions at any stage of conversion. We have investigated the cure kinetics of the title resin using differential scanning calorimetry and FT-IR spectroscopy, in order to obtain a correlation between the total conversion as monitored by differential scanning calorimetry, with the rates of formation and disappearance of specific functionalities, as monitored by FT-IR spectroscopy. Reaction rates measured under isothermal conditions at two temperatures yielded preliminary estimates of the principal reaction rates in this system within the experimental temperature range as well as heats (enthalpies) of reaction for each reaction.

Previous investigations of the cure kinetics in this system have either emphasized the changes in physical properties such as loss modulus and viscosity of the medium or chemical properties such as the concentration of epoxide or amine functionalities at various stages of cure. (1-7) In several earlier reports, we attempted to derive an overall mechanistic picture for this system which would recognize constraints due to both changing reactivity as well as increasing viscosity. (8-10)

## Experimental

Materials A commercial grade of tetraglycidyl diaminodiphenyl methane (TGDDM), namely MY720 supplied by Ciba Geigy was used as received. Diaminodiphenyl sulfone (DDS) was recrystallized twice to form off-white needles.

N,N'-dimethyldiphenyl sulfone (DMDDS) was synthesized as follows:  
31.7 g (0.1 mole) of 4,4'-dichlorodiphenyl sulfone; 62 ml of 60% aqueous methyl amine, and 5 g of  $\text{Cu}_2\text{Cl}_2$  were heated at

0097-6156/83/0227-0083\$06.00/0

© 1983 American Chemical Society



220°C for 24 hours in a high pressure bomb. The reaction product was then dissolved in boiling ethanol, treated with charcoal and filtered through celite. The product was isolated from the ethanol solution after cooling overnight at -10°C and recrystallized from ethanol one more time. The yield was 52% and the product has a melting point at 173°C. The results of the elemental analysis, as determined experimentally, are: %C -61.00, %H -5.85, %N -10.21 and %S -11.80.

N,N' tetramethyldiphenyl sulfone (TMDDS) was synthesized as follows:

In a 2-l three-necked flask fitted with a stirrer, thermometer, and a dropping funnel were placed 12.5 g (0.05 mole) of powdered 4,4'-diamino-diphenylsulfone, of sodium bicarbonate in 25 ml of water. The temperature was maintained at 20°C using an ice bath while 32 ml (0.34 mole) of dimethyl sulfate was added with stirring over a 30-50 50-minute.

When the addition of dimethyl sulfate is complete, stirring was continued for 1 hour at 20-25°C. Then the temperature was raised to 60-65° during 10 minutes and was kept at this value until the evolution of carbon dioxide ceased. After the addition of 25 ml of cold water, the reaction flask was cooled rapidly in an ice bath and 10 ml of ethanolamine was added. The resultant crystalline slurry was removed from the flask and the apparatus was rearranged using a distilling condenser, receiving flask, and a heating bath. To the reaction flask was added 30 ml of ethanolamine, and it is heated to 140°C with stirring. The slurry above is added in small portions over a 40- to 50-minute period. When heating bath is maintained at 230-240°, the addition slurry provides an inner temperature at 120-140° as the water distills. After the addition is complete, the dropping funnel is rinsed with 15 ml of water. As soon as the temperature has reached 160°C, 15 ml of ethanolamine is added and the temperature is maintained at 160-170° for 20 minutes. Water (25 ml) is added through the funnel at an inner temperature of 120-140° and heating is continued until the water is distilled off.

The flask is then cooled and the reaction mixture diluted with 100 ml of water. The product after filtration is washed several times with water and dried in vacuum. After drying, the product is reprecipitated from hot methanol (50 ml) and finally recrystallized from o-dichlorobenzene. Yield: 8 g (54%), m.p. 249-251°C Elemental analysis for  $C_{16}H_{20}N_2SO_2$ ; Theory: %C -63.12; %H -6.62; %N -9.20; %S -10.53; Found: %C -63.02; %H -6.64; %N -9.20; %S -10.69

Differential Scanning Calorimetry (DSC) A mixture of MY720 and DDS (containing 22 weight percent of DDS) was prepared at 120°C under high purity N<sub>2</sub>. This mixture was cured isothermally at 177°C (350°F) under a positive pressure of N<sub>2</sub> gas. The oven temperature was controlled by a thermocouple placed inside a metal plate on which samples were placed. The temperature of the plate was 177° ± 2°C. Samples were withdrawn at ten times intervals ranging from 10 minutes to 210 minutes (3 1/2 hrs.) and analyzed by differential scanning calorimetry in dynamic mode, scanned at 10°C per minute. Table I gives the thermal parameters such as the temperatures at which exotherms begin and at which they are maximum, as well as the total heat evolved per unit mass

TABLE I. DSC Results for MY720/DDS Samples Cured at 177°C

CURE TIME	T <sub>i</sub> ,(°C) <sup>1</sup>	T <sub>p</sub> ,(°C) <sup>2</sup>	T <sub>f</sub> ,(°C) <sup>3</sup>	ΔH,(J/g) <sup>4</sup>	ΔH,(Cal/g) <sup>4</sup>
(CONTROL)	160	267	280	505	120.6
10 min.	160	266.0	280	280	67.0
20 min.	160	265.0	280	194	46.3
30 min.	160	264.5	280	125	30.0
45 min.	160	263.5	280	100	24.0
1 hour	160	265.0	280	69	16.5
1 1/2 hours	180	263.0	280	63	15.0
2 hours	190	260.0	280	53	12.7
2 1/2 hours	200	260.0	276	52	12.4
3 hours	200	261.0	276	40	9.5
3 1/2 hours	210	258.0	276	35	8.4

1. T<sub>i</sub> = Onset temperature of exotherm; 2. T<sub>p</sub> = Peak temperature of exotherms; 3. T<sub>f</sub> = Final Temperature of exotherm; 4. ΔH = Total area under the exotherm.

of the sample. These measurements indicate that complete cure is never achieved at 177°C. The plot of conversion as measured by the decrease in the area of the exotherm recorded on the above described samples relative to a control sample vs. the isothermal curing time is shown in Figure 1.

Mixtures of MY720, DDS and DMDDS were prepared as shown in Table II. They were all mixed at the same temperature and DSC thermograms were recorded at various scanning rates. Figure 2 shows typical thermograms recorded for mixtures containing either DDS or DMDDS. Table II also gives parameters derived from the

TABLE II. DSC Results of Mixtures of MY720 with DDS and DMDDS

Sample No.	MY720 (g)	DDS (g)	DMDDS (g)	Scan Rate °C/min	Peak Temp. $T_p$ , °C	$\Delta H$ J/g
1	100	28	--	5	254	699
				10	264	597
				20	285	643
				40	310	644
2	100	25.	22.8	10	270	556
				20	290	567
3	100	21	7	10	276	558
				20	292	589
4	100	14	14	10	281	575
				20	300	564
5	100	7	21	10	286	549
				20	304	563
6	100	--	28	2.5	262	479
				5	276	465
				10	291	575
				20	310	510
				40	328	400

DSC data. It is apparent that the heat evolved per unit mass reaction is approximately the same for the primary amine and the secondary amine, after a correction is made for the higher molecular weight of DMDDS relative to DDS.

Isothermal cure was also carried out at  $153^\circ \pm 2^\circ\text{C}$  using the same batch of MY720 and DDS and the same equipment and procedure as for cure at  $177^\circ\text{C}$ , except that the initial mixing was carried out at  $110^\circ\text{C}$ . Table III gives the DSC results obtained on partially cured samples, as a function of cure time.



Figure 1. Plot of conversion vs. curing time for samples isothermally cured at 177°C, as determined from dynamic DSC analysis; scan rate = 10°C/min.

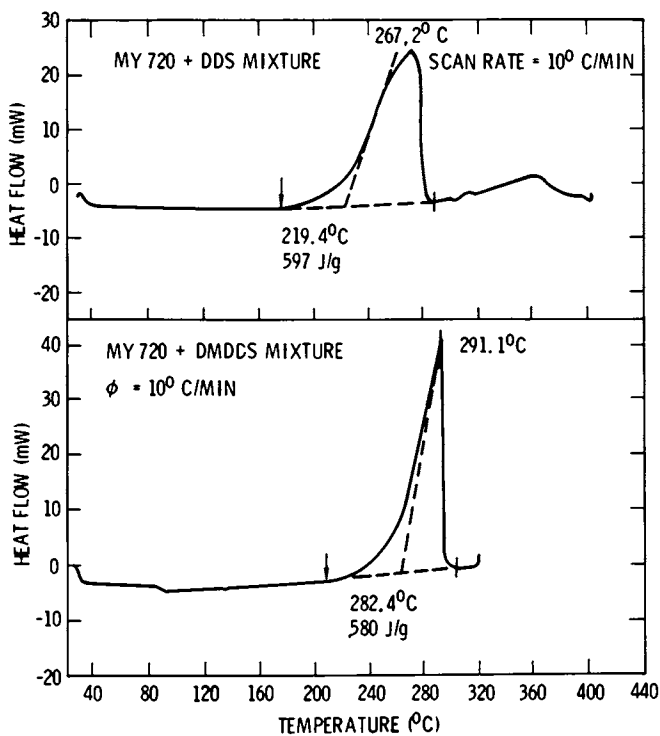


Figure 2. Typical dynamic DSC thermograms on MY720-DDS and MY720-DMDDS mixtures.

TABLE III. DSC Results on MY720/DDS Samples Cured at 153°C

Sample No.	Time of Isothermal Cure, Min.	T <sub>1</sub> , °C	T <sub>p</sub> , °C	T <sub>f</sub> , °C	ΔH(J/g)
1	0	162	268	286	778
2	15	162	266	282	592
3	30	162	268	284	520
4	45	162	270	284	472
5	60	162	268	284	365
6	90	162	270	284	352
7	120	162	269	284	267
8	150	172	269	286	222
9	180	182	268	284	194
10	240	182	268	284	160
11	300	190	268	284	140
12	360	194	270	282	131

FT-IR Spectroscopy The isothermally cured samples described above were also examined by transmission FT-IR spectroscopy. Typical spectra are shown in Figure 3. Comparison of the IR spectra of DDS and DMDDS indicated that the relative amplitudes of absorption maxima at 1105 and 1150  $\text{cm}^{-1}$ , assigned to S=O stretches go from 2.75 for DDS to 0.95 for DMDDS and 1.6 for TMDDS, if the ratio of areas of the peaks; i.e., 1105  $\text{cm}^{-1}$ /1150  $\text{cm}^{-1}$ , are measured. This reversal in peak heights and change in the peak area ratio are also noted in the partially cured samples. FT-IR spectra was also used to monitor the rate of loss of epoxide groups at 905  $\text{cm}^{-1}$  and the rate of formation of hydroxyl groups at 3400  $\text{cm}^{-1}$  for samples cured at 177°C, as shown in Figure 4.

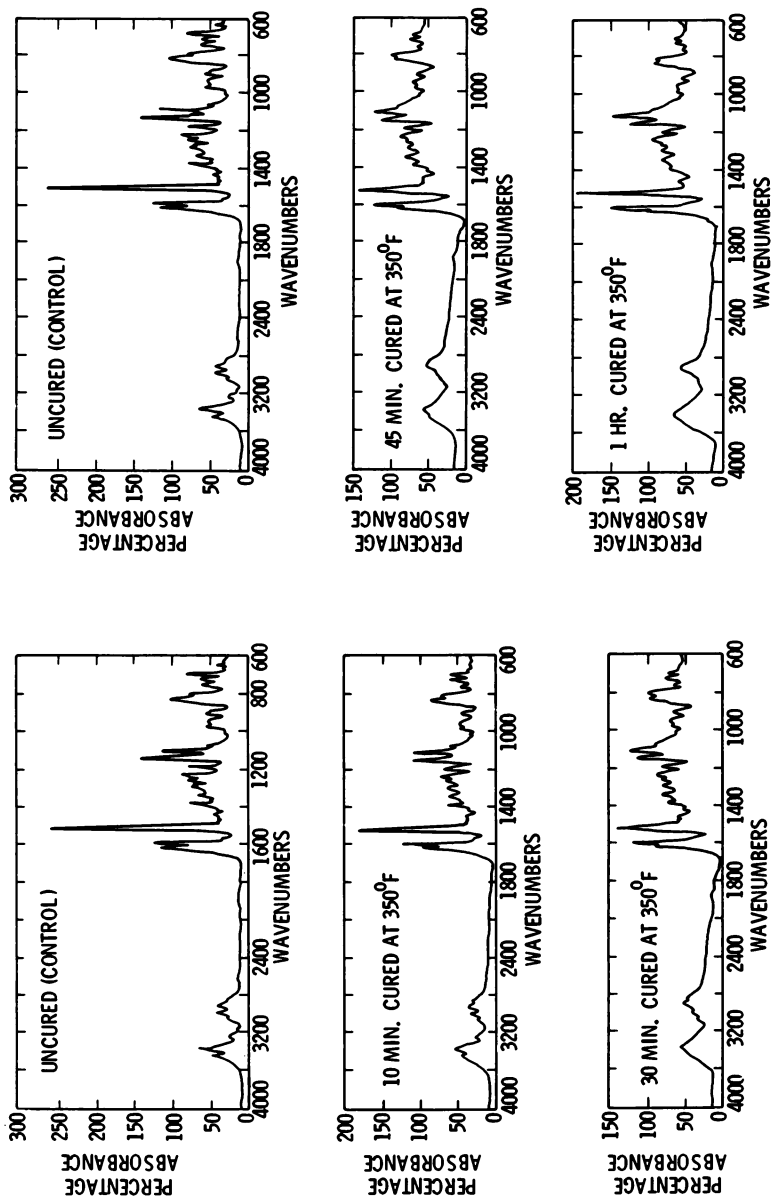


Figure 3. FT-IR monitoring of isothermal curing of the MY720-DDS system; curing temperature 177°C.

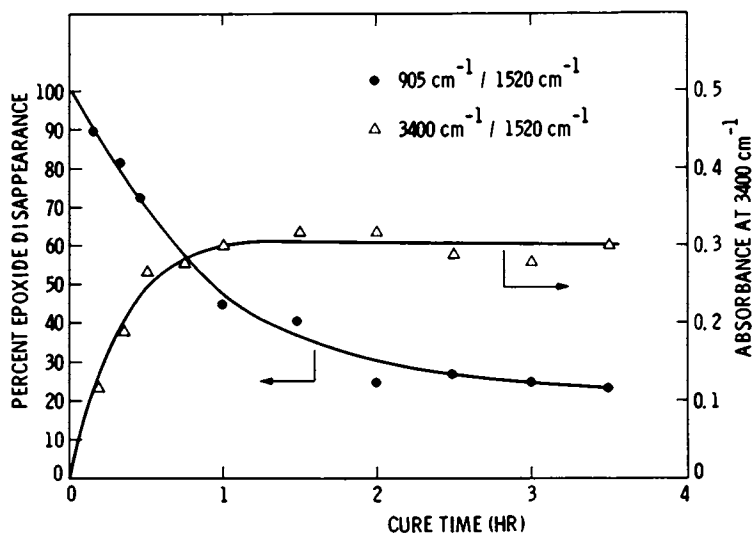
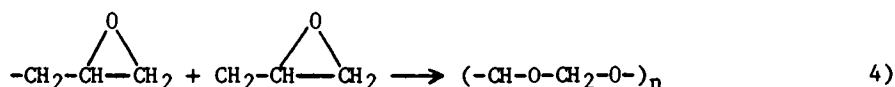
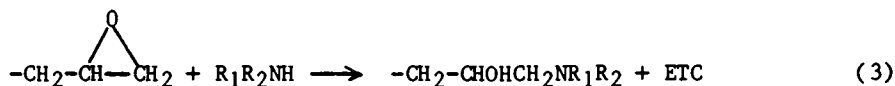
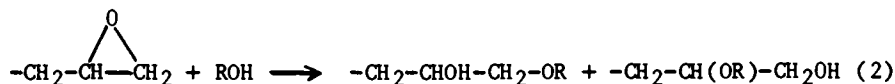
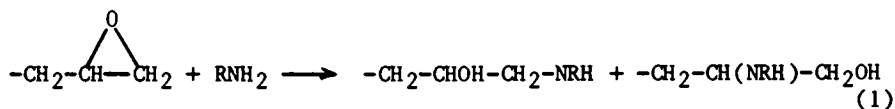


Figure 4. Plot of absorbance at  $905\text{ cm}^{-1}$  and  $3400\text{ cm}^{-1}$  vs. curing time from FT-IR analysis of MY720-DDS mixtures cured isothermally at  $177^\circ\text{C}$ .

Discussion

The main reactions in the TGDDM-DDS system are shown in Scheme 1.



SCHEME 1

First order plots of the conversion estimated from DSC data indicate that the overall process can be satisfactorily described in terms of two first order processes as shown in Figure 5. The initial reaction at both temperatures contributes proportionately more to the total heat evolution than one would expect from epoxide consumption measurements, monitored by FT-IR. The first order plot of appearance of hydroxyl groups on isothermal cure at 177°C is shown in Figure 6. The close agreement between the rate of appearance of hydroxyl groups and the overall rate of conversion is evidence that the major reaction during the first 100 minutes at 177°C is the epoxide-primary amine reaction, the end of which culminates in the consumption of a stoichiometric amount of primary amine and brings the Tg of the network up to 175°C. This stage is reached at 150-180 minutes at 153°C. Preliminary Tg measurements on samples cured at 153°C performed using a TMA apparatus indicate that that Tg of the sample cured for 180 minutes is 160°C. The plot of the sulfone peak ratio 1150 cm<sup>-1</sup>/1105 cm<sup>-1</sup> as well as the concentration of hydroxyl groups reach a plateau at the end of 60 minutes at 177°C, indicating that the secondary amine reaction is not important at 177°C. The same conclusion is also reached from DSC data on MY720 and DDS/DMDDS mixtures. Data recorded at the same scan rate indicate that the heat evolved per unit mole of reacting material is the same when DDS is replaced by DMDDS in the resin. A detailed N-15 nmr analysis of partially cured samples is being carried out in order to precisely elucidate the role of this



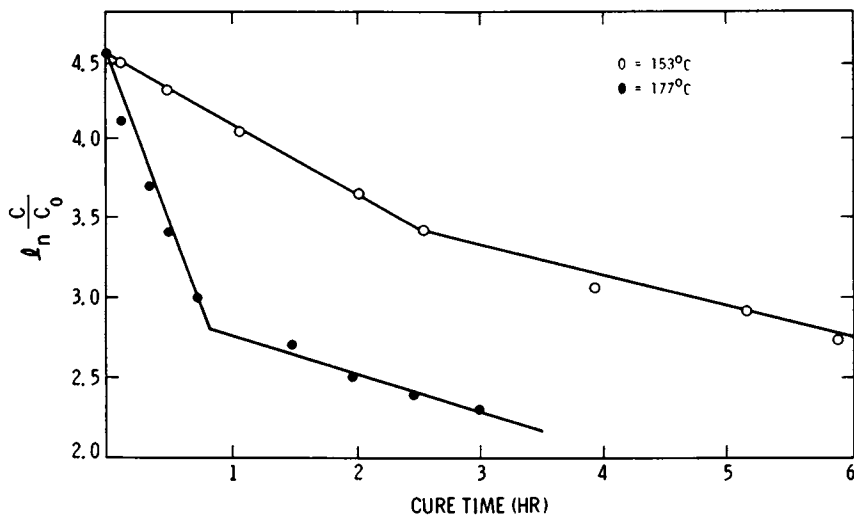


Figure 5. First order kinetic analysis of conversion rate data on the MY720-DDS system cured isothermally at 177°C and 153°C.

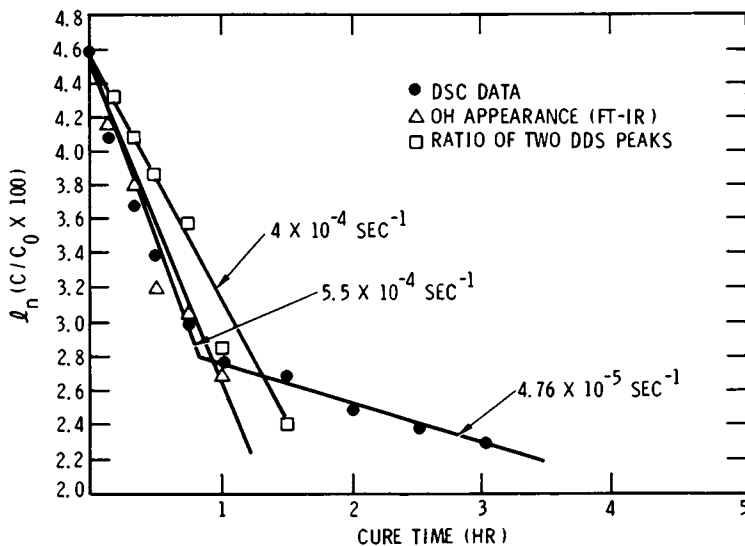


Figure 6. First order kinetic analysis of the rate of hydroxyl group appearance of 177°C.

reaction during the early cure. The secondary amine is probably involved in the post curing process, as pointed out by Morgan.<sup>(11)</sup> The lack of reactivity of the secondary amine which is a part of the network must be attributed as much to constraints imposed due to lack of diffusional transport to a reaction site as to its inaccessibility due to steric hinderance.

The constancy of the hydroxyl concentration during the later stages of the cure strongly implies that the epoxide consumption subsequent to the vitrification is mainly via the epoxide-hydroxyl reaction process. This reaction may proceed in an intramolecular fashion, resulting in the formation of cyclic morpholine type structures. The epoxide-hydroxyl reaction evidently requires a much lesser degree of intermolecular encounter, and hence can proceed in the vitrified phase at temperatures from 153-177°C. The rate of the epoxide-hydroxyl reaction is approximately an order of magnitude slower than the rate of the epoxide-primary amine reaction at 177°C with the consequence that at early stages of cure the rate of epoxide consumption is clearly controlled by the epoxide-primary amine reaction at this temperature. The two rates are much closer together at 153°C, which causes a significant degree of etherification to occur during the early stages of cure at 153°C. If we assume that etherification in a liquid medium would promote formation of intermolecular links, while etherification in the vitrified phase perhaps favors intramolecular reactions, the contribution to network topology by the ether links would be different at these two temperatures.

Using measured conversion rates and the heat evolution data, it is possible to estimate the relative heats of reaction of the epoxide-primary amine and the epoxide-hydroxyl reactions, the major reactions in this system. This calculation requires reliable estimates of the rate of appearance of hydroxyl groups and the rate of disappearance of the epoxide groups at early stages of the cure, as measured by FT-IR spectroscopy. These measurements can be corroborated by N-15 nmr monitoring of the rate of formation of secondary amines.

In conclusion, we have obtained a cure reactivity model for the TGDDM-DDS system within the temperature range 153-177°C. Extension of the model to higher and lower temperatures and its refinement via direct measurement of rates of specific reaction is in progress.

#### Acknowledgment

This paper represents the results of one phase of research carried out at the Jet Propulsion Laboratory, California Institute of Technology, under Contract No. NAS7-100, sponsored by the National Aeronautics and Space Administration.

Literature Cited

1. F. G. Musatti and C. W. Macosko, *Polymer Engr. Sci.*, 13, No. 3, 236, (1973).
2. M. J. Doyle, A. F. Lewis and H. M. Li, *Polymer Engr. Sci.*, 19, 687 (1979).
3. J. K. Gillham, *Polymer Engr. Sci.*, 19, 313 (1979).
4. G. A. Senich and W. J. MacKnight, *Polymer Engr. Sci.*, 19, 313 (1979).
5. A. F. Lewis, M. J. Doyle and J. K. Gillham, *Polymer Engr. Sci.*, 19, 683 (1979).
6. D. H. Kaelble, ACS, *Org. Coat. and Appl. Polymer Sci.*, Proceedings, Vol. 46, p. 241, 246 and 328 (1982).
7. J. B. Enns and J. K. Gillham, *Amer. Chem. Soc., Org. Coat. and Appl. Polymer Sci. Proceedings*, Vol. 46, p. 592 (1982).
8. M. Cizmecioglu and A. Gupta, *Soc. Plast. Ind. 37th Annual Conference of Reinforced Plastics/Composites Conference. Preprints*, January 1982, Washington, D.C. paper No. 20E.
9. M. Cizmecioglu and A. Gupta, *SAMPE Quarterly*, Vol. 13, No. 3, p. 16, April (1982).
10. A. Gupta, M. Cizmecioglu, D. Coulter, R. Liang, A. Yavrouian, F. D. Tsay and J. Moacanin, "The Mechanism of Cure of Tetraglycidyl Diaminodiphenyl Methane with Diaminodiphenyl Sulfone," *J. Appl. Polym. Sci.* (in press).
11. R. Morgan, Lawrence Livermore Labs, private communication.

RECEIVED May 2, 1983

# Moisture-Temperature Effects on the Dynamic Mechanical Properties of Epoxy Polymers

WAYNE J. MIKOLS<sup>1</sup> and JAMES C. SEFERIS<sup>2</sup>

Polymeric Composites Laboratory, Department of Chemical Engineering,  
University of Washington, Seattle, WA 98195

Dynamic mechanical properties are used in this work to develop an understanding of how epoxy based networks respond to different hygrothermal environments. A fundamental understanding of why property changes occur as a result of hygrothermal exposure is provided.

Numerous efforts have focused upon the nature of moisture transport of epoxy systems. Previous-sorption desorption work demonstrated that equilibrium moisture levels in an epoxy system can be related to thermodynamic states (1,2,3). Transient and equilibrium dynamic mechanical experiments are performed in this work with two epoxy systems TGEBA-TETA and N-5208. These experiments provide insight into the nature and extent that network changes have on the dynamic mechanical properties as a result of hygrothermal cycling.

## Experimental

Epoxy film samples were prepared with the DGEBA-TETA and N-5208 resins. Detailed information on the DGEBA-TETA and N-5208 resin cure and sample preparation has been previously provided (2,4). Films of the N-5208 resin were made with a curing agent concentration of 25 PHR-DDS (4); 14 PHR TETA was used for curing the DGEBA epoxy (2). Dynamic mechanical properties for films were measured on strip samples cut to nominal 0.02 cm x 0.3 cm x 6.0 cm dimensions.

Two different types of dynamic mechanical experiments were performed. First, the temperature dependence of "equilibrium" dynamic mechanical properties for all epoxy samples were obtained

<sup>1</sup> Currently with Shell Development Co. in Houston, TX

<sup>2</sup> Author to whom correspondence should be addressed

0097-6156/83/0227-0095\$06.00/0  
© 1983 American Chemical Society

with the Rheovibron DDVII as previously described (5). These experiments were performed at a frequency of 11 Hz over the temperature range beginning near  $-150^{\circ}\text{C}$  to just above the specific sample  $T_g$ . A heating rate of  $1^{\circ}\text{C}/\text{min}$ . was employed for all experiments. The samples for "equilibrium" -Rheovibron experiments were first allowed to equilibrate in a specified hygrothermal environment. They then were loaded into the Rheovibron environmental chamber and maintained in an atmosphere of dry nitrogen during the heating process imposed by the experiment. The data obtained were recorded in the form of the traditional  $\tan \delta$  moduli ( $E'$  and  $E''$ ) and dynamic mechanical compliances ( $S'$  and  $S''$ ) (5).

The second type of dynamic mechanical experiment involved collection of "transient" -Rheovibron data at a fix frequency as a function of time after a change in either the moisture or thermal environment. The experimental apparatus designed for this purpose is depicted in Figure 1.

### Discussion

Equilibrium Dynamic Mechanical Data. Dynamic mechanical properties of both the DGEBA-TETA and the N-5208 epoxy systems exhibit characteristic transitions observed in many polymeric materials. Figures 2a and 2b illustrate "equilibrium" dynamic mechanical  $\tan \delta$  as a function of temperature for samples saturated at different moisture levels.

At high temperatures, the exhibited  $\alpha$  transition is associated with the material's glass transition. Near  $-50^{\circ}\text{C}$ , both of these epoxies exhibit a familiar low temperature  $\beta$  transition. The low temperature  $\beta$  transition in glassy polymers is often a result of segmental chain mobility triggered by the system's thermal characteristics. This low temperature peak is quite broad indicating that a wide spectrum of motion types and/or activation energies are contributing to the transition (7).

The increase in magnitude of the low temperature  $\tan \delta$  associated with the  $\beta$ -transition peak can be rationalized due to a plasticization of the epoxy network. However, the significant differences in the  $\tan \delta$  magnitudes which arise above the  $25^{\circ}\text{C}$  for both epoxies are not attributable to plasticization. This shift is in fact a tertiary  $\omega$  dynamic mechanical transition (3, 4). This  $\omega$  transition is highly sensitive to the presence of polar solvents. Chu and Seferis (6) obtained dynamic mechanical data which demonstrate formation of such a tertiary  $\omega$  transition in a TGDDM-DDS epoxy system from residual amounts of acetone in the network. Keenan, et al (4) present data for the N-5208 epoxy system which indicate a slight drop in the temperature location of the  $\omega$  transition with increased moisture content. Broadening of the peak was also observed. Similar characteristics are inferred from  $\tan \delta$  curves for the

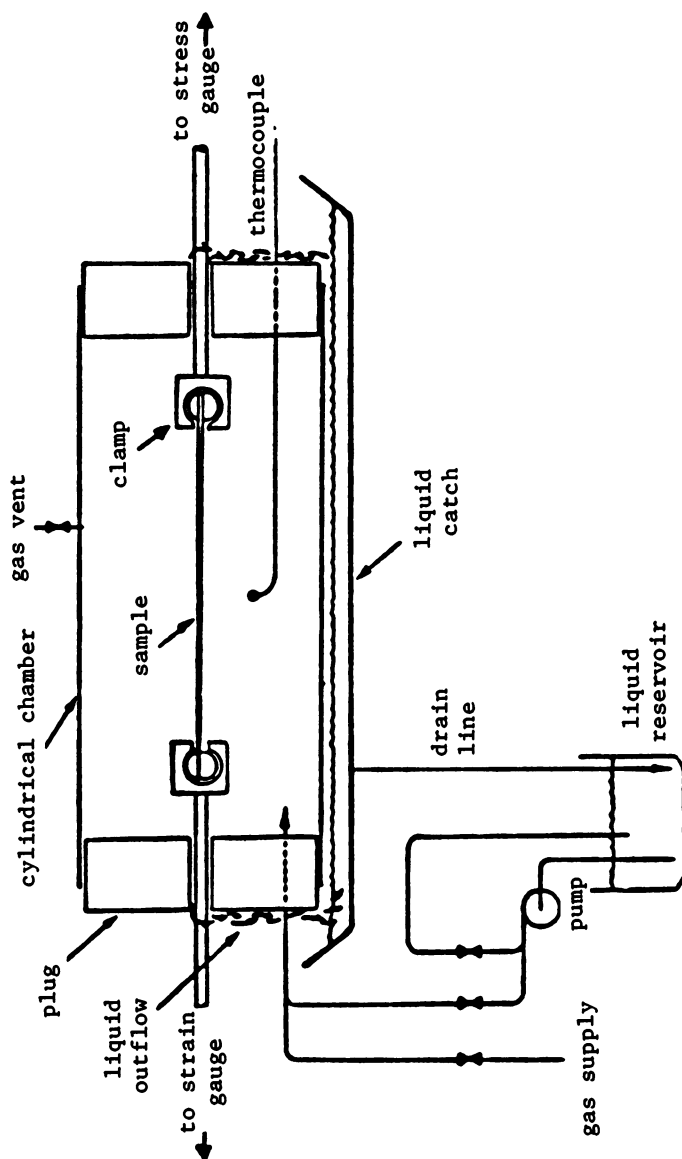


Figure 1. Test chamber for the dynamic mechanical moisture sorption/desorption experiments. The design of this chamber enables exposure of the sample to a variety of liquid and/or vapor environments. Temperature of the chamber can be controlled by adjusting flow or temperature in the liquid or gas supply lines. Alternatively, the chamber can be jacketed with cooling water or heat tape.

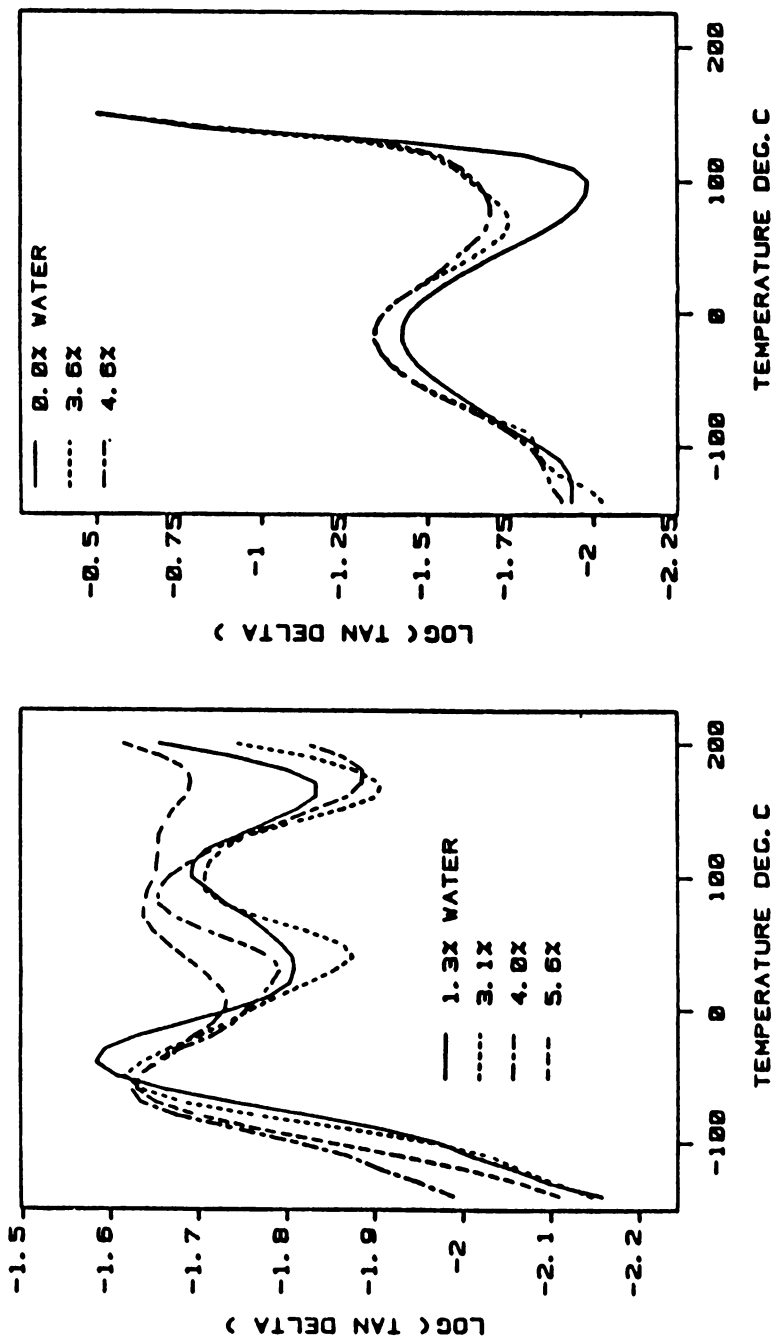


Figure 2. Tan ( $\delta$ ) as a function of temperature for samples with different equilibrium moisture contents. Key: left, N-5208 samples; and right, DGEBA-TETA.

DGEBA-TETA samples in Figure 2b. An increased moisture content results in the broadening of this  $\omega$  transition. However, no direct measurement of a temperature shift in this epoxy is possible since the increase occurs over such a broad temperature range. Moisture sorption in epoxies serves to disrupt the hydrogen bonding in the network of the cured system. This results in an increase in the network's free volume. As used herein free volume refers to intermolecular space of the network that has not been affected by moisture and/or the heat history of the material (11). Consequently, free volume changes should permit qualitative evaluation of relationships between a sample's moisture content and its mechanical loss properties(3).

A convenient way to quantify the increase in magnitude of the  $\omega$  transition with the increase in epoxy moisture content is to compare the area under this transition peak with sample moisture content. Several possible dynamic mechanical property comparisons exist. No identifiable trends were observed between the magnitude or area of the loss modulus ( $E''$ ) or  $\tan \delta$  and the amount of moisture in the N-5208 or DGEBA-TETA epoxy samples. The lack of identifiable loss modulus trends does not preclude the possibility that mechanical loss property trends exist. Loss modulus and loss compliance properties must both be studied to assess the impact of molecular changes in the network (5,8). Loss compliance ( $S''$ ) data for the samples from Figures 2a and 2b are given in Figures 3a and 3b.

When the area under the  $\text{Log}(S'')$  versus temperature curve is plotted against epoxy moisture<sup>10</sup> content, there is a definite increase with increased moisture content. One method for presentation of the data is to simply plot the area under the loss compliance  $\omega$  transition as a function of sample moisture content. This could be done for each epoxy under consideration. A more interesting plot would be one which puts the curves for several different epoxies on a comparable basis. While selection of a basis is somewhat arbitrary, the polar nature of the epoxy networks provides a foundation for such selection. In general, epoxies are noted for their wide range of polar type groups. The exact nature and number of polar sites in a given epoxy depend on the specific network crosslink agents or additives as well as the epoxy cure cycle. It is possible to identify chemical species in both the N-5208 and DGEBA-TETA systems which have potential for polar (or hydrogen) bond formation. In the N-5208 epoxy, the amine and sulfone groups produce dipoles capable of this bond formation. Amine groups of the TETA are identified for this purpose in the DGEBA-TETA system.

With respect to the amine groups in these epoxies, only the primary and secondary amine contribute to hydrogen bond formation. Steric considerations further serve to complicate the relative extent to which the amines and sulfone groups take part in the overall hydrogen bonding process. Consequently, it is apparent that the extent of reaction in such amine linked systems is one factor which influences the moisture uptake process. A



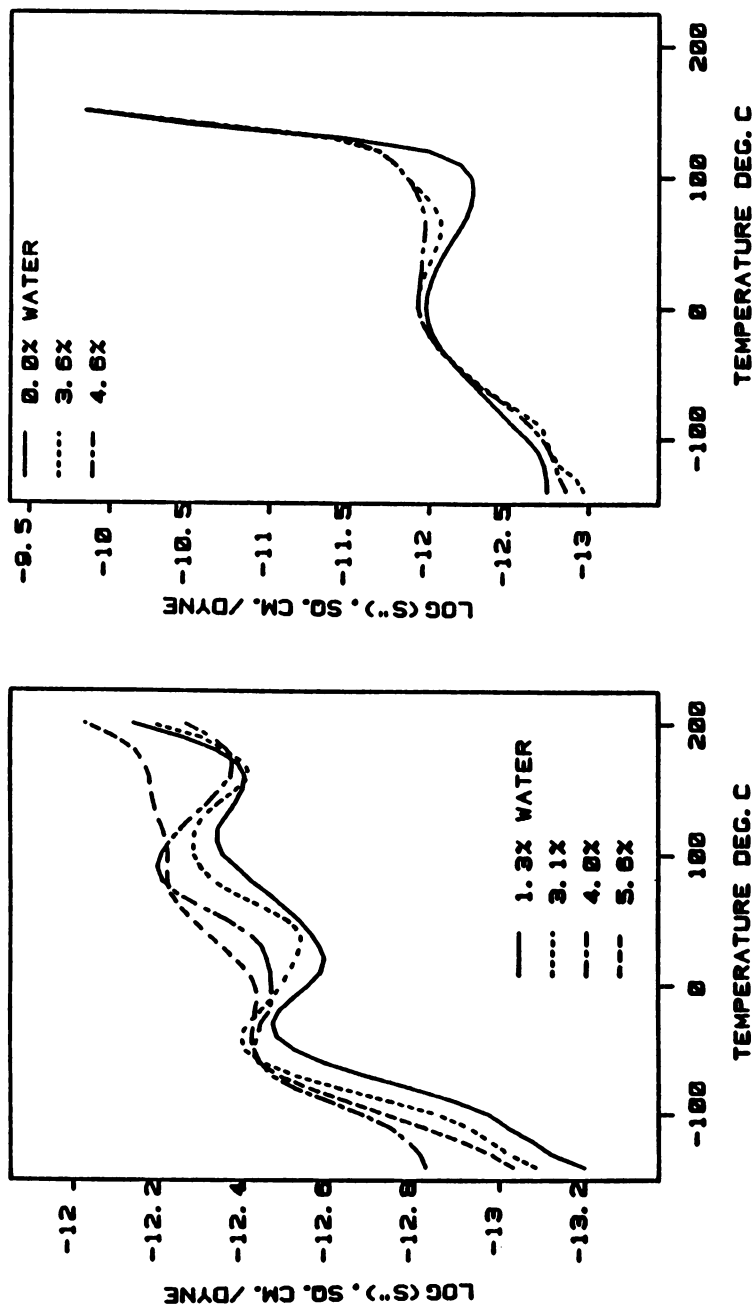


Figure 3. Loss compliance ( $S''$ ) as a function of temperature for samples with different equilibrium moisture contents. Key: left, N-5208 samples; and right, DGEBA-TETA.

comparison is made between dynamic mechanical loss compliance data and epoxy moisture content in Figure 4. The abscissa for this graph corresponds to the apparent equilibrium molar content of water in the epoxy per mole of nitrogen in the makeup batch of uncured epoxy resin. The ordinate is a measure of the differential area under the  $\omega$  peak in the  $\text{Log}_{10}(S'')$  versus temperature curve from Figures 3a or 3b. For each epoxy system, the differential area is defined as the difference between the  $\text{Log}_{10}(S'')$  versus temperature curves at a given moisture content and at zero moisture content. Numerical integration is done between these two curves under the  $\omega$  transition.

It is of interest to note that for both epoxies the differential area appears to increase steadily with the molar ratio of moisture to nitrogen content. Since each of the epoxies contain varying amounts of primary, secondary, and tertiary amines, the fact that both epoxy systems do not fall on the same line is expected. Sulfone groups in the N-5208 system further complicate analysis of the hypothesized relationship.

Useful insight can be gained by examining qualitatively the relationships between various sets of data of Figure 4. For the differential area under the curve for the DGEBA-TETA epoxy sample, it is observed that as the moisture content per mole of nitrogen is increased from zero, the differential area under the loss compliance versus temperature curve increases. Near an abscissa value of 0.6, the mechanical property data appears to plateau. Additional increases in epoxy moisture content play no further role in  $\omega$  transition loss compliance property changes. This should indeed occur if all available amine hydrogen bonding sites in the matrix become saturated. Additional moisture enters the network without introducing additional network hydrogen bonding or mechanical property changes.

The 25 PHR-DDS N-5208 epoxy sample covers a broader range of mole-moisture per mole-nitrogen values in Figure 4. However, at an abscissa value of 0.8, the differential loss compliance area does not appear saturated. The higher functionality of the N-5208 components result in a cured network with fewer tertiary amine links (6). This, in conjunction with the presence of the DDS sulfone groups, can be used to rationalize the lack of a plateau in the differential area curves of the 25 PHR-DDS epoxy data.

Transient Dynamic Mechanical Data. Data from Figures 2a and 2b for both the DGEBA-TETA and the N-5208 epoxy systems suggest that moisture serves to increase the relative molecular mobility of chain segments within the network structure. This is readily apparent from the increases in the  $\tan \delta$  values. However, these figures provide no information regarding the manner in which these changes occur. Insight into the network changes which

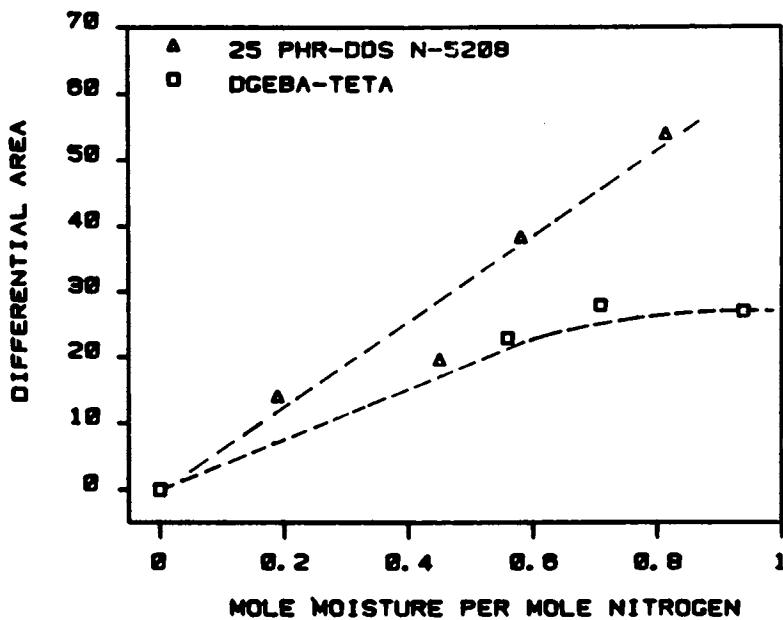


Figure 4. Differential area under the  $\text{Log}(S'')$  vs. temperature curve for DGEBA-TETA and 25 PHR-DDS N-5208 as a function of (molar-moisture per molar-nitrogen) content of the epoxy.

occur during the moisture sorption-desorption process can be gained by studying transient dynamic mechanical moisture data.

There are two basic types of transient dynamic mechanical experiments which were performed in this study. The first type involves isothermal cycling of an epoxy sample between a dry and wet environment. The second type of experiment involves cycling the epoxy sample between two different temperatures under a liquid water environment. In each case, the transient and equilibrium values of dynamic mechanical properties change in a unique manner.

**Isothermal Moisture Transients:** Isothermal experiments will first be discussed for the DGEBA-TETA systems. Film samples from this system were equilibrated in a desiccated environment and subsequently exposed to liquid water environment in the Rheovibron apparatus. Figure 5 summarizes typical results of these dynamic mechanical experiment. In addition to the  $\text{Log}_{10}(S')$  and  $\text{Log}_{10}(S'')$  dynamic mechanical properties, these figures also plot the percent elongational swell of the sample as a function of time.

The swell measurements were obtained from readings off the strain gauge dial on the Rheovibron according to our previously developed procedure (3,4). While swelling of the epoxy is not directly proportional to its moisture content, it certainly is indicative of the relative degree of moisture saturation (9).

Transition from the initial dry to subsequent wet environment caused an initial increase in the  $\tan \delta$  and loss mechanical properties for the sample as shown in Figure 5. This behavior may be explained in terms of a plasticizing effect. Small polar penetrant molecules enter the network and increase the average molecular distance between chain segments. Polarity of the penetrant serves to disrupt intra-chain hydrogen bonding between polar groups in the network allowing for this increase. The increase causes a macroscopic swelling of the network. The net result is creation of additional free volume within the structure. This increase in free volume permits an increased mobility for chain segments in the network structure. In such highly crosslinked systems, the effect does not significantly modify the overall stiffness properties. Hence, loss properties increase while storage properties remain relatively unaffected.

Transient experiments were expected to yield a smooth transition between the observed dry and wet equilibrium states in Figures 2a, 2b, 3a, and 3b. However, this expected behavior was restricted to a relatively short time segment following the initial change from a dry to a wet isothermal environment. It is helpful to focus on the  $\text{Log}_{10}(S'')$  and swelling curves of Figure 5 to better understand the nature of mechanical property changes which take place after the initial plasticization of the network. During the initial stages of the plasticization phenomena, moisture is entering available free volume in the network.

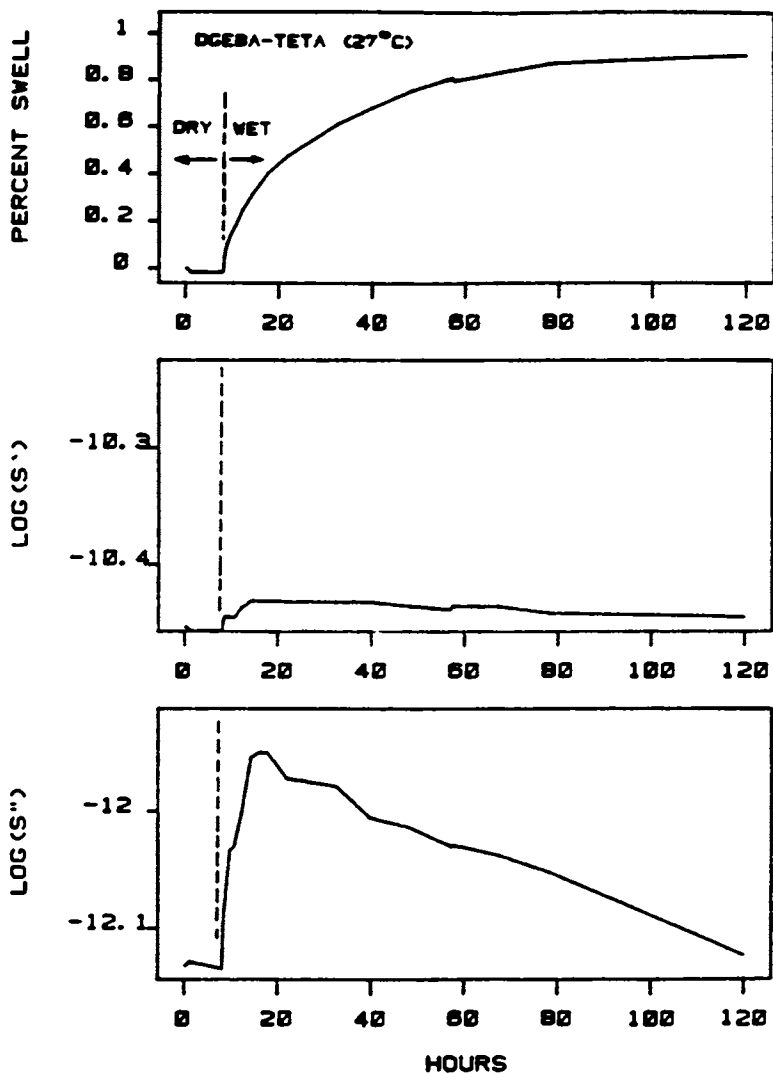


Figure 5. Dynamic mechanical and swelling behavior for a transient moisture sorption experiment on DGEBA-TETA.

Interruption of intra-chain hydrogen bonding creates additional free volume in the network. As saturation of the added available free space occurs, mobility of the network becomes restricted or "blocked." Epoxies are well known for their ability to absorb additional amounts of moisture over extended periods of time (4,10). As long as such a process continues to generate additional free volume for molecular motion, the plasticizing effect dominates. When free volume is consumed faster than it is generated, a blocking effect sets in. Since the changes of  $\tan \delta$  measurements in Figure 5 are extremely small, it is difficult to establish whether a true equilibrium value exists during the blocking stage of the process. Equilibration of dynamic mechanical data in short periods of time is unlikely on a theoretical basis in view of the prolonged moisture sorption behavior in epoxies (10).

The transient data of Figure 5 provides a new perspective on the physical significance of equilibrium experimental data. Long-time transient  $\tan \delta$  values show near indistinguishable differences from their original dry state values. This is in contrast to "equilibrium" dynamic mechanical  $\tan \delta$  values which show a modest increase as a result of moisture exposure. The difference in "equilibrium"  $\tan \delta$  values is the greatest in the 25-80°C  $\omega$  transition range. The magnitude of the initial rise in the dry to wet state transient  $\tan \delta$  data values correspond with the magnitude of the differences between dry and wet state "equilibrium" data at comparable temperatures. This observation suggest that samples equilibrated under different moisture conditions and loaded into the dry nitrogen environment of the Rheovibron for "equilibrium" experiments lose a small amount of their moisture prior to actual dynamic mechanical property testing. Such a loss changes the equilibrated epoxy sample from a "plasticized - blocked" state to one of a "plasticized - unblocked" state. Therefore, equilibrium dynamic mechanical properties of epoxy samples equilibrated at a variety of hygrothermal environments are not tested in their true equilibrium states. Some small portion of the final equilibrium moisture responsible for blocking of the network is lost. However, structural changes introduced into the network as a result of the former moisture presence appears to remain.

It should be re-emphasized that the equilibrium moisture responsible for swelling of the matrix also resulted in disruption of the intra-chain hydrogen bonding of the system. Although swelling and moisture content of a hygrothermally exposed sample is reduced when it is placed in a dry environment for an "equilibrium" dynamic mechanical experiment, network changes persist (3). If the changes which persist are permanent and chemical in nature, then removal of moisture resulting in subsequent network relaxation might result in a system with different mechanical property behavior than the original dry

state epoxy network. This does not appear to be the case. Previous diffusion work with DGEBA-TETA indicates that a moisture altered sample raised beyond the  $T_g$  apparently recovers the previous dry state characteristics<sup>g</sup>(1). This result is also coincident with information derived from dynamic mechanical experiments (3).

It is also of interest to evaluate subsequent sorption/desorption dynamic mechanical properties in view of the results from the simple single dry to wet cycle experiment. Figure 6 plots transient isothermal  $\tan \delta$  dynamic mechanical data for a 25 PHR-DDS N-5208 epoxy sample. This sample was initially exposed to a dry 50°C environment. This temperature was selected since it coincides with the vicinity of the dynamic mechanical  $\omega$  transition. Hence, differences between properties in the dry and wet states could be maximized. Behavior of the initial dry to wet state transient cycle was previously discussed for DGEBA-TETA epoxy sample of Figure 5. Similar behavior is noted for this N-5208 epoxy sample. There is an initial rise in the  $\tan \delta$  followed by a "blocking" and gradual reduction. After the  $\tan \delta$  appeared to approach a stable value, the environment in the sample chamber was switched from one of a 50°C liquid environment to a 50°C desiccated environment. Once again, a rapid increase in the mobility of the system occurred. After the sharp increase in  $\tan \delta$ , a gradual decrease followed.

The mechanical behavior of the dry-to-wet and wet-to-dry cycles complement each other. In the first sorption curve, blocking of the network structure was explained by sorption of a small quantity of moisture into free volume of the near saturated matrix. If this small quantity of moisture is allowed to escape, the network takes on mechanical behavior of the unblocked plasticized state. This transition occurs rapidly during the initial stages of drying. The peak  $\tan \delta$  value is representative of plasticized state properties. As further desorption takes place, mechanical properties approach the initial dry state values. A qualitative description of the diffusion-mechanical mechanisms associated with each segment of the sorption-desorption cycle is outlined in Figure 7.

It is of interest to note that subsequent cycling of the epoxy sample in Figure 6 results in a gradual increase of the "stable" dry and wet state  $\tan \delta$  values. This cumulative increase in network mobility continues with moisture cycling because the sample is never allowed a macroscopic network relaxation. Recovery of original dry state properties at least requires thermal excitation of the system to temperatures near the glass transition point (3).

Liquid water temperature transient experiments were also conducted on 25 PHR-DDS N-5208 epoxy samples. Each sample was first equilibrated in a desiccated environment. It was subsequently loaded into the Rheovibron chamber depicted in

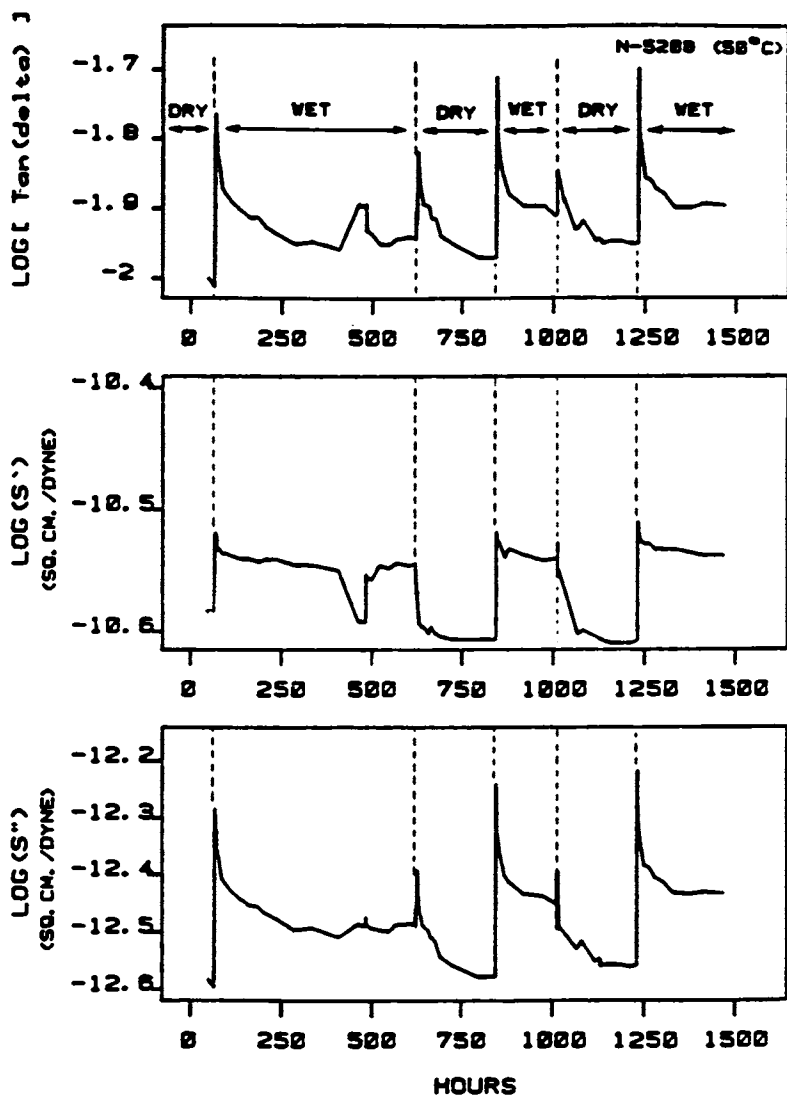


Figure 6. Dynamic mechanical properties for a transient moisture sorption experiment on 25 PHR-DDS N-5208.



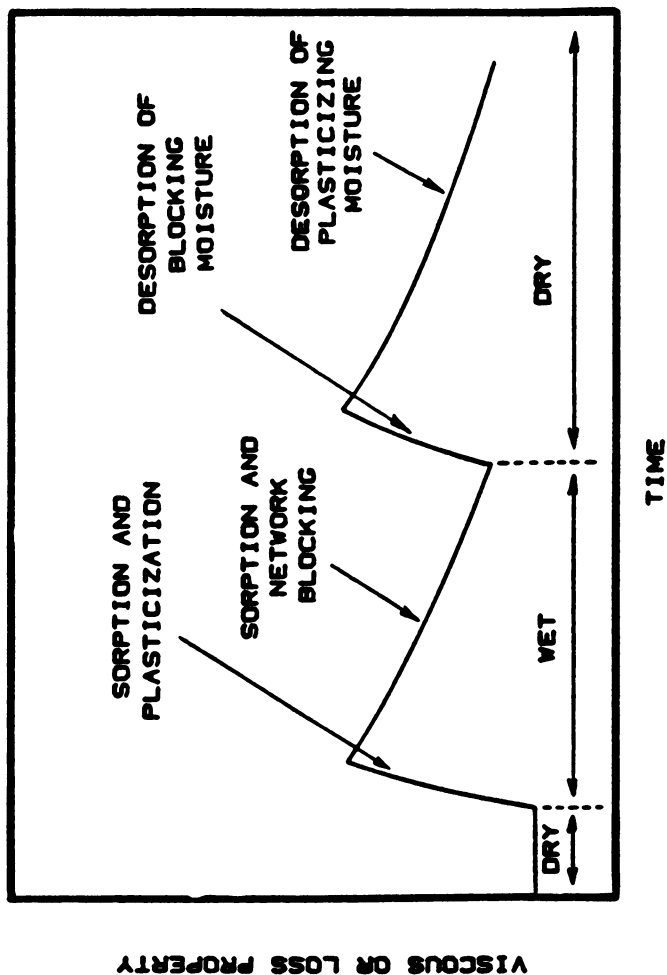


Figure 7. Qualitative description showing plasticizing and blocking effect of sorbed moisture on dynamic mechanical  $\tan (\delta)$  property behavior of an epoxy.

Figure 1. The sample was allowed to equilibrate at 20°C in this chamber under a dry nitrogen purge. At some initial time, 20°C liquid tap water was introduced and circulated through the environmental chamber. For each sample, the water temperature was subsequently cycled between 50°C and 20°C. These temperatures were selected since they correspond with the onset and peak values of the tertiary dynamic mechanical  $\tan \delta$ ,  $\omega$  transition. Enough time was allowed between temperature changes to establish "equilibrium" dynamic mechanical property values associated with each hygrothermal state.

$\tan \delta$ , storage compliance, and loss compliance values for these experiments are plotted as a function of time in Figure 8. This transient temperature cycle data illustrates interactions between the dynamic mechanical plasticization and blocking behavior just discussed as well as the epoxy's equilibrium moisture uptake behavior (3), and the temperature behavior of dynamic mechanical properties observed for this epoxy in Figure 2a. Perhaps the easiest comparison to consider involves the relationship between transient temperature cycling data of Figure 8 and the thermal behavior observed for N-5208 epoxy  $\tan \delta$  data of Figure 2a.

Based on "equilibrium" dynamic mechanical results of Figure 2a,  $\tan \delta$  properties associated with network thermal behavior at 20°C should be greater than comparable behavior at the 50°C thermal state. The difference in relative magnitudes stems from the relative positions of the 20°C and 50°C thermal states with respect to the low temperature  $\beta$  transition for this epoxy. This difference for the transient data is best observed in Figure 8. Equilibrated 20°C  $\tan \delta$  and loss property values for the 20°C hygrothermal state are greater than the subsequent 50°C hygrothermal state measurements.

The fundamental difference in property magnitudes stemming from the 20°C, 50°C, and  $\beta$  peak thermal locations is overlaid by the sorption/desorption "blocking" behavior previously explained for Figure 7 for isothermal cycling experiments. Similar behavior is noted for the liquid water thermal cycling experiments. The first 20°C liquid water cycle of Figure 8 follows the behavior outlined in Figure 7. There is an initial rise in the  $\tan \delta$  followed by a "blocking" behavior resulting in the  $\tan \delta$  decrease. When the thermal environment is changed from 20°C to 50°C, moisture sorption data indicates that additional moisture is absorbed into free volume of the polymer (3). Dynamic mechanical data of Figure 8 conforms with this behavior since additional plasticization occurs immediately after the initial 20°C to 50°C temperature change. The rapid rise is then followed by a decrease in the  $\tan \delta$  corresponding to a "blocking" of the network structure created by the 20°C - 50°C hygrothermal sequence.

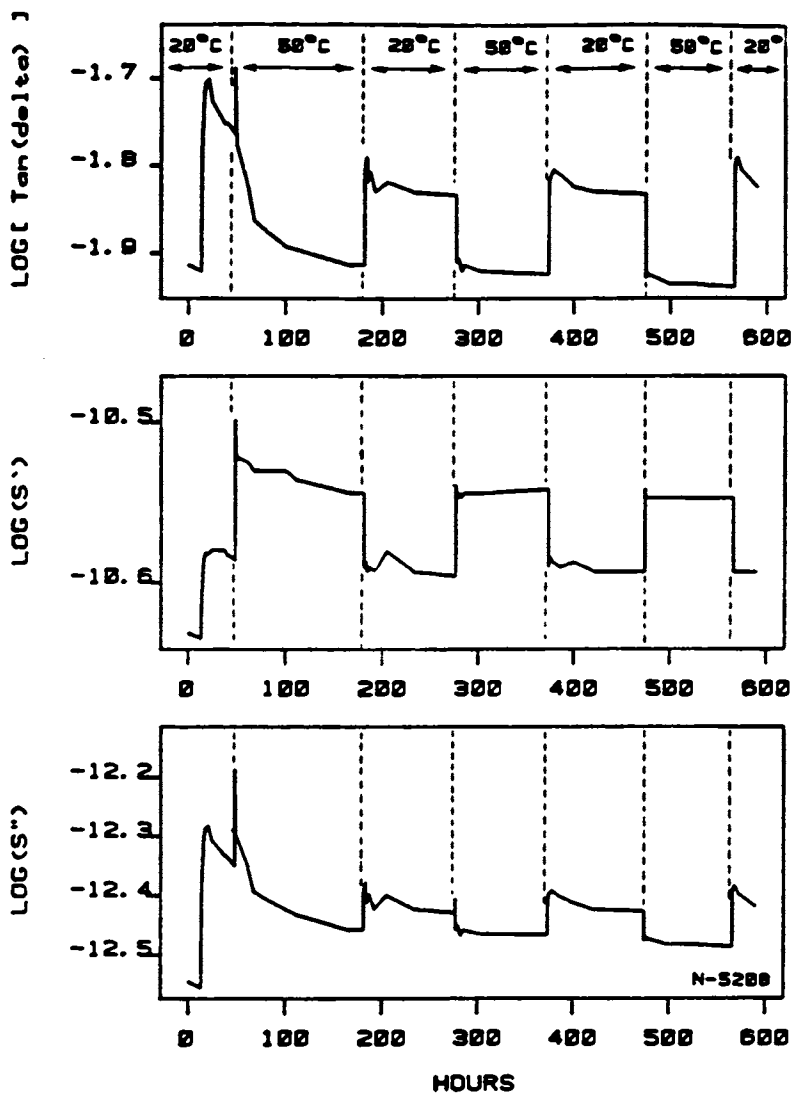


Figure 8. Transient dynamic mechanical properties of 25 PHR-DDS N-5208 epoxy sample during liquid water thermal cycling between 20 °C and 50 °C.

The next two steps in the thermal sequence are a 50°C to a 20°C change followed again by a 20°C to 50°C change. These two steps illustrate some key property behavior. The unique feature about the first 50°C to 20°C temperature step of Figure 8 is that once more, a slight plasticization occurs immediately after the thermal change. Moisture sorption data is consistent with this observation. When this epoxy is exposed to a low temperature liquid environment after a high temperature liquid environment, additional moisture is sorbed in the network (3). Unlike the first switch from 20°C to 50°C, the second switch 20°C to 50°C does not demonstrate any  $\tan \delta$  spike. This indicates that no free space is available for plasticization effects. Moisture is being squeezed out of the network as a result of a reduction in available free space at the new thermal condition (3). On every change from 50°C to 20°C there is plasticization followed by a blocking of the network. When subsequent changes are made from 20°C to 50°C, no network plasticization occurs since water is being "squeezed" from the epoxy network.

### Conclusions

Transient dynamic mechanical data on the DGEBA-TETA and high performance N-5208 epoxy based systems have been obtained and compared with "equilibrium" data. The transient data have demonstrated that moisture can act not only to plasticize an epoxy network but also to restrict and stiffen molecular chain movement. The behavior observed was explained by examining the synergistic effects that moisture and temperature have on the particular epoxy network structure.

### Acknowledgment

The authors express their appreciation to Drs. A. G. Miller and J. T. Quinlivan of the Boeing Commercial Airplane Company for helpful discussions. Financial assistance for this project was provided by the Boeing Commercial Airplane Company through the Polymeric Composites Laboratory.

### Literature Cited

1. A. Apicella, L. Nicolais, G. Astarita, and E. Drioli, *Polymer*, 20, 1143, (1979).
2. L. Nicolais, E. Drioli, A. Apicella, and D. Albanese, AFOSR 77-3369-01, (1978).

3. W. J. Mikols, J. C. Seferis, A. Apicella, and L. Nicolais, *Polymer Composites*, 3, 118, (1982); W. J. Mikols, *Hygrothermal Effect on the Mechanical Properties of Epoxies and Graphite Epoxy Composites*, Ph.D. Dissertation, Department of Chemical Engineering, University of Washington, Seattle, Washington (1982).
4. J. D. Keenan, J. C. Seferis, and J. T. Quinlivan, *J.A.P.S.*, 24, 2375, (1979); J. D. Keenan, *Structure and Dynamic Mechanical Properties of TGDDM-DDS Epoxy, Graphite Fibers and Their Composites*, M. S. Thesis, Department of Chemical Engineering, University of Washington, Seattle, Washington (1979).
5. A. R. Wedgewood and J. C. Seferis, *Polymer*, 22, 966, (1981).
6. H. S. Chu, *Processing-Structure-Property Relations for High Performance Amine-Cured Epoxy Polymers*, M. S. Thesis, Department of Chemical Engineering, University of Washington, Seattle, Washington, (1980).
7. C. A. May and F. E. Weir, *SPE Tech. Pap.* 8 2-2 (1962).
8. E. Passaglia and G. M. Martin, *J. Res. Nat. Bur. Std.*, 68A, 519, (1964).
9. M. Adamson, *J. Mater. Sci.*, 15I, 1736, (1980).
10. J. M. Whitney and C. E. Browning, *Advanced Composite Materials: Environmental Effects*, J. R. Vinson, Ed., ASTM-STP-658, 43, (1978).
11. H. Fujitz and A. Kishimoto, *J. Polymer Sci.* 28, 547 (1958).

RECEIVED May 10, 1983

# Cross-linking Reaction of an Epoxy Resin with Phthalic Anhydride

ELBERT W. CRANDALL and WINSTON MIH<sup>1</sup>

Pittsburg State University, Pittsburg, KS 66762

A study of the crosslinking of an epoxy resin with phthalic anhydride catalyzed by an imidazole catalyst has been carried out using differential scanning calorimetry, middle infrared and near infrared. The data from these methods indicate the process is a stepwise mechanism involving first anhydride ring opening, followed by epoxy ring opening and hydroxyl formation. Ether crosslinks begin to form after epoxy ring opening and the last step is formation of ester crosslinks.

A study has been undertaken to attempt to determine a possible mechanism for the crosslinking of an epoxy resin with phthalic anhydride using an imidazole derivative as the catalyst. In this study we have used differential scanning calorimetry (DSC) to measure the heat of reaction and time of curing process. Crosslinked polymers were studied by middle and near infrared. The middle IR could be used to look at the C-O ester and ether bands and the secondary hydroxyl in the 1000 to 1500  $\text{cm}^{-1}$  region. However, more useful were the results from the near IR in which the epoxy C-H, C=O, and O-H bands can be compared to the first overtone of the 3.5  $\mu\text{M}$  C-H band which appears at 1.66  $\mu\text{M}$  in the near IR. DCS and near IR data have been obtained on samples in which time of curing and concentrations of phthalic anhydride and imidazole catalyst have been varied.

Several authors (1-6) have proposed that the crosslinking reactions of epoxy resins with anhydrides is a two or three step process: formation of the monoester, formation of the diester and formation of ether crosslinks. It is hoped that this work may assist in a better understanding of this process.

## Experimental

The epoxy prepolymer used was Dow Chemical's D.E.R. 331,

<sup>1</sup> Current address: California State University, Chico, CA 95929

molecular weight 390. Reagent grade phthalic anhydride was purchased from General Chemical Company under the Baker and Adamson label. The amine catalyst used was Curezol 2E4MZ-CN 3 (2-ethyl-4-methylimidazolyl) propanenitrile, obtained from Shikoku Chemicals Corporation.

The DSC data were obtained on a Perkin-Elmer DSC-1B by sealing samples weighed on a six place balance into volatile sample pans. The samples were prepared by weighing the proper amount of epoxy resin and finely divided phthalic anhydride and mixing. This mixture was placed on a clay plate and ground with a spatula until a homogeneous mixture was obtained. The instrument was operated at 10<sup>0</sup>K per minute on range 8. The areas under the curve were determined with a planimeter and the  $\Delta H$  of curing were calculated as described in the Perkin-Elmer manual (7).

The samples for the middle IR were obtained by curing the epoxy, phthalic anhydride mixtures in metal placets with covers to prevent sublimation. The samples were then heated in an oven set at the proper temperature. After curing, the samples were ground to a fine powder and made into a window using a KBr minipress. Samples for the near IR were prepared as given for the middle IR or were cured between glass plates in an oven set at the proper temperature. Spectra were run on a Beckman DK-2A.

### Discussion

The reaction of the epoxy resin with phthalic anhydride using curezol catalyst, 3(2-ethyl-4-methylimidazolyl) propanenitrile, shows an exotherm with its minimum at 154<sup>0</sup>C and a curing time of five to six minutes depending on the concentration of phthalic anhydride (Figure 1). At mole ratios of epoxy/phthalic anhydride of 1.7-1, 2-1, and 3.5-1 a small exotherm appears at 117<sup>0</sup>C before the main exotherm at 154<sup>0</sup>C. This exotherm decreases in intensity with decreasing phthalic anhydride concentration. The heats of reaction for the curing process are given in Table I.

Table I. DSC Data<sup>a</sup>

<u>Mole Ratio</u>	
<u>Epoxy/Phthalic Anhydride</u>	<u>H (Cal/gram)</u>
No P.A.	-54.
12-1	-51.66
5-1	-49.38
3.5-1	-43.13
2-1	-32.98
1.7-1	-26.00

<sup>a</sup>Catalyst concentration 0.19 mole curazol/mole epoxy resin

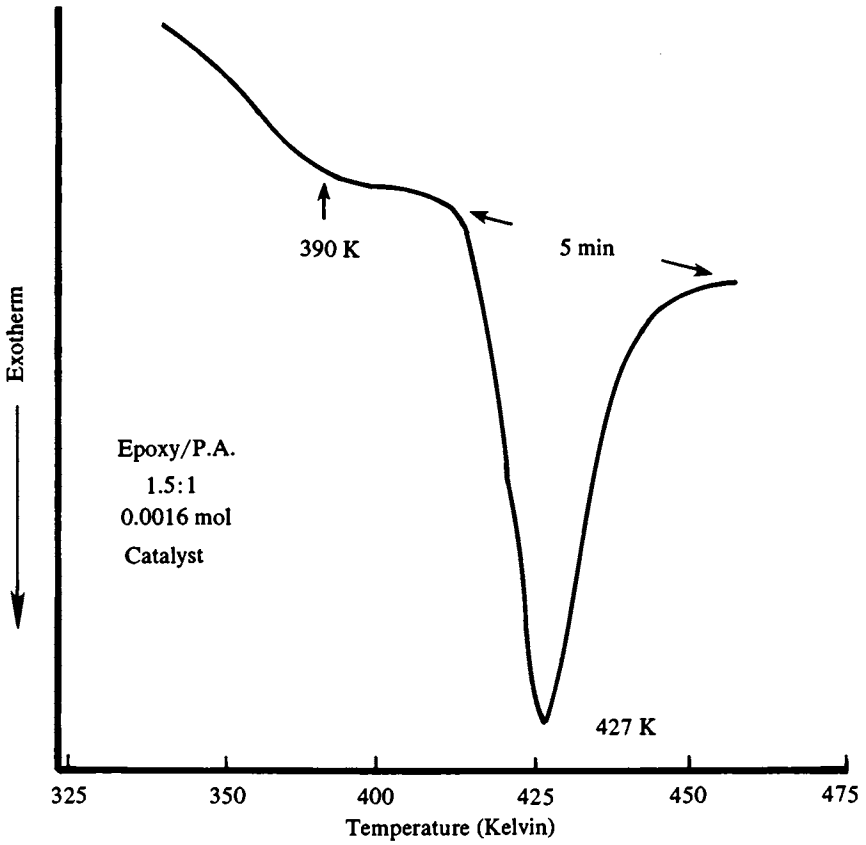


Figure 1. Thermogram of Catalyzed Cure.



Two trends are observed from these data. The heat of reaction decreases with increasing concentration of phthalic anhydride and increases as catalyst concentration is increased. The values obtained are in line with those given by Fava (8) and Malavasic et al. (9). Using somewhat different systems, Fava gives values of 54-87 cal/gram, while Malavasic gives exothermic values of 74-80 cal/gram. When no phthalic anhydride is present, using only the imidazole catalyst, an exothermic value of 54 cal/gram is obtained. Since the latter involves epoxy ring opening and formation of ether crosslinks, it must be assumed that these processes are exothermic. The lower exotherm with the anhydride systems indicates that the heat of formation of the ester linkages is lower than that resulting from ether formation.

The small exotherm at 117°C preceding the main exotherm at 154°C is dependent on the concentration of phthalic anhydride it appearing at higher concentrations of phthalic anhydride. A mixture of phthalic anhydride and imidazole catalyst with no epoxy resin present shows a broad, low exotherm starting at 125°C. This suggests that anhydride ring opening occurs as the first step in the process.

The middle infrared region of the cured crosslinked polymers shows bands in the 3480  $\text{cm}^{-1}$ , the 1200-1300  $\text{cm}^{-1}$  and the 1000-1100  $\text{cm}^{-1}$  region, the latter two increase with phthalic anhydride concentration. A band at 1420  $\text{cm}^{-1}$  along with the 3480  $\text{cm}^{-1}$  O-H stretch band appears in the spectra of the epoxy resin cured with curezol only. This band is a weak band in the uncured epoxy resin and is interpreted to be associated with a secondary hydroxyl group arising from epoxy ring opening (10). Bands at 1080  $\text{cm}^{-1}$  and 1290  $\text{cm}^{-1}$  also are present and are probably the C-O stretch bands of ether crosslinks. Upon the addition of phthalic anhydride new bands appear at 1110  $\text{cm}^{-1}$ , 1160 $^{-1}$  and 1280 $^{-1}$ , which are assumed to be the C-O stretching of ester groups. Whereas the ether and ester bands increase with increasing phthalic anhydride concentration the 1420  $\text{cm}^{-1}$  and 3480  $\text{cm}^{-1}$  hydroxyl bands remain constant.

The near infrared region has been shown to be very useful in studying polymer systems (11, 12). A mixture of epoxy resin and phthalic anhydride before addition of catalyst and heat shows a very strong C-H band in the 2.19  $\mu$  M region which has been shown to be a hydrogen attached to an epoxy group (13). In the 2.16.  $\mu$  M region the C-H bands of the aryl rings appear. The 2.0 - 2.5.  $\mu$ M region is the region of alkyl and aryl C-H combination bands. The second overtone of the 5.7.  $\mu$  M C=O shows up at 1.91.  $\mu$  M which in the mixture is very weak. In addition the first overtone of the 3.5.  $\mu$  M C-H stretch appears at 1.66.  $\mu$  M, and the first overtone of the 2.8.  $\mu$  M O-H stretch is seen at 1.42  $\mu$ M.

Upon addition of catalyst and heat, three changes appear in the near IR spectra. The epoxy band decreases rapidly, the O-H band increases and the C=O band at 1.91 shows a large increase (Tables II and III). Table II shows the effects of phthalic anhydride concentration. Using the 1.66  $\mu$ M band as an internal standard according to the method of Henniker (14), the 1.91  $\mu$ M carbonyl and the 1.42  $\mu$ M hydroxyl were compared to the 1.66  $\mu$ M C-H band. Increasing the concentration of phthalic anhydride causes an increase in the intensity of the carbonyl band which becomes a maximum at a mole ratio of 1.7 to 1. This carbonyl could be due to monoester or diester in the final product. The hydroxyl band at 1.42  $\mu$ M on the other hand remains fairly constant.

Table II. Near Infrared Band Ratios: Effect of Concentration<sup>a</sup>

<u>Epoxy/P.A.</u> <u>Mole Ratio</u>	<u>O-H</u> <u>C-H</u>	<u>C=O</u> <u>C-H</u>	<u>Catalyst</u> <u>Mole x 10<sup>-4</sup></u>
12-1	0.26	0.34	8
	0.39	0.46	12
5-1	0.29	0.38	8
	0.31	0.44	12
3.5-1	0.29	0.58	24
	0.33	0.54	24
2-1	0.35	0.65	28
	0.33	0.43	20
1.7-1	0.38	0.61	32
	0.33	0.64	40

<sup>a</sup>All samples cured at 200°C for 8 min.

A study of curing times is recorded in Table III. Three changes are occurring during the curing process. Initially the epoxy band goes to a minimum within the first minute. The carbonyl increases slowly and attains a maximum after six minutes, while the hydroxyl band increases for one minute and then remains fairly constant.

While the curing process is complex and involves several steps, some of the steps can be deduced from the data described here. The appearance of the exotherm preceding the main exotherm in the DSC suggests that anhydride ring opening occurs as the first step to give a carboxy anion as suggested by Fischer (15). The rapid formation of hydroxyl and decrease of epoxy bands indicates that in the early stages of the curing process, the carboxy anion is leading to epoxy ring opening and the formation of pendant hydroxyl groups. While this is occurring, ether crosslinks are forming, the last part of the curing curve appears to be formation of ester links. The data suggests that the pendant hydroxyl groups are probably not involved in ester formation to any extent.

## Conclusions

DSC, middle IR and near IR data suggest that the crosslinking reaction of an epoxy resin with phthalic anhydride is a stepwise process as follows.

1. anhydride ring opening
2. epoxy ring opening and formation of pendant hydroxyl groups
3. ether links begin to form
4. formation of ester crosslinks

Table III. Near Infrared Data: Effect of Time  
Minutes

	0	1	2	6
<u>160°C</u>				
<u>C=O</u>				
<u>C-H</u>	0.	0.	0.09	0.54
<u>O-H</u>				
<u>C-H</u>	0.26	0.51	0.37	0.41
<u>Epoxy</u>				
<u>C-H</u>	0.47	0.17	0.11	0.13
<u>200°C</u>				
<u>C=O</u>				
<u>C-H</u>	0.	0.14	0.15	0.50
<u>O-H</u>				
<u>C-H</u>	0.26	0.31	0.32	0.44
<u>Epoxy</u>				
<u>C-H</u>	0.47	0.10	0.10	0.08

## Literature Cited

1. Fisch, W.; Hofmann, W. Makromol. Chem. 1961,44,8.
2. Shechter, L.; Wynstra, J. Ind. Eng. Chem. 1956,48,86.
3. Kannebly, G. Kunststoffe. 1957,47,693.
4. Fischer, R.F. J. Polym. Sci. 1960,44,155.
5. Arnold, R.J. Mod. Plast. 1964,41,149.
6. Batzer, H.; Porret, D.; Lohse, F. Makromol. Chem. 1966,91,195.
7. Instructions for Differential Scanning Calorimeter, Perkin-Elmer, Norwalk, Conn. April 1974.
8. Fava, R.A. Polymer. 1968,9,137.
9. Malavasic, T.; Moze, A.; Vizovisek, I.; Lapanje, S. Makromol. Chem. 1975,44,89.
10. Meloan, C.E. "Elementary Infrared Spectroscopy". Macmillan Company. New York, NY 1963.
11. Crandall, E.W.; Johnson, E.L.; Smith, C.H. J. Appl. Polym. Sci. 1975,19, 897.

12. Crandall, E.W.; Jagtap, A.N. *J. Appl. Polym. Sci.* 1977,21,449.
13. Goddu, R.F.; Delker, D.A. *Anal. Chem.* 1953,30,2013.
14. Henniker, J.C. "Infrared Spectroscopy of Industrial Polymers", Academic Press, London and New York, 1967, p. 153.
15. Fischer, F.R. *Ind. Eng. Chem.* 1960,52,321.

RECEIVED May 10, 1983

## Chemiluminescence of Thermosetting Resins

CLARENCE J. WOLF, DALE L. FANTER, and MICHAEL A. GRAYSON  
McDonnell Douglas Research Laboratories, St. Louis, MO 63166

The use of organic materials in modern aerospace systems encompasses a wide variety of applications ranging from elastomers and sealants to structural members. The long-term stability of these materials, particularly when exposed to the hostile environment of present-day aircraft, is not known. By many standards, these materials are considered stable; the deleterious reactions are slow, requiring many years to cause component-failure. Realistic test procedures and methods are required that can reliably predict the long-term properties of these materials based on short-duration tests. Chemiluminescence, sometimes called oxyluminescence, was used to monitor chemical and physical changes in the epoxy resin system, MY720/Eporal (Ciba-Geigy). Test coupons were exposed to accelerated aging conditions in which the temperature, humidity, and external tensile stress were varied over a considerable range. Chemiluminescence (CL) intensity-temperature-time (ITt) profiles of all aged resin coupons were measured. Changes in ITt profiles of the aged resin samples were related to changes in the chemical and mechanical properties of the resin system.

Polymers and composites are finding ever-increasing use as structural components in aerospace systems because of their attractive strength/weight characteristics. During the past 20 years, their use in military aircraft has increased from essentially zero in F-4 jets to over 25% in the advanced AV8-B Harrier II. Thermosetting resins, particularly epoxies and polyimides, are of prime interest for use in structural applications.

The aerospace industry has developed fabrication and testing procedures for resins that are radically different from those traditionally used with metals. However, little is known about the long-term durability of these relatively new nonmetallic composites, and their full potential has not been realized. By most standards, these materials are considered extremely stable, and if deleterious aging reactions occur, they are slow, requiring many years to cause component failure.

0097-6156/83/0227-0121\$06.00/0  
© 1983 American Chemical Society

Because of the slow reaction rates, even under accelerated aging conditions, sensitive methods are required to measure these effects. Recently, new and highly sensitive physical-analytical techniques have been developed which may be useful in describing both the chemical and physical aging processes in organic-matrix composite materials. The chemical reactions which occur within the resin systems vary from oxidation to cross-linking and may result from a variety of external factors such as heat or ultraviolet radiation. In many instances the morphology of the resins change because of relaxation processes, i.e., the free volume of the system changes, which occurs after the resin is cured.

Normally, accelerated aging tests are conducted by exposing the sample to a specific environment at high temperature for short periods, possibly as long as several months. The short-time, high-temperature, high-intensity data then are extrapolated to the environmental-use envelope for the corresponding long service periods. Since the aging mechanism at high temperature may not be identical to the mechanism operative at service conditions, such extrapolations are suspect; therefore the results of accelerated aging experiments are of questionable validity. Realistic test procedures and methods are required that can reliably predict the long-term properties of these materials from short-duration (weeks to months) tests.

A relatively new analytical technique, chemiluminescence (CL), is an ultrasensitive technique, and it has been reported that reaction rates as low as  $10^{-14}$  mole/year can be measured (1-5). Thus, it could monitor the aging reactions on a real-time basis while the resins are exposed to a simulated service environment. If the method can be shown to be sufficiently sensitive and reliable, the errors inherent in extrapolating accelerated aging data to the actual conditions encountered can be eliminated (6-8).

## Experimental

**Resin Components:** Epoxy resins used in this study were fabricated from the same components employed to prepare most of the commercially available graphite-epoxy prepreg resins used in military aircraft, namely Narmco 5208, AS 3501-6, Hercules 3501-5, and Fiberite 934. The epoxide (MY720, Ciba-Geigy) and amine hardener (Eporal, Ciba-Geigy) were obtained from the manufacturer in quantities sufficient for fabricating all samples used in the experimental program. As recommended by the manufacturer, MY720 was stored at  $-20^{\circ}\text{C}$  until needed. Eporal was stored in a sealed container at room temperature until needed. Both the epoxide and hardener were used without further purification.

**Resin Preparation:** Approximately 1 kg of MY720 was heated briefly to  $70^{\circ}\text{C}$  and mixed with 27 parts Eporal per hundred parts (phr) MY720. The temperature was gradually increased to  $150^{\circ}\text{C}$  while stirring to facilitate mixing. The mixture was cooled to room temperature, stored at  $-20^{\circ}\text{C}$ , and used as a master batch.

**Mold Fabrication:** Fifteen silicone rubber molds were cast from a master stainless steel template machined in the shape of a dogbone with gauge dimensions of 4 x 12 x 25 mm. The grip portion of the sample was terminated in a

cylindrical shape. The molds were cast according to the method described by Fanter (9). A two-part silicone-rubber casting material (RTV-664, General Electric) was poured into a form containing the pattern and cured at room temperature for 24 h. The molds were post-cured at 177°C for 5 h.

**Casting:** The silicone-rubber molds and premixed resin were heated to 150°C prior to casting. After the Eporal was totally dissolved, the resin was deaerated in a vacuum bell jar, reheated to 150°C, and poured into the preheated molds. The samples were cured for 1 h at 150°C, followed by 5 h at 177°C; then the oven was turned off and the samples were allowed to cool slowly to room temperature.

**Chemiluminescence:** The CL detection system is shown in Figure 1. Samples can be exposed to selected combinations of atmosphere, temperature, and tensile stress while measuring the luminescence emitted from the sample (6). Generally, air or oxygen is used to purge the sample chamber. A gearmotor, belt, and worm-drive mechanism apply tensile stress to the sample through two grips attached to cylinders cast in the tensile coupons. Tensile loads up to 100 kg can be applied to polymer coupons and are recorded by the load transducer attached to the fixed grip. Electrical pulses from the photomultiplier tube (PMT) are processed by an amplifier/discriminator and counted for selected times by a photon counting system (E.G.&G., Princeton Applied Research, models 1121 and 1112). Sample surface temperatures are measured directly by a thermocouple and digitized for computer processing.

A microcomputer (Digital Equipment Co. MINC 23 and VT105 CRT terminal) controls the experiment and processes the data (10). The CL experimental variables, photon counts per second, sample temperature, stress, and strain, are monitored continuously by the computer and recorded at selected time intervals for closed-loop control of the CL experiment and subsequent off-line storage on flexible disk.

**Environmental Chamber:** The samples were aged in an environmental exposure chamber (Tenney model BTRS) which is capable of operating and maintaining (up to several months) a hot, humid atmosphere which can be varied to 100°C while the relative humidity can be varied from 20 to 98% (for temperatures up to 85°C). The internal dimensions of the chamber are 0.5 x 0.5 x 0.5 m permitting the simultaneous aging of many specimens mounted in stress rigs.

**Mechanical Loading:** A mechanical load was applied to approximately half of the samples during environmental exposure. The shape of the molded samples matched slots in the stress rig so that the sample slides into the stress rig. The design of the rig and the shape of the molded samples are such that the sample is automatically aligned when it is installed in the stress rig.

The total force applied to the sample in the stress rig was determined immediately prior to loading the sample. A load transducer was installed in the stress rig, and the torque on the loading nut, which gives the desired total force on the sample, was determined. The sample was then installed in place of the

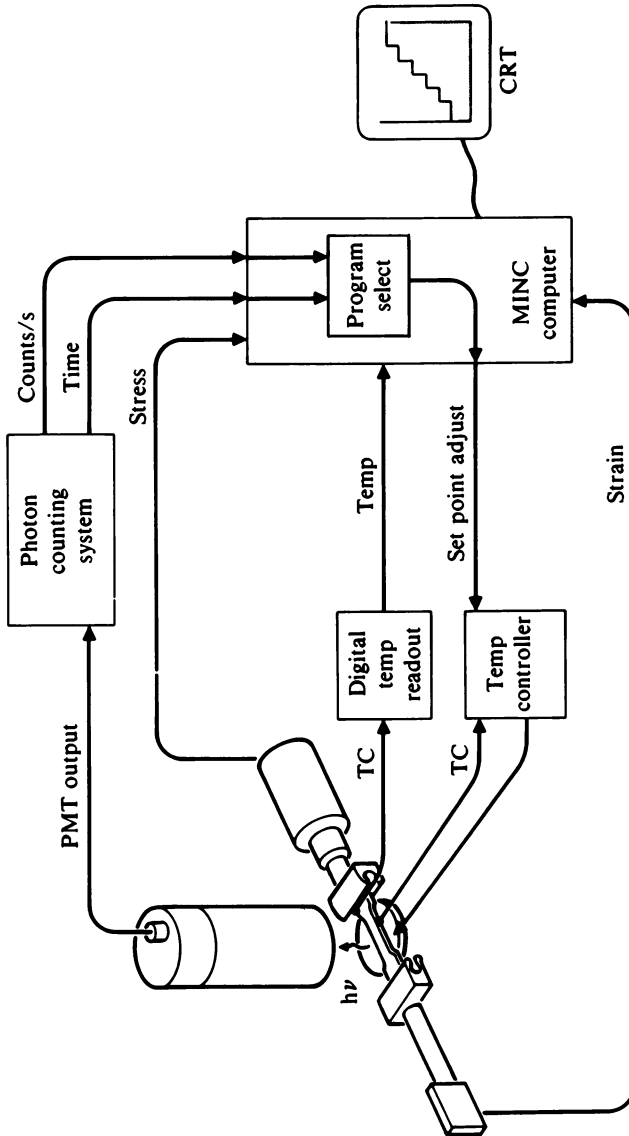


Figure 1. Block diagram of the CL system.



load transducer, and the nut was tightened to the desired torque. A spring in the stress rig minimizes changes in tensile load during the experiment.

**Chemical Analysis:** One of the primary objectives of this program was to carefully monitor microchemical changes that occur in the resin system during the aging processes; therefore sensitive methods were required to characterize the starting materials, the fresh and the aged resin.

**Liquid Chromatography:** Resin coupons used throughout this program were prepared from a single batch of epoxy resin, MY720 and Eporal. These starting materials were characterized by liquid chromatography. The analyses were conducted with a liquid chromatograph (Spectra Physics 8000) containing a 9.4 mm diam x 50 cm column (Whitman Partisil Magnum-9).

The solvent was acetonitrile/water in the gradient elution mode; the gradient ranged from 20% to 100% acetonitrile in 130 min. The MY720 was approximately 72% tetraglycidyl-diaminodiphenyl methane and contained six other compounds, primarily higher-molecular-weight analogs and triglycidyl derivatives whose concentrations ranged from 1.5% to 14%. The Eporal was approximately 91% pure diaminodiphenyl sulfone and contained four major impurities whose concentrations ranged from less than 1% to almost 4%.

TGDDM was purified by preparative liquid chromatography (11). Fifty-gram aliquots of MY720 were dissolved in 1000 mL dichloromethane and separated with a preparative liquid chromatograph (Waters model 500A). Two columns (Waters Prep/Pak 500/Silica) were connected in series, and the solvent flow rate was 50 mL/min. The effluent from the entire chromatographic separation was collected in seven 1000 mL aliquots. The solvent was evaporated using gentle heating under reduced pressure in a rotary evaporator (Polyscience V-1). The sample residues were analyzed by mass spectrometry. Approximately 20 g of TGDDM (96% pure) was recovered from each separation. The clear, light-colored TGDDM was stored at  $-15^{\circ}\text{C}$  until used.

A new set of columns was used for each separation. The columns were contaminated with at least three higher-molecular-weight components, which appeared as two well-resolved purple bands and a yellow band. These compounds were held tenaciously by the packing material and could not be removed by extended  $\text{CH}_2\text{Cl}_2$  extraction in a Soxhlet extractor.

**Vaporization Gas-Chromatography/Mass-Spectrometry:** Vaporization gas-chromatography/mass-spectrometry (Vap GC/MS) is a technique developed at MDRL specifically to analyze for trace compounds in an intractable matrix (12).

Thin shavings, approximately 10–20  $\mu\text{m}$  thick, were milled from the aged resin coupons. The shavings were placed in a tared quartz tube, weighed, and connected to flowing helium in the gas chromatograph. Volatile compounds desorb from the sample shavings when they are inserted into the heated region of the Vap CG oven. The compounds are transferred by the carrier gas to an in-line low-temperature trap. The sample can be heated at any temperature from ambient to  $250^{\circ}\text{C}$  for periods as long as several hours. Chromatographic analysis

is accomplished by removing the sample from the heated zone, heating the column trap, and starting the chromatographic temperature program. The GC column is interfaced with a MS-30 mass spectrometer (Kratos, formerly AEI) for compound identification. Vap GC is extremely sensitive, permitting the qualitative detection of as little as  $10^{-9}$  g of volatile compound per gram of resin.

## Results

The CL intensity-temperature-time (ITt) profiles of resin coupons aged for various periods of time, temperature, humidity, and tensile stress were measured. ITt profiles of resin coupons were measured immediately after removal from the fabrication mold and after selected aging. In the plots and all ITt profiles, the temperature (T) of the sample during CL measurement is shown by a dashed line (the temperature scale is the left ordinate), the CL intensity by the solid line (intensity flux is the right ordinate), and, on the abscissa, the time (t) after the measurement commenced. A ITt profile of a resin coupon measured immediately after removal from the fabrication mold is shown in Figure 2.

The initial peak that occurs when the sample is inserted in the CL chamber is highly variable and depends upon many factors including the photochemical history of the sample; therefore it is not used for analysis and is disregarded. A sharp increase in CL intensity occurs each time the temperature is increased; these CL peaks are specified by a subscript. For example,  $CL_{50-65}$  refers to the intensity of the CL peak observed when the temperature is increased from  $50^{\circ}$  to  $65^{\circ}\text{C}$ . The peaks from both the  $49^{\circ}$  to  $62^{\circ}\text{C}$  and  $62^{\circ}$  to  $74^{\circ}\text{C}$  thermal transitions are rather sharp and have half-widths of approximately 100 s. Aging, even for relatively short periods of time, broadens these peaks.

The ITt profile of the uncured resin components, MY720 and Eporal (DDS), are considerably different. The CL intensity from the unpolymerized MY720 is an order-of-magnitude greater than that observed in the cured resin and, the general shape of the ITt profile is different. The CL intensity from Eporal is small, approximately three orders-of-magnitude less than that observed in the MY720 and two orders-of-magnitude less than that found in the resin. Although the CL intensity from Eporal is low, the curve follows the same general shape noted in the resin. The differences in intensity and form of the ITt profile from MY720, Eporal, and the cured resin show that the CL observed from the cured resin is a property of the resin and is not due to either unpolymerized MY720 or Eporal.

The origin of the CL in the resin system was investigated by separating the MY720 into several fractions and measuring the CL of each. Since MY720 is a complex mixture whose main constituent is TGDDM, the ITt profiles of coupons prepared from neat MY720 and pure TGDDM (cured with DDS) were measured and compared.

The reproducibility of the CL method is clearly indicated by the data given in Table I. The intensities of the peaks corresponding to the temperature changes  $60^{\circ} \rightarrow 80^{\circ}$ ,  $80^{\circ} \rightarrow 100^{\circ}$ , and  $100^{\circ} \rightarrow 120^{\circ}$  are essentially identical for three independent resin samples prepared from both MY720 and TGDDM; the standard deviation of the intensities is approximately 5%. The ratio of the CL intensity

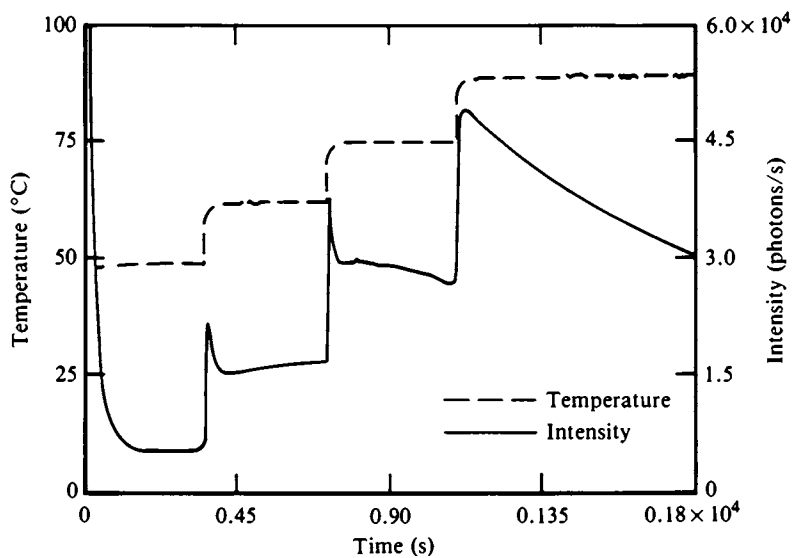


**Figure 2.** Chemiluminescence intensity-temperature-time profile for resin directly after removal from mold.

**Table I. CL peak intensity from MY720 and pure TGDDM resin after casting.**

Sample	Peak	Peak	Peak
	60 – 80° (x 10 <sup>3</sup> )	80 – 100° (x 10 <sup>3</sup> )	100 – 125° (x 10 <sup>3</sup> )
MY720	44.8	60.2	103.2
	42.4	59.2	102.0
	41.4	58.4	95.4
	average* 42.9 ± 1.7	59.3 ± 0.9	100.0 ± 4.2
Pure TGDDM	63.2	73.0	140.0
	65.6	76.0	132.4
	67.2	81.8	135.2
	average 65.3 ± 2.0	76.9 ± 4.5	135.9 ± 3.8

\*Includes standard deviation

GP21-0920-13

observed in the resin prepared from MY720 to that prepared from TGDDM for each of the three peaks is summarized in Table II. The average peak ratio is 72% which is consistent with the hypothesis that the primary source of CL arises from the TGDDM (which comprises approximately 70% of MY720).

The ITt profiles for the resin aged at 85°C in an air atmosphere with 50% humidity in the absence of applied tensile stress are shown in Figure 3; samples aged for 5, 21, 50.5, 68, 168, 240, 365, 650, and 1008 h are shown in Figure 3. The CL intensity decreases as a function of aging, and the peaks change from relatively sharp spikes to much broader peaks. The CL peak intensities from the 50° to 62°C, the 62° to 76°C, and the 76° to 90°C thermal transitions as well as the constant intensity regions, i.e., the plateau, all decrease during environmental aging. The decrease suggests that CL and aging are inversely related. A plot of the reciprocal of the peak CL intensity from the 62° to 76°C thermal transition as a function of aging time ( $\tau_A$ ) is shown in Figure 4. The least-squares fit to the data is shown by the solid line, which corresponds to the equation:

$$[\text{CL} - \text{CL}_0]_{85^\circ, 50,0}^{-1} = 2.69 \times 10^{-7} \tau_A + 2.08 \times 10^{-5} \quad (1)$$

**Table II. Ratio of CL peak intensity in MY720 to pure TGDDM.**

	Average CL intensity		
	$I_{\text{Pk}60-80^\circ}$	$I_{\text{Pk}60-100^\circ}$	$I_{\text{Pk}60-125^\circ}$
$\frac{\text{MY720}}{\text{Pure TGDDM}}$	0.66	0.77	0.74

$$\text{Ratio: } \frac{\text{MY720}}{\text{Pure TGDDM}} = 0.72 \pm 0.06$$

GP21-0920-14

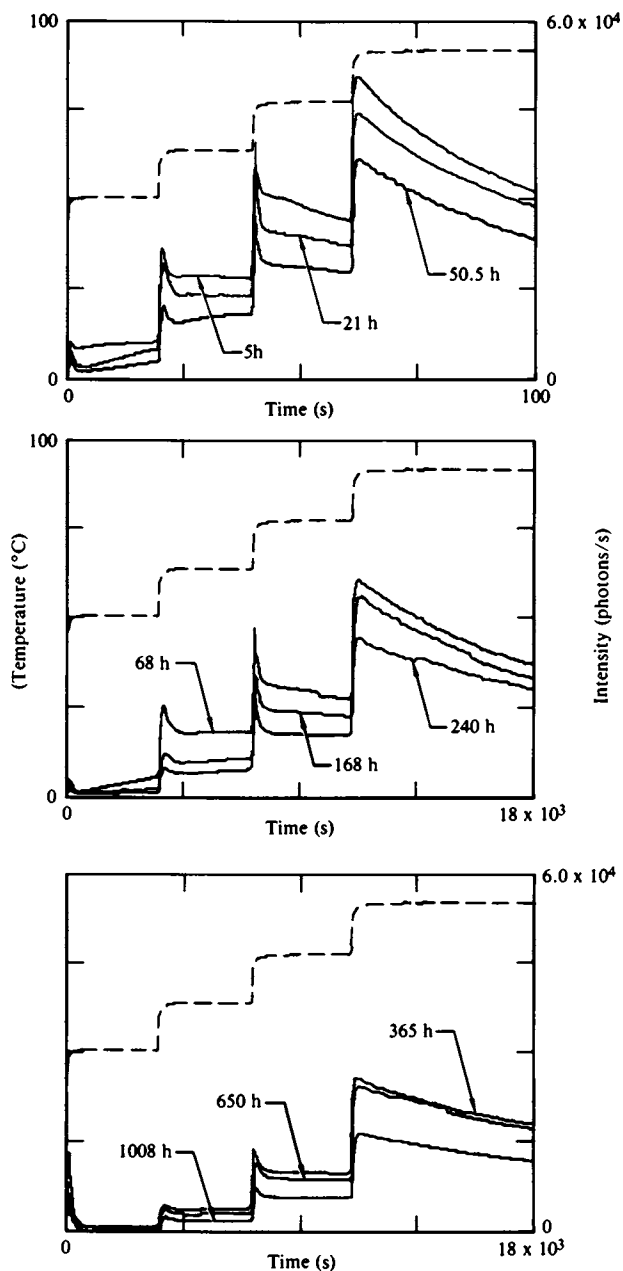


**Figure 3. Chemiluminescence intensity-temperature-time profiles for resin aged at 85°C and 50% RH in the absence of mechanical stress.**

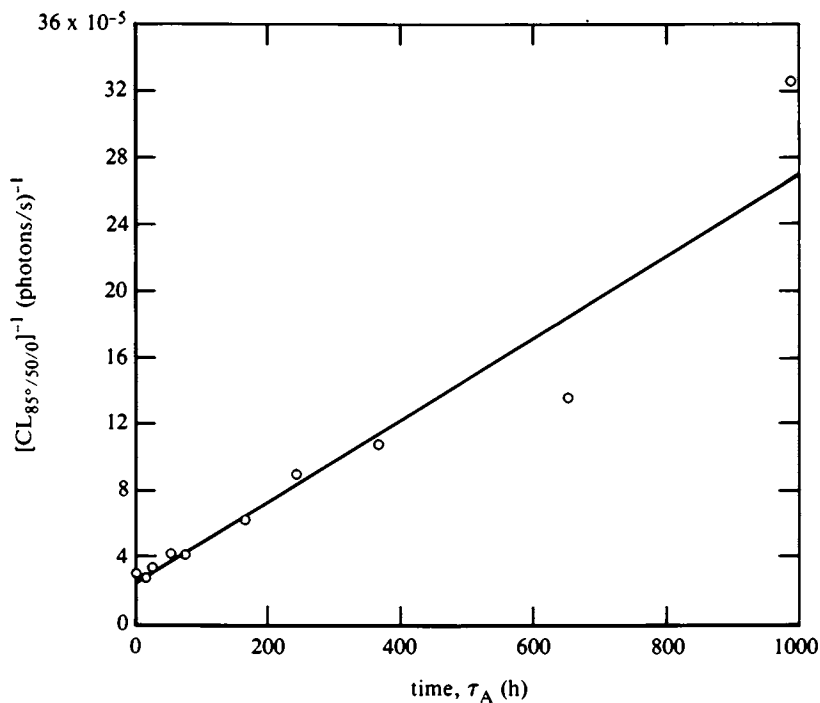


**Figure 4.** Reciprocal of the chemiluminescence peak (corresponding to the 60°C to 70°C temperature change) as a function of aging time at 85°C and 50% RH in the absence of mechanical stress.

where CL is the intensity in photons/s,  $CL_0 = 5000$  photons/s, and time ( $\tau_A$ ) is in hours. All the aging data can be treated in a similar fashion. CL analyses also were performed on resin samples aged at 85°C in a dry atmosphere (less than 2% RH) and in the presence and absence of external mechanical stress (stressed in tension to 50% of the ultimate tensile stress (UTS)).

The data summarizing the linear relationship between the reciprocal of the CL peak intensity and the aging time are given in Table III where the slope of the line is given for each of the environmental aging conditions investigated. The samples exposed to the dry environment exhibit considerably smaller slopes than those exposed to a humid environment. The reason(s) for this difference is not known, but it may result from one of two factors: (1) wet samples age faster and undergo more bond cleavage, or (2) oxygen is more soluble in the wet resin, thereby increasing the rate of chemiluminescence.

**Table III. Summary of coefficients relating aging time at 85°C to reciprocal chemiluminescence intensity.**

Temp (°C)	Humidity (%)	Stress (UTS) (%)	Coefficient (s/photon-h)
85	0	0	$0.54 \times 10^{-7}$
85	0	50	0.99
85	50	0	2.69
85	50	50	1.14

The activation energies (actually the temperature coefficients in an Arrhenius plot) for the change in CL intensity accompany each temperature increase, i.e., the peaks in the ITt profile, were calculated and are summarized in Table IV. The activation energies for the three peaks, corresponding to a temperature change from 50° to 65°C ( $\Delta E_{50-65^\circ}$ ), from 65° to 75°C ( $\Delta E_{65-75^\circ}$ ), and from 75° to 90°C ( $\Delta E_{75-90^\circ}$ ), are given. Although the peak intensity decreases appreciably during the aging process, the activation energies for the production of CL from each thermal transition is essentially unchanged during aging. The result indicates that the mechanism responsible for the production of CL does not change appreciably during aging, which suggests that CL can be used over a broad temperature range for real-time studies. A summary of the average activation energies and standard deviation ( $1\sigma$ ) for the three CL peaks observed in the resin samples aged at 85°C is given in Table V.

The ITt profiles from the resin aged at 150°C while stressed to 50% UTS for 136, 357, and 744 h is shown in Figure 5. The ITt profiles from coupons aged at 150°C in the absence of stress is quite similar but is not shown. The CL from samples aged at 150°C, even for relatively short periods of time such as 130–160 h,

**Table IV. Activation energies for the production of chemiluminescence from resin aged at 85°C.**

Aging Time (h)	Humidity (%)	Stress (UTS) (%)	$\Delta E_{50-65^\circ}$ (kJ/mole)	$\Delta E_{60-75^\circ}$ (kJ/mole)	$\Delta E_{75-90^\circ}$ (kJ/mole)
183	0	0	135	123	89
406	0	0	121	109	96
696	0	0	112	109	84
1152	0	0	121	114	91
167	0	50	133	133	84
432	0	50	110	107	89
696	0	50	110	98	79
5	50	0	95	79	51
21	50	0	96	81	53
505	50	0	103	81	56
68	50	0	103	81	60
168	50	0	109	91	68
240	50	0	109	95	67
650	50	0	126	112	84
1008	50	0	107	89	72
984	50	50	119	102	86
1560	50	50	103	105	77
2448	50	50	100	96	86
4056	50	50	123	119	98

**Table V. Average activation energies for the production of chemiluminescence from aged resin.**

Aging temp (°C)	Humidity (%)	Stress (UTS) (%)	$\Delta E_{50-65^\circ}$ (kJ/mole)	$\Delta E_{60-75^\circ}$ (kJ/mole)	$\Delta E_{75-90^\circ}$ (kJ/mole)
85	0	0	122 ± 10	114 ± 6	87 ± 3
85	0	50	117 ± 12	112 ± 19	84 ± 5
85	50	0	105 ± 10	88 ± 11	64 ± 11
85	50	50	112 ± 11	107 ± 9	86 ± 9



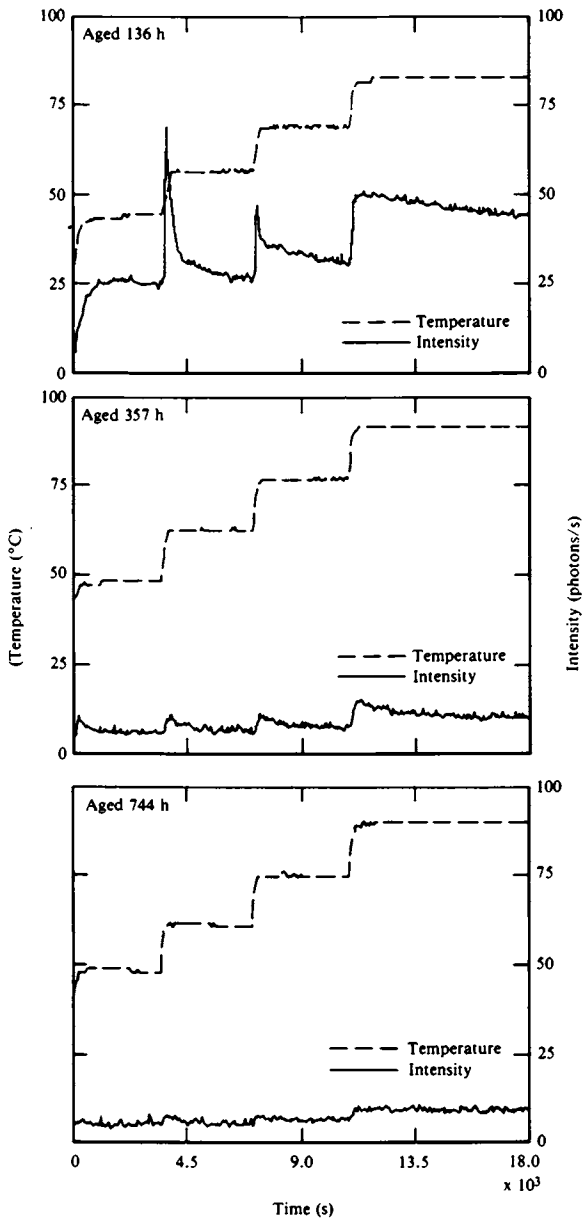


**Figure 5.** Chemiluminescence intensity-temperature-time profiles of the resin as a function of aging time at 150°C while stressed to 50% UTS.

is reduced markedly from that of samples aged at lower temperatures. The overall CL intensity at any point in the ITt profile is approximately three orders-of-magnitude less than that observed in ambient aged coupons. The general form of the ITt profile is different from that observed from samples aged at lower temperatures. The maximum CL peak intensity occurs at the 50–60°C thermal transition, and CL does not increase with temperature. After aging for 200–300 h, the CL intensity is essentially equal to that of the background.

In addition to major changes in CL, the mechanical properties of the resin aged at 150°C are reduced significantly. Three of the samples aged at 50% UTS for time intervals greater than 500 h broke while in the environmental oven. All the samples, even those stored for 130 h, were markedly darker than the unaged samples. Aging at 150°C drastically changed the chemical and physical properties of the resin even though the samples were post cured at 177°C for 5 h.

**Vaporization Gas Chromatography and Mass Spectrometry of Aged Resin:** The volatile low-molecular-weight compounds indigenous to the cured resin were determined by Vap GC. All samples were ground to uniform size prior to analysis to minimize differences resulting from inhomogeneities within the resin. The compounds released following a controlled heating were separated by gas chromatography and identified by mass spectrometry. A single sample was sequentially heated at the same temperature to yield a series of chromatograms indicating both the composition and quantity of volatile compounds released.

A series of Vap GC analyses on approximately 50 mg of all the aged resin samples was conducted. Ethanal, propanal, isobutyraldehyde, propenal, butenal, methyl ethyl ketone (MEK), and methyl penetenal were positively identified by mass spectrometry. With the exception of MEK, all compounds identified (the major products) were aldehydes. Methyl ethyl ketone, the solvent used in MY720, remains even after cure. The aldehydes, however, are not impurities in either the MY720 or DDS and represent compounds which are characteristic of the resin alone. These compounds are either produced during the curing process or are formed from the thermal decomposition of a labile compound which is formed during cure.

A typical set of chromatograms of the compounds released from an aged resin is shown in Figure 6. The compounds released after heating for 20 min at 125°C is shown in Figure 6a. The chromatograms from the second and third heating at 125° are shown in Figure 6b and 6c, respectively. The total quantity of material released from the second and third heating is an order-of-magnitude less than that from the first. The resin then was heated to 175°C for 20 min, and the chromatogram of the products is shown in Figure 6d; the chromatogram of the compounds collected from the second and third 20 min heating at 175°C are shown in Figure 6e and 6f, respectively. The large increase in the amount of propenal observed from the resin heated at 175°C compared with that observed from the third heating at 125°C suggests that propenal is thermally produced at 175°C.

An analysis of the Vap GC data from a series of resin samples aged at 85°C in the presence and absence of moisture and/or external tensile stress shows three compounds of particular interest: MEK, propanal, and propenal. The normalized

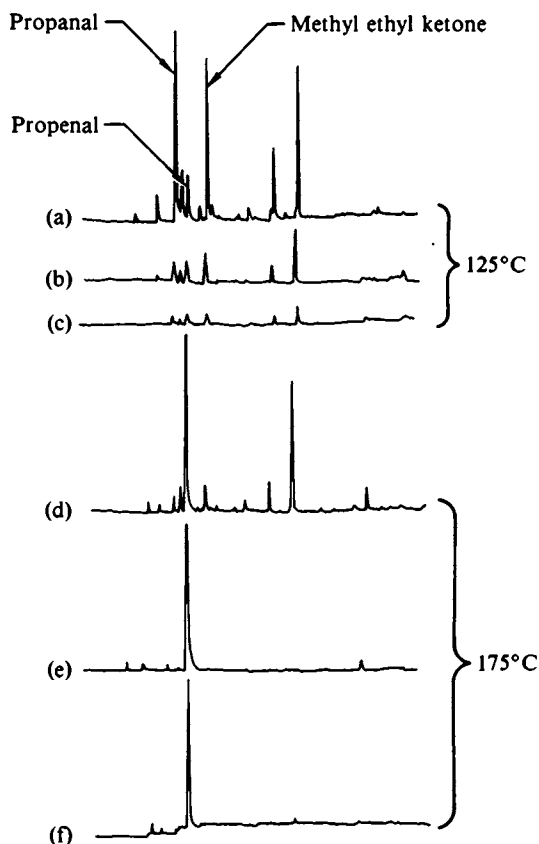


**Figure 6.** Vaporization gas chromatograms of the compounds released from the resin aged for 169 days at 85°C in a humid atmosphere (50% RH) in the absence of external stress. The sample was successively heated for (a) 20 min at 125°C, (b) a second heating for 125°C at 20 min, (c) a third heating for 20 min at 125°C, (d) 20 min at 175°C, (e) a second heating for 20 min at 175°C, and (f) a third heating for 20 min. at 175°C.

quantities (i.e., the chromatographic peak area divided by the weight of the powdered resin analyzed) of propanal, and propenal released during each of the six heating periods (three at 125°C and three at 175°C) are shown in Figure 7, respectively. Although only methyl ethyl ketone is not shown in the figure, relatively large quantities of both MEK and propanal were released during the first heating at 125°C, but little was released during subsequent heating at either 125° or 175°C. This result suggests that both of these compounds are indigenous volatile materials trapped in the resin matrix at the time of cure. The release of propenal is, however, quite different; the quantity released at 175°C is considerably greater than that released at 125°C for all samples investigated. The most pronounced difference occurred in the resin aged for 48 days in a dry atmosphere in the absence of mechanical stress. The ratio of the quantity released at 175°C to that released at 125°C is essentially the same regardless of the aging environment. These ratios together with the calculated temperature coefficients (activation energies) for propenal production from 125° to 175°C are summarized in Table VI. The average value of the ratio of the quantities released at 175°C to that released at 125°C is 25.6, and the corresponding activation energy and its standard deviation ( $1\sigma$ ) is  $96 \pm 4$  kJ/mole. It is not likely that the propenal observed in the Vap GC experiments is the result of residual material trapped in the matrix. Several observations support this hypothesis: 1) little propenal was observed during Vap GC analysis of unpolymerized MY720, 2) the amount of propenal released at 175°C is 25 times greater than that released at 125°C, and 3) propenal is a relatively reactive, unstable liquid at room temperature (13). Propenal may be formed by the decomposition and subsequent arrangement of the unreacted glycidyl group or by the cyclization of two neighboring glycidyl groups followed by subsequent decomposition.

**Table VI. Activation energies for the release of propenal from aged resin samples.**

Aging conditions					
Temp (°C)	Humidity (%)	Stress (UTS) (%)	Time (days)	Ratio propenal released at 175°/125°	$\Delta$ (kJ/mole)
85	0	0	48	27.1	98
85	0	50	49	27.3	98
85	50	50	196	26.0	96
85	50	0	169	19.5	88
85	50	0	195	28.3	99
Average				(25.6 ± 3.5)	(96 ± 4)

GP21-0920-20

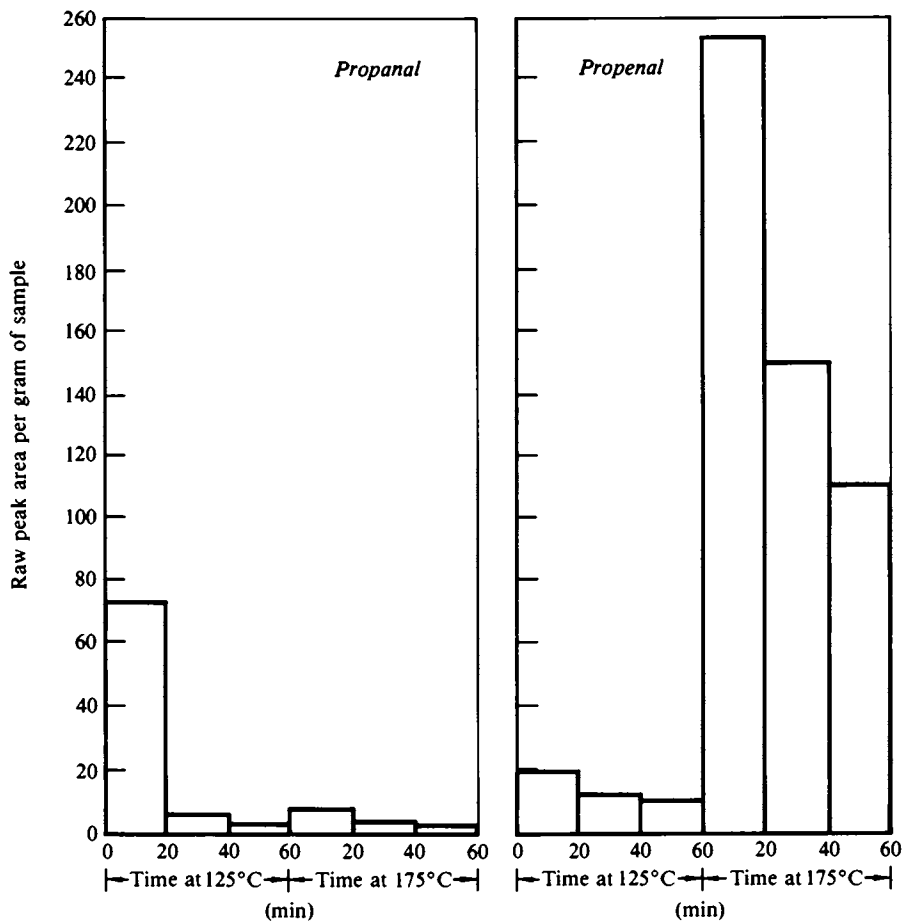


Figure 7. Volatiles released from epoxy resin.

## Discussion

Chemiluminescence (CL) intensity-temperature-time (ITt) profiles of the aged resin were measured at four temperatures. The reciprocal of the maximum CL intensity occurring at each temperature increment was a linear function of the environmental aging period ( $\tau_A$ ). Vaporization gas chromatography (Vap GC) measurements of the aged resins indicate that propenal (acrolein) is formed during the relatively low-temperature thermal aging ( $\sim 150^\circ\text{C}$ ). The activation energies for the CL process and propenal production are similar, approximately 90–105 kJ/mol, and suggest that the reaction(s) forming propenal may be involved in the production of CL. These observations are consistent with the general hypothesis that the glycidyl group is responsible for both CL and propenal production.

The data indicate that the mechanism responsible for the CL production in this resin system does not change appreciably within the temperature range investigated, i.e., up to  $90^\circ\text{C}$ . This result suggests that CL may be a good method to monitor real-time aging within the service environment.

## Acknowledgment

This work was supported by the Naval Air Systems Command under contract N00019-80-C-0102.

## Literature Cited

1. Nathan, R. A., Mendenhall, G. D., and Hassell, J. A., "Application of Chemiluminescence to the Characterization of Polymeric Materials," in **Proceedings of the TTCP-3 Critical Review: Techniques for the Characterization of Polymeric Materials** (Army Materials and Mechanics Research Center, 1977), p. 123.
2. Fanter, D. L., and Levy, R. L., *Chemtech* 1979 **9**, 682.
3. Fanter, D. L., and Levy, R. L., *Organic Coatings and Plastics Chem.* 1978 **39**, 599.
4. Fanter, D. L., and Levy, R. L., "The Application of Chemiluminescence for the Study of Polymer Mechanochemistry," **Durability of Macromolecular Materials** (R. K. Eby, Ed.) (American Chemical Society, Washington, DC, 1979), p. 211.
5. Fanter, D. L., Levy, R. L., and Wolf, C. J., 15th American Chemical Society Midwest Regional Meeting, St. Louis, MO (Nov 1979).
6. George, G. A., **Use of Chemiluminescence to Study the Kinetics of Oxidation of Solid Polymers** (N. Grassie, Ed.) Applied Science, London, 1981), Chap. 6.
7. George, G. A., *Polymer. Deg. Stabil.* 1979, **1**, 217.
8. Wolf, C. J. and Fanter, D. L., "The Use of Chemiluminescence to Monitor the Aging Processes in Polymers and Composites," in **Proceedings of the Critical Review; Techniques for the Characterization of Composite Materials** (Army Materials and Mechanics Research Center, 1982), p. 311.

9. Fanter, D. L., *Rev. Sci. Instru.* 1978, **49**, 1005.
10. Brennenstuhl C., and Fanter, D. L., **Proc. Digital Equipment Computer User's Society** (Digital Equipment Corporation, Maynard, MA, 1981), Vol. 7, p. 1049.
11. Hagnauer, G., *Ind. Res. and Dev.* 1981 (April) 128.
12. Levy, R. L., Wolf, C. J., and Oro', J., *J. Chromatogr.* (1970) **8**, 524.
13. According to L. F. Fieser and M. Fieser [**Organic Chemistry**, (D. C. Heath and Co. Boston, 1950) p. 200], Acrolein (the old name for propenal) is a highly reactive, volatile liquid with a sharp irritating odor and a marked tendency to polymerize.

RECEIVED May 10, 1983

# Poly(*n*-Butyl Methacrylate) and Poly(Butyl Methacrylate-co-Acrylic Acid) Films Dried from Solutions of Hydrogen Bonding Capability

MICHAEL S. CHUU, CARL J. KNAUSS, RICHARD J. RUCH, and  
RAYMOND R. MYERS

Department of Chemistry, Kent State University, Kent, OH 44242

The adhesion and wettability of thin films of poly(*n*-butyl methacrylate)(PBMA) and (butyl methacrylate/co-acrylic acid)(AA/BMA) cast from various solvents was studied. Most PBMA films showed adhesive failure regardless of the solvent from which they were cast. The AA/BMA films showed better adhesive properties when cast from the hydrogen-bonding solvents *t*-butanol and *p*-dioxane. Wetting by water of AA/BMA films indicated that in freshly contacted films, the wettability increased due to the exposure of the polar carboxyl groups, as the hydrogen-bonding capability of the solvent increased. Longer exposure time to water leveled the availability of hydrophilic groups at the film/air interface.

The copolymerization of species having hydrophilic side groups with hydrophobic monomer units has led to the development of water-dispersible coatings of considerable promise. The morphology of these polymers and the orientation that takes place at the interface are of particular importance, for organic cosolvents are used in the copolymer synthesis and also as solubilizers.

Water-thinnable acrylic polymers dissolved in cosolvent aggregate on dilution. The aggregates are highly swollen with water in the region of the functional groups and with cosolvent around the hydrophobic backbone. Clearly, the nature of the cosolvent-water-polymer interaction is a major factor in the polymer conformation. The effect on the orientation of the carboxyl groups, on which adhesion and water sensitivity depend, is unknown.

One deduction from rheological studies of drying (1) is that triads of carboxylate ions be avoided. One way to proceed in this direction would be to copolymerize with such control over the

0097-6156/83/0227-0141\$06.00/0  
© 1983 American Chemical Society



sequence distribution that the carboxyl groups would be spaced every ten mer units (in the 1:9 ratios used for acrylics). A more practical solution is to repress the ionization (2). In either case the preferred orientation of the groups is outward, away from the polymer coils and convolutions, and directed toward the substrate where polar attractions enhance adhesion.

The extent to which the cosolvent provides control over orientation depends on its hydrogen-bonding capability. This dependence is the subject of the present paper.

### Experimental

Polymers. High molecular weight poly(n-butyl methacrylate) (PBMA) was obtained from Scientific Polymer Products Inc. and used as such. The viscosity-average molecular weight,  $\bar{M}_v$ , was determined by the Mark-Houwink-Sakurada equation

$$\eta = KM^a$$

The values of K and a for PBMA in acetone at 25°C are  $18.4 \times 10^{-5}$  dl/g and 0.62 respectively (3). The calculated  $\bar{M}_v$  is  $2.62 \times 10^5$ .

A copolymer of butyl methacrylate with acrylic acid (AA/BMA) was prepared by Loren Hill, then of North Dakota State University. Its  $\bar{M}_n$  was 6,200 and  $\bar{M}_w/\bar{M}_n$  was 3.5. The acid value was 68.

Solvents. Toluene, t-butanol, and p-dioxane obtained from Fisher Co. were doubly distilled. Their melting points were -95°C, 24°C, and 11°C respectively.

Procedures. The polymer was diluted to 3% by weight of solid as the initial concentration. No water was used in this series of experiments which consisted of determinations of the development of rigidity as the dilute solution dried on a flat quartz surface.

Mechanical Measurements. Shear moduli  $G'$  were determined at  $1.4 \times 10^7$  Hz by the attenuated reflection of pulses (ARP) method described previously (4-6). In this method a 4  $\mu$ sec pulse of ultrasonic energy applied in the shear mode is made to traverse a quartz substrate, impinging on the underside of the film as it reflects repeatedly from the ends of the substrate.

Modulus is calculated (7) from the attenuation coefficient per echo by the relation,

$$G' \approx 2.5 \times 10^{10} [(1 - r)/(1 + r)]^2 \text{ dynes/cm}^2$$

where  $\log r = -\Delta/40$ .

Increases in modulus as the coating dries occur as a consequence of its conversion to a solid. The magnitude of the increase is inversely related to the amount of plasticization wrought by the residual solvent. For this reason, weight losses

were measured by a single-pan balance supporting a glass slide of the same dimensions as the quartz substrate. Both samples were monitored simultaneously in the same humidity chamber.

Drying studies were made at two relative humidities: 10% and 80%. The temperature of drying was 35°C. Because the rate of evaporation of solvent depends on RH, some caution must be exercised in drawing conclusions from the results at the two humidity levels.

Wetting Measurements. Wetting measurements with water were made on copolymer films formed by evaporation of 3% by weight solutions of the copolymer from t-butanol, p-dioxane, and toluene. The films were formed on glass microscope slides and were the order of 10 microns in thickness. The films were allowed to form over a 24-hour period in a drying box at a relative humidity of 20%.

Contact angles were calculated from the profile of the water as it was advanced or receded over the surface for dynamic values or from the stationary drop for static values.

## Results

Acrylic Ester. Drying curves of poly(n-butyl methacrylate) from the three solvents are given in Figure 1 (10% RH) and Figure 2 (80% RH).

Residual stress capable of partially delaminating the coating built up in all cases except from p-dioxane at high RH. Before the onset of adhesive failure (at the peaks in the drying curves) drying from all three solvents proceeded at about the same pace at low RH; toluene outpaced the two hydrogen-bonding solvents at high RH. t-Butanol boils at 83°C, whereas the two remaining boil above 100°C; therefore, volatility alone did not account for any of these phenomena.

Hydrogen bonding appeared to increase the resistance of the drying film to adhesive failure. Films dried from toluene failed at an earlier time and at a lower or equal rigidity than did the films from the H-bonding solvents. Cohesive energy density is enhanced by H bonding, whereas in the case of a polymer containing only ester groups the effect on adhesion is slight.

Acrylic Acid Copolymer. Drying results for the 10% copolymer of acrylic acid and butyl methacrylate are given in Figure 3 (10% RH) and Figure 4 (80% RH).

Less tendency toward adhesive failure is noted, as expected for a functional polymer. The only catastrophic incident occurred in drying from toluene at high RH.

Delayed removal of the last vestiges of solvent was observed from the hydrogen-bonding solvents at high RH, whereas no such tendencies were noted in any of the other drying episodes.

Modulus levels of all of the dried films varied little with drying conditions. Toluene gave the lowest modulus, overall; dioxane and butanol vied for top position.

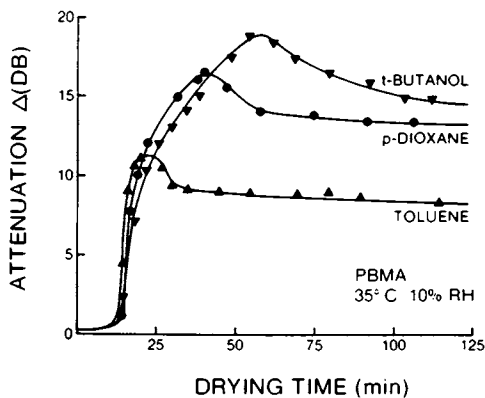


Figure 1. Drying of PBMA cast from various solvents at 10% RH.

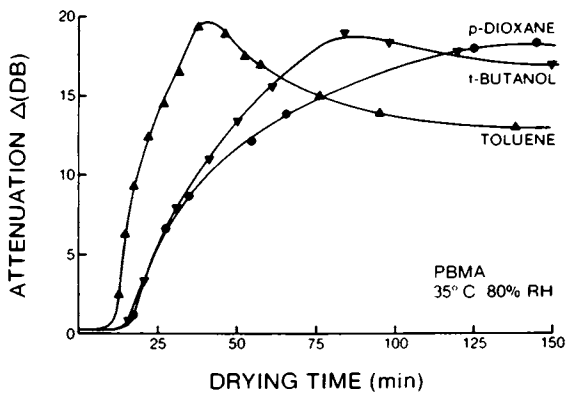


Figure 2. Drying of PBMA cast from various solvents at 80% RH.

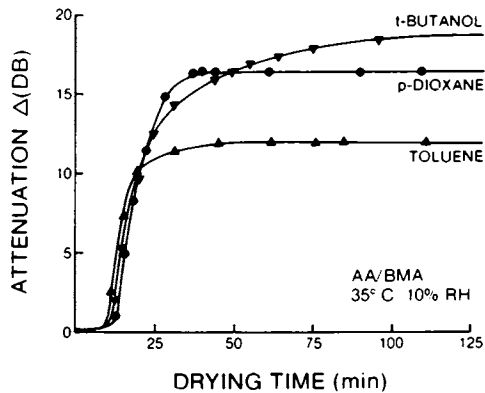


Figure 3. Drying of AA/BMA copolymer cast from various solvents at 10% RH.

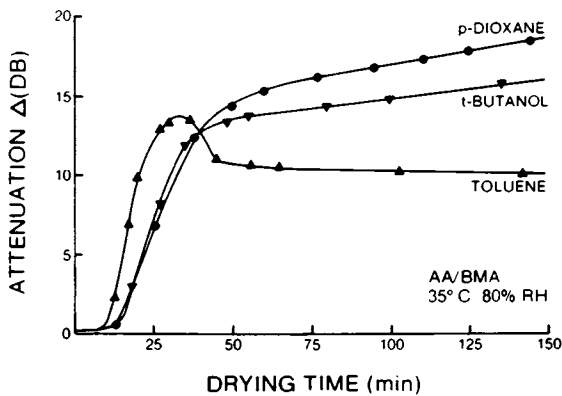


Figure 4. Drying of AA/BMA copolymer cast from various solvents at 80% RH.

The results of wetting studies on the copolymer films are shown in Table I. The advancing angle of all films was nearly the same at 80-85°. The receding angle was lower (55°) for films cast from t-butanol than from either p-dioxane (65°) or toluene (65°). The initial static angle increased in the order of decreasing hydrogen bonding capability of the casting solvents: t-butanol (64°), p-dioxane (86°), and toluene (101°). The static contact angle after one hour most nearly paralleled the dynamic receding angle: t-butanol (55° vs 55°), p-dioxane (57° vs 65°), and toluene (60° vs 65°).

Table I. Comparison of the Water Wettability of AA/BMA Copolymer Films Cast from Different Solvents

<u>Contact Angle</u>	<u>t-butanol</u>	<u>p-dioxane</u>	<u>toluene</u>
Advancing	80 ± 4°	85 ± 4°	84 ± 2°
Receding	55 ± 5°	65 ± 3°	65 ± 3°
Initial Static	64 ± 8°	86 ± 1°	101 ± 5°
1-hr. Static	55 ± 5°	57 ± 4°	60 ± 4°

### Discussion

The trends shown in Figures 1 and 2 for the acrylic ester appear to be more morphological than interfacial. Interactions between polymer and solvent are able to control the orientation at the interface, but without a highly polar functional group present there is little opportunity for orientation to override Brownian movement and induce the ester group to point toward the quartz surface.

There was a distinct change in morphology, however, for the drying conducted at low RH. At comparable evaporation rates the residual stresses in the film dried from toluene were appreciably greater than from the two polar solvents. Toluene, of course, plasticizes the polymer by its attraction to the hydrophobic backbone, whereas dioxane and t-butanol cluster around the side chains. Since glass transitions were not involved in these drying studies the distinction is not particularly important, as attested to by the similar behavior patterns. Whether side chains or backbones remain clustered until the end of the drying period is not of great importance.

The situation is different when carboxyl functionality is present, as in the copolymer drying curves, Figures 3 and 4. Smoother trends attest to better adhesion, as observed above. Hydrogen bonding enhances rigidity, possibly through the interfacial orientation of the carboxyl groups. In the copolymer the changes in morphology, however subtle, are reflected in improved performance.

For a given solids concentration beyond the gel point, the increase of the modulus for the acrylate coating cast from toluene was higher than that from the hydrogen-bonding solvent. This trend agrees with the one observed by Walter (8) and discussed by Ferry (9). Hydrogen-bonded gels appear to have a lower "intrinsic rigidity" than do hydrophobic gels. That is, the dependence of rigidity on concentration appears to be greater when hydrogen bonding is absent than when it is present.

Baier and Zisman (10) found that polyamide films cast from different solvents gave different degrees of adhesion as well as affecting the conformation of the film as detected by wetting behavior toward hydrogen and non-hydrogen bonding solvents. In the present study, acrylic acid copolymer films cast on glass microscope slides gave wetting results suggesting that the polar groups were more readily accessible to water in the t-butanol cast film than in those cast from p-dioxane or toluene. Contact angles of water on the films cast from the three solvents became comparable in magnitude only after the films were in contact with the water for an hour.

The wetting results in this study also agree with those found by Gregonis, et al. (11), who studied the wetting by water of films of copolymers of poly(hydroxyethyl) methacrylate (HEMA) with poly(methyl methacrylate) (MMA). The hydroxy group would impart a hydrophilicity to these copolymers analogous to that of the carboxyl group in the AA/BMA copolymer in the present study. There is good agreement in wetting behavior between the AA/BMA film (16 mole % AA) cast from t-butanol and HEMA/MMA (5 mole % HEMA) for the advancing angle ( $80^\circ$  vs  $80^\circ$ ), the receding angle ( $55^\circ$  vs  $52^\circ$ ), and the static angle on aging ( $55^\circ$  vs  $56^\circ$ ). The hydroxyethyl group may be more accessible than the carboxyl group since the butyl group in AA/BMA is bulkier than the methyl group in HEMA/MMA.

Advancing angles are a measure of the low energy regions of the film surface. Since the contact angles of water on the AA/BMA films were nearly constant regardless of the casting solvent, it appears that low energy butyl group regions were equally accessible in all cases. The receding angle, however, is more indicative of the higher energy regions and the results indicate that the films cast from the hydrogen bonding solvent, t-butanol, had virtually the maximum number of low energy sites available during the initial dynamic measurement of the receding angles.

The initial static contact angles show that the wetting behavior parallels the expected degree of hydrophobicity of the fresh film surfaces. The carboxyl groups should be least accessible in the films cast from toluene and most accessible in those cast from t-butanol. However, after exposure to water for an hour, the static angle was a much less definitive measure of the original film hydrophobicity indicating that the water is able to penetrate the film surface and gain access to previously unexposed carboxyl groups. This same phenomenon has been noted in studies of hydrogels by Holly (12).

**American Chemical**

**Society Library**

**1155 16th St. N. W.**

**Washington, D. C. 20036**

The interpretation of the wetting results at the film/air interface is in agreement with those conclusions reached from the interpretation of the mechanical results. How general the wetting behavior at the film/air interface reflects behavior at the film/substrate interface needs further study.

### Conclusions

Hydrogen bonding between the solvent and acrylic acid/butyl methacrylate copolymer led to better adherence of the dried films than when H bonding was absent. The effect was absent in the case of poly(butyl methacrylate).

Increasing the ambient relative humidity decreased the modulus levels but did not decrease the effect of hydrogen bonding.

Protection of the functional group until the end of drying enhances adhesion.

A subtle version of chemorheology involving hydrogen bonding of polar groups is involved in the drying of water-dispersible polymers.

### Literature Cited

1. Tsutsui, K.; Myers, R. R. I&EC Prod. R&D 1980, 19, (3), 310-314.
2. Raju, K. S.; Myers, R. R. J. Coat. Technol. 1981, 53, (676), 31-39.
3. Kurata, M.; Iwama, M.; Kamada, K., Part IV in "Polymer Handbook," Brandrup, J.; Immergut, E. H., Eds., Interscience Publishers: New York, 1966; p. 24.
4. Myers, R. R.; Schultz, R. K. J. Appl. Poly. Sci. 1964, 8, 755-764.
5. Myers, R. R.; Knauss, C. J. J. Paint Technol. 1968, 40, (523) 315-319.
6. Myers, R. R.; Klimek, J.; Knauss, C. J. J. Paint Technol. 1966, 38, (500) 479-484.
7. Myers, R. R. J. Poly. Sci. 1971, Part C, 35, 3-21.
8. Walter, A. T. J. Poly. Sci. 1954, 13, 207.
9. Ferry, J. D. "Viscoelastic Properties of Polymers"; 2nd ed., John Wiley: New York, 1970; pp. 562-563.
10. Baier, R. E.; Zisman, W. A. Macromolecules 1970, 3, 462.
11. Gregonis, D. E.; Hsu, R.; Buerger, D. E.; Smith, L. M.; Andrade, J. M. in "Macromolecular Solutions," Seymour, R. B.; Stahl, G. A., Eds.; Pergamon Press: New York, 1982; p. 120.
12. Holly, F. J. in "Medical Polymers: Chemical Problems," Sedlacek, B.; Overberger, C. G.; Mark, H. F., Eds., J. Poly. Sci.: Polymer Symposium No.66, John Wiley & Sons: 1979; p. 409.

RECEIVED March 31, 1983

## Cure of Intaglio Printing Inks

D. L. HUNSTON and J. L. RUSHFORD

National Bureau of Standards, Polymer Division, Washington, DC 20234

W. R. NEWITT and B. A. VANDREUIL

Bureau of Engraving and Printing, Research Division, Washington, DC 20228

The intaglio inks used to print currency in the United States contain relatively little solvent and dry primarily by chain extension and cross-linking reactions in the vehicles. To obtain good performance, the initially fluid ink must change rheologically in the manner required to give proper transfer to the plate and then to the paper and to obtain sufficient hardness at the end of the process so that the printed sheets do not smear when stacked. To study these changes, the rheology of two ink formulations with very different press performances was examined, first in the uncured state and then during curing. The uncured inks exhibited complex rheological properties including time dependence, yield behavior, elasticity, and non-linearity. Curing of the inks produced an increase in both viscosity and elasticity. The viscosity change could be roughly fitted to a first order type equation. Comparisons between these results and the performance of the inks on the press show that if the rate at which properties change during cure falls outside a certain range, acceptable print quality cannot be achieved.

The manufacture of paper currency in the United States is the responsibility of the Bureau of Engraving and Printing (BEP) which is the world's largest securities manufacturing establishment. BEP produces, on average, 16 million notes per day which represents an annual face value of 43 billion dollars. An intaglio printing process is used because it is the most difficult process to perform and thus to counterfeit (1). Other processes lack the fidelity of fine lines and the distinctive third-dimensional effect of raised line on paper inherent in intaglio printing (1). The plates are hand-tooled by highly skilled engravers who engrave the designs using grooves of varying depths. The currency is then printed on high-speed sheet-fed rotary presses that employ two or four plates containing 32 notes each. The presses are capable of

This chapter not subject to U.S. copyright.  
Published 1983, American Chemical Society



printing 9,000 sheets per hour. The ink is supplied to the roller containing the plates from the ink trough, or fountain, by a series of feed rollers. The ink in the fountain is heated and kept in slow but usually constant motion. After the hot ink is transferred by the feed rollers to the plate, ink is removed from the elevated portions of the plate by a series of three wiping cloths. A sheet of paper is then forced under heavy pressure against the plate so that it picks up most of the ink remaining in the fine engraved lines. The sheets are immediately stacked by the press and on a subsequent day the reverse side of the sheets are printed in the same way.

To efficiently produce a high quality product requires the use of special formula, fast-drying inks, developed in BEP's laboratories. The rapid drying eliminates the time-consuming need for tissinging or interleaving between sheets to prevent smearing when stacked. Rapid drying on the sheets alone however is not sufficient to guarantee good results. The proper transfer of the initially liquid ink from the fountain to the plate via the feed rollers, the complete removal of the ink from the high portions of the plate by the wiping cloths, and the necessary transfer of the remaining ink to the paper require that the ink be in the proper rheological states at the appropriate times. As a result the rheological changes that occur during drying must proceed both rapidly and correctly if proper print quality is to be achieved.

To minimize the problems associated with poorly performing inks, a number of quality control (QC) tests are presently being used. Unfortunately, the complexity of the printing process is such that undetected variations in ink batches are still present and this leads to a higher than desirable percentage of ink batches with unacceptable performance. To help minimize the problem, a cooperative study was initiated between the National Bureau of Standards and BEP with the objective of obtaining a more complete picture of the basic rheological properties of the ink and how these properties change as the ink cures. This information combined with the results of other studies (2-6) will provide both the basis for more reliable Q.C. techniques and the data required to help design improved ink formulations in the future.

### Background

The inks used in currency printing are complex formulations based on natural drying oils such as tung oil and linseed oil. These oils contain multiple double bonds which act as polymerization sites when exposed to oxygen. Although the details of the chemistry are not fully understood, some important observations can be made. If a bulk ink sample is exposed to air for several days a hard skin forms on the surface. Underneath this skin, however, the mechanical properties of the ink remain virtually

unchanged for many months. Thus the polymerization requires direct exposure to oxygen and so the cure can be accurately studied only with experiments using films. The reactions are also greatly accelerated by increased temperature. Changes which require many hours at room temperature will occur in minutes or seconds at press temperatures.

It is the black currency ink which has been the most troublesome and is therefore the subject of this study. This ink contains very little solvent--drying experiments show a weight loss of less than 1% to full cure--and thus the hardening must proceed by polymerization and cross-linking reactions. In a recent study of this ink (2) it was demonstrated that cure reactions are a critical factor in the performance of the ink on the press. Consequently, an examination of curing behavior is necessary to the development of an understanding of ink performance.

In the present study two different ink formulations were examined. They are designated as BK-62 and BK-60 modification 17 (hereafter designed simply as BK-60). Formulation BK-60 was used for a number of years and gave acceptable performance although there was room for improvement. Formulation BK-62 was developed more recently as a trial material with a much simpler composition. Experiments with this ink on the press showed that it had unacceptable performance and this has led to a modification in the BK-62 formulation. This new version which shows marked improvement (2) is now being utilized in production and studied in this program. For the present discussion, however, it is useful to examine the original BK-62 and BK-60 as examples of an unacceptable ink and an acceptable, although not ideal, ink. It is also helpful to note that although a number of problems were observed with BK-62, a major difficulty (2) was "excessive drying on the plate".

### Experimental Section

Various samples of the two different ink formulations were evaluated for mechanical properties prior to and during cure. Both formulations are based on natural vehicles and are highly filled with pigments and additives. There are a number of differences between the two formulations but the most important is that the samples designated BK-60 contain a linseed oil vehicle system while those designated BK-62 contain a tung oil system. Details of the ink's composition are given in Table I.

The inks were examined by using transient, steady flow, and oscillatory tests performed at room temperature,  $22 \pm 0.5^\circ\text{C}$ . These experiments were performed on a specially modified and computerized cone and plate viscometer. The cone utilized was 2.5 cm in diameter and 0.5 degrees in angle. Details of the data acquisition system for this device have been described previously (7) and will only be summarized here. The plate can be driven in

Table I. Composition of Ink Formulations

Ingredients	BK-60	BK-62
Pigments	51.4	36
Barytes	-	30
Calcium Carbonate	17.4	17
Linseed Oil Vehicle	16.5	-
Varnish	6.5	9
Bodied Tung Oil	-	8
Amorphous Silica	5.7	-
Driers	1.9	-
Petroleum Solvent	0.6	-
Total	100	100

steady rotation or oscillatory rotation. The motion of the cone, which is attached to a torsion bar and held in line by an air bearing, is monitored to provide a measure of the stress. In the oscillatory experiments, the drive shaft is attached to a shaft angle encoder that generates 360 equally spaced pulse per cycle. Each pulse triggers the acquisition of position data from displacement transducers attached to the cone and the plate. This information is transferred to a minicomputer for storage and analysis. From this data the stress and strain in the sample can be calculated and thus the mechanical properties can be determined. In some cases it is useful to examine the stress curve itself and for this purpose the digitized data can be accessed. These data are in arbitrary units but for the test conditions used here they can be converted to stress in dynes/cm<sup>2</sup> by multiplying by 8.120. The experiments were performed at frequencies from 10 Hz to 6x10<sup>-4</sup> Hz and amplitudes between 4x10<sup>-4</sup> radians and 4x10<sup>-2</sup> radians.

In the initiation of steady shear flow and the steady shear flow experiments, the shaft angle encoder was attached to a timing motor and data acquisition proceeds in the same way as in the oscillatory experiments. These tests were performed at shear rates between 5x10<sup>-2</sup> sec<sup>-1</sup> and 2000 sec<sup>-1</sup>.

After characterizing the basic shear properties of the inks, their cure behavior was investigated by placing samples on a specially designed 2 roller apparatus where one of the rolls was heated to 80°C (roughly equivalent to the press temperature). This setup provides some of the important conditions seen on the press, i.e. the application of heat, the formation of a thin film for maximum exposure to oxygen, and the constant renewal of the free surface to prevent a hard crust from forming. After various cure times a small portion of the ink was removed from the mill and characterized for shear properties using the same techniques described previously. Once curing had begun on the mill, it

continued even after the ink was removed and cooled to room temperature. Nevertheless, the cooling sufficiently slowed the changes in mechanical properties due to curing so that short term characterization tests could be performed. On the mill complete curing of the ink film required more than half an hour. This is much longer than required on the press. The difference can be attributed, at least in part, to the fact that the film thickness on the mill is much larger than that on the press. Despite the differences in cure rate, however, this technique was thought to be a useful method for comparing the cure of different ink formulations and for determining the rheological changes associated with cure.

### Results and Discussion

Uncured Ink. The behavior of both ink formulations can be roughly divided into three regions: initiation behavior, short term steady flow, and long term steady flow. This can be illustrated by experiments on the start-up of steady shear. When the ink is allowed to rest in the instrument for 15 minutes or more and then steady shear is initiated, there is a significant stress overshoot (Figure 1). Subsequently, the stress level shows a significant time dependence for a period of time that depends on the experimental conditions but is generally less than 10 seconds. After this initial period the stress appears to level-off at what will be termed the short term steady flow value. If the steady shear is maintained for long periods of time, however, it is found that the stress is not constant but shows a small and very slow decrease. For the range of conditions tested here, the stress, and therefore the viscosity, drops by about 15% in one hour (Figure 2). The decrease is approximately linear in a  $\log(\eta)$  vs  $\log(\text{time})$  plot.

If the shear flow is stopped and then reinitiated within a few minutes, the stress will return to the level achieved just prior to stopping the flow with little or no overshoot. Only if the ink is allowed to recover for a significant period of time, say 15 minutes, will the response be similar to that observed initially.

All three aspects of the ink behavior--initiation, short term steady flow, and long term response--may have importance in ink performance and are being studied in this program. This paper, however, focuses only on the short term steady flow regime and small amplitude oscillatory experiments.

Steady Shear (Uncured Inks). The short term steady flow stress levels (average values achieved between 30 and 120 seconds) were determined as a function of shear rate and used to calculate viscosities. Values of these viscosities for samples of the two ink formulations are plotted against shear rate in Figure 3.

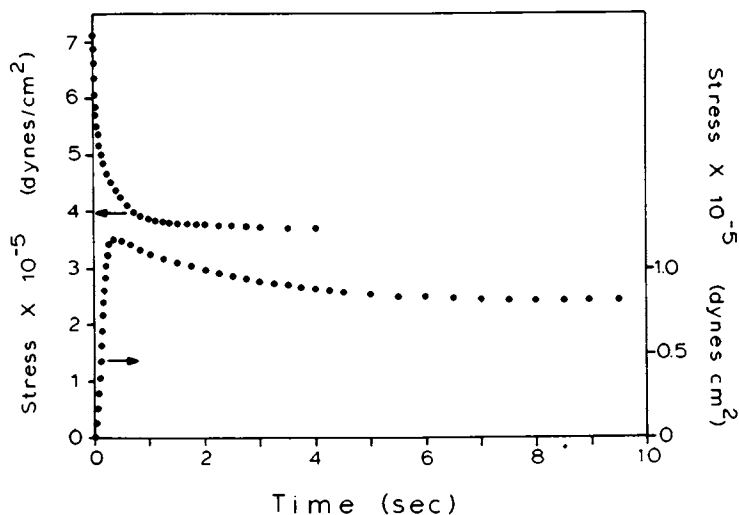


Figure 1. The stress associated with the initiation of steady shear flow in BK-60 at shear rates of  $55.7 \text{ sec}^{-1}$  (A) and  $5.6 \text{ sec}^{-1}$  (B).

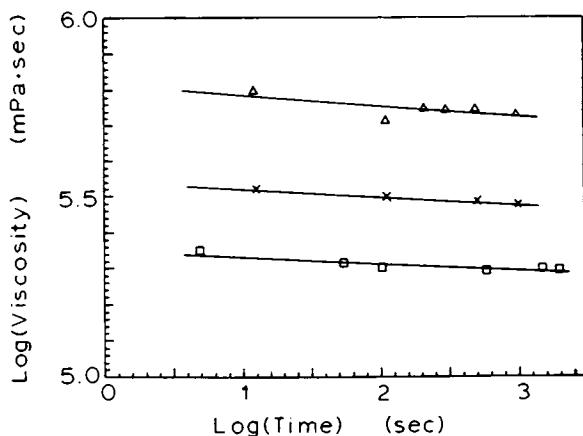


Figure 2. Viscosity of BK-62 as a function of time for steady shear flow at shear rates of  $1.76 \text{ sec}^{-1}$  ( $\Delta$ ),  $5.57 \text{ sec}^{-1}$  (X), and  $17.6 \text{ sec}^{-1}$  ( $\square$ ).

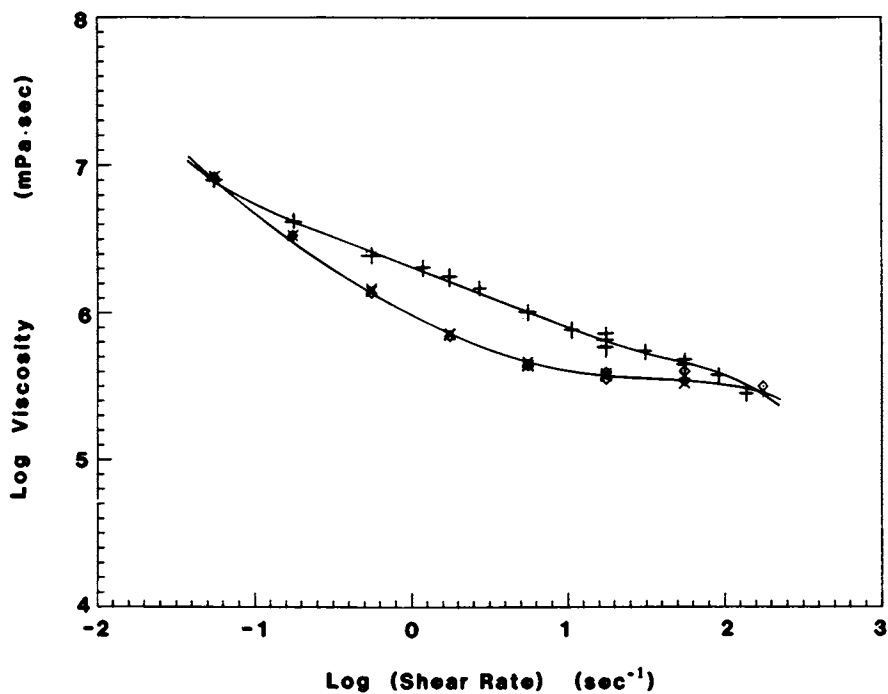


Figure 3. Short term steady flow viscosity vs. shear rate for two samples of BK-62: X & ◊ and two samples of BK-60: ◻ & +.

Above shear rates of  $500 \text{ sec}^{-1}$  the data are unreliable because there is often a loss of adhesion between the sample and the cone or plate; however, the indications are that the viscosity may drop significantly at high shear rates. In the region between 80 and  $500 \text{ sec}^{-1}$  as well as the region between  $6 \times 10^{-2}$  and  $0.6 \text{ sec}^{-1}$ , the viscosities for the two ink formulations are similar. Only at the intermediate shear rates, 0.6 to  $80 \text{ sec}^{-1}$ , is the behavior substantially different. In this region the viscosity of BK-60 reaches values more than 3 times as large as those for BK-62.

This difference is important because a number of the mixing steps required to prepare these inks involve shear rates in this intermediate range. On the press, however, the ink sees only very low shear rates in the fountain and very high shear rates during printing. For these conditions the behavior of both inks is similar in Figure 3. Since the results in this Figure are for room temperature while the ink on the press is hot ( $50^\circ\text{C}$  to  $80^\circ\text{C}$ ), additional tests (2) were performed at high shear rates ( $475 \text{ sec}^{-1}$ ) and elevated temperatures ( $60^\circ\text{C}$ ). Here again the behavior of the two ink formulations was similar. Consequently, although the differences in short term steady flow viscosities may have an effect on ink preparation, they do not appear to be a likely cause of the poor performance for BK-62.

Oscillatory Shear (Uncured Inks). Because the viscosities of these inks are highly non-linear the oscillatory behavior is quite complex. For example, Figure 4 shows the stress curves associated with a pure sine wave strain imposed on samples of BK-60 at 3 different frequencies. For the lowest frequency the stress curve is approximately sinusoidal although shifted in phase, but the curves become increasingly non-sinusoidal as the frequency is increased. Moreover, even at the lowest frequency, if the sample is subjected to steady shear for a few minutes before the oscillatory test, a non-linear response is obtained (Figure 5). A comparison between the behavior of the two ink formulations indicates a general similarity in the effects of changing the amplitude or frequency or shearing the sample before the test. In most cases, however, the stress levels are greater in BK-60 while the non-linearity is greater in BK-62 (Figure 6).

In light of this complexity only a simple analysis of the oscillatory results was performed. Nevertheless, this analysis provides several interesting general conclusions. First, the behavior of the inks is viscoelastic in that the stress leads the strain (Figure 4-6) by an angle between  $0^\circ$  (elastic) and  $90^\circ$  (viscous). Second, a simple Fourier analysis indicates that the stress curves can be fit quite well with a response involving the fundamental frequency and the first two odd harmonics. For example, Figure 7 shows the measured and calculated curves for the case that gave the poorest fit of all the experimental conditions analyzed. Even for this case the agreement is reason-

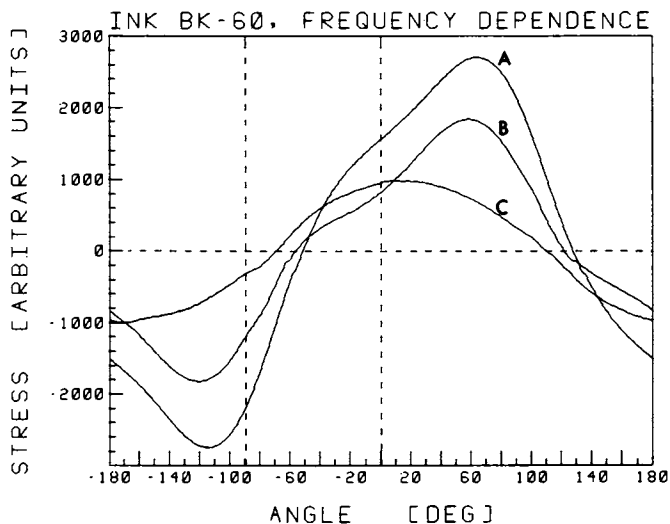


Figure 4. The stress curves for BK-60 associated with a sine wave strain at an amplitude of  $1.5 \times 10^{-3}$  radians and frequencies of 6.0 Hz (A), 0.6 Hz (B), and 0.06 Hz (C).

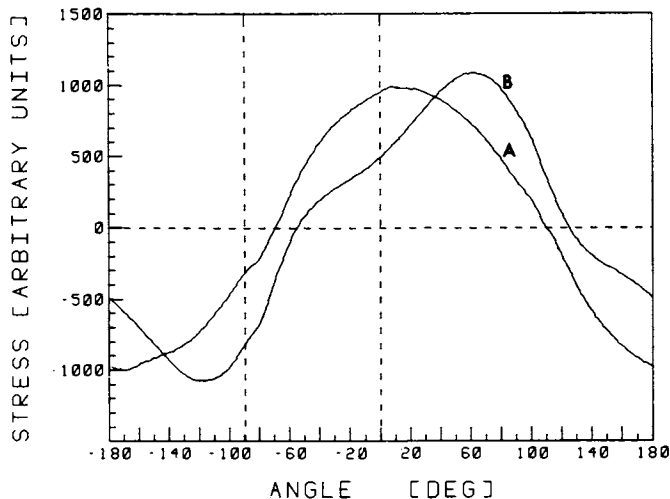


Figure 5. The stress curves for BK-60 associated with a sine wave strain of amplitude  $1.5 \times 10^{-3}$  radians and frequency of 0.06 Hz before (A) and after (B) shearing with steady shear flow (shear rate  $60 \text{ sec}^{-1}$ ) for 1 minute.



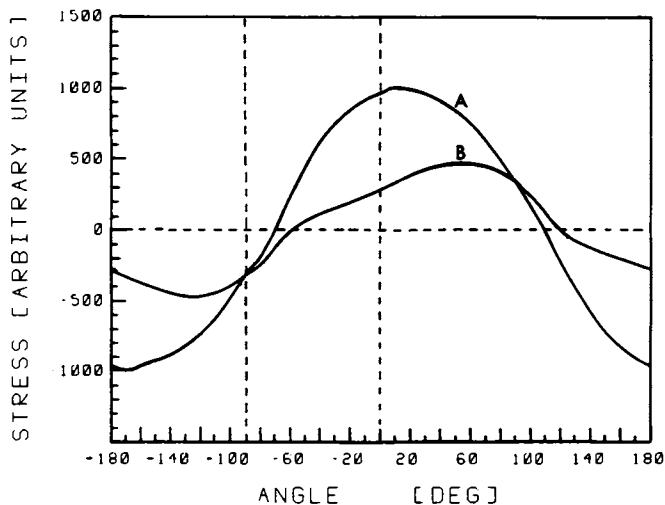


Figure 6. The stress curves for BK-60 (A) and BK-62 (B) associated with a sine wave strain of amplitude  $1.5 \times 10^{-3}$  radians and frequency 0.06 Hz.

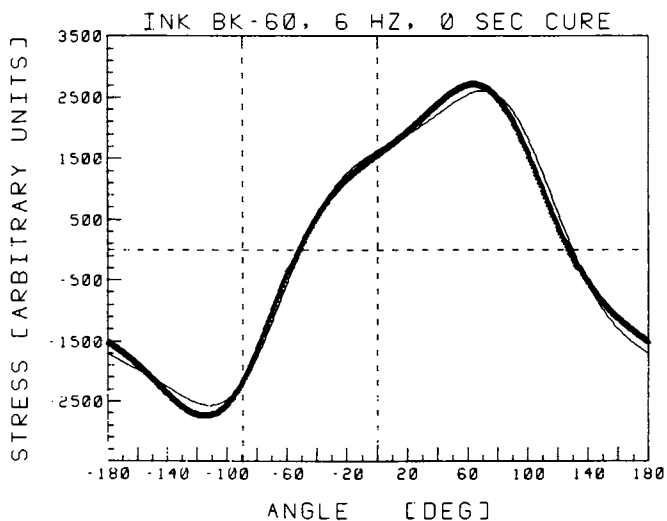


Figure 7. Comparison between the measured stress curve (overlapping data points appear as heavy line) and calculated curve (thin line) for BK-60 at frequency of 6 Hz and sine wave strain of amplitude  $1.5 \times 10^{-3}$  radians.

ably good. An examination of the results also indicates that in the calculated curves the total amplitude of the harmonics is in all cases less than 14% of that for the fundamental and in many cases less than 7%. Thus to a large extent the fundamental frequency dominates the response.

As a result it is of interest to examine some of the general characteristics of this component of the total response. If the real part of the dynamic shear viscosity is calculated for this component,  $\eta_1'$ , it is found to be a strong function of the strain amplitude and frequency. Data were obtained for BK-60 at 6 different amplitudes and 9 different frequencies. In an effort to systematize this information, the dependence of  $\eta_1'$  on the shear rate was examined by plotting  $\log(\eta_1')$  against the time average shear rate during the oscillatory cycle (Figure 8)

$$\text{time average shear rate} = \frac{2 \omega A}{\pi \tan \theta} \quad (1)$$

where  $\omega$  is the angular velocity,  $A$  is the amplitude of oscillation (radians), and  $\theta$  is the cone angle. Although this does not collapse the data to a single curve, it does compress the variations to a narrow band which is quite narrow at low shear rates and broadens somewhat as the shear rate is increased. If the short term steady flow data are added to the graph, they fall roughly within this same band. A much less extensive study using formulation BK-62 gave similar results. Consequently, although the oscillatory behavior is quite complex, there is an interesting correlation between the oscillatory data and the short term steady shear results.

Curing Study. Although the data on the mechanical properties of the uncured inks provide information that is useful in fabricating the inks, no explanation for the poor performance of BK-62 was found. As a result, experiments aimed at examining the cure behavior of the inks were conducted. Samples of the inks were cured on a heated 2 roller apparatus, and, after various curing times, small portions of ink were removed and characterized for oscillatory and short term steady flow viscosity. In view of the complexity of the oscillatory behavior, most of the emphasis is on the steady flow tests; however, it is useful to examine the general trends exhibited in the oscillatory data.

Steady Shear (Curing Study). Figures 9 and 10 illustrate the types of changes that are observed in the short term steady flow viscosity as the ink cures. Over the entire range of shear rates tested, the curing produces an increase in viscosity. For a given curing time the data for BK-60 show an approximately equal increase in  $\log(\eta)$  at all but the highest shear rates. For BK-62 the longer cure times show the same trend but the 7.5 minute cure produces larger changes at the low shear rates than

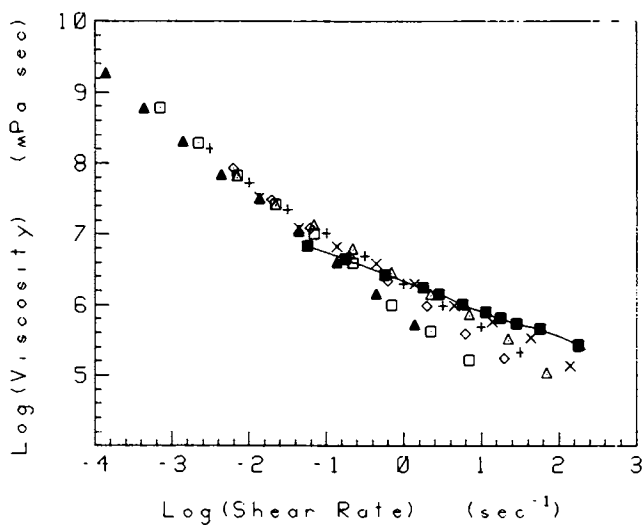


Figure 8. The dependence of  $\log(\eta_1')$  on time average shear rate for BK-60 at amplitudes of  $4.5 \times 10^{-4}$  rad ( $\Delta$ ),  $2.2 \times 10^{-3}$  rad ( $\square$ ),  $6.4 \times 10^{-3}$  rad ( $\diamond$ ),  $9.8 \times 10^{-3}$  rad (+),  $2.2 \times 10^{-2}$  rad ( $\Delta$ ), and  $4.5 \times 10^{-2}$  rad (X). Short term steady flow viscosity vs. shear rate ( $-\square-$ ).

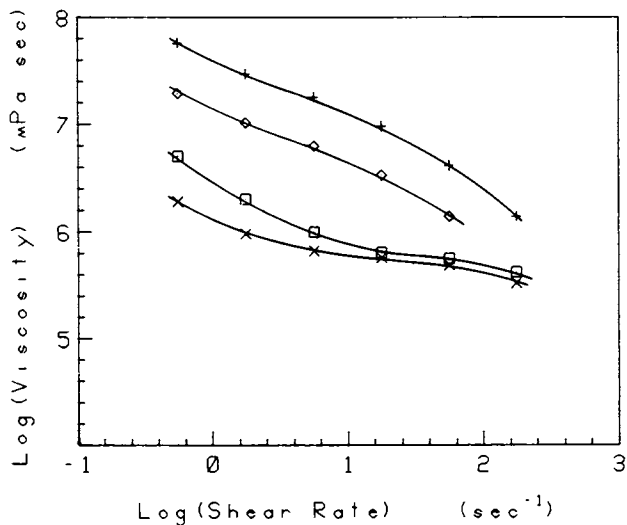


Figure 9. Short term steady flow viscosity vs. shear rate data for samples of BK-62 cured for 0 min (X), 7.5 min ( $\square$ ), 20 min ( $\diamond$ ), and 30 min (+).

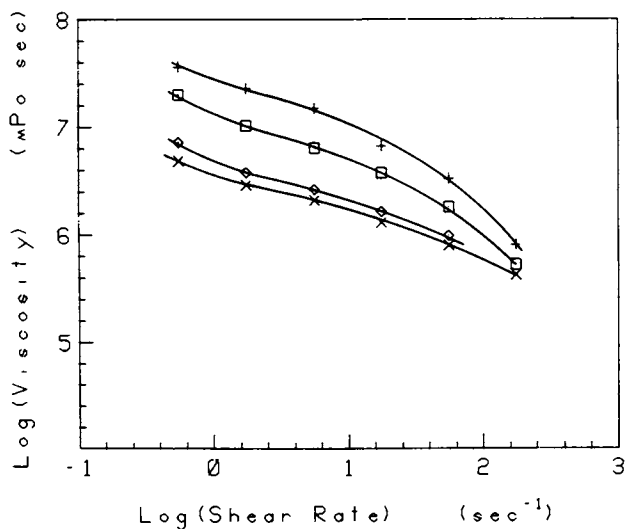


Figure 10. Short term steady flow viscosity vs. shear rate data for samples of BK-60 cured for 0 min (X), 10 min ( $\diamond$ ), 20 min ( $\square$ ), and 30 min (+).

at the intermediate and high shear rates. One factor that could contribute to this difference in behavior at short cure times is the possibility of an induction period. Thermal experiments (2) have demonstrated that the cure reactions do not begin immediately but only after the sample has been held at the cure temperature for a few minutes. In the present experiment the cure temperature is reached very rapidly but as will be seen later, there is evidence for an induction period.

Before curing begins, BK-60 has a higher viscosity over most of the shear rate range than BK-62. Once curing starts however, the rate of increase in  $\eta$  is much greater for BK-62. Consequently, within a short time the viscosity for BK-62 is larger than that for BK-60. It is clear therefore that the two ink formulations have very different curing behaviors.

Oscillatory Shear (Curing Study). Very similar trends are seen in the oscillatory data. Figures 11 and 12 show the stress curves associated with a sine wave strain for ink samples cured various lengths of time. As shown previously, the initial stress levels in BK-62 are much lower than in BK-60. The changes associated with curing, however, are substantially larger for BK-62 and within a short time the stress levels in BK-62 are larger than those in BK-60. In view of the correlation that was found between the oscillatory and short term steady flow experiments on the uncured inks, the similar trends in the curing tests are a logical result. With both inks there is a decrease in non-linearity as the inks cure; i.e., the stress curves become more sinusoidal. The angle by which the stress leads the strain (sine wave) also decreases with curing indicating that although both the elastic and viscous components of the response increase, the elasticity increases more rapidly at least in the initial phase of cure.

Analysis of Cure. A simple analysis of the cure results for short term steady flow can be performed by noting that for a number of polymerization reactions, the early stages of cure can be described by a first order type equation (9,10). In the simplest case this would mean that  $\log(\eta)$  would vary linearly with time. To examine this possibility the data for various shear rates were analyzed by plotting  $\log(\eta)$  vs. time (Figures 13 and 14). If the initial points (zero cure time data) are excluded, the data for each shear rate can be fit, to a first approximation, with a straight line. The fact that the zero cure time points do not fall near the lines suggests that the mechanical property results show an initiation time just as was found previously in thermal experiments (2).

The slopes,  $k$ , of the lines in Figures 13 and 14 provide a measure of the rate of change of viscosity with time during curing. The initiation period can also be characterized by determining the time,  $t_0$ , corresponding to the point on each

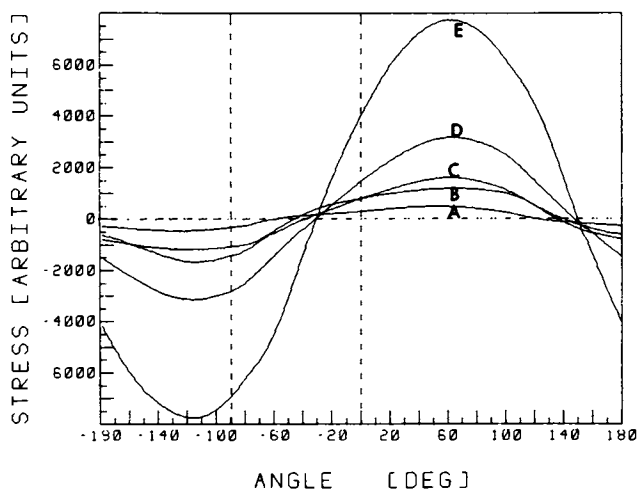


Figure 11. The stress curves for BK-62 associated with a sine wave strain of amplitude  $1.5 \times 10^{-3}$  radians and frequency 0.06 Hz cured for 0 min (A), 5 min (B), 10 min (C), 20 min (D), and 30 min (E).

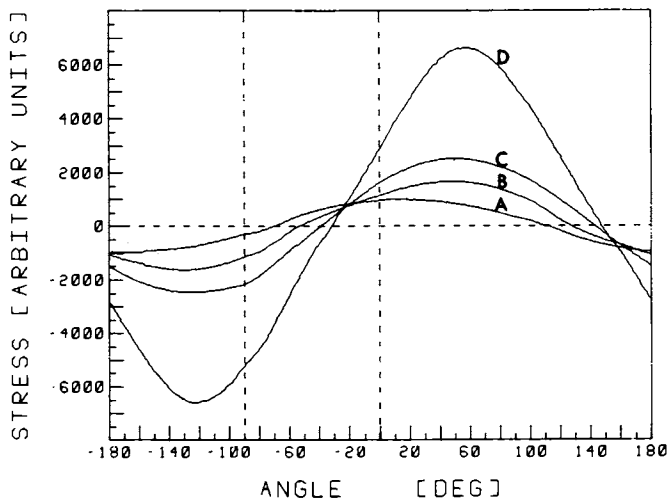


Figure 12. The stress curves for BK-60 associated with a sine wave strain of amplitude  $1.5 \times 10^{-3}$  radians and frequency 0.06 Hz cured for 0 min (A), 10 min (B), 20 min (C), and 30 min (D).

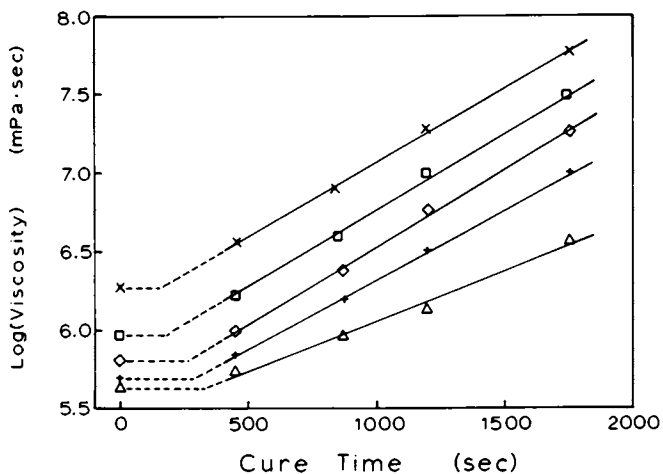


Figure 13. Short term steady flow viscosity of BK-62 vs. cure time at shear rates of  $0.56 \text{ sec}^{-1}$  (X),  $1.76 \text{ sec}^{-1}$  (□),  $5.57 \text{ sec}^{-1}$  (◇),  $17.6 \text{ sec}^{-1}$  (+), and  $55.6 \text{ sec}^{-1}$  (Δ).

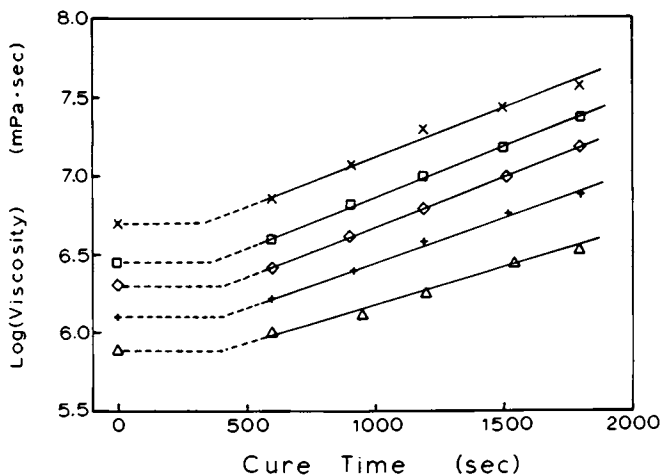


Figure 14. Short term steady flow viscosity of BK-60 vs. cure time at shear rates of  $0.56 \text{ sec}^{-1}$  (X),  $1.76 \text{ sec}^{-1}$  (□),  $5.57 \text{ sec}^{-1}$  (◇),  $17.6 \text{ sec}^{-1}$  (+), and  $55.6 \text{ sec}^{-1}$  (Δ).

straight line where the viscosity equals the zero cure time viscosity of the ink at that shear rate. Values of  $k$  and  $t_0$  for the various shear rates and inks are given in Table II.

Table II. Cure Parameters

Shear Rate ( $\text{sec}^{-1}$ )	BK-60		BK62	
	$k \times 10^4$	$t_0$ (sec)	$k \times 10^4$	$t_0$ (sec)
0.56	6.1	330	9.4	150
1.76	6.4	360	9.6	180
5.56	6.1	410	9.8	270
17.60	5.6	410	8.8	280
55.60	4.7	420	6.4	340
55.60a	5.0	500	7.2	530

<sup>a</sup> Does not include data point for shortest non-zero cure time.

Over most of the measured shear rate range, the slopes are quite similar. At the two highest shear rates the slopes are less as would be suggested by the data in Figures 9 and 10. It should be noted, however, that the initiation times are greater at these shear rates, and as a result the data points at the shortest non-zero cure time may be in the initiation region. If straight lines are fit to the data for the shear rate of  $55.6 \text{ sec}^{-1}$  without including the results for either zero cure time or the shortest non-zero cure time, the slopes are greater although still not as large as the values obtained at lower shear rates (Table II). Consequently, although the data here are limited, the changes do appear to be somewhat slower at the higher shear rates.

The results in Table II help quantify the differences in cure behavior between BK-60 and BK-62. Previous experiments (2) using thermal analysis techniques have found that the initiation period for BK-62 is shorter than that for BK-60. The same trend is seen in the mechanical properties data. Moreover, the rate at which the properties change once curing has begun is approximately 50% greater for BK-62 than for BK-60. When these results are combined with the observation that a major problem with the performance of BK-62 on the press is excessive drying on the plate, the inescapable conclusion is that the differences in curing behavior are a major source of the problems with BK-62.

It is easy to see how these differences in curing could lead to excessive drying on the plate. Even under conditions where excessive drying on the plate is not observed, however, there will still be significant differences in the mechanical properties of the two ink formulations due to the curing behavior. This would affect transfer on the feed rollers, wiping of the



plate, and pick-up of ink by the paper and thus other problems with BK-62 may also be related to the cure behavior. In general it would appear that the changes in ink properties during cure must fall within a given range if proper performance on the press is to be achieved. Unfortunately, the original BK-62 ink fails to meet this criterion.

### Conclusion

The rheology of two intaglio ink formulations with very different performance on the press was examined prior to and during the early phases of cure. The uncured inks exhibit complex viscoelastic properties with stress overshoot, time dependence, and non-linearity. A major aspect of the non-linearity is a large shear rate dependence of the viscosity. Curing of the inks produces changes in both the viscosity and elasticity of the inks. After a short initiation period, the increase in the logarithm of the short term, steady flow viscosity is linear with respect to time so the slopes of the best-fit straight lines at various shear rates can be used to characterize the rate of change in properties. Over a wide range of shear rates the slopes of these lines show only a small variation. A comparison between the two formulations, however, reveals significant differences: BK-62 has a shorter initiation period than BK-60 and a rate of increase in viscosity during curing that is 50% greater than BK-60. These differences in curing behavior play a major role in the poor performance of BK-62.

### Acknowledgment

The equipment utilized in this work was developed and used in cooperation with the Naval Research Laboratory. Without their assistance this work would not have been possible.

### Literature Cited

1. "Production of Government Securities," Bureau of Engraving and Printing, Public Brochure, P.15 - REV 9-80.
2. Newitt, W. R.; Lipman, B.; Vandreuil, B. A.; Bureau of Engraving and Printing Research Report BEP-81-013, February, 1982.
3. Hirayama, K.; Research Bulletin Printing Bureau, Ministry of Finance, Japan 1979, 47, 1.
4. Shurz, J.; Kashmoula, T.; Papier 1976, 30, V52.
5. Oittinen, P.; Acto Polytechnica Scandinavica 1976, 131, 1.
6. Amari, T.; Watanabe, K.; Rep. Prog. Polym. Phys. in Japan 1979, 22, 101 and 105.
7. Huston, D. L.; Bascon, W. D.; Wells, E. E.; Fahey, J. D.; Bitner, J. L.; "Adhesion and Adsorption of Polymers,," Lee, L.H., Ed; Plenum Press: New York, 1980, Part A, p 321.

8. Hollands, K. M.; Kalnin, I. L.; "Epoxy Resins," *Advances in Chemistry Series No. 92*, ACS: Washington, D.C., 1970; p.60.
9. Roller, M. B.; Poly. Eng. Sci. 1975, 15, 406.

RECEIVED May 11, 1983

# Curing Behavior of Segmented Polyurethane Adhesives

D. MARK HOFFMAN

Lawrence Livermore National Laboratory, Livermore, CA 94550

Seven polyurethane adhesives, called Halthanes, were developed by the polymer group at Lawrence Livermore National Laboratory (LLNL) to meet design requirements of LLNL engineers while avoiding the use of OSHA restricted curing agent MOCA, methylene bis(2-chloroaniline). Four of these adhesives, the 73 series Halthanes, were made from 4,4' methylene bis(phenylisocyanate), MDI, terminated poly(tetramethylene oxide) prepolymers cured with a blend of butanediol and polyols. Three adhesives, the 87 and 88 series Halthanes, were made from 4,4' methylene bis(cyclohexylisocyanate), HMDI, terminated prepolymer cured with aromatic diamines. These segmented polyurethanes (1) consist of hard and soft segments whose concentration and chemical structure have been tailored for either more elastomeric character or tougher adhesive properties (2-4). Based on structure-property relationships, we have developed adhesives that bond rapidly and well, have low to intermediate modulus over a wide temperature range, and appear to be reasonably compatible with other components.

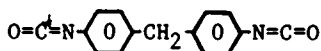
Among the design requirements for these adhesives were initial viscosities lower than 40 Pa.-sec., working times of about an hour, and cure times which permit removal of tools and clamping fixtures after 16 hours. LLNL engineers also wanted adhesives which would set up in 4-8 hours rather than 16 for some applications. More rapid cure rates were achieved by accelerators and aromatic diamine curing agents. An adhesive curing behavior may be followed by a variety of techniques (5,6). One of the most important for engineering purposes is the increase in viscosity during cure. The curing behavior of these segmented polyurethane adhesives was followed by dynamic viscosity measurements with time under isothermal conditions. Viscosity measurements can be used to estimate the kinetic rate constants and the activation energy of the reactions occurring between the prepolymer and curing agent. Changing the hard segment former from MDI/BDO to HMDI/ADA significantly increased the cure rate. The accelerator, ferric acetoacetate, used in

0097-6156/83/0227-0169\$06.00/0

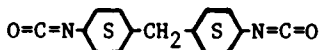
© 1983 American Chemical Society

Abbreviations Used in TextAbbreviationsStructure

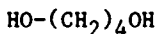
MDI = 4,4' methylene bis  
(phenyl isocyanate)



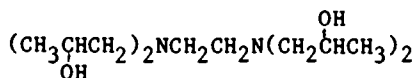
HMDI = Hylene W (saturated MDI)



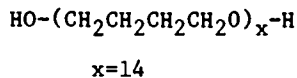
BDO = butanediol



Q = quadrol



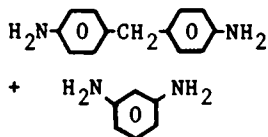
Polymeg 1000 =  
poly(tetramethylene oxide)



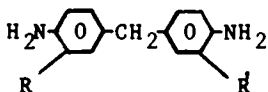
Polymeg 2000 =  
poly(tetramethylene oxide)

x=28

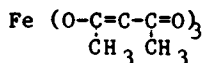
TONOX = mixture of aromatic diamines  
4,4' methylene dianiline and  
m-phenylene dianiline



XU-205 = mixture of substituted  
aromatic diamines of 4,4'  
methylene dianiline



FAA = ferric acetylacetonate



combination with a tetrafunctional alcohol increased the cure rate of the MDI adhesive system to nearly that of the HMDI system. Unfortunately, kinetic data extracted from viscosity measurements does not always correlate with that derived from more conventional chemical techniques for a variety of reasons. The viscosity of an unreacting liquid decreases with temperature. During the curing reaction the rate of increase in the polymer number average molecular weight is directly related to kinetics, but viscosity is related to the weight average molecular weight and the dependence of viscosity on molecular weight changes from being linear at low molecular weight to a 3.4 power dependence at high molecular weight (8). Under isothermal conditions the initial viscosity will depend on the temperature. As the material cures the viscosity should follow the molecular weight increase.

These prepolymers are made by reacting the polyol with excess isocyanate. Since the polyol oligomers are crystalline, they are warmed prior to addition of the isocyanate. With time the MDI terminated polyols in the prepolymer recrystallize and the excess isocyanate will phase separate. Prepolymer crystallization has a long induction time so that if the prepolymer is warmed, it will remain liquified for several hours. However the MDI terminated polyols are not completely miscible with the excess MDI. The milky appearance associated with liquid-liquid phase separation persists even in the room temperature cured adhesive as macroscopic phase separation, i.e., opaque polymer. In the curing adhesive, with increasing temperature macroscopic phase separation of the excess MDI in the MDI terminated prepolymer is compatibilized by the curing agent. Thus MDI/BDO/PTMG1 systems are clear when cured at above 60 °C. This does not affect the hard-soft block structure which controls the adhesive properties. All components of the HMDI/ ADA/ PTMG2 systems can be compatibilized at 60°C and will remain dissolved for several hours at room temperature. Therefore, these systems are dark but clear when cured.

### Experimental

The compositions of these adhesives are given in tables I and II. Further information on preparative procedures for the prepolymers, curing agents, and final adhesives are described in depth elsewhere (4). Prepolymer and curing agents were mixed in the ratios given in the tables and then degassed to remove entrapped air as rapidly as possible (3-8 minutes). In most cases, freshly prepared adhesive was immediately transferred to preheated fixtures.

Dynamic viscosity was followed as a function of time at room temperature (23-25°C), 40, 60, 80, and 100°C using 25 mm diameter cone and plate fixtures with 0.1 radian cone angle on a Rheometrics Mechanical Spectrometer. The oscillating frequency

Table I. 73 series prepolymer and curing agent formulations.

Curing Agents				
Component	73-14	73-15	73-18	73-19
Polymeg 1000	90	90	85	85
1,4-butanediol	10	10	10	10
quadrol	-	-	5	5
FAA	-	0.0156	-	0.0107
Prepolymer				
Polymeg 1000	47.6	47.6	47.6	47.6
Polymeg 2000	7.4	7.4	7.4	7.4
MDI	45.0	45.0	45.0	45.0
Prepolymer/ curing agent	62/38	62/38	65/35	65/35

Table II. Prepolymer and curing agent formulations for polyurea hard segment adhesives.

Curing Agents			
Component	87-1	87-2	88-2
Tonox 60/40	100	-	-
XU-205	-	100	100
Prepolymer			
Polymeg 2000	77.6	77.6	74.0
HMDI	22.4	22.4	26.0
Prepolymer/ Curing agent	93/7	92/8	88/12

was held constant at 1.0 Hz. or 1.59 Hz. (10 rad/ sec) in some instances. Further discussion of the equations and use of these fixtures is given elsewhere (7,8).

### Results

73 (MDI/ Butanediol/ Polyol) Systems. Halthane 73 series adhesives contain MDI - butanediol hard segments and polyether soft segments. The incorporation of small amounts of higher molecular weight soft segment reduces the tendency of the soft segment to crystallize and improves elongation to break. 73-14 and 73-15 are essentially linear segmented polyurethanes. The addition of the tetrafunctional alcohol N,N,N',N' tetrakis(2-hydroxypropyl)ethylenediamine or Quadrol improves the modulus of the 73-18 and 73-19 adhesives above the hard segment glass transition temperature (~70°C) by crosslinking the system to prevent the onset of viscous flow. Our results (2-4) are consistent with a number of other studies on MDI - butanediol hard segment polyurethane systems (9-12).

In this paper we examine the effect of temperature on the dynamic viscosity of these adhesives. Figures 1 and 2 are isothermal viscosity - time curves for 73-18 and 73-19. As expected, the rate of change of viscosity with time increases with temperature since this depends on cure kinetics. The initial viscosity decreases with temperature because the temperature dependence of viscosity affects the reacting mixture more rapidly than kinetics. On close examination the addition of ferric acetylacetonate is seen to increase the logarithmic rate of change of viscosity in the 73-19 system by about a factor of 2. This is not an exceptionally fast catalyst, but is sufficient to reduce the handling time from 16 to 4 hours (4). 73-18 mixes may be refrigerated for short periods and reused, but after 24 hours at -10°C 73-19 viscosity has been increased beyond a useful limit as shown in figure 2. The viscosity change with time after refrigeration is identical to the 40°C freshly mixed adhesive except that it is shifted upward about an order of magnitude. Note that the dynamic viscosity curves of fully cured 73-19 at 100°C and 80°C are lower than the curve at full cure for 60 °C. This is probably caused by side reactions of the isocyanate occurring at the higher cure temperatures which have a dilatorious effect on the mechanical properties.

The initial viscosity  $\eta(0,T)$  of the unreacted prepolymer/curing agent mixture will vary inversely with temperature according to equation (1) (13,14).

$$\eta(0,T) = A \exp (\Delta E/RT) \quad (1)$$

where A and R are constants,  $\Delta E$  is the activation energy for viscous flow, and T is the temperature. Semilog plots of the initial viscosities of the 73 series polyurethanes versus

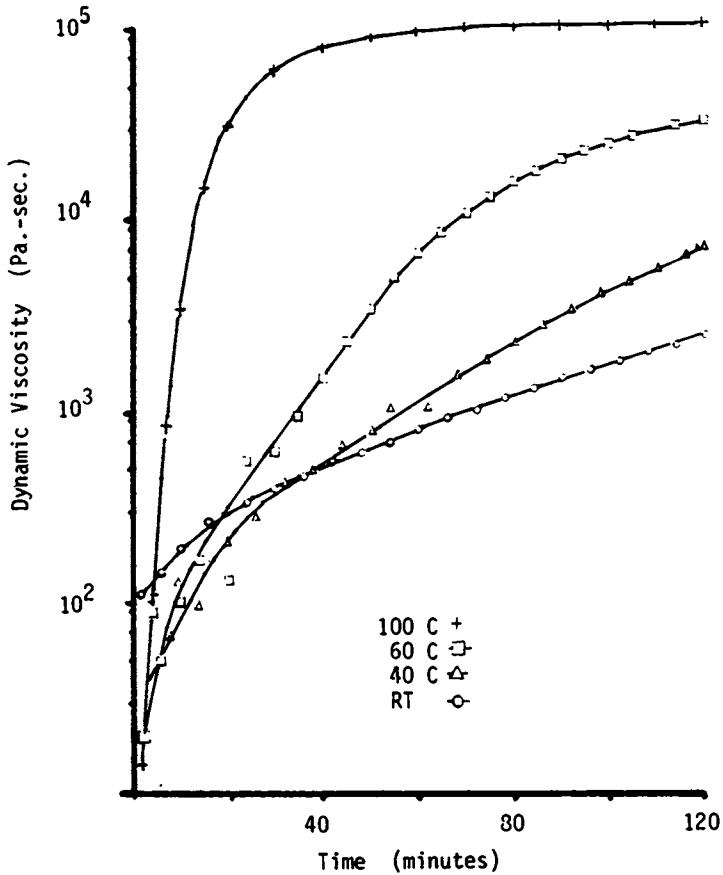


Figure 1. The dynamic viscosity ( $G''/\omega$  in pascal seconds) of Halthane 73-18 segmented polyurethane adhesive increases with time until the chemorheology of cure is complete. Cure curves for four different temperatures show a positive temperature coefficient which should be proportional to the overall reaction rate.



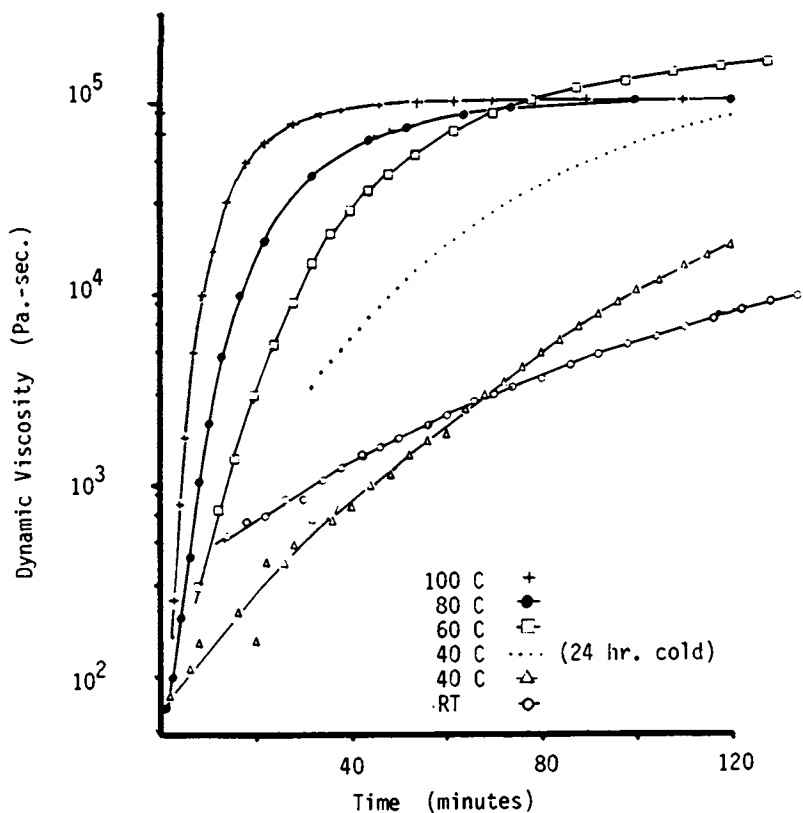


Figure 2. Examining the cure chemorheology of Halthane 73-19 polyurethanes reveals the effect of temperature on initial viscosity, cold storage on shelf life, and side reactions on final cured properties.

reciprocal temperature are given in figure 3. The addition of 5% quadrol, a viscous tetrafunctional alcohol, increases the initial viscosity of 73-18 and 73-19 above that of 73-15. As expected, the iron catalyst does not affect the initial viscosities. The activation energies for viscous flow are  $10 \pm 2$  Kcal/mole for these adhesives. Scatter in the data is high since at higher temperatures the viscosity increases very rapidly and extrapolation to zero time is difficult.

Assuming the viscosity,  $\eta(t,T)$ , change is directly proportional to polymerization under steady state conditions, equation (2) is expected to hold (13,14).

$$[\ln \eta(t,T)/dt] = A' \exp(-\Delta E / RT) \quad (2)$$

where  $t$  is the time,  $T$  is temperature,  $A'$  and  $R$  are constants and  $\Delta E$  is the energy of activation of the overall curing process. The slope of the early time portion of the dynamic viscosity versus time curves of the 73 series urethanes is plotted in figure 3. Estimation of the rate constants from the initial slopes of the viscosity-time curves results in activation energies of 8-10 Kcal/mole. These results are too low compared to values from kinetic measurements on model systems (15) and IR and thermal measurements on segmented polyurethanes (16). The reason for this appears to be the influence of molecular weight on the viscosity (17). The effect of the ferric acetylacetonate catalyst is to increase  $\ln \eta/dt$  or the rate constant by about a factor of 2. Whereas the initial viscosity is affected by the addition of 5% viscous quadrol making 73-18 and 73-19 comparable, the kinetics of cure are affected by catalyst and thus 73-15 and 73-19 fall on the same line while the uncatalyzed 73-18 has lower activation energy and rate constants (see figure 3).

Another surprising result is that no maximum occurs in either the loss modulus or tangent delta during cure of these systems at temperatures above 40°C (see figure 4). One would expect that the onset of gelation would produce maxima as has been observed for epoxy systems (18) and peroxide cured polysiloxanes (19). Vitrification of the hard segments should also produce peaks in the loss modulus and/or tan delta (20). The vitrification of MDI - butanediol hard segments has been reported (21) in systems similar to ours during polymerization as indicated by DSC. In the 73 series adhesives differences in  $G''$  and tan delta would be expected above and below the hard segment glass transition temperature. Above the hard segment transition (60°C) vitrification would not be observed. We attribute the broad maximum sixty minutes into the 40°C loss curve (shown in figure 4) to hard segment vitrification. There is excessive scatter in the data in this region probably due to poor segregation of the MDI-BDO hard segments. Above the hard segment glass transition temperature no vitrification peak would be expected but the gelation peak should be observed and is not.

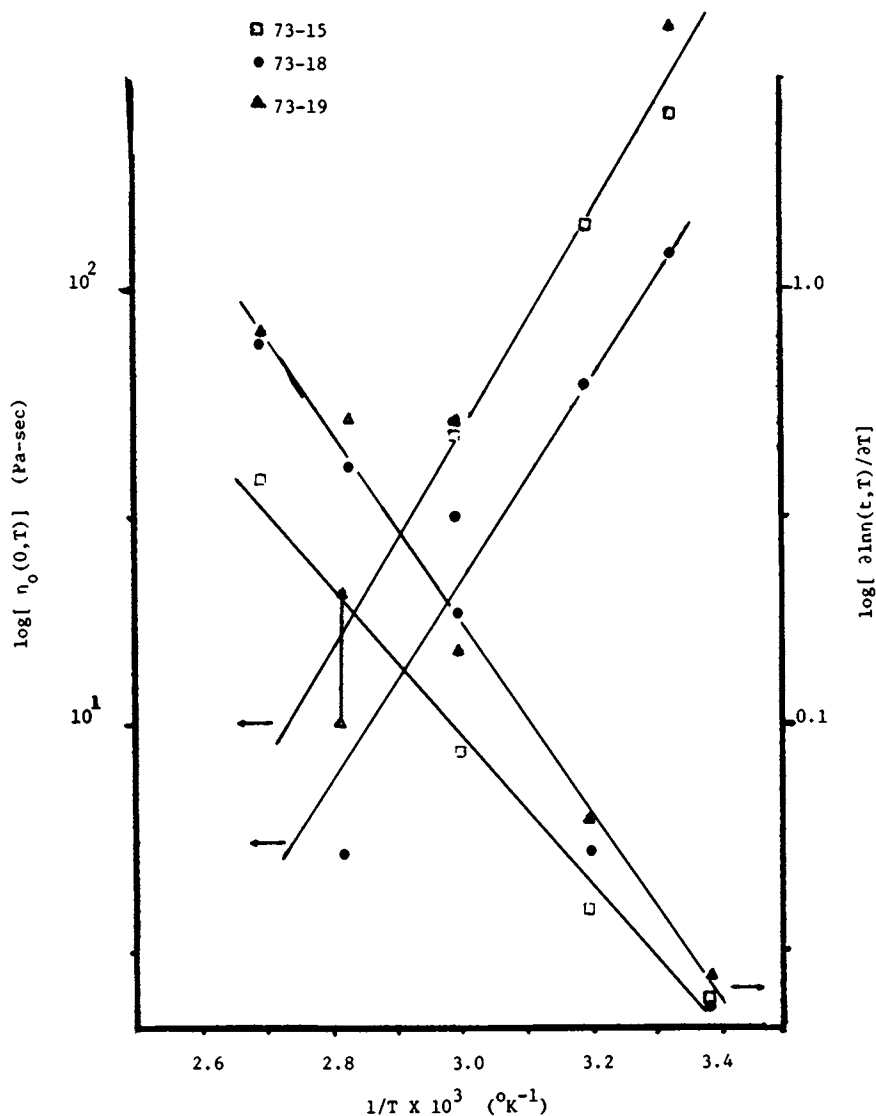


Figure 3. Plots of the log of the initial viscosity versus inverse temperature exhibit Arrhenius behavior with activation energies for viscous flows of about 10 Kcal/mole. Plots of the change in viscosity with temperature versus inverse temperature have negative slope and activation energies for overall curing kinetics of 8-10 Kcal/mole.

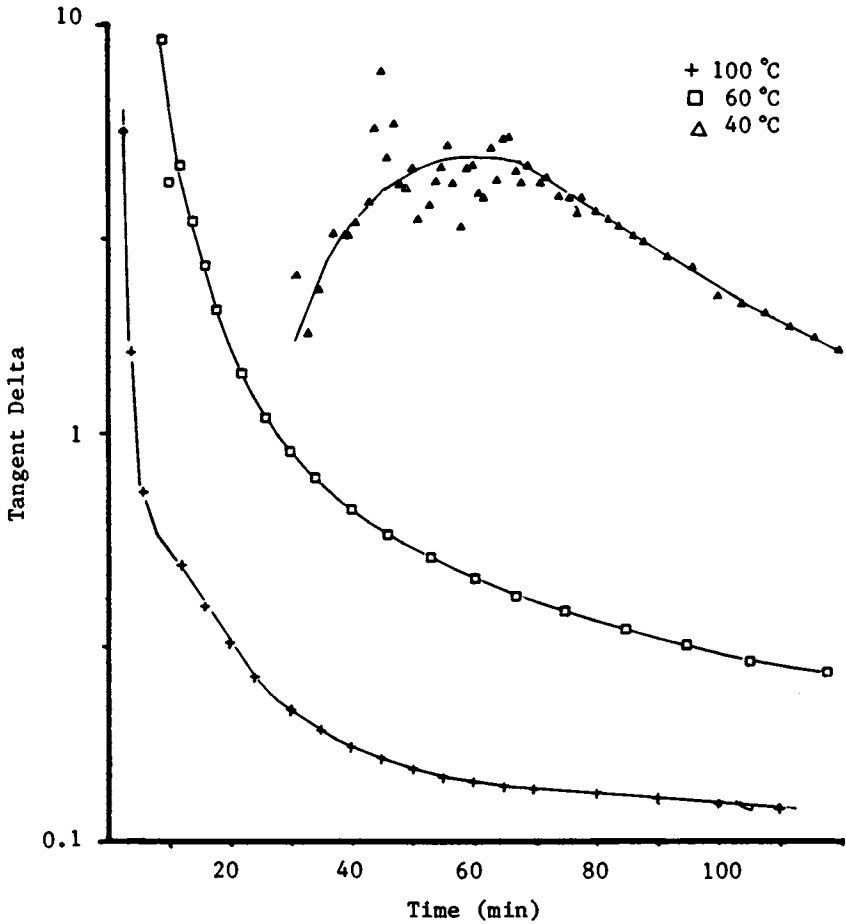


Figure 4. The large broad "maximum" in the loss tangent isotherm of 73-19 polyurethane adhesive at 40 °C is attributed to hard segment development. This peak is not observed above 50 °C because the hard segment glass transition temperature has been exceeded.

Currently the reason for the absence of maxima in the dynamic mechanical properties is not known.

One further phenomena observed in all 73 systems is the decrease in opacity on curing at elevated temperatures. Above about 60°C the poly(tetramethylene glycol) and excess isocyanate become miscible. This miscibility may be assisted by the fact that the MDI-BDO hard segments are above their glass transition temperature. To an extent which has not been quantified as yet, liquid-liquid phase separation of MDI and MDI terminated polyol in the prepolymer at low temperatures persists into the final adhesive. The dynamic mechanical behavior of transparent or opaque adhesive, i.e., cured at 60-100 °C compared to room temperature are virtually identical. Similar immiscibility has been observed in other prepolymers (20). This does not appear to adversely affect the adhesive properties of these Halthanes.

87 and 88 (HMDI/ Aromatic diamine/ Polyol) Systems. The 87 and 88 series adhesives contain aromatic - cycloaliphatic polyurea hard segments which have a considerably higher glass transition temperature ( 190 °C). The soft segments are 2000 molecular weight macro glycols which reduce the soft segment glass transition temperature to -77°C (2). The high polyurea hard segment glass transition temperatures extend the elastomeric behavior of these adhesives to fairly high temperatures for polyurethanes. The increased incompatibility of the polyurea hard segment with the polyol soft segments tends to increase the stiffness and strength of these adhesives compared to the 73 systems. Our results are similar to other literature results (22-25). In fact, aliphatic diamines are equally effective for obtaining high glass temperature hard segments according to Paik Sung, et. al. (25).

Figures 5 and 6 are isothermal viscosity time curves for Halthanes 87-1 and 88-2. Again the initial viscosity depends inversely on temperature. The higher concentration of hard segment formers in 88-2 causes more rapid cure compared to 87-1. Substitution of ethyl groups on the 2 positions of 4,4' methylene dianiline (XU-205) in 87-2 for 4,4' methylene dianiline/m-phenylene diamine (tonox) in 87-1 has very little influence on the viscosity isotherms and so the 87-2 curves are not shown. From equation (1) the initial viscosity decreases with increasing temperature according to an Arrhenius relationship with activation energies for viscous flow of 9-12 Kcal/mole (see figure 7). Because of the rapid reaction rate at high temperatures accurate viscosities are difficult to determine. Apparent activation energies of 6.6 - 7.6 Kcal/mole from the initial slopes of the viscosity curves with inverse temperature, as per equation (2), are below the values expected for these systems (15,20) and further study is needed in this area.

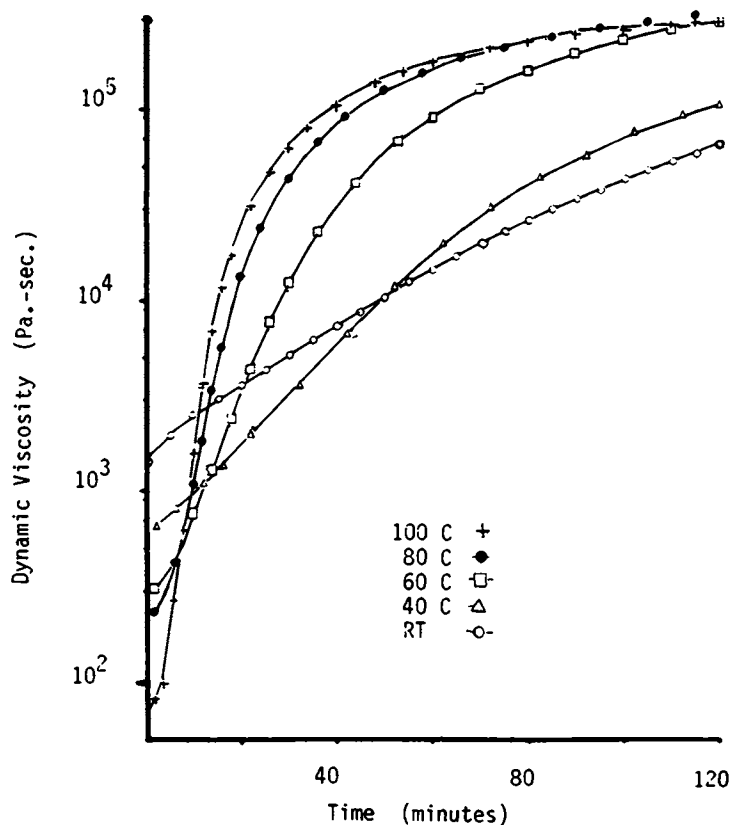


Figure 5. The change in dynamic viscosity of Halthane 87-1 segmented poly(urea-urethane) adhesive with time increases dramatically with temperature. Since the initial viscosity decreases with temperature, the plot cross through each other.

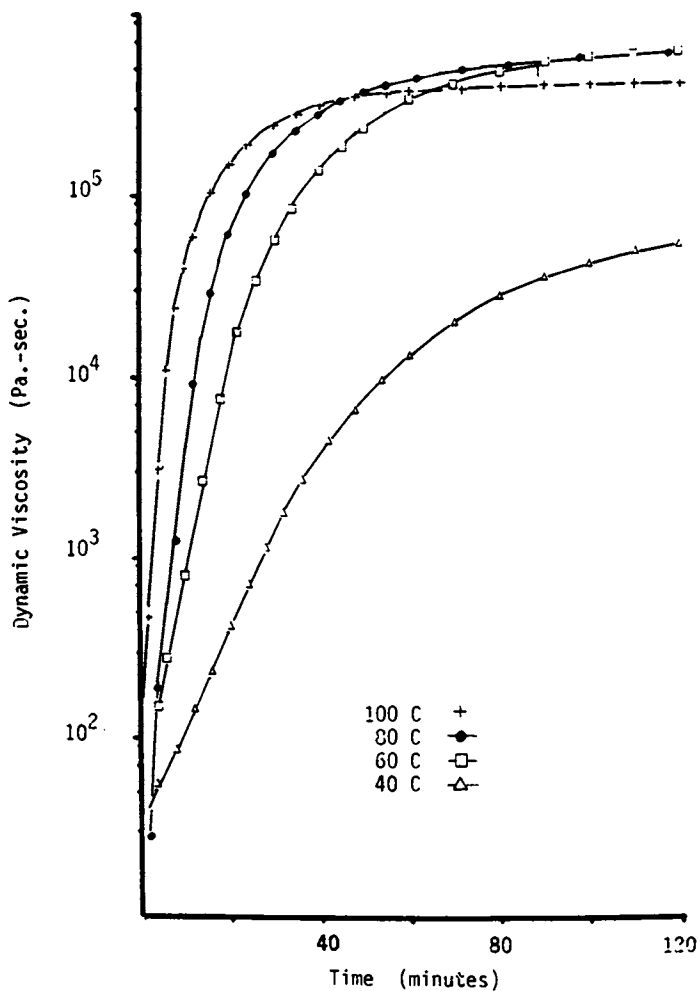


Figure 6. Because of the rapid increase in dynamic viscosity of Halthane 88-2 poly(urea-urethane) adhesive caused by a higher concentration of HMDI- aromatic diamine chain extender, the initial viscosities are difficult to determine accurately.

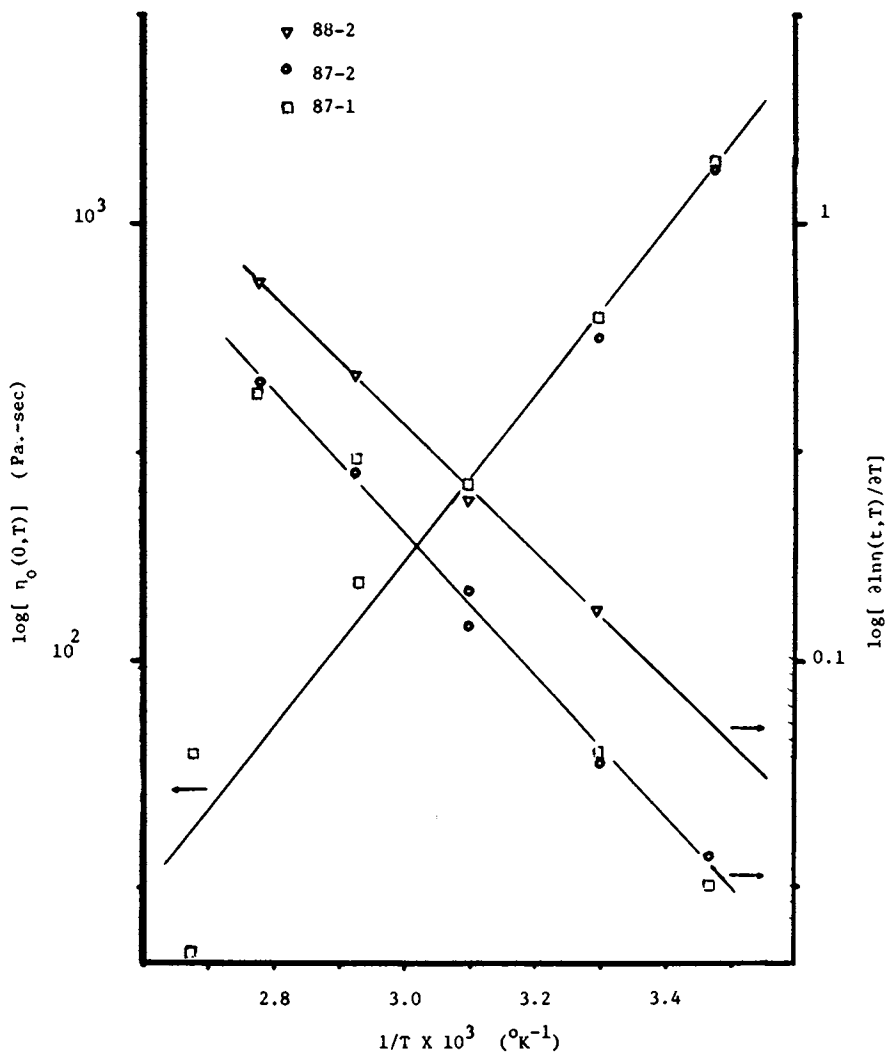


Figure 7. The inverse temperature dependence of initial viscosity and direct dependence of cure chemorheology for poly(urea-urethane) adhesives yield activation energies of 9-12 Kcal/mole for viscous flow and 6-8 Kcal/mole for overall cure, respectively.



As pointed out previously, dynamic mechanical loss measurements should show  $G''$  and  $\tan \delta$  peaks during gelation and hard segment vitrification. We have arbitrarily introduced peaks in the scatter of the  $\tan \delta$  data shown in figure 8 for the 87-1 system. Unfortunately, the scattering behavior is not consistent appearing to give peaks in the 80°C and 40°C  $\tan \delta$  curves but not in the 60°C or 100°C (not shown) curves. Neither can the room temperature loss curve data be resolved into a peak. It would be equally accurate to draw the loss curves for this system without maxima. Perhaps with a more sensitive transducer the early time loss behavior of these rapid curing amine systems could be resolved. In the 87 and 88 polyurea-urethanes macrophase separation does not occur, i.e., the components are miscible, and the broad maxima found in the MDI-BDO systems cured below the hard segment glass transition are not observed. Again in these systems no clear evidence of gelation or vitrification is found from our dynamic mechanical measurements.

### Conclusions

Investigation into the dynamic viscosity change on curing of seven segmented polyurethane polymers has shown that initial viscosities decrease with temperature while the rate of cure and change in viscosity depend directly on temperature. The polyurea hard segment (87 and 88) systems cured more rapidly than polyurethane hard segment (73) systems. By using iron catalysts the cure rate of the polyurethane hard segment systems begins to approach that of the 87 and 88 systems. For an as yet undetermined reason no definite evidence of gelation or vitrification was found in the dynamic mechanical measurements on these systems during cure even though the hard segment glass transitions for the polyurea systems are well above the cure temperature. The observed liquid liquid phase separation in 73 systems at low curing temperatures implies the presence of an upper critical solution temperature and/or chemical compatibilization of the MDI terminated polyether during cure at the higher temperatures. All of these cured adhesives have low to intermediate moduli over a wide temperature range, bond rapidly and well to most substrates, and can be cured at room temperature or accelerated with heat in modestly dry environments. At cure temperatures above 60-80 °C some side reactions may occur reducing the properties of the cured adhesives.

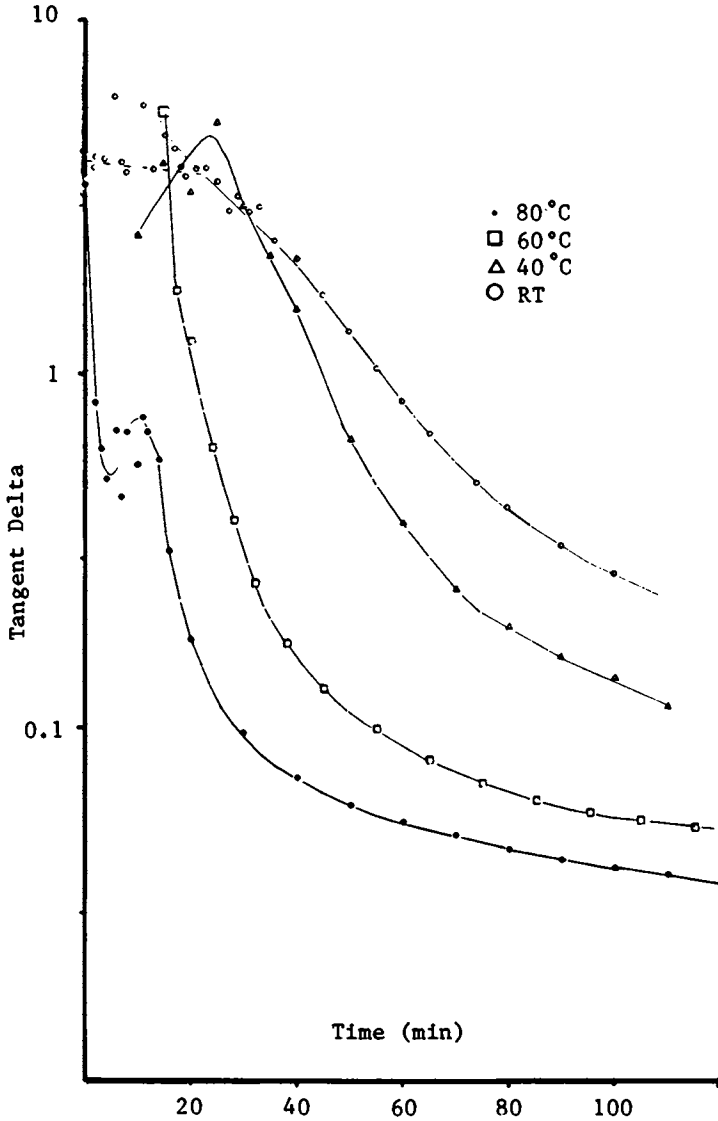


Figure 8. The scatter in the loss tangent data for 87-1 poly(urea-urethane) makes identification of the onset of gelation or hard segment vitrification impossible. Although we have drawn peaks in some of the isotherms, Statistical fits do not justify them.

### Acknowledgments

We would like to thank Barbara McKinley for assistance in preparing and testing these adhesives and LeRoy Althouse for his advise and discussions.

Work performed under the auspices of the U.S. Department of Energy by Lawrence Livermore National Laboratory under contract No. W-7405-Eng-48.

### Disclaimer

This document was prepared as an account of work sponsored by an agency of the United States Government. Neither the United States Government nor the University of California nor any of their employees, makes any warranty, expressed or implied, or assumes any legal liability or responsibility for the accuracy, completeness, or usefulness of any information, apparatus, product, or process disclosed, or represents that its use would not infringe privately owned rights. Reference herein to any specific commercial products, process, or service by trade name, trade mark, manufacturer, or otherwise, does not necessarily constitute or imply its endorsement, recommendation, or favoring by the United States Government or the University of California. The views and opinions of the authors expressed herein do not necessarily state or reflect those of the United States Government, and shall not be used for advertising or product endorsement purposes.

### Literature Cited

1. Estes, G.M.; Cooper S.L.; Tobolsky, A.V. J. Macromol. Sci., Rev. Macromol. Chem. 1970, C4, 167.
2. Hoffman, D.M. in "Urethane Chemistry and Applications," Edwards, K.N. Ed. ACS SYMPOSIUM SERIES ACS: Washington, D.C., 1981; p. 343.
3. Hoffman, D.M.; Hammon, H.G.; Althouse, L.P. SPE Ann. Tech. Papers 1981, 39, 314.
4. Hammon, H.G.; Althouse, L.P.; Hoffman, D.M. "Development of Halthane Adhesives for Phase 3 Weapons: Summary Report"; UCRL- 52943, December, 1980.
5. Prime, R.B. in "Thermal Characterization of Polymeric Materials" Turi, E.A., Ed.; Academic : New York, 1981, Chap. 3.
6. Collins, E.A.; Bares, J.; Billmeyer, F.W., Jr., "Experiments in Polymer Science" John Wiley: New York, 1973, Chap. 5.
7. Rheometrics Mechanical Spectrometer Operating Manual, Rheometrics Inc., 1974.
8. Middleman, S. "The Flow of High Polymers"; John Wiley: New York, 1968.

9. Kajiyama T.; MacKnight, W.J. Trans. Soc. Rheol. 1979, 13, 527.
10. Huk D.S.; Cooper, S.L. Polym. Eng. Sci. 1971, 11, 369.
11. Schollenberger C.S.; Dinbergs, K. J. Polym. Sci. Symposium, 1978, 64, 315.  
C.S. Schollener, in "Multiphase Polymers", Cooper, S.L.; Estes, G.M., Eds.; ADVANCES in CHEMISTRY SERIES No. 176, ACS: Washington, D.C., 1979; p. 83.
12. Dzierza, W. J. Appl. Polym. Sci., 1978, 22, 1331.
13. Roller, M.B.; Polym. Eng. Sci., 1975, 15, 406.
14. White, R.B., Jr., Polym Eng. Sci. 1974, 14, 50.
15. Reegen, S.L.; Frisch, K.C.; Adv. in Urethane Sci. and Technol., 1971, 1, 1.
16. Richter, E.B.; Macosko, C.W. Polym. Eng. Sci., 1978, 18, 1012.
17. Lipshitz, S.D.; Macosko, C.W. Polym. Eng. Sci., 1976, 16, 803.
20. Gillham, J.K. Polym. Eng. Sci., 1979, 19, 676.  
Enns, J.B.; Gillham, J.K. ACS Org. Coatings Appl. Polym. Sci. Prepr., 1982, 46, 592.
21. Hager S.L.; MacRury, T.B.; Gerkin, R.M.; Critchfield, F.E. in "Urethane Chemistry and Applications", Edwards, K.C., Ed. ACS SYMPOSIUM SERIES No. 172, ACS: Washington, D.C., 1982; p. 149.
22. Work, J.L. Macromol., 1976, 9, 759.
23. Illinger, J.L.; Schneider, N.S.; Karasz, F.E. Polym. Eng. sci., 1972, 12, 25.
24. Paik Sung, C.S.; Hu, H.B.; Wu, C.S. Macromol. 1980, 13, 117, 111.
25. Van Bogart, J.W.C.; Lipaonitkal, A.; Cooper, S.L. in "Multiphase Polymers", Cooper, S.L.; Estes, G.M., Eds.; ACS Advances in Chemistry Series No. 176, ACS: Washington, D.C., 1979, p. 1.

RECEIVED March 31, 1983

## **Rheological Cure Transformation Diagrams for Evaluating Polymer Cure Dynamics**

**RICHARD J. HINRICHS**

Applied Polymer Technology, Inc., Costa Mesa, CA 92627

Structural engineering polymers (epoxies, phenolics, polyimides) are complex oligomeric mixtures which result in multiple reaction pathways. Unfortunately, the structural engineer is faced with the physical problem of producing an article whose manufacturing behavior is dependent on how the polymer reacts to various thermal histories. This paper will deal with the development of a laboratory procedure (based on the rheological visco-elastic properties of the polymer) which accurately describes the polymer cure behavior. In addition, the data is translated from the chemical semantics into engineering transformation diagrams which process engineers can easily interpret. The converted data in graphics form can then be used to model various manufacturing constraints (tooling, thermal vessel response parameters, etc.) to determine their affects on the polymer reaction behavior. This leads directly to predicting allowable efficient thermal profiles for the manufacturing of structural polymers.

The purpose of this paper is to present a technique whereby manufacturing process dynamics for structural polymers can be accurately defined through efficient laboratory rheological characterization. Structural polymers, in this paper, refer principally to the thermosetting epoxides, phenolics and polyimides. This type of test pattern, however, is generally applicable to the production and utilization of most polymers. The engineering applications associated with these polymers involves primary and secondary aerospace articles. In this situation, failure to meet performance criteria could result in catastrophic loss of the vehicle and associated cargo.

The typical application situation is where a new material or structure is being implemented. The question to be resolved is what thermal cure profile (time, temperature, pressure) should be specified. The current approach has been to expend much time and material producing simulated panels for validation. This process is neither rigorous

0097-6156/83/0227-0187\$06.00/0

© 1983 American Chemical Society

(control over fabrication techniques, tooling variations, environmental factors, etc.) or time effective (autoclave-press operations expense, labor force manning requirements, sequential laminate experiments required to feedback data for next test, etc.) The cure cycle development costs generally exceed \$30,000 to \$50,000 and generally require a minimum of six months time.

The problem really centers on understanding that these polymers are reactive chemical systems. They have variable kinetics, form numerous adducts and phase morphology as a function of the actual process (time, temperature, pressure, etc.) pathway incurred. The ability of a material to uniformly exhibit consistent process behavior and mechanical properties will therefore depend on controlling the variations within a materials chemical process boundaries.

### Test Objectives

The objectives of this test pattern is to analytically resolve these problems into three manageable segments. The first task will be to define the viscoelastic kinetic properties of a material as a function of various reaction temperatures. These properties (viscosity, viscous modulus, elastic modulus, tan delta) define the rate of change in the polymers overall reaction "character" as it will relate to article flow consolidation, phase separation particle distribution, bond line thickness and gas-liquid transport mechanics. These are the properties primarily responsible for consistent production behavior and structural properties. This test is also utilized as a quality assurance technique for incoming materials. The reaction rates are an excellent screening criteria to ensure the polymer system is "behaviorally" identical to its predecessor. The second objective is to allow modeling for effects of process variables. This will allow the material to undergo environmental exposure situations which could be encountered during production. It can measure the effects of out time during fabrication, heat rate variations, or formula anomalies. This test series again utilizes the conditioned samples rheological response under process simulation. The third goal is to translate this information into engineering cure transformation diagrams. These diagrams are designed to convey the entire chemical test data into a reaction phase diagram that engineering personnel (not rheologists, chemists, or material scientists) can readily interpret to design the necessary process specification requirements. They will provide accurate information for the appropriate most optimum dwell times-temperatures, allowable part thermal deviation which will still maintain consistent reaction properties, and identify when to optimize application of pressure.

### Instrument Requirements

The rheological equipment requires certain capabilities in order to effectively measure composite adhesive resin systems. The transducer must have a dynamic range from 1 to  $10^6$  poise. This is a result of achieving a very low viscosity during an elevated temperature cure and

the subsequent reaction to high viscosity polymer upon gelation. To help increase its sensitivity for low viscosity resin systems, 50 mm parallel plate fixtures are beneficial. High viscosity systems (i.e.; adhesives) use 25 mm parallel plates. Strain and frequency sweep options are necessary to evaluate the materials linear response region and affects of shear rate. The rheological properties are shear-stress dependent. Thus, these options measure the materials' response and select the appropriate linear instrument parameters. The instrument needs a variable heating rate chamber with computer controlled linear ramping capability. This is used to model various cure cycles and heating rates.

The instrument is operated in a sinusoidal, oscillating mode. The oscillating mode is preferred to minimize shear plane and rate effects associated with continuous 360° rotation. The system computes the torque response and the resultant phase angle. The phase angle is directly related to the storage ( $G'$ ) and loss ( $G''$ ) modulus by the following equations:

$$G' = G^* \times \cos \delta$$

$$G'' = G^* \times \sin \delta$$

$G^*$  = Complex Modulus = Ratio of stress to strain amplitude for a given instrument condition.

$$\eta^* = \frac{G^*}{W} = \sqrt{[(G')^2 + (G'')^2]} / W$$

Where  $\eta^*$  = Dynamic Viscosity

$W$  = Frequency (radians per second)

### Sample Handling

Care must be exercised in preparing a sample for rheological characterization. The observed polymer properties are strongly influenced by several factors. First, moisture, absorbed from the laboratory humidity, can cause a 50% deviation in observed viscosity after only a few hours of exposure. Emulsified non-homogeneous samples prevent proper contact of the plate-resin surface and induce data scatter. Many thermoset polymers are capable of reacting slowly even at room temperature. This advancement causes changes in rheological properties. The following handling practice is recommended to prevent these distortions:

- 1) Maintain samples in a dessicated environment. A sample brought to the laboratory in a non-controlled container should be dessicated 24 hours before attempting to characterize the material.
- 2) Avoid touching the sample surface directly as much as possible. The water, oils, and other chemicals from the laboratory will transfer and obscure the test results.
- 3) Transfer from the control environment directly to the instrument in as short a time as possible.
- 4) Store the samples in a sealed container at 0°F. Let freely warm to room temperature in a dessicated environment prior to opening

the container. Cold resin immediately condenses water into the matrix.

### Operational Parameters

The actual operational parameters must be determined for each individual material. This involves running the frequency and strain sweeps mentioned earlier at the various temperatures of interest. It is then a matter of deciding the best linear operating conditions to be employed. There are several operator techniques, however, which will greatly increase precision if followed.

- a) Calibrate the instrument using silicone putty as suggested by the manufacturer. The transducers can easily be damaged and we recommend checking its response once a week. Also, check, using a calibrated external thermocouple, the temperature response of the system. Even 1° can significantly change the isothermal properties.
- b) Zero the parallel plates and place the resin sample onto the fixtures. Reduce the gap to within 0.04mm of the desired setting. Remove excess resin from around the plate, let the chamber warm to the desired starting temperature, and then reduce the gap to the actual desired size (0.06 mm for formulated polymers and 0.3 mm for low viscosity simple monomers). This keeps a consistent edge bleed of resin on the plates. It has been found that not keeping this technique constant caused 10% to 15% variation in properties.

Note: For adhesive film samples, this is not practical. Samples are cut to the appropriate diameter (generally 25 mm parallel plates, due to their high viscosity profile) and 2 to 3 plies placed on the fixture.

This predetermines the gap size to be the film thickness.

- c) The initial low temperature is allowed to stabilize four minutes before acquiring data.
- d) Begin test experiment or frequency and strain sweep mode as desired.

Though the parallel plate method is described here, cone and plate options are also available. These will more accurately describe the shear stress dependence of the material if that is the experimental goal.

### Applications

The principle rheological properties which reflect the polymer process dynamics are the loss modulus ( $G''$ ), storage modulus ( $G'$ ), dynamic complex viscosity ( $\eta^*$ ), and tan delta parameters. In simplified form the loss modulus describes the viscous or fluid component of viscosity. That is, how easily the molecules can move past each other. The storage modulus describes the elastic or network entanglement structure of the polymers. It is, therefore, sensitive to cross linking, reaction formation and the elastomeric modifiers. The complex dynamic viscosity is the combined effect of both moduli discussed. It, therefore,



will relate to the overall reaction cure dynamics of the polymer and the process properties described earlier. The tan delta is the ratio of the loss to storage modulus. It is very useful in describing the effects of variations in the polymer chemistry due to some applied variable. For example, in the presence of moisture, tan delta may increase initially during cure, but dramatically decrease at 110°C compared to a control dry sample. This indicates an initial fluidity (plasticization) effect followed by cure acceleration. These are important parameters to understand in order to model cure process effects.

### Experimental

The first test is a series of isothermal temperature hold experiments measuring the visco-elastic kinetic cure properties (Figure 1). The temperature values selected bracket every 10°F, the range in which processing is to occur. The four properties measured are the loss modulus (viscous modulus  $G''$ ), storage modulus (elastic modulus  $G'$ ), complex viscosity ( $\eta^*$ ), and tan delta ( $G''/G'$ ). However, when mainly newtonian liquids or monomers are present ( $G'' \gg G'$  and  $\tan \delta > 10$ ), viscosity is sufficient to use for the evaluation criteria.

The viscosity and tan delta parameters are plotted as a function of time for various temperatures. The regions of importance are more easily observed in Figure 2. This is an identical configuration graph as Figure 1 but marked with critical engineering transitions. This represents the classical polymer phase states. (1) That is, as we first heat the polymer it will melt or flow and be in a liquid state. The reaction will proceed until such time that sufficient network structure will build into insoluble infinite molecular weight entities known as gelation. Here the polymer will form an elastomeric type network until finally vitrification occurs and a gelled glass phase polymer exists. The points of importance in this scenario are when network structure is measurably beginning to increase. This represents a cautionary zone when the "character" of the polymer is beginning to change from a viscous fluid viscosity towards an elastic rubber type of viscosity. It is still fully processable here but this serves as an indicator of events forth coming. The next point is when gelation is occurring. This has been correlated with  $\tan \delta = 1.0$  from an engineering view point. (2) Thus, the range of processable polymer states (fluid to elastic) is definable for each reaction temperature. These points are marked on Figure 2. In addition, out time aging data can be evaluated and superimposed on these diagrams. The data indicates the general trend to be the higher the process temperature the less the effect of room temperature aging. Figure 3 is an important illustration of an elastomeric modified epoxy system. Here there is a phase precipitation occurring before gelation. The importance of that precipitation is in the rubber particle size distribution which forms as it is effectively forced out of the increasing polymer network structure. This change in solubility characteristic as a function of increasing viscosity induces the elastomers to separate into discrete globules. These globules are responsible for the fracture toughness and crack propagation characteris-

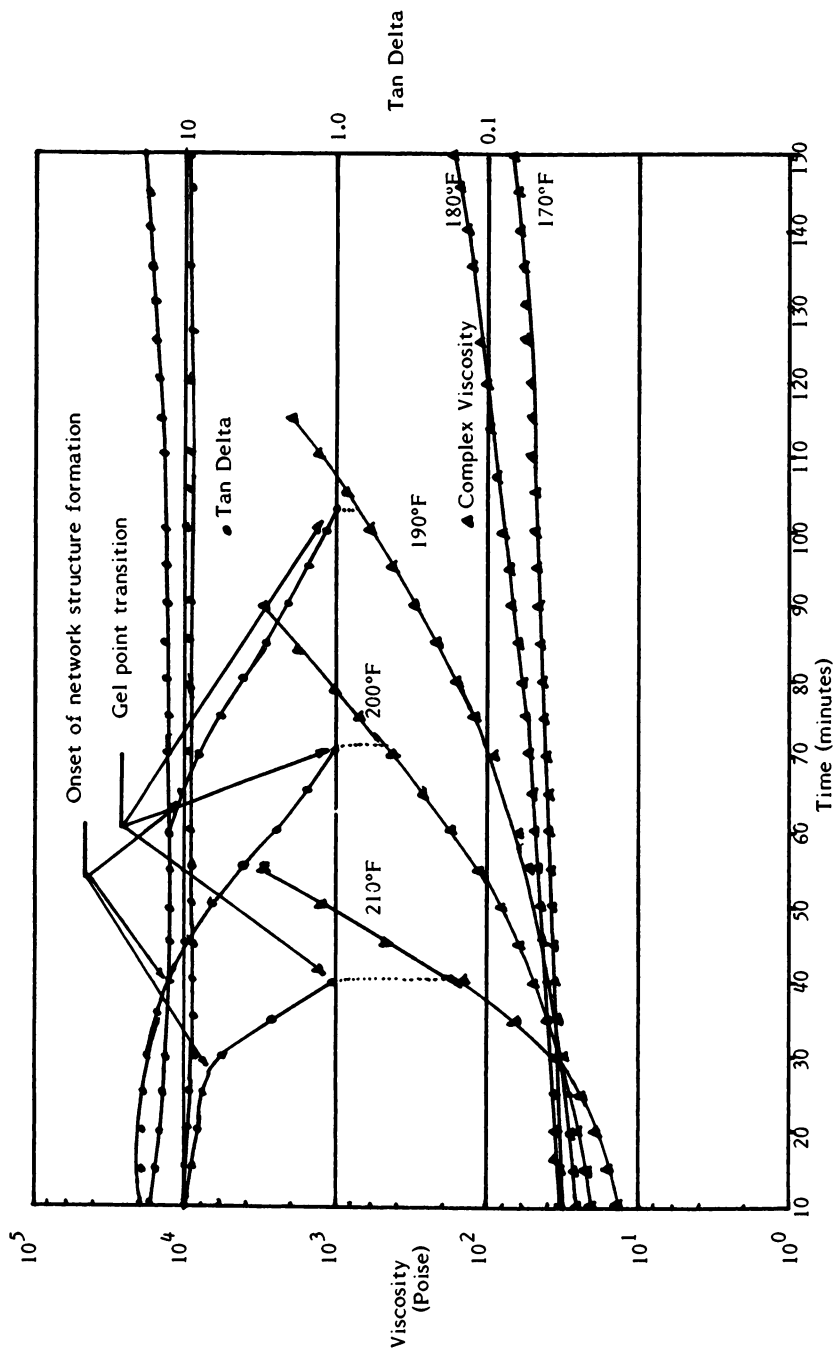


Figure 1. Isothermal Kinetic Behavior - Accelerated Epoxy System.

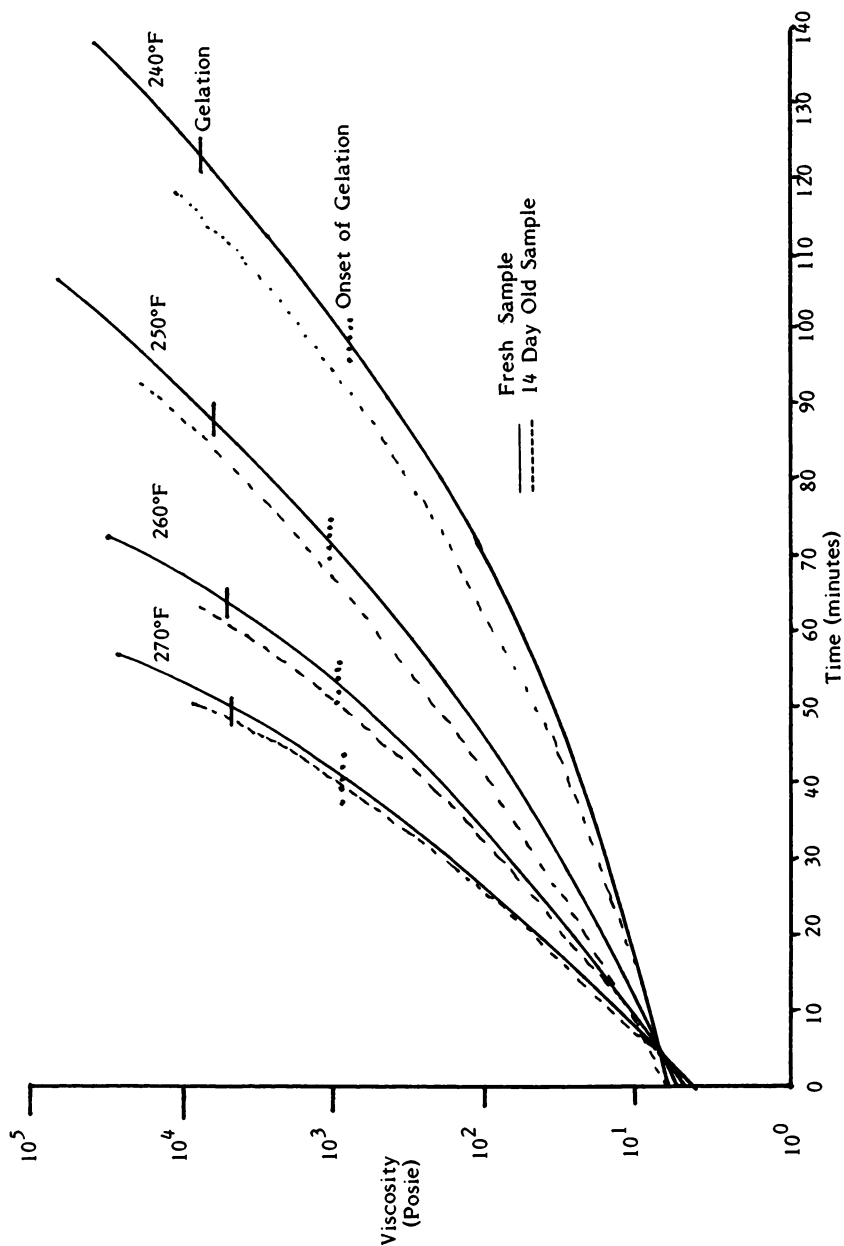


Figure 2. Isothermal Kinetic Phase Diagram Affect of Room Temperature Aging.

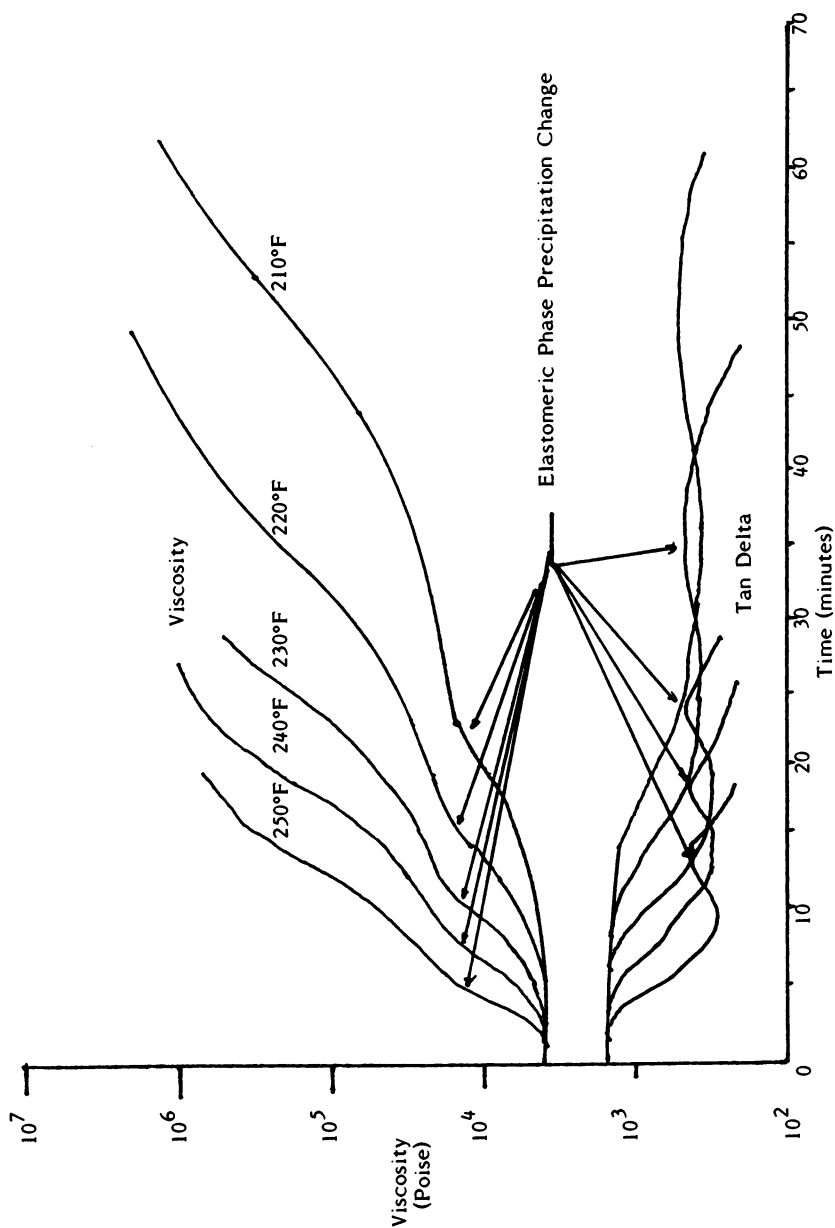


Figure 3. Isothermal Kinetic Diagram Illustrating Phase Precipitation Effects.

tics of a given formula. A problem can arise if incorrect or nonconsistent precipitation distribution occurs. Figure 3 clearly indicates the variability in precipitation time as increased temperatures are employed. Thus, small globules are formed under short precipitation conditions and larger agglomerations form when given greater time to coalesce. A subnote can be mentioned here in that the peak area in the tan delta curve has been found to be representative of the quantity of modifier present.

The next type of test is a heat rate effect evaluation. Here the sample is heated at various rates over the process range to define any effects on reaction initiation temperatures or kinetics. Figure 4 illustrates the effect of low rates allowing sufficient time for chemical reactions to change the process behavior. The higher heat rates indicate that no significant reaction products have had the opportunity to influence the process behavior. This type of information is useful for the engineering staff to set process boundary limits to maintain flow consistency.

Another variable easily studied under these rheological conditions is environmental effects. Humidity exposure under shop conditions can easily effect the reaction kinetics. Figure 5 illustrates the effect of moisture on an accelerated epoxy formula. For clarification, accelerators are considered like consumable catalysts which promote the system to cure at lower temperatures than would otherwise be possible for the particular curing agent employed. The curing agent is the reacting component which supplies the cross linking capacity to the formula. In this case, one can see that moisture is blocking the effectiveness of the accelerator. This could result in the formula behaving as a non-accelerated formula and not properly cured (low glass transition and mechanical properties). It should be noted that previous work on non-accelerated systems have found the opposite effect where moisture can help accelerate amine-epoxide formulas. (3-4) This single test pattern accurately defines what problems may occur and how to design allowable specifications to accomodate the situation.

These two basic rheological tests (isothermal reaction kinetics and heat rate tests) have been seen to generate a complete picture of a materials' response to production situations. Unfortunately, the data is not in a convenient form to translate this information into easily recognizable engineering process diagrams. This is accomplished by rearranging the previous data into isoviscosity engineering cure transformation diagrams (Figure 6). The diagram is made by rearranging the axis into temperature (data available from the various isothermal kinetic tests) and time. The result is a picture of the time it will take to reach a given viscosity level for any reaction temperature. This is actually the least important point of this diagram. Here the liquid, cautionary liquid to elastic transition and gel-elastic regions are easily identified. Further, the engineer can define exactly the process viscosity range desired and can draw a process window. For any given location of that viscosity range (i.e.;  $P_1 - P_2$ ) the engineer can read the temperature axis to define the allowable thermal variation tolerable by this material, process temperature required under those conditions, and exactly what

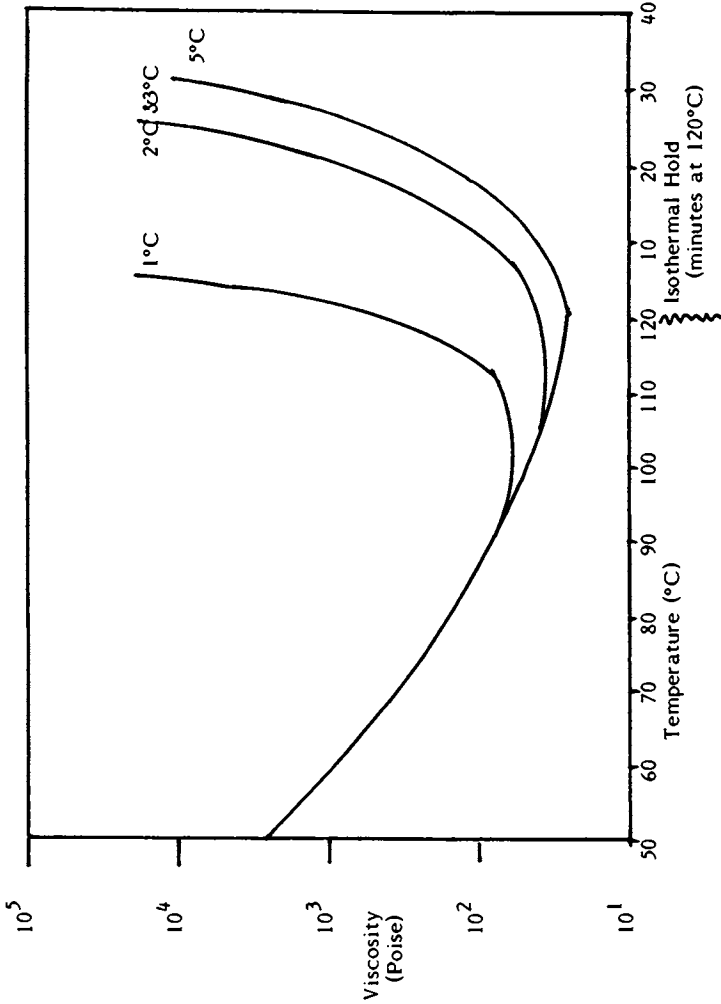


Figure 4. Affect of Varying Heat Rates.

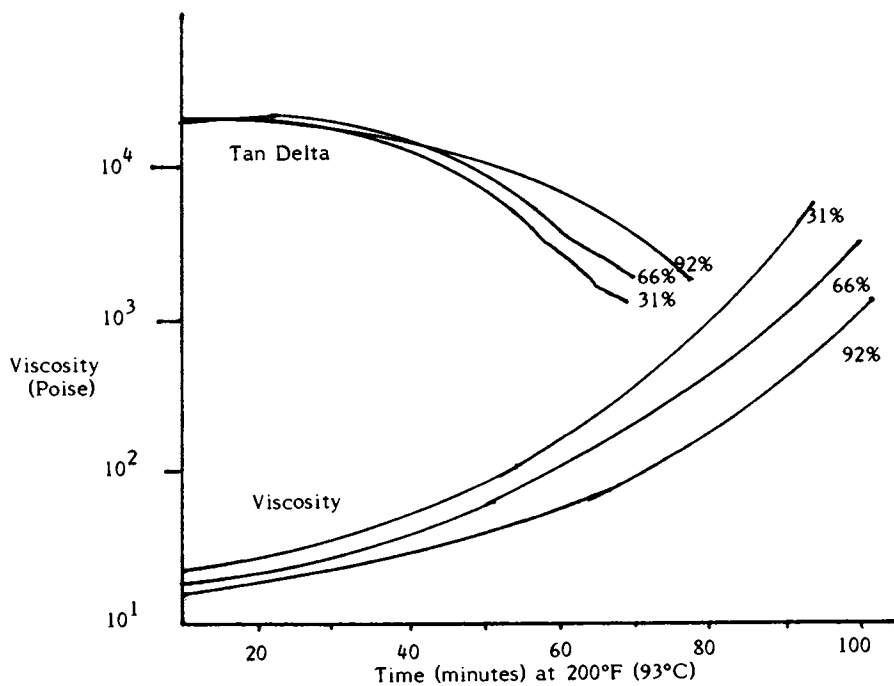


Figure 5. Moisture Effects on Viscosity and Tan Delta.

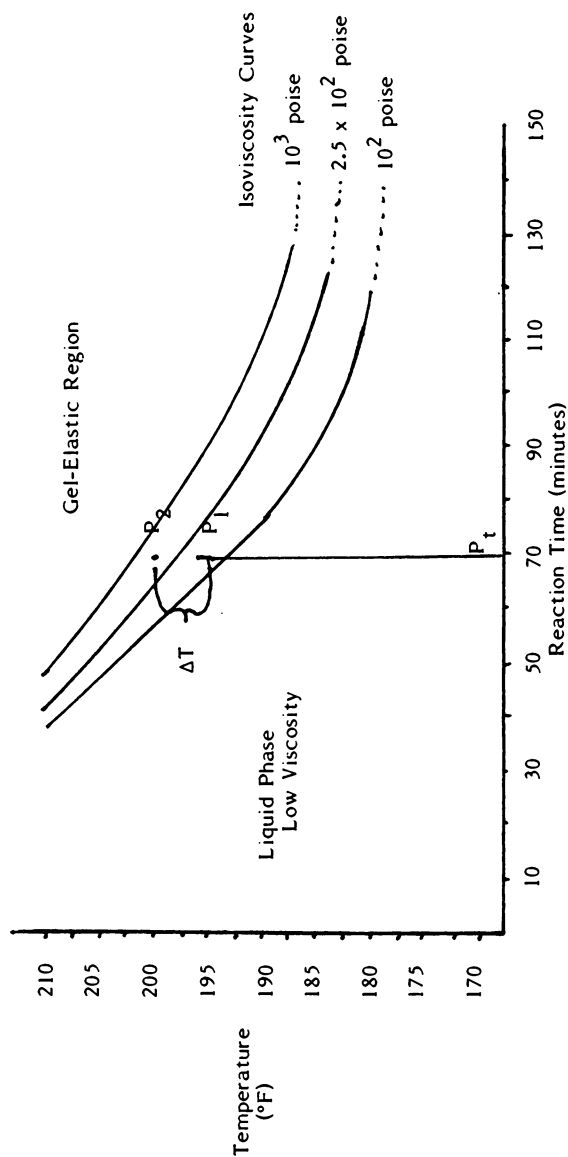


Figure 6. Engineering Cure Transformation Diagram Accelerated Epoxy System.



time ( $P_c$ ) pressurization is required such that all the parts will be in the same chemical-viscosity condition. In addition, it is evident that for production efficiency a short process time would be desirable. But note that the allowable part thermal variance is narrower and process temperatures are higher. If the manufacturing system cannot tolerate that level of control, you can simply move downward on the curves to longer times but larger thermal variation tolerances. This completes the scope of chemical information the process engineer requires to develop material process requirements.

### Conclusion

This rheological technique described accomplishes our test objectives and accurately portrays chemical data in terms manufacturing engineers can utilize to optimize their specific manufacturing situation. Reaction kinetics, thermal variations, environmental effects, and out time aging are readily quantifiable effects which can be defined under these laboratory test conditions. This test pattern can be completed within one month labor time and is thus far more efficient than conventional trial panel techniques. The engineering cure transformation diagram is an effective tool for presenting process engineering the results of the rheological data for implementation of process specifications based on a materials' chemical behavior.

### Literature Cited

1. Gilham, J. Polymer Engineering & Science 1979, Vol. 19, No. 10.
2. Tung, J.; Dynes, P. Proc. ASTM Conference Oct. 1981.
3. Hinrichs, R.; Thuen, J. SAMPE Journal 1979, Vol. 15, No.6, 12-20.
4. Thuen, J.; Hinrichs, R. Proc. 1980 National SAMPE Symposium Vol. 25.

RECEIVED March 31, 1983

## Curing Kinetics of Unsaturated Polyester and Vinyl Ester Resins

CHANG DAE HAN and KWOK-WAI LEM

Department of Chemical Engineering, Polytechnic Institute of New York,  
Brooklyn, NY 11201

Unsaturated polyester resins are one of the most important thermosetting resins used for preparing molding compounds for hot-press matched molding, cold molding, and contact molding.

Polyester resins of commercial interest, containing carbon-to-carbon double bonds, are generally classified into three types: Alkyds, polyallyl esters, and linear unsaturated polyesters. Alkyd resins, which are prepared from polyhydric alcohols and dibasic acids or their corresponding anhydrides, together with modifying oils or their corresponding acids, find extensive use in surface coatings. Both polyallyl esters and linear unsaturated polyester resins are used primarily in moldings and castings. Polyallyl esters are prepared from the monomers derived from the reactions of allyl esters of dibasic acids or their corresponding anhydrides, the most important monomers being diallyl phthalates and diallyl isophthalates. The molded articles produced with diallyl phthalates are generally expensive and therefore find use in special applications, such as in manufacturing electrical components requiring good electric insulation and dimensional stability (1).

On the other hand, the linear unsaturated polyester resins find use in many commercial applications, such as in producing solventless lacquers, and thermosetting molding compounds. The resin is normally prepared by the reaction of a saturated diol with a mixture of an unsaturated dibasic acid and a 'modifying' dibasic acid or its corresponding anhydride. It is commonly referred to as

0097-6156/83/0227-0201\$06.25/0

© 1983 American Chemical Society

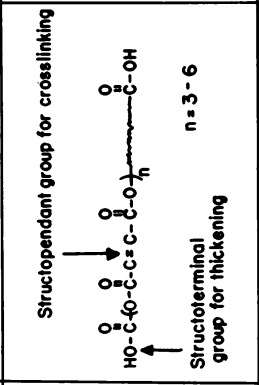
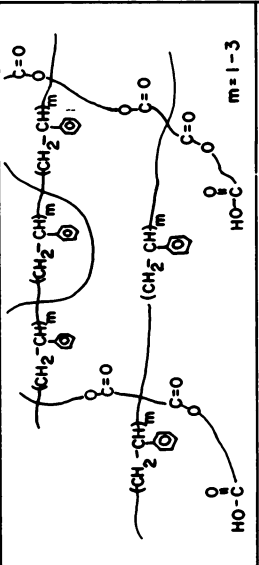
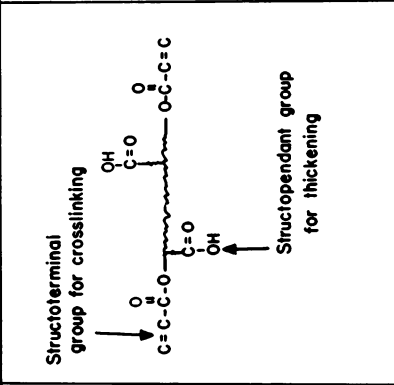
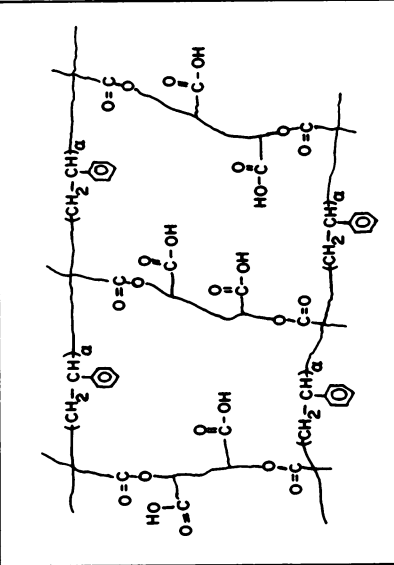
'conventional unsaturated polyester,' and typical examples are bisphenol A-fumaric acid polyester and isophthalic polyester. Commercially, the resin is available in the form of solutions containing 60-70 wt. % of a prepolymer dissolved in a reactive solvent (e.g., styrene). The conventional polyester resins reinforced with glass fibers are used in roofing and building insulation, automobiles, paneling for lorries, and boat hulls (2).

As illustrated in Table I, in conventional polyester resins, the ester groups and carbon-to-carbon double bond linkages are located along the polymer chains, thus referred to as structopendant (3), and they are distributed randomly in the polymer network after the polymer has been crosslinked with styrene. The cured resins are rigid, heat stable, and have good chemical resistance to most inorganic and organic acids and, also, to a wide range of organic solvents. However, the ester groups and the unreacted carbon-to-carbon double bonds in the network provide sites for hydrolytic attack, oxidation, and/or halogenation. This makes the cured resin unsuitable for use in aggressive environments (1,2).

To overcome these drawbacks, in recent years much attention has been paid to the development of resins which can be fabricated with the same processes as those for conventional polyester resins, but having superior properties. Vinyl ester resins are the result of such development efforts (4-6). Vinyl ester resins are addition products of various epoxide resins and ethylenically unsaturated monocarboxylic acids (5). It combines the excellent mechanical, chemical and solvent resistance of epoxy resins with the properties found in the unsaturated polyester resins. In general, the cured vinyl ester resin has physical properties superior to the cured conventional ester resin, particularly corrosion resistance. This arises from the differences in the number and arrangement of polar groups such as ester and hydroxyl groups and carbon-to-carbon double bonds present in the polymer chains.

As illustrated in Table I, in the vinyl ester resins, the ester groups and carbon-to-carbon double bond linkages are located at the end of the polymer

Table I. Speculative Prepolymer and Crosslinked Polymer Structures

Resin	Speculative Prepolymer Structure	Speculative Crosslinked Polymer Structure
<p>Unsaturated Polyester Resin</p> 		
<p>Vinyl Ester Resin</p> 		

chains, thus referred to as structoterminal (3), and they are distributed regularly in the network after the polymer has been cured. As a result, the cured vinyl ester resin is tougher and has higher resistance to crazing or cracking during service than the cured conventional polyester resin. Note that the distance between crosslinks, i.e., approximately the entire chain length of the prepolymer molecule, is available for absorbing mechanical and/or thermal shocks under stress.

In view of the technological importance of conventional polyester and vinyl ester resins, we have recently embarked on a research program to investigate their rheological behavior during thickening and during cure. In our previous paper (7), we have reported that, during thickening, vinyl ester resins attained a constant value of viscosity much sooner than did conventional polyester resin, and at a lower value. We also reported that thickened conventional polyester resins exhibited larger normal stress effects and had a higher value of flow activation energy than thickened vinyl ester resins. In this paper, we will report the highlights of our findings on the chemorheology and curing kinetics of the two resins.

### Experimental

A general purpose (i.e., conventional) unsaturated polyester resin (Aropol 7030, Ashland Chemical Company) and a vinyl ester resin (XD-7608.05, Dow Chemical Company) were used for the study. Benzoyl peroxide in granular form (Cadox BFF-60 WET, Noury Chemical Corp.) was used as initiator, and a solution of 5 wt. % N,N-dimethylaniline (Aldrich Chemical Company) diluted in styrene was used as promoter.

In preparing the sample for curing, the formulation used was: resin/initiator/promoter = 60/2.0/1.2 (by weight). We prepared Solution A by mixing the resin and initiator, and Solution B by mixing the resin and promoter. The individual solutions were kept separately in glass jars equipped with glass stoppers, sealed with silicone grease, in order to prevent the evaporation of styrene. The solutions

were kept in a refrigerator maintained at 10°C to avoid any premature polymerization when they were not in use. They were discarded after three weeks storage and fresh samples were then prepared. When needed, we mixed equal amounts of Solution A and Solution B, stirred the mixture vigorously with a wooden tongue blade for about 30 seconds at room temperature, and placed the sample immediately either into a rheometer for rheological measurements or into a hermetic DSC aluminum pan for thermokinetic measurements.

For rheological measurements we used a model R-16 Weissenberg rheogoniometer, fitted with a flat plate, and a 2.5 cm diameter, 4° cone (Sangamo-Weston Controls, Bognor Regis, Sussex, England). We conducted steady shearing flow measurements under isothermal conditions, at various temperatures. In the analysis of the experimental data, we assumed that the effect of temperature variation during cure (due to the exothermic reaction) on the rheological data obtained was negligible, since the gap opening between the cone and plate was very small (160  $\mu\text{m}$ ).

Differential scanning calorimetry (DSC) was used in investigating the curing kinetics of the unsaturated polyester resin. For the study, we used a DuPont 1090 Thermal Analyzer, equipped with a 910 DSC Module. Indium was used for temperature and calorimetric calibrations, following the procedure described in the operating manual of the instrument. The experimental procedure employed is very similar to that described in the literature (8-13) and we have discussed it elsewhere (14).

## Results

Figure 1 gives plots of shear viscosity  $\eta$  versus cure time, and Figure 2 gives plots of first normal stress difference  $\tau_{11} - \tau_{22}$  versus cure time, with shear rate as parameter, at a 60°C cure temperature for both the Ashland polyester resin and the Dow vinyl ester resin.

As indicated in Figure 1, the viscosity increases slowly during the early stage of curing and then increases very rapidly, approaching a very large value as the cure progresses. After this very rapid

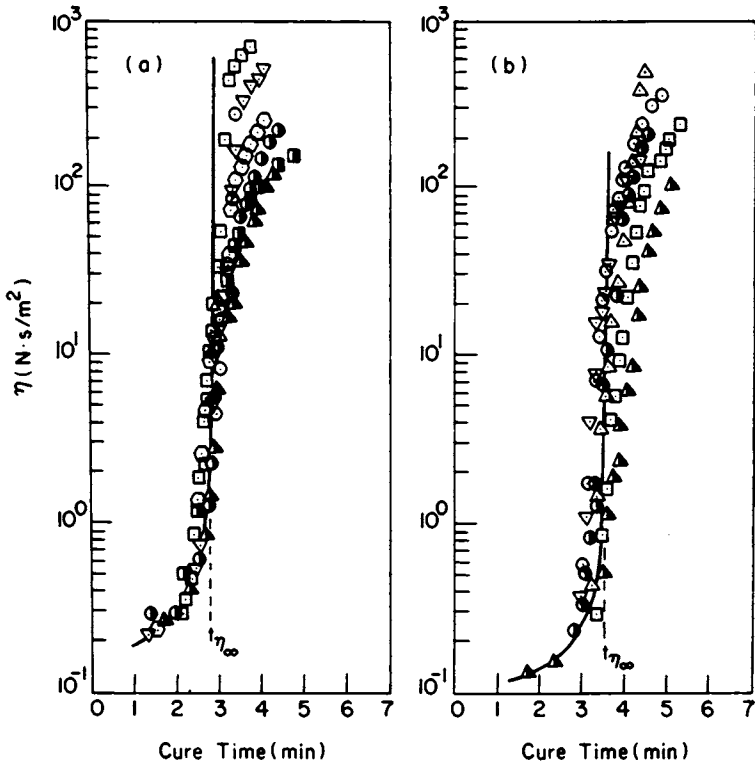


Figure 1.

$\eta$  versus cure time at  $60^\circ\text{C}$  for (a) the Ashland polyester resin and (b) the Dow vinyl ester resin, at various shear rates ( $\text{S}^{-1}$ ): ( $\odot$ ) 0.27; ( $\triangle$ ) 1.07; ( $\square$ ) 2.69; ( $\nabla$ ) 4.27; ( $\odot$ ) 6.77; ( $\bullet$ ) 10.7; ( $\blacktriangle$ ) 17.0; ( $\blacksquare$ ) 26.9.

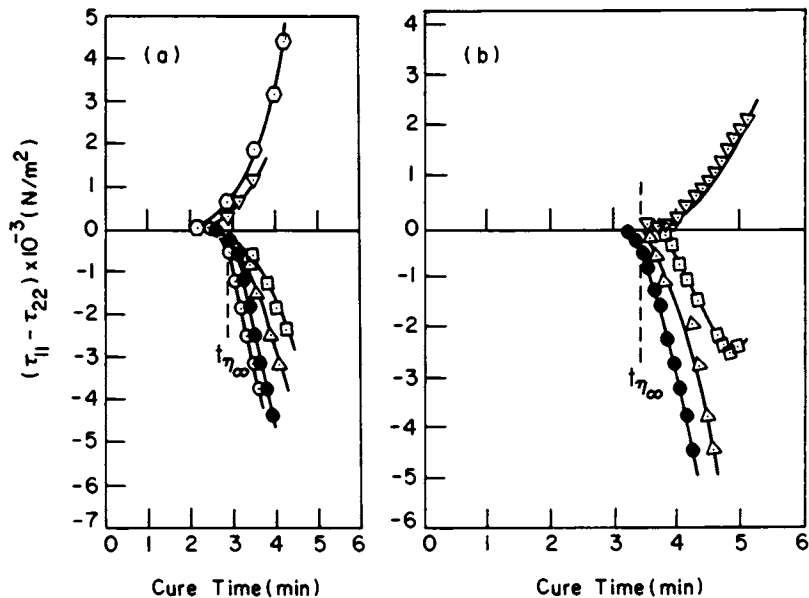


Figure 2.

$\tau_{11} - \tau_{22}$  versus cure time at 60°C. (a) Ashland polyester resin at various shear rates ( $\text{s}^{-1}$ ): ( $\bullet$ ) 0.00; ( $\odot$ ) 0.03; ( $\Delta$ ) 0.11; ( $\square$ ) 1.07; ( $\nabla$ ) 6.77; ( $\ominus$ ) 17.0. (b) Dow vinyl ester resin at various shear rates ( $\text{s}^{-1}$ ): ( $\bullet$ ) 0.00; ( $\Delta$ ) 2.69; ( $\square$ ) 6.77; ( $\ominus$ ) 17.0.



increase, the rate of increase in viscosity started to slow down at a critical cure time. As a matter of fact, when this happened, we noticed irregular torque output signals and also noticed an exudation of material from the gap between the cone and plate, indicating that the flow had become unstable. Therefore, from the point of view of rigor, the values of viscosity to the right of the vertical lines (i.e., above  $t_{\eta_{\infty}}$ ) in Figure 1 have little rheological significance.

In view of the fact that fluid elasticity develops as the curing reaction progresses (i.e., as the size of the molecules becomes larger due to polymerization) and that the fluid elasticity increases with shear rate, the deviation of the viscosity-cure time curve from the vertical line at  $t_{\eta_{\infty}}$  is attributable to the onset of flow instability due to fluid elasticity.

When a sample was placed in the rheometer at the rest position (i.e., no flow), we observed that the plates were pulled together which, we believe, is attributable to the shrinkage of the material during cure. The normal force ( $F$ ) measured was used to calculate  $\tau_{11}-\tau_{22}$  using the expression  $\tau_{11}-\tau_{22} = 2F/\pi R^2$ , in which  $R$  is the radius of the plate. The negative sign of  $\tau_{11}-\tau_{22}$  in Figure 2 refers to the inward direction of plate movement. Note that the sign of  $\tau_{11}-\tau_{22}$  is positive when the plates move apart from each other. Note further that, when a sample is subjected to shearing motion, the normal force generated by the motion of the fluid overcomes the shrinkage force and that, at high shear rates,  $\tau_{11}-\tau_{22}$  increases very rapidly with cure time, giving rise to positive values, as may be seen in Figure 2.

We realize that, from the point of view of rigor,  $\tau_{11}-\tau_{22}$  calculated from the expression,  $\tau_{11}-\tau_{22}=2F/\pi R^2$ , when the fluid undergoes shrinkage during flow, is of little rheological significance. This is because some of the assumptions made in deriving the expression from the equations of motion are violated (15,16). For instance, the available surface area of the fluid undergoing shearing deformation becomes time-dependent when shrinkage occurs. This affects both the boundary

conditions and the shape of the fluid at the rim (i.e., the meniscus).

In spite of the fact that the rheological behavior during cure of the Ashland polyester resin looks very similar to that of the Dow vinyl ester resin, the Ashland polyester resin is found to be more reactive than the Dow vinyl ester resin, with the same formulation and initiator system used in this study. Some important differences in the rheological responses are reflected on: (1) the values of  $t_{\eta}$ ; (2) the time at which shrinkage begins to occur when the fluid is at rest; and (3) the slope of the  $-(\tau_{11}-\tau_{22})$  versus cure time curve.

Figure 3 gives plots of the rate of heat generated versus cure time under isothermal DSC conditions, at various temperatures, for both the Ashland polyester and the Dow vinyl ester resins. It is seen that the amount of heat generated (i.e., the area under the  $dQ/dt$ -cure time curve) increases as the cure temperature increases, as would be expected for exothermic chemical reactions.

Figure 4 describes the following facts: (1) the heat generated ( $Q_T$ ) which was obtained by integrating the  $dQ/dt$ -cure time curve given in Figure 3; (2) the heat of curing ( $Q_M$ ) under isothermal conditions, which was calculated by curve fitting the experimental data to the following quadratic expression

$$Q_M(T) = C_0 + C_1T + C_2T^2 \quad (1)$$

following the suggestion of Kamal and coworkers (8-10); (3) the residual heat ( $Q_R$ ) that was released when the sample was heated to 200°C, upon completion of an isothermal cure, at a rate of 10°C/min; (4) the total heat of curing ( $Q_{TOT}$ ), which is the sum of  $Q_T$  and  $Q_R$ , i.e.,

$$Q_{TOT} = Q_T + Q_R \quad (2)$$

It is of great interest to note in Figure 4 that, for both the Ashland polyester and the Dow vinyl ester resins, the value of  $Q_{TOT}$  turns out to be a constant,

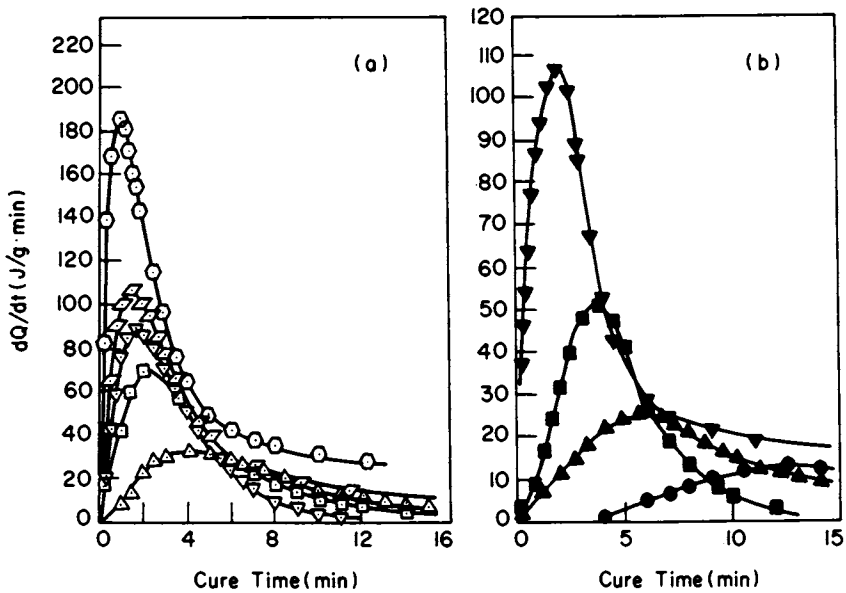


Figure 3.

$dQ/dt$  versus cure time. (a) Ashland polyester resin at various temperatures ( $^{\circ}C$ ): ( $\Delta$ ) 40; ( $\square$ ) 45; ( $\nabla$ ) 50; ( $\diamond$ ) 55; ( $\circ$ ) 60. (b) Dow vinyl ester resin at various temperatures ( $^{\circ}C$ ): ( $\bullet$ ) 30; ( $\blacktriangle$ ) 40; ( $\blacksquare$ ) 45; ( $\blacktriangledown$ ) 50.

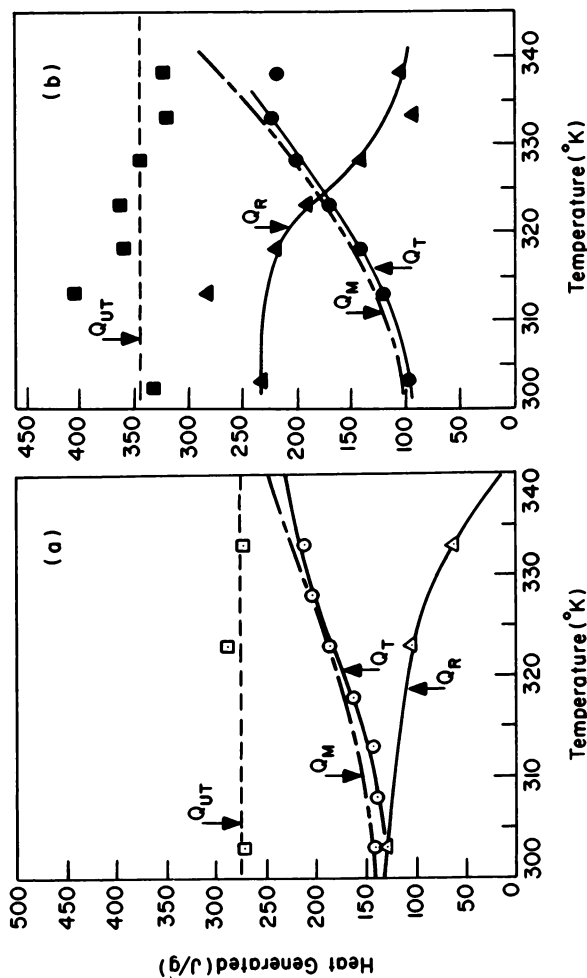


Figure 4.  
Heat generated versus isothermal cure temperature for  
(a) the Ashland polyester resin, and (b) the Dow vinyl  
ester resin.

which is almost independent of the temperature chosen for isothermal curing.

Following the assumption made by previous investigators (8-13) that the amount of heat generated due to curing is directly proportional to the degree of cure, one can now define:

$$\alpha_M = Q_i(T)/Q_M(T) \quad (3)$$

and

$$\alpha_{UT} = Q_i(T)/Q_{UT} \quad (4)$$

depending upon the choice of the total heat generated,  $Q_M$  or  $Q_{UT}$ . Note that  $Q_i(T)$  refers to the heat generated at a particular time  $t$  at an isothermal curing temperature  $T$ , and  $Q_{UT}$  is the ultimate heat of reaction, being the average value of several measurements, taken at various temperatures, of the total heat of reaction  $Q_{TOT}$ .

Figure 5 gives plots of  $\alpha_{UT}$  and  $\alpha_M$  versus cure time for the Ashland polyester resin, and Figure 6 gives similar plots for the Dow vinyl ester resin. It is seen that in both cases the use of  $\alpha_M$  gives rise to very high values for the degree of cure (approaching 1.0) at the end of each isothermal cure, compared to that obtained when  $\alpha_{UT}$  was used. We know that the curing reaction cannot approach its completion at such low temperatures, say at 50°C, because the ratio of the residual heat ( $Q_R$ ) to the ultimate heat ( $Q_{UT}$ ) is fairly large: 0.376 for the Ashland polyester resin and 0.557 for the Dow vinyl ester resin.

Our study indicates that the choice of  $\alpha_{UT}$ , instead of  $\alpha_M$ , gives rise to more realistic values of the degree of cure. For this reason, we have chosen to use  $\alpha_{UT}$  (hereafter the subscript UT will be omitted) in constructing the plots of the rate of cure (i.e.,  $d\alpha/dt$ ) versus the degree of cure ( $\alpha$ ), as given in Figure 7. Having constructed plots of  $d\alpha/dt$  versus  $\alpha$ , we have determined the parameters in the kinetic expression (8,9),

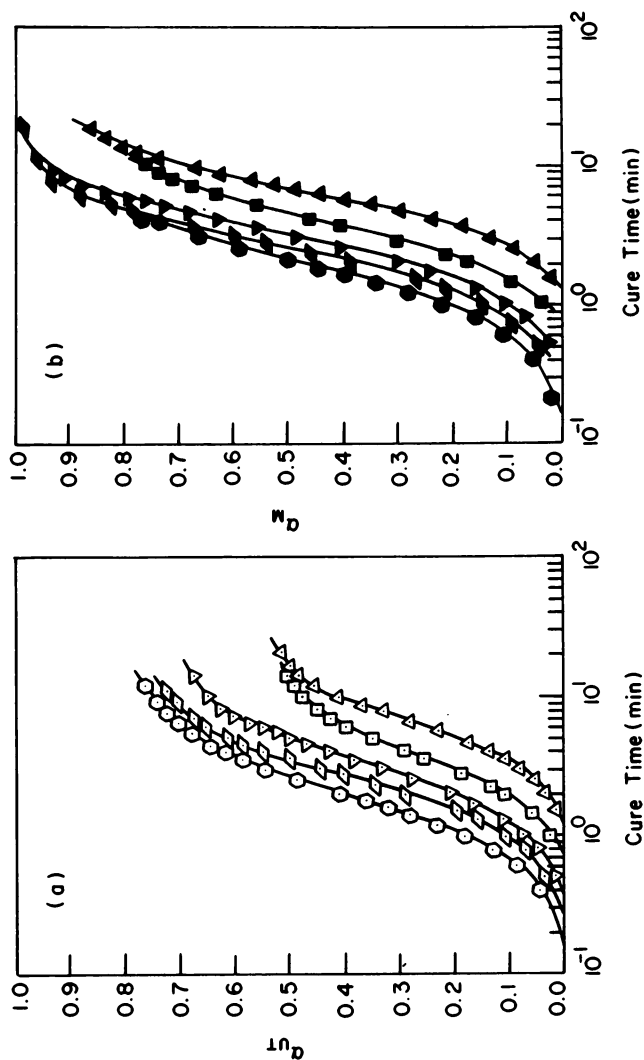


Figure 5.  
 $\alpha_{UT}$  and  $\alpha_M$  versus cure time for the Ashland polyester resin, at various temperatures ( $^{\circ}\text{C}$ ): ( $\Delta, \blacktriangle$ ) 40; ( $\square, \blacksquare$ ) 45; ( $\nabla, \blacktriangledown$ ) 50; ( $\diamond, \blacklozenge$ ) 55; ( $\diamond, \bullet$ ) 60.

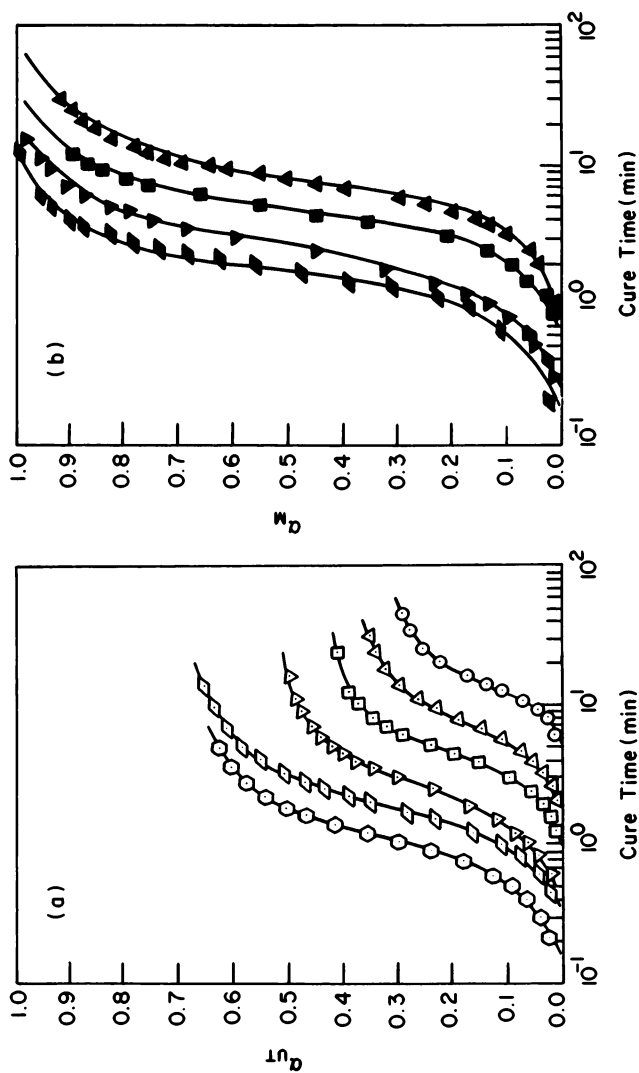


Figure 6.  
 $\alpha_{UT}$  and  $\alpha_M$  versus cure time for the Dow vinyl ester resin,  
 at various temperatures ( $^{\circ}\text{C}$ ): (○); (△,▲) 40; (□,■) 45;  
 (▽,▼) 50; (◄,◃) 60; (◊) 65.

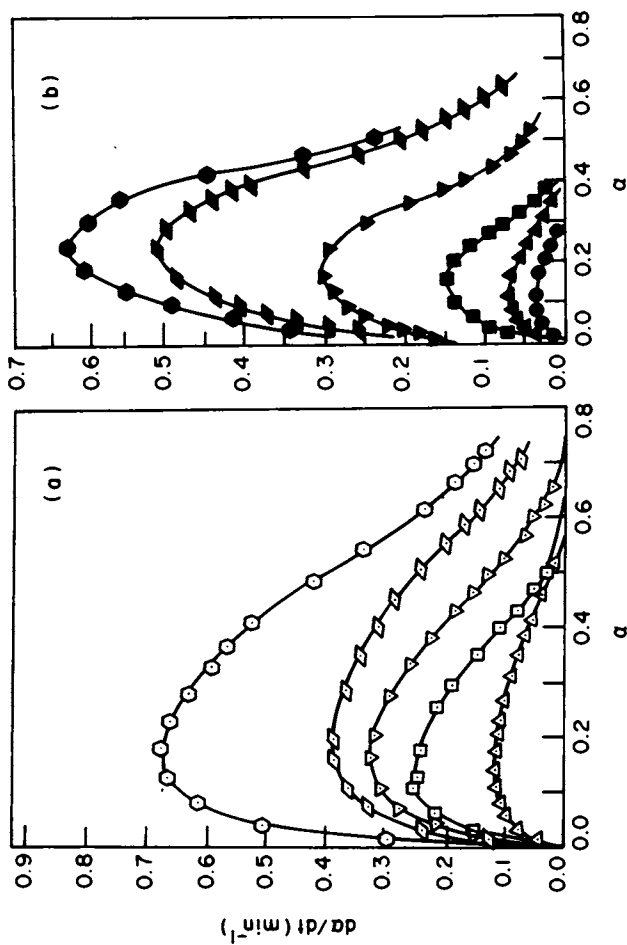


Figure 7.  $d\alpha/dt$  versus  $\alpha$ . (a) Ashland polyester resin at various temperatures ( $^{\circ}\text{C}$ ): ( $\Delta$ ) 40; ( $\square$ ) 45; ( $\nabla$ ) 50; ( $\diamond$ ) 55; ( $\circ$ ) 60. (b) Dow vinyl ester resin at various temperatures ( $^{\circ}\text{C}$ ): ( $\bullet$ ) 30; ( $\blacktriangle$ ) 40; ( $\blacksquare$ ) 45; ( $\blacktriangledown$ ) 50; ( $\blacklozenge$ ) 60; ( $\bullet$ ) 65.



$$\frac{d\alpha}{dt} = (k_1 + k_2 \alpha^m)(1 - \alpha)^n \quad (5)$$

A summary of the kinetic parameters in Equation (5) evaluated for both resins is given in Table II. In calculating these parameters, we assumed a second-order reaction (i.e.,  $m+n=2$ ) as suggested by Kamal and coworkers (8,9), and used the procedure suggested by Ryan and Dutta (13). It is seen in Table II that, over the range of the isothermal curing temperatures investigated, the values of  $m$  and  $n$  are found to be sensitive to temperature, and the values of  $k_1$  and  $k_2$  increase with temperature, following the Arrhenius relationship.

Having obtained information on the viscosity ( $\eta$ ) and the degree of cure ( $\alpha$ ), both of which vary with cure time (see, for example, Figures 1 and 5), we now can construct plots describing how  $\eta$  varies with  $\alpha$ , as given in Figure 8 for both resins. It is seen that, as the temperature increases, one can achieve a higher degree of cure before the viscosity approaches a very large value. This observation is in consonance with that reported by Imai (17) and Funke (18).

### Discussion

In spite of the fact that the carbon-to-carbon double bonds in the Dow vinyl ester prepolymer chains are structoterminal and those in the Ashland polyester resin are structopendant, the Dow vinyl ester resin is less reactive than the Ashland polyester resin with the same formulation and initiator system. This difference in reactivity or rate of reaction can be discussed with the aid of the DSC measurements presented above.

First, it is seen in Figure 3 that the maximum value of  $dQ/dt$  (i.e.,  $(dQ/dt)_p$ ) increases, and the time ( $t_p$ ) at which the maximum of  $dQ/dt$  occurs decreases, as the cure temperature (hence the rate of cure) increases. Over the range of temperatures investigated, the Ashland polyester resin exhibits higher values of  $(dQ/dt)_p$  and lower values of  $t_p$  than the Dow vinyl ester resin, indicating that the former is more reactive than the latter. Second, although

Table II. Summary of the Kinetic Parameters Evaluated

Temperature ( $^{\circ}\text{K}$ )	$k_1$ ( $\text{min}^{-1}$ )	$k_2$ ( $\text{min}^{-1}$ )	m	n
(a) Ashland Polyester Resin				
313	0.0048	0.203	0.29	1.71
318	0.0131	0.351	0.23	1.77
323	0.0278	0.793	0.35	1.65
328	0.0607	1.110	0.43	1.57
333	0.0924	1.570	0.40	1.60
(b) Dow Vinyl Ester Resin				
313	0.0054	0.129	0.24	1.76
318	0.0073	0.219	0.33	1.67
323	0.0151	0.998	0.35	1.65
333	0.0624	1.590	0.49	1.51
338	0.0828	1.910	0.51	1.49

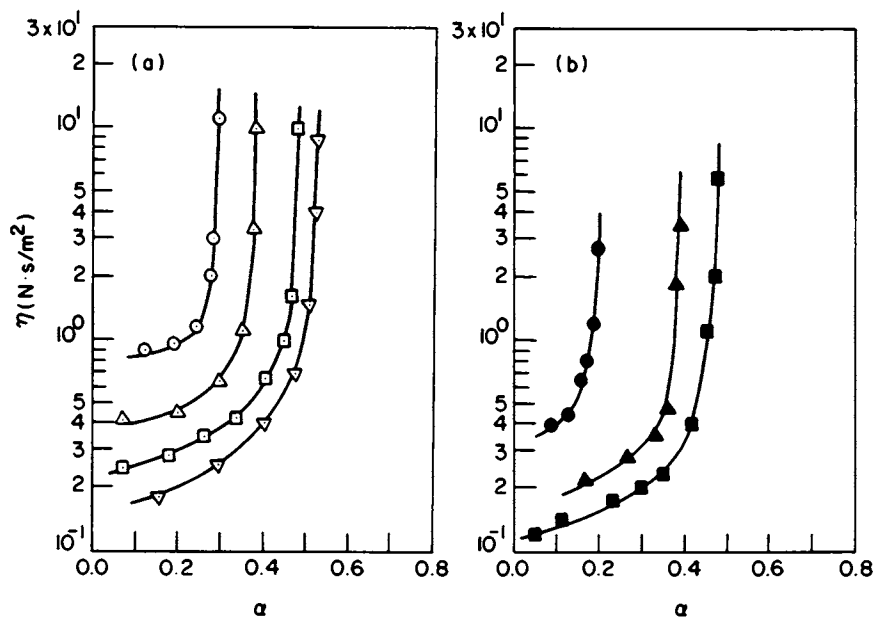


Figure 8.

$\eta$  versus  $\alpha$ . (a) Ashland polyester resin at various temperatures ( $^{\circ}\text{C}$ ): ( $\odot$ ) 30; ( $\triangle$ ) 40; ( $\square$ ) 50; ( $\nabla$ ) 60. (b) Dow vinyl ester resin at various temperatures ( $^{\circ}\text{C}$ ): ( $\bullet$ ) 40; ( $\blacktriangle$ ) 50; ( $\blacksquare$ ) 60.

the ultimate heat generated ( $Q_{UT}$ ) by the Dow vinyl ester resin ( $Q_{UT} = 345.5 \text{ J/gm}$ ) is greater than that by the Ashland polyester resin ( $Q_{UT} = 275 \text{ J/gm}$ ), (see Figure 4), the ratio of  $Q_R$  to  $Q_{UT}$  for the Dow resin is much higher than that for the Ashland resin, over the range of temperatures investigated. Since we have assumed that the amount of the heat generated due to the curing reaction is directly proportional to the degree of cure, the  $Q_R/Q_{UT}$  ratio may be used as a measure of the amount of unreacted functional groups present in the resin, upon completion of an isothermal cure. Note that the  $Q_R/Q_{UT}$  ratio decreases with increasing temperature or rate of reaction. Thus we can conclude that the Dow vinyl ester resin is less reactive than the Ashland polyester resin. Third, as may be seen in Figures 5 and 6, the Ashland polyester resin approaches a higher value for the degree of cure than the Dow vinyl ester resin, upon the completion of an isothermal cure.

As may be seen in Table II, in both resins the reaction rate constants  $k_1$  and  $k_2$  appearing in eq. (5) increase with the isothermal curing temperature. In most cases, the magnitudes of  $k_1$  and  $k_2$  (only at low temperatures) are greater for the Ashland polyester resin than for the Dow vinyl ester resin. It is of interest to note in Table II that the values of  $m$  and  $n$  appearing in eq. (5) also vary somewhat with temperature, especially at isothermal curing temperatures below  $55^\circ\text{C}$ . It should be remembered that we have assumed that, overall, the curing reaction is of the second-order (i.e.,  $m+n=2$ ). The fact that  $m$  and  $n$  are dependent upon the curing temperature appears to suggest that different reaction mechanisms might prevail at low temperature curing.

It is a well-recognized fact today that the process of curing and the nature of resin chemistry greatly influence the mechanical properties of cured resins. In order to have an insight into this problem, we have taken measurements of the dynamic mechanical properties of fully cured samples, using both the Ashland polyester resin and the Dow vinyl ester resin. The fully cured samples were prepared by first curing a resin at  $30^\circ\text{C}$  for 2 hours, and then post-curing it at  $150^\circ\text{C}$  for 12 hours under 30 in. Hg vacuum. The measurements were taken using a DuPont 1090 Thermal Analyzer equipped with a 981 Dynamic Mechanical

Analyzer (DMA) module. Figure 9 gives the dynamic mechanical spectra of the Ashland polyester and Dow vinyl ester resins. It is seen in Figure 9 that the Ashland resin has a higher Young's modulus than the Dow resin, over a wide range of temperatures.

The differences in prepolymer chemistry between the two resins investigated may be observed in their relaxation transitions at both low and high temperatures. Of particular interest is the existence of two major relaxation transitions observed in the Dow vinyl ester resin at high temperatures. We believe that the second relaxation occurring at 80°C is not the same as the  $\beta$  transition reported in the literature (19,20). Furthermore, we speculate that the Dow vinyl ester resin employed in our study might have been a blend of two resins. This speculation will be tested in a future investigation.

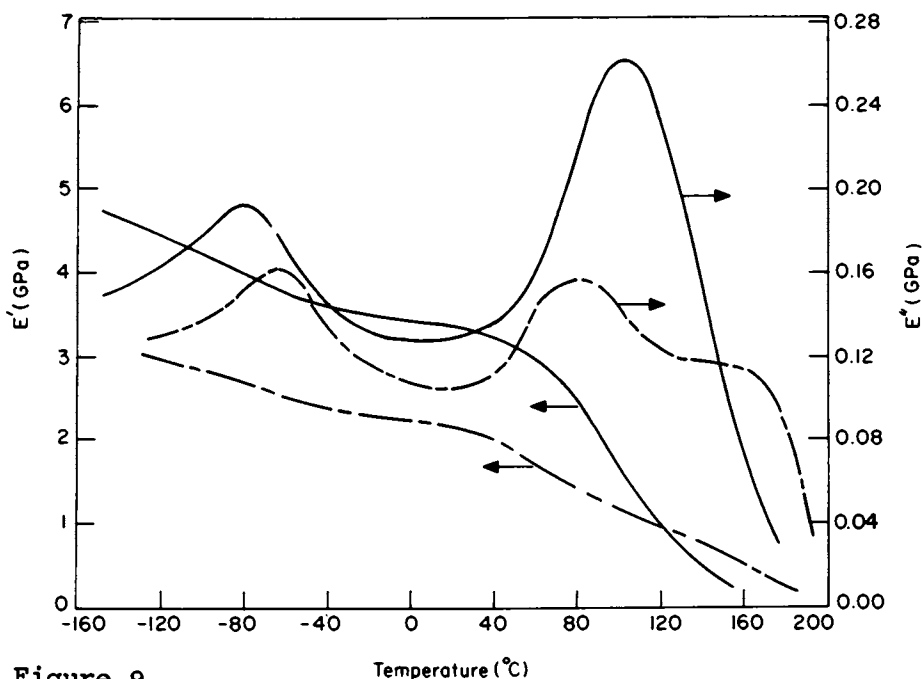


Figure 9.

$E'$  and  $E''$  versus temperature for the Ashland polyester resin denoted by the solid line, (—), and for the Dow vinyl ester resin denoted by the broken line (---).

Literature Cited

1. Saunders, K.J. "Organic Polymer Chemistry"; Chapman Hall: London, 1973.
2. Brydson, J.A. "Plastics Materials"; Third Edition, Newnes-Butterworths: London, 1975.
3. Rider, S.H.; Hardy, E.E. in "Polymerization and Polycondensation Processes"; N.A.J. Platzer, Ed.; ADVANCES IN CHEMISTRY SERIES No. 34, ACS: Washington, D.C., 1962, p. 173.
4. Longenecker, D.M. in "Unsaturated Polyester Technology"; P.F. Bruins, Ed.; Gordon & Breach: New York, 1976, p. 279.
5. Young, R.E. in "Unsaturated Polyester Technology"; P.F. Bruins, Ed.; Gordon & Breach: New York, 1976, p. 315.
6. Kelly, M.E. in "Unsaturated Polyester Technology"; P.F. Bruins, Ed.; Gordon & Breach: New York, 1976, p. 343.
7. Han, C.D.; Lem, K.W. J. Appl. Polym. Sci. in press.
8. Kamal, M.R.; Sourour, S. Polym. Eng. Sci. 1973, 13, 59.
9. Kamal, M.R.; Sourour, S.; Ryan, M.E. Preprints of SPE ANTEC 1973, p. 187.
10. Kamal, M.R. Polym. Eng. Sci. 1974, 14, 232.
11. Hagnauer, G.L.; Labiberte, B.R.; Dunn, D.A. Preprints of Organic Coat. Plast. ACS: Washington, D.C. 1982, 46, p. 646.
12. Pusatciaglu, S.Y.; Fricke, A.L.; Hassler, J.C. J. Appl. Polym. Sci. 1979, 24, 937.
13. Ryan, M.E.; Dutta, A. Polymer, 1979, 20, 203.
14. Han, C.D.; Lem, K.W. J. Appl. Polym. Sci. in press.
15. Adams, N.; Lodge, A.S. Trans. Phil. Roy. Soc. (London) 1964, A256, 149.
16. Olabisi, O.; Williams, M.C. Trans. Soc. Rheol. 1972, 16, 727.
17. Imai, T. J. Appl. Polym. Sci. 1967, 11, 575.
18. Funke, W. J. Polym. Sci. Part C, 1967, 16, 1497.
19. Douglas, W.E.; Pritchard, G. J. Polym. Sci. Polym. Phys. Ed. 1982, 20, 1223.
20. Cook, W.D.; Delatycki, O. J. Polym. Sci. Polym. Phys. Ed. 1974, 12, 2111.

RECEIVED May 5, 1983

## Dynamic Mechanical and Dielectric Properties of an Epoxy Resin During Cure

W. X. ZUKAS, W. J. MacKNIGHT, and N. S. SCHNEIDER <sup>1</sup>

Chemical Engineering Department and Polymer Science and Engineering Department, University of Massachusetts, Amherst, MA 01003

The curing behavior of a commercially formulated epoxy resin composed of a tetrafunctional epoxy, tetraglycidyl methylene dianiline, and a tetrafunctional amine, diaminodiphenyl sulfone, was followed by dynamic spring analysis (DSA) and dielectric relaxation measurements. Both methods yielded two peaks in their loss tangent vs. time traces. The first peak in dynamic spring analysis was used as a measure of the onset of gelation, whereas the second peak appeared to be related to vitrification. The first dielectric relaxation peak was due to a surface charge-related phenomenon while the origin of the second peak is unclear. Results from additional mechanical relaxation studies of thin-films of known cure history support the interpretation of the DSA second peak as due to vitrification and reveal three dispersion regions. In order of increasing temperature these are associated with a glass transition near the temperature of molding (curing), further reaction, and the ultimate glass transition of the "fully cured" network.

The changes which occur in thermosetting resins undergoing cure have been studied by a variety of techniques. Supported sample methods have been used to monitor the relative changes in modulus and damping behavior from the initial low viscosity liquid to the fully cured rubbery or glassy state. Torsional braid analysis (TBA) employs a resin sample impregnated on a

<sup>1</sup> Current address: Polymer and Chemistry Division, Army Materials and Mechanics Research Center, Watertown, MA 02172

glass fiber braid as the mechanical element in a torsion pendulum. This method has been used extensively by Gillham and coworkers (1-13) who developed a pseudo-phase diagram to describe the general features of the thermosetting process. A technique similar to TBA, reported by Lee and Goldfarb (4), involves the use of a resin impregnated glass cloth which is oscillated in the torsional mode of a Rheometrics mechanical spectrometer. An advantage of this method is the ability to observe the frequency dependence of the dispersion phenomena.

Using such techniques, it is generally not possible to obtain the viscoelastic properties of the resin from the measured behavior of the composite (resin plus support). In dynamic spring analysis (DSA) the sample is coated on a spring mounted in the Rheovibron dynamic viscoelastometer (5,6). It was shown by Senich and MacKnight (7) that it was possible to estimate the viscoelastic response of the resin by assuming a simple parallel model of the spring-resin composite and using the measured characteristics of the spring. This method of analysis was applied to the study of the curing of two epoxy resins (8). In addition to the supported sample methods, the viscoelastic properties of partially cured epoxy resins have been obtained directly from temperature scans in the Rheovibron carried out on unsupported films (4,8,9).

Another approach which has received considerable attention involves measuring the changes in the electrical properties of the curing resins, but there is considerable disagreement about the molecular origin of the observed effects. Delmonte (10) determined the change in dissipation factor, dielectric constant, and volume resistivity of several epoxy resins during isothermal cure and attributed a peak observed in the dissipation factor to gelation. Haran et al. (11) used a similar peak to control the physical properties of the cured resins, but did not believe that it represented gelation. Adamec (12) developed an empirical relationship between the a.c. conductivity and the degree of cure represented by the relative concentration of epoxy groups determined by infrared analysis. Dandurant and Huraux (13) observed a broad dielectric relaxation in a Cole-Cole representation of the results of a curing epoxy resin. Other recent studies of the dielectric response by Lawless (14) and by Crabtree (15) used cure cycles which simulate an actual commercial cure process rather than an isothermal cure and therefore were not readily interpreted in terms of the reaction kinetics. A new development in technique was described by Senturia et al. (16) who used a charge flow transistor to monitor isothermally curing resins and developed a simple circuit model to interpret the dielectric response of the resin. A sharp decrease in permittivity and loss factor with cure time was attributed to the rapid rise in viscosity which marks the onset of gelation.

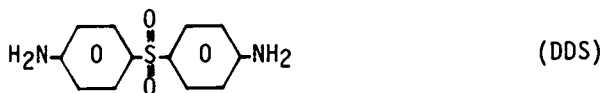
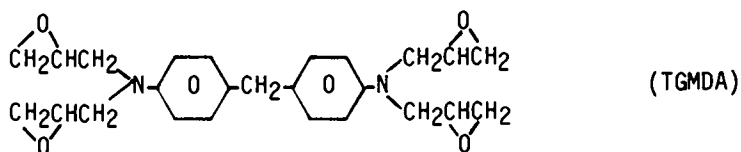
The present work is concerned with measurements of the curing



behavior of the Narmco 5208 resin both by the dynamic spring and dielectric methods. This resin is one of the high temperature epoxies which have been developed for aerospace composites and it has been the subject of extensive characterization. Mechanical property characterization of cured resins has been carried out by Morgan et al. (17). Recent studies on such resins also include dielectric and dynamic mechanical by Crabtree (15), FTIR and HPLC analyses by Cizmecioglu (18), FTIR by Mones and Morgan (19), and spin trapping studies by Tsay et al. (20).

## EXPERIMENTAL

The subject of this study is a commercially formulated resin (Narmco Materials Division of Celanese Corp.) referred to as Resin 5208. May et al. (21) have shown that the primary constituents of this resin are Ciba-Geigy Corporation's Araldite MY720, diaminodiphenyl sulfone (DDS), and a glycidyl ether of a bisphenol A based novolac (Celanese SU-8). The principle component of MY720 is tetraglycidyl methylene dianiline (TGMDA).



Resin 5208 is a tacky solid at room temperature and has an approximate amine to epoxy equivalent of 0.6:1.0 (18). Samples were stored in sealed vials at 0°C and briefly warmed to room temperature before removing for analysis. The recommended commercial cure is 177°C for 2 hrs. (22).

The isothermal DSA analysis, utilizing the Rheovibron DDV-IIB dynamic viscoelastometer, has been described elsewhere (7). A steel spring 2.9 mm in outer diameter of 0.30 mm diameter wire, seventeen turns in length was placed in the Rheovibron. The temperature chamber was then brought to constant cure temperature,  $T_c$ , the spring stretched to achieve a pitch of 0.1 mm, and the sample applied by hypodermic syringe as a 50% by weight solution in methylene chloride. The viscoelastic response of the spring supported resin was then followed in a dry nitrogen atmosphere as a function of time. About 10 to 15 mg of resin per run was required.

Dielectric measurements were made using a GenRad 1620 Precision Capacitance Measurement System (modified for high loss materials) equipped with a Balsbaugh Three-Terminal Research Cell. Dielectric relaxation data for isothermal cures were obtained from thin-films essentially "compression molded" in the parallel plate measuring cell. The resin was separated from the upper guard electrode by a thin sheet of PTFE and from the bottom electrode by a thin sheet of aluminum foil (Figure 1a). A PTFE shim with a circular hole 50 mm in diameter constrained the resin to an approximate thickness of 0.7 mm (Figure 1b). The measuring cell was first allowed to equilibrate thermally at the cure temperature, then the resin, sandwiched between the PTFE and aluminum sheets, was placed and clamped between the two plates of the measuring cell. After a short (2-5 minutes) thermal equilibration period the isothermal dielectric response was followed as a function of time at frequencies of 0.05, 0.10, 0.20, 0.50, 1.0, 2.0, 5.0, 10, 20, 50, and 100 kHz. This procedure was repeated for various cure temperatures. Approximately 2 g of resin was required for each analysis.

Thin-film samples of specific isothermal cure histories were prepared for dynamic tensile testing on the Rheovibron by compression molding 0.6 to 0.7 mm thick samples at a pressure of 14 MPa. The samples were air quenched after various times at constant cure temperature. The thin-films were then mounted in the Rheovibron and the temperature increased from room temperature to approximately 310°C at 2°C/min in a dry nitrogen atmosphere. DSA and thin-film experiments were carried out at frequencies of 3.5, 11, 35, and 110 Hz.

### Results and Discussion

DSA. Isothermal cures of Resin 5208 in the temperature range of 125 to 181°C were examined by the DSA technique. Figure 2 shows the composite loss tangent response as a function of the natural logarithm of time for a cure at 147°C at several frequencies. Two  $\tan \delta$  peaks are observed. At fixed temperature both peaks become smaller, shift to longer times, and exhibit improved resolution as the frequency is decreased. Figure 3 displays the composite loss tangent as a function of the natural logarithm of time at a fixed frequency of 3.5 Hz for cures at several temperatures. At this, the lowest frequency of measurement, the two peaks are best resolved, smallest, and occur soonest in time as the temperature is increased.

As noted previously by Senich et al. (8), the usefulness of the DSA technique in following the cure of epoxy curing systems stems from the fact that a relative maximum is produced in the composite loss tangent when the viscosity of the resin reaches a predetermined value. In a previous study (23) which considered a series of polystyrenes of varying molecular weights characterized

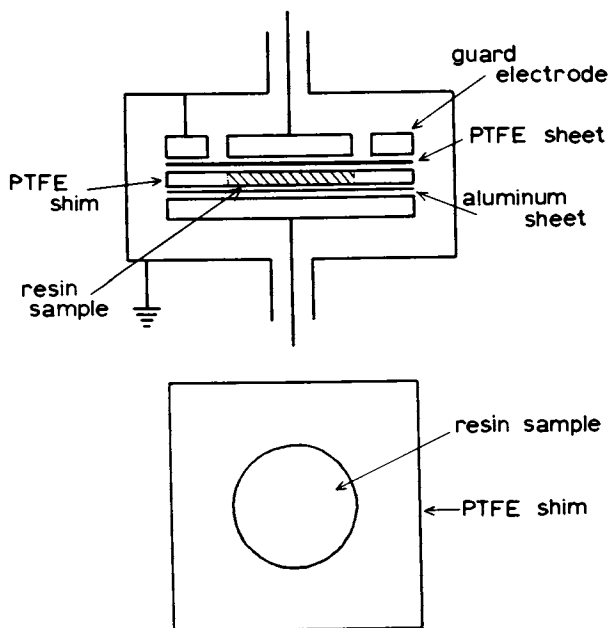


Figure 1. Dielectric cell.

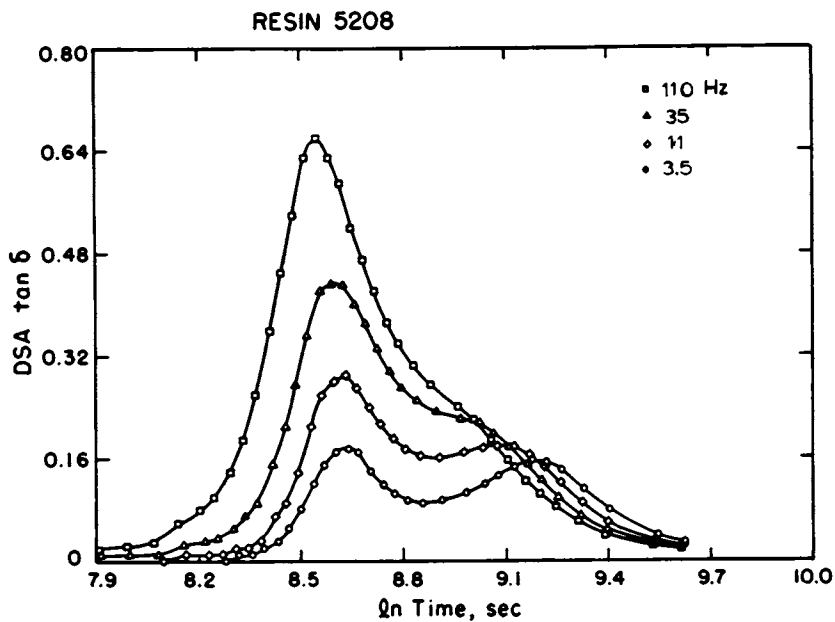


Figure 2. DSA  $\tan \delta$  vs.  $\ln$  (time, sec) at fixed temperature (147 °C).

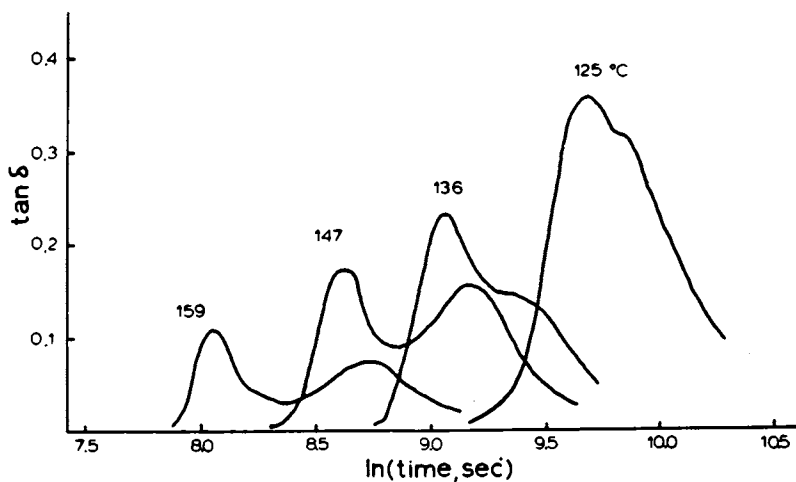


Figure 3. DSA  $\tan \delta$  vs.  $\ln$  (time, sec) at fixed frequency (3.5 Hz).

by DSA, the theoretical basis for understanding the viscosity related peak was established. The study also showed that the T<sub>g</sub> or vitrification process was not observed by DSA for this series of PS samples. The appearance of a second peak well beyond the T<sub>g</sub> of two high molecular weight polystyrene samples was attributed to the relaxation of entanglements.

The location of the first peak represents the time required to reach a specific viscosity, and, providing the reaction mechanism does not change as a function of temperature, represents the time to reach a fixed chemical conversion for a specific frequency. These peaks can then be used as a measure of the rate of reaction at each temperature where the reaction velocity constant can be treated as inversely proportional to the time to the peak maximum,  $t_{\max}$ :

$$\ln \left( \frac{1}{t_{\max}} \right) = - \frac{H_a}{RT} + C \quad (1)$$

where  $H_a$  is the activation energy of the reaction. The slope of a plot of the natural logarithm of  $t_{\max}$  vs. the inverse of absolute temperature can then be used to determine the activation energy. Figure 4 contains the DSA and TBA (24) results on Resin 5208 plotted in this way. A linear least squares fit was applied to the data and the activation energies are listed in Table 1. A frequency dependent activation energy results which changes from 14.7 to 16.0 kcal/mole for frequencies of 110 and 3.5 Hz, respectively, for DSA results (125 to 160°C). This may be compared to a value of 19.3 kcal/mole obtained from TBA at a nominal frequency of 1 Hz (150 to 180°C). In addition, the curing times for DSA were found to be approximately 40% longer than the TBA values for similar temperatures (150 to 160°C).

Resin 5208 exhibits a second peak at longer times than the viscosity related maximum. Gillham (1) attributed a second peak observed by TBA to vitrification. Figure 5 displays the plots of the natural logarithm of  $t_{\max}$  vs. the reciprocal of absolute temperature for the second peaks from DSA and TBA. The activation energies derived from the slope of a linear least squares fit of the results from both are somewhat different as indicated in Figure 5 and Table 1.

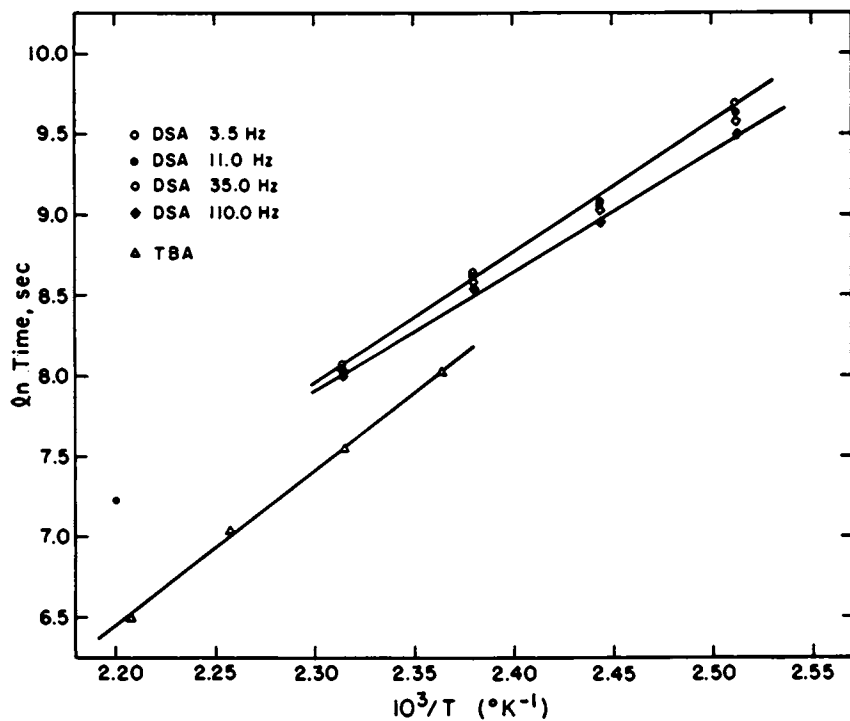


Figure 4. Arrhenius plots of DSA and TBA first peaks.

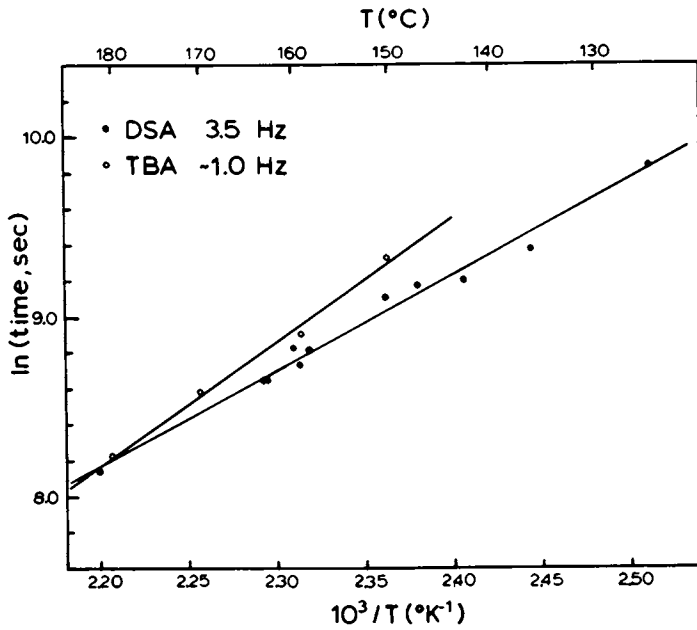


Figure 5. Arrhenius plots of DSA and TBA second peaks.

TABLE I. Dynamic Mechanical (DSA and TBA) Activation Energies

Peak	Frequency (Hz)	Analysis	$H_a$ (kcal/mole)
1st	110	DSA	14.7
	35	DSA	15.3
	11	DSA	15.6
	3.5	DSA	16.0
	~1.0	TBA	19.3
2nd	3.5	DSA	10.5
	~1.0	TBA	13.7

The DSA technique allows for the calculation of the storage and loss components of the resin modulus from the composite response using a simple parallel mechanical model:

$$M_C^* = M_S^* + M_P^* \quad (2)$$

where  $M_C^*$ ,  $M_S^*$ , and  $M_P^*$  are the complex moduli of the composite, spring, and material of interest, respectively. Figure 6 shows the results of such an analysis applied to the Resin 5208 cure at 147°C shown in Figure 2. Similar analyses were done for the entire temperature range.

If the above model correctly describes the behavior of the resin then it is possible to identify the behavior in the storage modulus ( $E'$ ) and the loss modulus ( $E''$ ) responsible for the composite  $\tan \delta$  peaks. The first  $\tan \delta$  peak corresponds to an increasing resin  $E'$  that reaches a value at  $t_{\max}$  which is approximately frequency independent for each isothermal cure as shown in Figure 6 for a 147°C cure. This  $E'$  value is observed in similarly derived curves ranging from 20 to 55 kPa as the isothermal cure temperatures are lowered from 181 to 125°C. This first peak also corresponds to a shoulder in the resin  $E''$ . Apparently, the increase in the magnitude of  $E''$  with frequency at this position is responsible for the change in magnitude of  $\tan \delta$  with increasing frequency seen in Figure 2.

The second maximum in the composite  $\tan \delta$  corresponds to an approximate plateau value of 700 kPa in resin  $E'$  and a peak in resin  $E''$ . The frequency shift of the  $E''$  peak to longer times appears to be responsible for the increasing separation of gel and vitrification  $\tan \delta$  peaks with decreasing frequency. Higher temperature cures with a well separated second peak show a small inflection in  $E'$  very similar in shape to what one would expect for a glass transition, but not of the order of magnitude observed in linear or lightly crosslinked polymers. This supports the contention that the second peak is correlated with a vitrification of



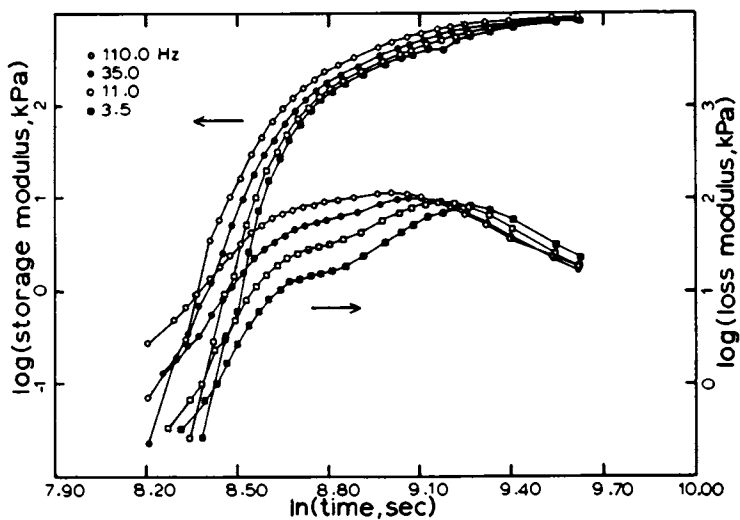


Figure 6. DSA moduli vs.  $\ln$  (time, sec) for  $147^{\circ}\text{C}$  cure of resin 5208.

the curing epoxy resin, but the weakness of the DSA transition indicates the limit of sensitivity of the technique is being approached or that the resin is already highly crosslinked before it vitrifies.

Significant differences are observed between the present study on Resin 5208 and the previous studies on two dicy-containing epoxy resins by DSA (8) and by TBA (25).

- Two  $\tan \delta$  peaks are observed by DSA compared to one peak in the previous study.
- Differences in the temperature dependence between DSA and TBA are observed in the present study.
- The frequency dependence in the cure times obtained by DSA was not previously observed.

These points will be addressed in order.

First, it is important to recognize that the DSA and TBA peaks do not correspond to the same stage of cure. Figure 7 illustrates the DSA and TBA results for isothermal cures of Resin I at 112 and 92°C from the previous studies and for isothermal cures of Resin 5208 at 180 and 150°C. The TBA logarithm of rigidity and logarithm of the mechanical damping index are plotted as functions of the logarithm of time. The times corresponding to the DSA  $\tan \delta$  maxima are indicated as arrows on the TBA rigidity traces. Figure 8 shows  $E'$  and  $E''$  for Resin I at 80.2°C computed from the composite DSA results by the analysis used to produce Figure 6. The DSA data were taken from the previous study. A similar frequency independent storage modulus value is observed for Resin I as for Resin 5208 (Figures 6 and 8). The first DSA peak positions indicated on the TBA rigidity curves in Figure 7 also correspond to approximately the same rigidity values. It is apparent that the DSA peak occurs later in the reaction than the TBA peak. The first DSA peak occurs upon the attainment of a modulus close to that of the rubbery plateau while the corresponding TBA peak occurs at the point where the relative rigidity begins to increase. Hedvat (26) has shown that changes in peak position in TBA are possible depending on the ratio of the sample rigidity to the support rigidity. Considering the differences in the nature of the supports and the types of deformation occurring in DSA and TBA it is not possible to rule out effects of this type as an explanation for the differences in the TBA and DSA peak times.

The significant increase in the TBA rigidity after the first DSA maximum is not observed in the derived resin modulus traces from DSA in Figures 6 and 8 indicating lack of DSA sensitivity in the glassy region. A second DSA maximum is apparently observed for Resin 5208. This could be due to the somewhat larger separation in time between the first DSA peak and a more distinct vitrification process observed by TBA (Figure 7). The TBA rigidity traces for Resin 5208 predict the observed larger separation between the two DSA peaks in the logarithm of time as the cure temperatures are increased.

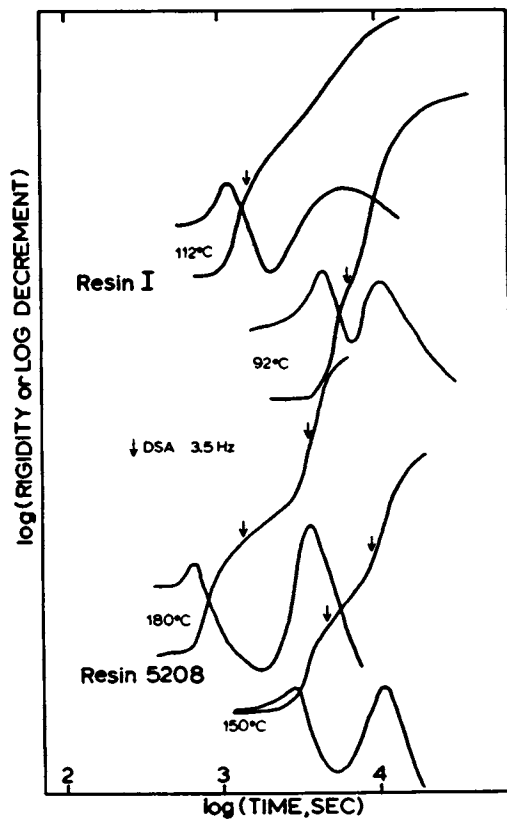


Figure 7. TBA and DSA for Resin I and Resin 5208.

The previous studies showed no significant differences in the temperature dependencies of the first DSA and TBA peaks. Results for Resin I show the DSA peak to occur approximately 25% later in time over the temperature range studied (80 to 112°C) compared to approximately 40% later for Resin 5208. The activation energies derived for Resin 5208 extrapolate to a larger difference between DSA and TBA at temperatures above 160°C and to a smaller difference below 150°C between the two techniques. The fact that the first DSA peak occurs much later in time than the TBA peak means that the reaction responsible for the TBA and DSA peaks might differ due to complexities of the curing mechanism. This could account for some of the differences in activation energy.

The kinetic effect involved in the TBA procedure for an isothermal cure also accounts for some of the differences observed in activation energies for Resin 5208. Typically, a resin solution impregnated braid is introduced to the sample chamber at room temperature (or the temperature of the low boiling solvent) and brought to the cure temperature at a nominal 10°C/min. If the equivalent isothermal curing time is calculated (assuming an approximate activation energy) and the TBA data suitably corrected, an activation energy of 17.5 kcal/mole is observed vs. 19.3 kcal/mole for the uncorrected data (Table 1).

A frequency dependence of activation energies in DSA appears to be fairly well explained by the overlapping of the two  $\tan \delta$  peaks observed. The 110 Hz data show only one (superimposed) peak at low temperatures and a shoulder at the higher temperatures. Correcting the times to the first peak would tend to yield a slightly higher activation energy. The opposite would take place with the 3.5 Hz data which are resolved into two peaks at the higher temperatures and overlap at the lower temperatures. Correction would yield somewhat lower activation energies. A linear least squares fit of the completely resolved 3.5 Hz peaks (inclusion of the 181°C data and exclusion of the 125°C data) reduces the activation energy from 16.0 to 15.4 kcal/mole. A frequency independent value of 15.0 to 15.5 kcal/mole would appear to be the result of corrected DSA data (Table 1).

In summary, the differences observed between DSA and TBA can be accounted for to some extent by careful consideration of the meaning of the observed viscoelastic phenomena. An explanation of the frequency dependence of the magnitude of the first peak and strong frequency dependence of the time to the second peak by DSA for Resin 5208 is beyond the scope of this work.

Dielectric Measurements. The dielectric properties of Resin 5208 were followed for isothermal cures of 110, 125, 137, 148, and 162°C at several frequencies. Figure 7 shows the time dependence of the dielectric loss tangent for the combination of the PTFE

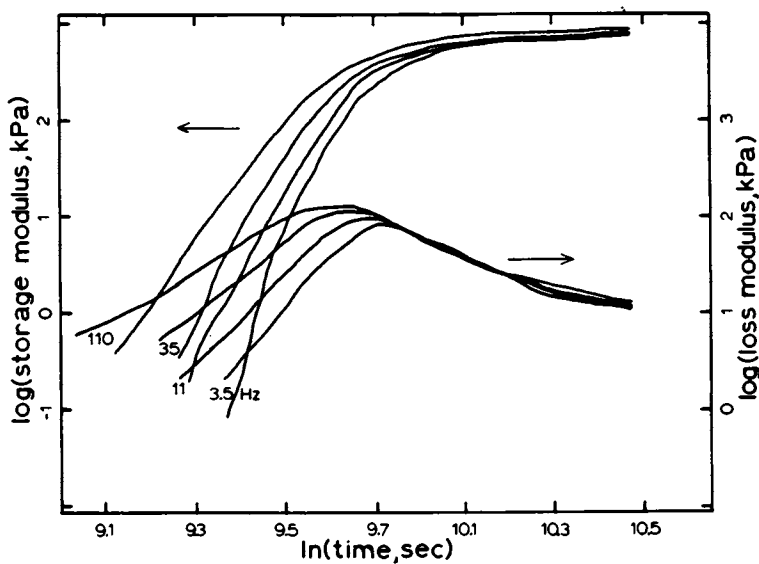


Figure 8. DSA moduli ca.  $\ln(\text{time, sec})$  for  $80.2^\circ\text{C}$  cure of resin 1.

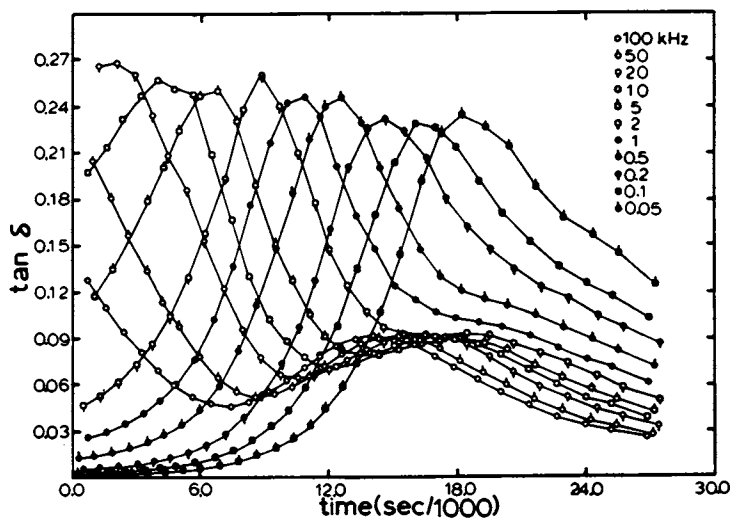


Figure 9. Dielectric composite  $\tan\delta$  vs. time for  $110^\circ\text{C}$  cure.

film and epoxy resin as experimentally measured. Through the analysis presented in Appendix 1 the actual material response is derived and shown in Figure 10 for the same 110°C cure in Figure 6 as a plot of the logarithm of the dielectric constant,  $\epsilon'$ , and the dielectric loss factor,  $\epsilon''$ , vs. time.

Figure 10 shows a high initial value of about 250 for  $\epsilon'$  of the resin at the lower frequencies (0.05 to 0.50 kHz) and a low initial value of about 11 for the higher frequencies (20 to 100 kHz). The lower frequencies show a pronounced frequency dependent drop in  $\epsilon'$  after an initial more gradual decrease through the course of reaction. The fairly steady initial values of the higher frequency runs also show a drop at some frequency dependent point in time with all frequencies showing an approach to an  $\epsilon'$  value consistent with literature values (27) for cured resins in the range of 3.5 to 4.0. Two main dispersion regions are observed for the time dependence of  $\epsilon''$  (Figure 10). Initial high values of  $\epsilon''$  develop into a large dispersion with a strong dependence on frequency as the frequency is lowered. A smaller dispersion is also observed at a later time and with a smaller dependence on frequency than the larger, short time dispersion. The smaller dispersion is observed only at the higher frequencies.

An analysis of the dielectric data similar to that for the dynamic mechanical data was undertaken. The natural logarithm of the time to peak maximum vs.  $1/T$  was plotted for the two peak maxima observed in the dielectric loss tangent as shown in Figure 11. The activation energies derived from linear least squares fit of the data in these plots are listed in Table II.

TABLE II. Dielectric Activation Energies

<u>Peak</u>	<u>Frequency</u>	<u>H<sub>a</sub> (kcal/mole)</u>
1st	50 Hz	11.2
	100	10.8
	200	11.3
	500	11.4
	1000	10.6
2nd	20 kHz	13.3
	50	13.1
	100	13.5

An average activation energy of 11.0 kcal/mole was found for the first peak at frequencies of 50 to 1000 Hz. An average activation energy of 13.3 kcal/mole was found for the second smaller dispersion for the 20, 50, and 100 kHz frequencies. The second peak occurs approximately 40% sooner in time than the DSA second peak. The dielectric relaxation strength ( $\Delta\epsilon'$ ) associated with this peak

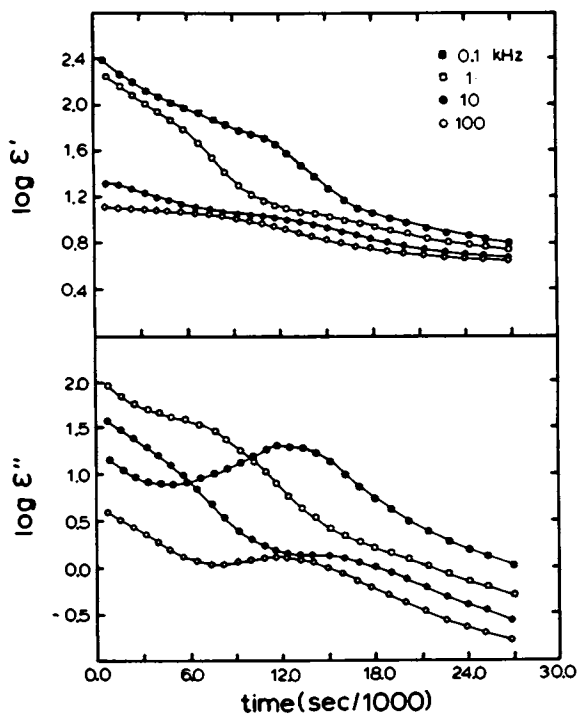


Figure 10. Dielectric resin  $\epsilon'$  and  $\epsilon''$  vs. time for 110 °C cure.

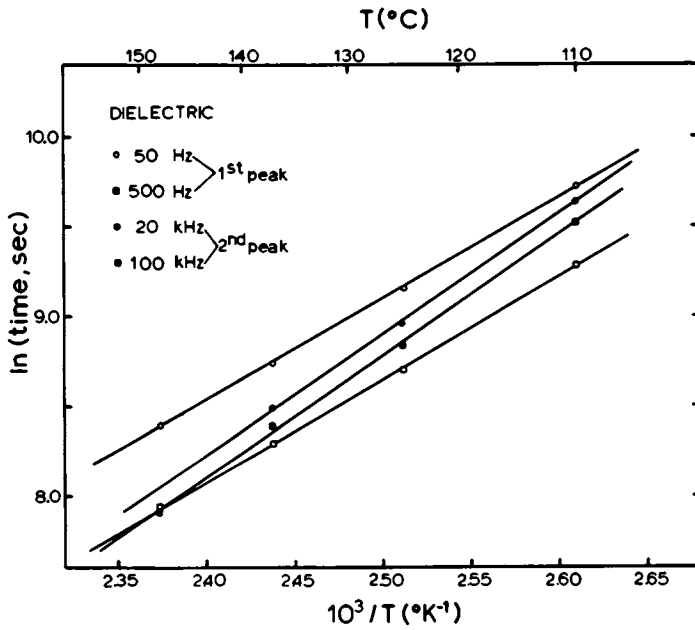


Figure 11. Arrhenius plots of dielectric first and second peaks.



is much closer to the magnitudes to be expected from dipolar reorientation mechanisms than is the relaxation strength of the first peak. An approximate frequency shift of the dielectric second peak (20 to 100 kHz) to the dynamic mechanical frequency range (1 to 100 Hz) shows fairly good agreement at similar cure temperatures with the time to vitrification by DSA and TBA. Although good agreement in the temperature dependence with TBA exists and order of magnitude agreement in time with DSA and TBA second peaks exist, the large separation in real time and limited frequency data prevent unequivocal assignment of vitrification as the cause of the second dielectric dispersion.

Some well documented reasons exist concerning difficulties in interpretation of dielectric data. The dielectric loss spectrum will be significantly affected by material electrical conductance. McCrum et al. (28) show the d.c. conductivity can be separated from the total dielectric loss factor as follows:

$$\epsilon''(\omega) = \epsilon_0''(\omega) + \epsilon_1''(\omega)$$

where  $\epsilon_0''(\omega)$  is the part due to conductivity,  $G_0$ :

$$\epsilon_0''(\omega) = \frac{G_0}{\omega C_0}$$

and  $\epsilon_1''(\omega)$  is the part due to the actual material dielectric loss mechanisms. Increasing the frequency should decrease the  $\epsilon_0''$  term which is observed in Figure 10. Starting values for d.c. conductivity in the temperature range studied agree in order of magnitude with those observed by Delmonte (10) and Adamec (12) ( $1 \times 10^{-6}$  to  $1 \times 10^{-7}$  ohm $^{-1}$  cm $^{-1}$ ). The PTFE film in Figure 1a was originally utilized to prevent shorting across the guard ring.

According to Blythe (29) polarization effects at electrodes become most prominent when the material of a specimen shows some appreciable bulk conductivity. At low frequencies there is sufficient time for any slight conduction to transfer charge to the specimen surface forming an ion double-layer. The result is an enormous increase in the measured capacitance which is observed in Figure 10. A Cole-Cole plot of the data from Figure 9 is shown in Figure 12 as a large dispersion modelled by a single Debye-type relaxation time at 15, 50, 100, and 200 minutes into the 110°C cure. This single relaxation time appears to be associated with charge transport in a viscous medium. The relaxation stems from charge migration to form the ion double-layer instead of from polymer dipolar orientation. Dipolar reorientation in polymers invariably results in a broad distribution of relaxation times. The decrease in the size of the Cole-Cole semicircle with time is

consistent with the above interpretation of the dispersion because of the increase in viscosity of the medium during cure decreases the rate of migration of ions. The second peak in time is much smaller and is difficult to resolve from the main peak. It is observable as a shoulder on the low  $\epsilon'$  end of the 200 minute Cole-Cole plot (Figure 12).

Similar to the findings in other electrical property studies, correlations may be drawn between electrical and mechanical data, but the large effects of conduction and ion double-layer formation mask such correlations in the present case.

Thin-Films. Dynamic tensile testing was carried out on thin-films of Resin 5208 molded with specific isothermal cure histories. The temperature dependence of the loss tangent at several frequencies of one of these samples cured at 124°C for 5 hours is shown in Figure 13. The state of the cure of the sample corresponds to that of a resin studied isothermally by DSA at a time between the two observed DSA  $\tan \delta$  peaks.

The frequency dependence of the loss peak in a temperature scanning experiment indicates whether it arises from viscoelastic relaxation or is associated with chemical reaction. One would expect a peak associated with a viscoelastic relaxation to occur at higher temperatures at higher frequencies, which is true for the lowest and highest temperature peaks observed (Figure 13). For a peak associated with chemical reaction (leading to increased molecular weight) one would expect the peak to occur at lower temperatures at higher frequencies as observed for the intermediate temperature peak (Figure 13). For longer compression molding times at 124°C (or higher temperature cures) the intermediate temperature peak becomes less well resolved from the lowest temperature peak because the extent of further reaction decreases.

Figures 14a and 14b show the logarithm of the storage,  $E'$ , and loss,  $E''$ , moduli vs. temperature for specimens cured at 124°C for 5 and 11.5 hours, respectively. The 5 hour sample, as mentioned above, corresponds to a time between the two DSA peaks at 3.5 Hz isothermal scans while the 11.5 hour sample corresponds to a time longer than those of both DSA loss tangent peaks. The  $E'$  shows an initial decrease (greater in the case of the 5 hour sample than the 11.5 hour sample) followed by an increase and a final decrease at about 250°C.  $E''$  exhibits three dispersion regions in order of increasing temperature. The first is associated with the softening manifested by the decrease in  $E'$ , followed by a peak due to chemical reaction, and finally a peak associated with the glass transition of the fully cured resin. The softening peak in  $E''$  at 3.5 Hz for the 5 hour cure occurs at about 91°C while the same peaks for the 11.5 hour cure occur at approximately 129°C. This indicates the resin is significantly below its glass transition temperature at times after the first DSA peak in the isothermal 124°C scan, whereas the resin is in the

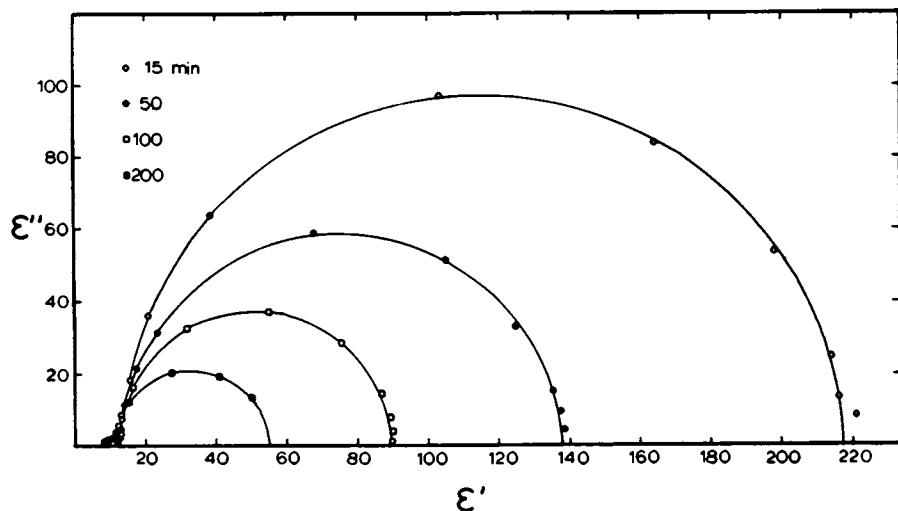


Figure 12. Cole-Cole plots as a function of time for 110 °C cure.

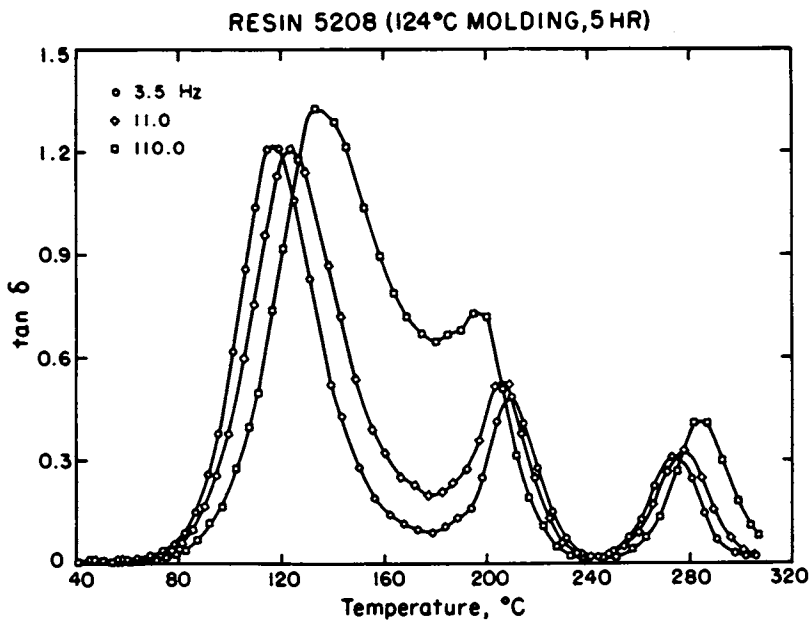


Figure 13. Thin-film  $\tan \delta$  vs. temperature for 5 hr premolded at 124 °C.

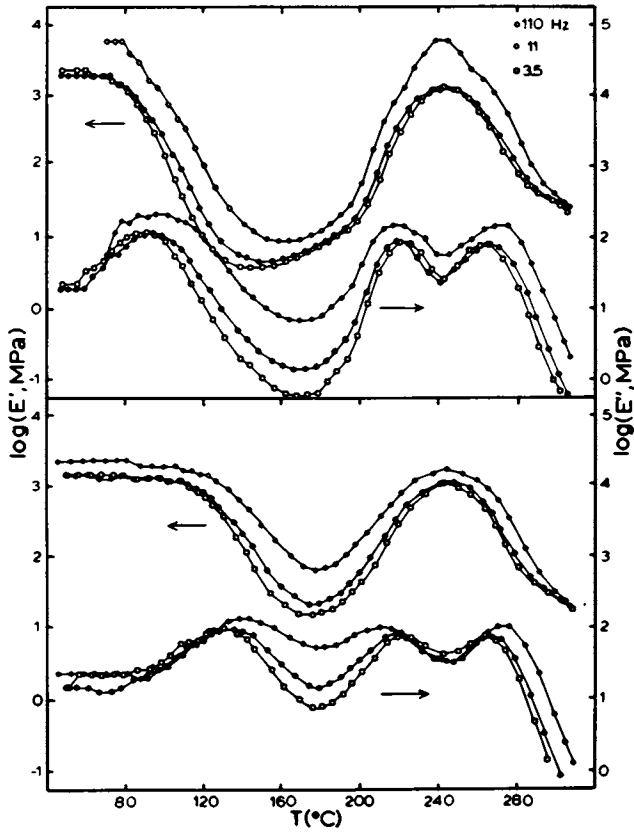


Figure 14. Thin-film moduli vs. temperature for 5 and 11.5 hr premolded at 124 °C.

glassy state at times after the second DSA peak in the isothermal 124°C scan. This implies that the second peak in DSA is associated with vitrification and that significant reaction takes place between the two DSA peaks observed for Resin 5208 in isothermal scans at 3.5 Hz and 124°C.

The viscoelastic response of a sample previously heated to approximately 310°C is shown in Figure 15a. In this case only a single relaxation region exists and this is associated with the glass transition temperature of the fully cured resin formed at 2°C/min.

Previous work (8) on partially cured thin-films of two other epoxy resins showed much less temperature separation between softening, further reaction, and ultimate glass transition than is the case with Resin 5208. In fact, overlap between the dispersion regions made it impossible to identify the chemical reaction process.

Keenan et. al. (30) observe a peak due to the softening of the sample and another peak associated with the glass transition of the fully cured resin on similar type resin systems. Samples in their study were molded at higher temperatures thus no evidence of a reaction peak was observed. They also report the existence of two other processes during the thermal scan of thin films. a  $\beta$  transition at approximately -50°C attributed to the crankshaft motion of the glycidyl portion of the polymeric chain and a  $\omega$  transition at approximately 100°C attributed to the motions of unreacted molecular segments and/or inhomogeneities arising from dissimilar crosslink densities. Thermal scans of the samples in this study were not carried out in this  $\beta$  transition region and no evidence of the  $\omega$  transition is observed for the fully cured resin as seen as in Figure 15 for Resin 5208 between 40 and 300°C. The lower molding temperatures in this study apparently give rise to large softening and reaction effects which possibly mask the observation of the  $\omega$  transition in the partially cured materials.

## Conclusions

DSA analysis of Resin 5208 exhibits two dispersion regions. The first is related to gelation and the second is related to vitrification. The first DSA peak occurs on the attainment of a value for the resin storage modulus slightly lower than that of the rubbery plateau. The first TBA peak occurs at the point where the composite (braid and resin) attains measurable rigidity.

Activation energies are derived from the dynamic mechanical experiments assuming that the kinetic mechanism does not change with temperature. The thus arrived at activation energy represents a lumped kinetic parameter for the reactions which have led to the point in time of the dynamics mechanical dispersion being measured. Activation energies for the first dispersion by DSA

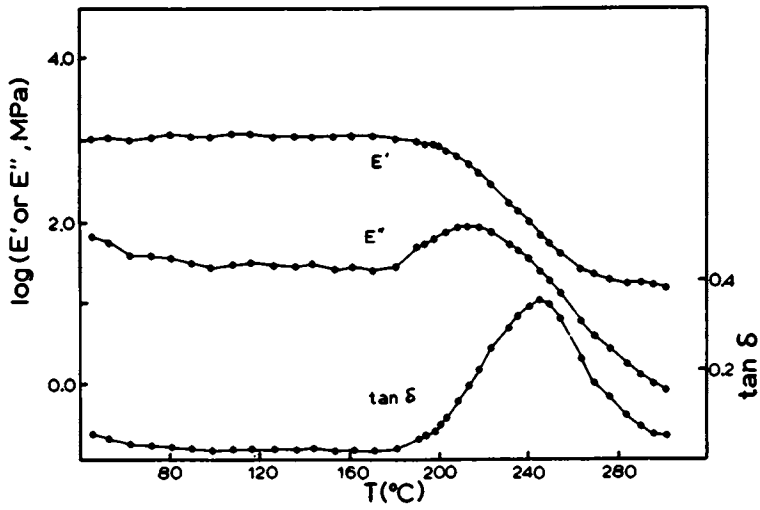


Figure 15. Thin-film  $E'$ ,  $E''$ , and  $\tan \delta$  vs. temperature for  $T_g \infty$ .

range from 14.7 to 16.0 kcal/mole whereas the TBA value is 19.3. Activation energies of 15.0 to 15.5 kcal/mole for DSA and 17.5 for TBA were derived by elimination of the overlap of the second dispersion in DSA and consideration of the kinetic effect in the heating procedure of TBA. The first peaks by DSA and TBA occur at significantly different times (extents of reaction) into the cure and a change in reaction mechanism may account for the difference observed.

Molecular dipolar polarization was difficult to define from dielectric measurements. A large first dispersion in time for isothermal cures of Resin 5208 is attributed to charge migration in a viscous medium. High values of dielectric constant and dielectric loss factor are attributed to the formation of an ion double-layer and sample conductivity, respectively. Limited frequency data on a smaller second dispersion prevent unequivocal assignment of its relationship to molecular changes.

It is useful to make a comparison of the capabilities and limitations of the three techniques used in this work for characterizing the isothermal curing behavior of epoxy resin formulations. DSA has the advantage that storage and loss modulus values for the resin can be computed employing a simple model for the resin-spring composite. The data are reliable only during the early stages of cure due to a loss of sensitivity as the resin vitrifies and greater deformations occur in the ends of the spring. With DSA it is also possible to examine the frequency dependence of the changing viscoelastic characteristics of the resin during cure. TBA allows a broader relative view of the entire process, but adds the mathematical complexity of the braid/resin composite and allows observations only at a resonant frequency. The dielectric analysis first dispersion appears to arise from the influence of the changing viscosity during cure on charge migration rather than from the rapid change in viscosity which marks the onset of gelation in the other two techniques. This method could provide an accurate means of measuring the change in viscosity during the cure. Due to the strength of this dispersion the vitrification region is masked in the equivalent mechanical frequency range of the dielectric analysis. Thus, it appears that the three methods are complementary in the information which they are capable of providing about the properties and characteristics of the resin during cure.

Thin-films of Resin 5208 with specific isothermal cure histories exhibit three dispersion regions upon heating. The first is attributed to softening, followed by further chemical reaction and finally a peak due to the glass transition of the fully cured resin. Dynamic mechanical testing on thin-films shows that significant reaction takes place between the two DSA loss tangent peaks and that the second DSA peak is associated with vitrification.

**American Chemical  
Society Library  
1155 16th St. N. W.  
Washington, D. C. 20036**

### Acknowledgments

We are grateful to the Army Materials and Mechanics Research Center, Watertown, Massachusetts for support of this research under contract no. DAAG 46-80-C-0019 and to the Narmco Materials Division of Celanese Corp. for providing samples. We are also grateful to Dr. R.M. Neumann for helpful discussions and critique of this manuscript.

### Literature Cited

1. Gillham, J.K. A.I.Ch.E.J., 1974, 20, 1066.
2. Gillham, J.K. Polym. Eng. Sci., 1979, 19, 676.
3. Lewis, A.F.; Doyle, M.J.; Gillham, J.K. Polym. Eng. Sci., 1979, 19, 683.
4. Lee, C.-Y.-C.; Goldfarb, I.J. Polym. Eng. Sci. 1981, 21, 390.
5. Naganuma, S.; Sakurai, T.; Takahashi, Y.; Takahashi, S. Kobunshi Kagaku, 1972, 29, 105.
6. Naganuma, S.; Sakurai, T.; Takahashi, Y.; Takahashi, S. Kobunshi Kagaku, 1972, 29, 105.
7. Senich, G.A.; MacKnight, W.J. J. Appl. Polym. Sci., 1978, 22, 2633.
8. Senich, G.A.; MacKnight, W.J.; Schneider, N.S. Polym. Eng. Sci., 1979, 19, 313.
9. Murayama, T.; Bell, J.P. J. Polym. Sci., Part A-2, 1970, 8, 437.
10. Delmonte, J. J. Appl. Polym. Sci., 1959, 2, 108.
11. Haran, E.N.; Gringras, H.; Katz, D. J. Appl. Polym. Sci., 1965, 9, 3505.
12. Adamec, V. J. Polym. Sci., Part A-1, 1972, 10, 1277.
13. Dandurant, D.; Huraux, C. Pr. Nauk. Inst. Podstaw Elektrotech. Elektrotechnol. Politech. Wroclaw., 1977, #16, 275.
14. Lawless, G.W. Polym. Eng. Sci., 1980, 20, 546.
15. Crabtree, D.J. Am. Chem. Soc., Prepr., Div. Polym. Chem., 1981, 22, #2, 233.
16. Senturia, S.D.; Sheppard, N.F.; Poh, S.Y.; Appelman, H.R. Polym. Eng. Sci., 1981, 21, 113.
17. Morgan, R.J.; O'Neal, J.E.; Miller, D.B. J. Mater. Sci., 1979, 14, 109.
18. Cizmecioglu, M.; Hong, S.D.; Moacanin, J.; Gupta, A. Am. Chem. Soc., Prepr., Div. Polym. Chem. 1981, 22 #2, 224.
19. Mones, E.T.; Morgan, R.J. Am. Chem. Soc., Prepr. Div. Polym. Chem., 1981, 22, 249.
20. Tsay, F.E.; Hong, S.D.; Moacanin, J.; Gupta, A. Am. Chem. Soc., Prepr., Div. Polym. Chem., 1981, 22, #2, 231.
21. May, C.A.; Fritzen, J.S.; Whearty, D.K. AFML-TR-76-112, June 1976.
22. Schneider, N.S.; Gillham, J.K. Polymer Composites, 1980, 1, 97.



23. Neumann, R.M.; Senich, G.A.; MacKnight, W.J. Polym. Eng. Sci., 1978, 18, 624.
24. Schneider, N.S.; personal communication.
25. Schneider, N.S.; Sprouse, J.F.; Hagnauer, G.L.; Gilham, J.K. Polym. Eng. Sci., 1979, 19, 304.
26. Hedvat, S. Polym. Eng. Sci., 1981, 21, 129.
27. "CRC Handbook of Chemistry and Physics", 51st edition, The Chemical Rubber Co., Cleveland (1970).
28. McCrum, N.G.; Read, B.E.; Williams, G. "Anelastic and Dielectric Effects in Polymeric Solids", John Wiley and Sons, London (1967).
29. Blythe, A.R. "Electrical Properties of Polymers", Cambridge University Press, Cambridge, 1979.
30. Keenan, J.D.; Seferis, J.C.; Quinlivan, J.T. J. Appl. Polym. Sci. 1979, 24, 2375.
31. Hill, N.E. "Dielectric Properties and Molecular Behaviour", Van Nostrand Reinhold Co., London (1969).

### Appendix

Composite Dielectric Analysis. The dielectric response from the experimental set-up shown in Figure 1 is that of the epoxy resin and upper PTFE sheet. In order to observe the dielectric response of the resin alone one must first subtract the PTFE response from the total response.

The total complex capacitance ( $C^*_{total}$ ) can be expressed as a series combination of the complex capacitances of the resin and PTFE sheet ( $C^*_{resin}$  and  $C^*_{PTFE}$ ) as follows:

$$\frac{1}{C^*_{total}} = \frac{1}{C^*_{PTFE}} + \frac{1}{C^*_{resin}} \quad [1]$$

A complex capacitance can be expressed as the product of the complex dielectric constant,  $\epsilon^*$ , and a geometrical constant,  $C_0$ , of the sample:

$$C^* = \epsilon^* \cdot C_0 \quad [2]$$

where the complex dielectric constant is defined by a real ( $\epsilon'$ ) and an imaginary ( $i\epsilon''$ ) component as follows:

$$\epsilon^* = \epsilon' - i\epsilon'' \quad [3]$$

Assuming no dielectric loss factor ( $\epsilon''_{PTFE} = 0$ ) for the PTFE response over the temperature range studied, combining [1], [2], and [3] shows:

$$\frac{1}{(\epsilon' - i\epsilon'')_{\text{total}} \cdot (C_0)_{\text{total}}} = \frac{1}{\epsilon'_{\text{PTFE}} \cdot (C_0)_{\text{PTFE}}} + \frac{1}{(\epsilon' - i\epsilon'')_{\text{resin}} \cdot (C_0)_{\text{resin}}}$$

Rearranging [4] for the complex resin dielectric constant yields:

$$\epsilon'_{\text{resin}} - i\epsilon''_{\text{resin}} = \frac{1}{(C_0)_{\text{resin}}} \cdot \left( \frac{\epsilon'_{\text{total}} \cdot \epsilon'_{\text{PTFE}} \cdot (C_0)_{\text{total}} \cdot (C_0)_{\text{PTFE}}}{\epsilon'_{\text{PTFE}} \cdot (C_0)_{\text{PTFE}} - \epsilon'_{\text{total}} \cdot (C_0)_{\text{total}}} \right) + \left( \frac{-i\epsilon''_{\text{total}} \cdot \epsilon'_{\text{PTFE}} \cdot (C_0)_{\text{total}} \cdot (C_0)_{\text{PTFE}}}{+i\epsilon''_{\text{total}} \cdot (C_0)_{\text{total}}} \right) \quad [5]$$

Separating and equating the real and imaginary parts of [5] yield the actual resin response:

$$\epsilon'_{\text{resin}} = \frac{1}{(C_0)_{\text{resin}}} \cdot \left( \frac{A \cdot C - B \cdot D}{C^2 + D^2} \right) \quad [6]$$

$$\epsilon''_{\text{resin}} = \frac{1}{(C_0)_{\text{resin}}} \cdot \left( \frac{A \cdot D + B \cdot C}{C^2 + D^2} \right) \quad [7]$$

where A, B, C, and D are all functions of experimentally measurable quantities:

$$A = \epsilon'_{\text{total}} \cdot \epsilon'_{\text{PTFE}} \cdot (C_0)_{\text{total}} \cdot (C_0)_{\text{PTFE}} \quad [8]$$

$$B = \epsilon''_{\text{total}} \cdot \epsilon'_{\text{PTFE}} \cdot (C_0)_{\text{total}} \cdot (C_0)_{\text{PTFE}} \quad [9]$$

$$C = \epsilon'_{\text{PTFE}} \cdot (C_0)_{\text{PTFE}} - \epsilon'_{\text{total}} \cdot (C_0)_{\text{total}} \quad [10]$$

$$D = \epsilon''_{\text{total}} \cdot (C_0)_{\text{total}} \quad [11]$$

A somewhat similar analysis for a conducting layer and a parallel non-conducting layer is presented by Hill (31).

RECEIVED May 17, 1983

## Reactive Systems—Finite Element Analysis

CRAIG DOUGLAS and DAVID ROYLANCE

Department of Materials Science and Engineering, Massachusetts Institute of Technology, Cambridge, MA 02139

This paper outlines the equations which govern the nonisothermal flow of reactive fluids, and describes the means by which finite element analysis can be used to solve these equations for the sort of arbitrary boundary conditions encountered in industrial practice. The performance of the computer code is illustrated by several trial problems, selected more for their value in providing insight to polymer processing flows than as practical production problems. Although a good deal remains to be learned as to the performance and proper use of this numerical technique, it is undeniably useful in providing better understanding of today's complicated polymer processing problems.

Finite element analysis offers great promise for reducing the empiricism often found in polymer processing design, since it is well suited for modeling the complicated boundary conditions and material properties encountered in industrial practice. Although the method is now well accepted in structural stress analysis, its use in fluid transport situations is less widespread. We have sought to exploit some of the many advantages of the finite element method in polymer fluid processing analysis, and this paper describes some of our work in chemorheology.

Reactive flows have several advantages in polymer processing in comparison with more traditional melt-flow techniques. Perhaps the most significant of these is the energy savings which result from the elimination of the several melting stages necessary in such technologies as extrusion or injection molding. However, these advantages are offset to some degree by the complexity of the process, which renders the empirical approach to process development difficult in the extreme. The flow velocities in such processes are governed by the fluid viscosity, which is a strong

0097-6156/83/0227-0251\$06.00/0  
© 1983 American Chemical Society

function of temperature and molecular weight. The temperature in turn is affected by the viscous dissipation and the heat released or consumed by the reaction, and the reaction rate is also a strong function of temperature. All of these variables interact and change in such a way as to make an intuitive grasp of the process almost impossible, and there is obviously an advantage to being able to provide some sort of mathematical or numerical simulation of the process.

The finite element scheme to be described below is very useful for obtaining numerical solutions for reactive flows with arbitrary boundaries, and such a technique is well suited for detailed analysis of real industrial processes. However, we argue that the greatest value of the method may not be in these detailed calculations, but in the degree to which the method can enhance the process designer's intuition. For this latter purpose, it is often sufficient to run only very small and inexpensive trial problems; these can elucidate the manner in which the various problem parameters interact, so that the designer develops a much improved "feel" for the problem. It is likely that most real advances in processing technology will continue to be made more by Edisonian innovation than by detailed mathematical calculations. But since today's processes have become so complicated, such a technique as the finite element method can be a powerful adjunct to intelligent intuition.

### Theoretical background

The equations which govern the nonisothermal flow of a reactive fluid are derived in several texts on transport phenomena and polymer processing (e.g. refs. 1,2). Regarding velocity, temperature, and concentration of unreacted species as the fundamental variables, the governing equations can be written as:

$$\begin{aligned}\rho [\partial u / \partial t + u \cdot \nabla u] &= -\nabla p + \eta \nabla^2 u \\ \rho C [\partial T / \partial t + u \cdot \nabla T] &= Q + k \nabla^2 T \\ [\partial C / \partial t + u \cdot \nabla C] &= R + D \nabla^2 C\end{aligned}$$

(A list of nomenclature is attached.) The similarity of these equations is clear. In all cases, the time rate of change of the transported variable (velocity, temperature, or concentration) is balanced by the convective or flow transport terms (e.g.  $u \cdot \nabla C$ ), the diffusive transport (e.g.  $D \nabla^2 C$ ), and a generation term (e.g.  $R$ ).

The analyst seeks expressions for the space- and time-dependent velocities, temperatures and concentrations which satisfy these equations and also the problem's boundary conditions. It is generally the boundary conditions which make real problems intractable: even if one were able to describe the boundaries mathematically, the resulting expressions would not likely be amenable to closed-form solution. In addition, many of the

"constants" in the above equations are often nonlinear functions of the problem variables. In reactive polymer processing, one might encounter such expressions as the following:

$$\begin{aligned}\eta &= \eta_0 \dot{\gamma}^{n-1} \exp[E_1/R_g T] \exp(\beta p) (m w^{3.4}) \\ Q &= (\eta/2) (\dot{\gamma}:\dot{\gamma}) + R(\Delta H) \\ R &= -k_m \exp(E_2/R_g T) C^m\end{aligned}$$

It is clear that all of these expressions, taken together, constitute a mathematical situation which must be approached with caution. Even though it is not overly difficult to incorporate them into a numerical scheme, which we have done, it is important to proceed slowly enough to develop the proper experience in the computer code's behavior before tackling full-blown problems.

### Computer Model

We have sought to develop a finite element code which is able to predict polymer fluid velocities, stresses, temperatures, and degrees of chemical conversion in a variety of flow geometries and for a variety of fluid material properties. Space limitations prohibit our listing here the full derivation of the finite element equations from the above differential equations, but there exist several well developed means by which this may be done. The reader is directed to standard texts (3,4) for a more complete description, and we will just state here that we employ the Galerkin method of weighted residuals, together with isoparametric mapping and interpolation, to replace the differentials by integrals which can be evaluated numerically over small subregions ("elements"). The results of these numerical integrations are then assembled into a set of simultaneous algebraic equations which can be solved numerically.

The salient features of our code can be listed briefly as follows: (1) Velocity, temperature, and chemical conversion are taken as nodal unknowns, so that coupled incompressible viscous flow and diffusive-convective heat and mass transport may be modeled. (2) Incompressibility is enforced by a "penalty" formulation employing selective reduced integration. This approach requires the use of double precision arithmetic with a concomitant reduction in the amount of available core, but it has several programming advantages which usually outweigh this drawback. (3) The code is developed primarily for plane and axisymmetric flows. We have coded a three-dimensional capability, but generally feel that the expense of running three-dimensional problems is not justified for most of our modeling research. (4) The code includes several models for the effect of shear rate, temperature, pressure, and chemical conversion on the fluid viscosity. These nonlinear models have not yet been researched extensively, however, and the exploration of the interactive schemes needed for their proper use constitutes a major goal for

future research. We have also coded a capability for viscoelastic fluid effects (ref. 5), but currently feel that this difficult aspect of polymer flow is being researched satisfactorily by other workers. (5) Convective transport of heat or chemical species can be handled either by a conventional Galerkin treatment or by the convenient but still controversial "optimal upwinding" approach. (6) The code can treat transient problems by means a two-point "theta-method" time-stepping algorithm. The dynamic algorithm is also useful in nonlinear problems, in which the final fluid state may be approached dynamically from an estimated initial state. (7) The code is capable of a variety of iterative treatments of nonlinear problems, including Newton-Raphson iteration and incremental load methods.

Some additional discussion is warranted concerning the treatment of convective effects beyond what has been mentioned in item (5) above. Momentum convection ( $\rho u \cdot \nabla u$ ) is generally negligible in comparison with the viscous terms due to the high viscosities of polymer fluids, but the convective terms tend to dominate the energy and mass transport equations due to the generally low thermal and mass diffusivities. The programming of the convective terms presents no special problems in the Galerkin approach beyond the need to store and solve unsymmetric matrices, but it is well known that the presence of strong convective terms tends to create oscillations in the final solutions which can be large enough to destroy their value. This instability is related to the tendency of convection to produce large downstream gradients which the finite element grid cannot resolve. A largely ad hoc procedure known as "upwinding" has been used in both finite element and finite difference work which seems to alleviate this problem by providing a greater numerical weight to the upstream portion of the element. Hughes (6) has published a very convenient means of upwinding, in which the sampling points in the numerical integration scheme are simply moved upstream an appropriate distance. We have made extensive use of the Hughes upwinding technique, but the reader is cautioned that this method is regarded as controversial by many workers. A provocative paper by Gresho (7) details many of the possible pitfalls in upwinding, and states a strong preference for grid refinement as the appropriate cure for convection-induced instabilities.

#### Selected Numerical Result

The operation of the numerical model will be illustrated by means of three computer experiments, chosen more for their value in visualizing reactive flow than as detailed numerical simulations of real industrial processes. Simple fluid property models will be used in which material parameters such as viscosity and reaction order are not allowed to vary during the process, although real situations are often much more complicated than this. The numerical model does have the capability of performing

a variety of iterative schemes to model real situations in which nonlinear and time-varying fluid properties are present, but such complicated simulations are often not as revealing as simple trial problems, at least in the earlier stages of research.

Nonreactive entry flow. Figure 1 shows the streamlines for a 4:1 entry flow. Here a grid of 100 four-node linear elements was used to model the upper symmetric half of a plane capillary, and a fully-developed Poiseuille velocity was imposed on the reservoir entry as a boundary condition. The streamlines are identical with published experimental and numerical results, although the grid used here was not intended to be fine enough to capture the weak recirculation which develops in the stagnant corner of the reservoir.

The temperature contours for convectionless flow are shown in figure 2, which shows a hot region at the entrance of the capillary due to the combination of high viscous energy dissipation there and its distance from cool boundaries to which heat may be conducted. These isotherms are normalized on the maximum centerline temperature expected for Poiseuille flow in the capillary.

The importance of thermal convection relative to conduction is given approximately by the Peclet number  $Pe = UL\rho c/k$ , where  $U$  and  $L$  are a characteristic velocity and length. Figure 3 plots the variation of temperature along the centerline for various values of the Peclet number, and it can be seen that the effect of increased thermal convection is to sweep the cooler upstream flow particles into the capillary, with a resulting lowering of the temperatures overall and a shift downstream of the hot spot near the throat. The relatively coarse grid used in this problem produced unstable Galerkin results for Peclet numbers higher than approximately ten, and the higher degrees of thermal convection were computed using the upwinding formulation. Further tests with refined grids should be completed to assess the accuracy of the upwinded solutions, although the plots in figure 3 appear reasonable.

One-dimensional reactive flow. As a preliminary trial problem in our computations of reactive flow, we have studied a simple situation in which a fluid obeying first-order chemical kinetics moves at constant velocity and temperature in the positive  $x$  direction. Here only the mass-transport equation is operative, and it takes the simple form:

$$u(dC/dx) = -KC + D(d^2C/dx^2)$$

This equation is solved easily, and for nonzero values of the diffusion coefficient  $D$  two boundary values for  $C$  must be specified. One of these is the initial concentration at the inlet, and the other requires a consideration of the outlet conditions. Here several possibilities exist, and we have studied the case in which

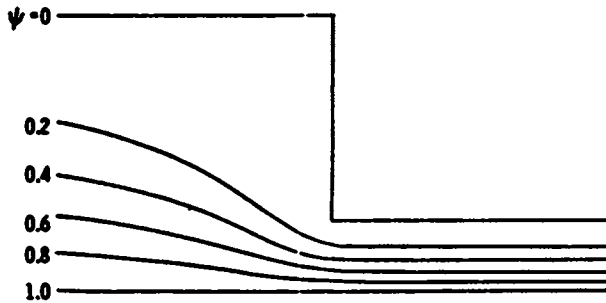


Figure 1. Streamlines for nonreactive 4:1 entry flow, Newtonian fluid with imposed Poiseuille flow at inlet.

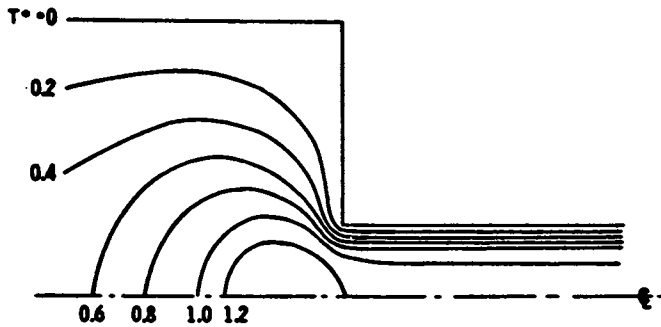


Figure 2. Contours of constant temperature for convectionless entry flow, with heat generation by viscous dissipation only.



the concentration of the outlet reservoir is allowed to rise to meet that supplied by the flow; this is equivalent to specifying a zero concentration gradient at the outlet. For the case of negligible diffusion ( $D=0$ ), the second-order term vanishes from the above equation and the downstream boundary condition cannot be specified. The solution is then a simple exponential, in which the reactive species vanish according to first-order kinetics as they are carried downstream at constant velocity.

Figure 4 shows the computed and exact predictions for reactive group concentration as a function of distance along the channel. The Galerkin values are nearly exact, but it is clear that upwinding leads to erroneous results in the small-diffusion case. The upwinding has introduced an artificially high diffusivity and a zero concentration gradient at the outlet, and such artifacts must be considered as possibilities when upwinding is used.

Two-dimensional nonisothermal reactive flow. Figure 5 shows the contours of constant conversion for a two-dimensional analog of the flow discussed in the previous section. Here again, a simple uncoupled problem is treated in which the material parameters are taken to be independent of the solution variables, and in which the velocity conditions are prescribed. The concentration is taken to have a fixed value at the inlet and a zero gradient at the outlet, as before. The two-dimensionality of the problem is contained in two features: the velocity is taken to be parabolic, ranging from a maximum at the centerline to zero at the walls (a Poiseuille flow); and now diffusive heat and mass transport can occur in both the  $x$  and  $y$  direction. For the low diffusivities shown, mass diffusion in the  $x$  direction is negligible, as was demonstrated in the previous section. However, the concentration gradients in the  $y$  direction are substantial, so that diffusive transport in that direction is appreciable even at  $D = 0.01$ . At  $D = 0.001$ , even the  $y$ -diffusion is negligible, so the concentration contours simply represent a fluid which moves in the  $x$ -direction while reacting by first-order kinetics. The concentrations along the centerline are then identical with the  $D = 0.01$  curve of figure 4.

Figure 6 shows the contours of constant temperature which result from this flow (with  $D = .001$ ), where the temperature boundary conditions were set to zero at the entry and along the top and bottom surfaces. The temperature gradient at the outlet was allowed to become zero, similar to the concentration gradient. The results obtained for the temperature field are of course dependent on the values chosen for fluid properties. To avoid using space here for a detailed discussion of the dimensional analysis used for selecting these parameters, we will state simply that in figure 6 the viscous dissipation and reaction heat make approximately equal contributions to the internal heating (Brinkman and Damkoehler numbers both equal to three).

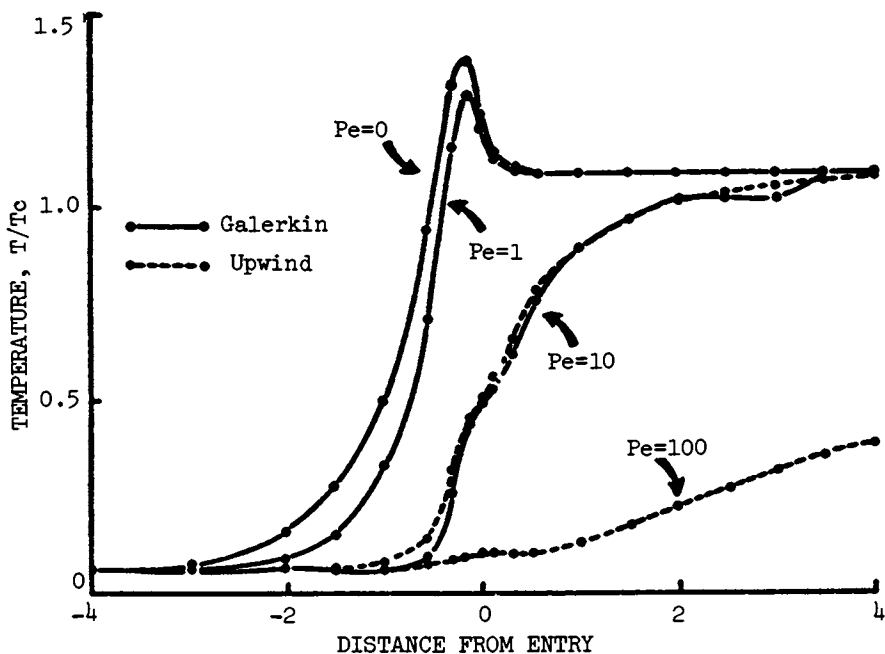


Figure 3. Entry flow centerline temperatures at various Peclet numbers.

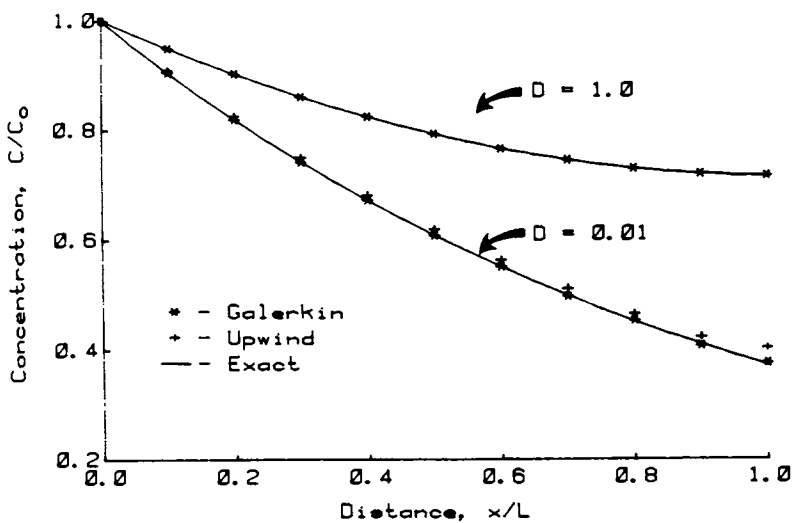


Figure 4. Degree of conversion along channel in one-dimensional reactive flow.

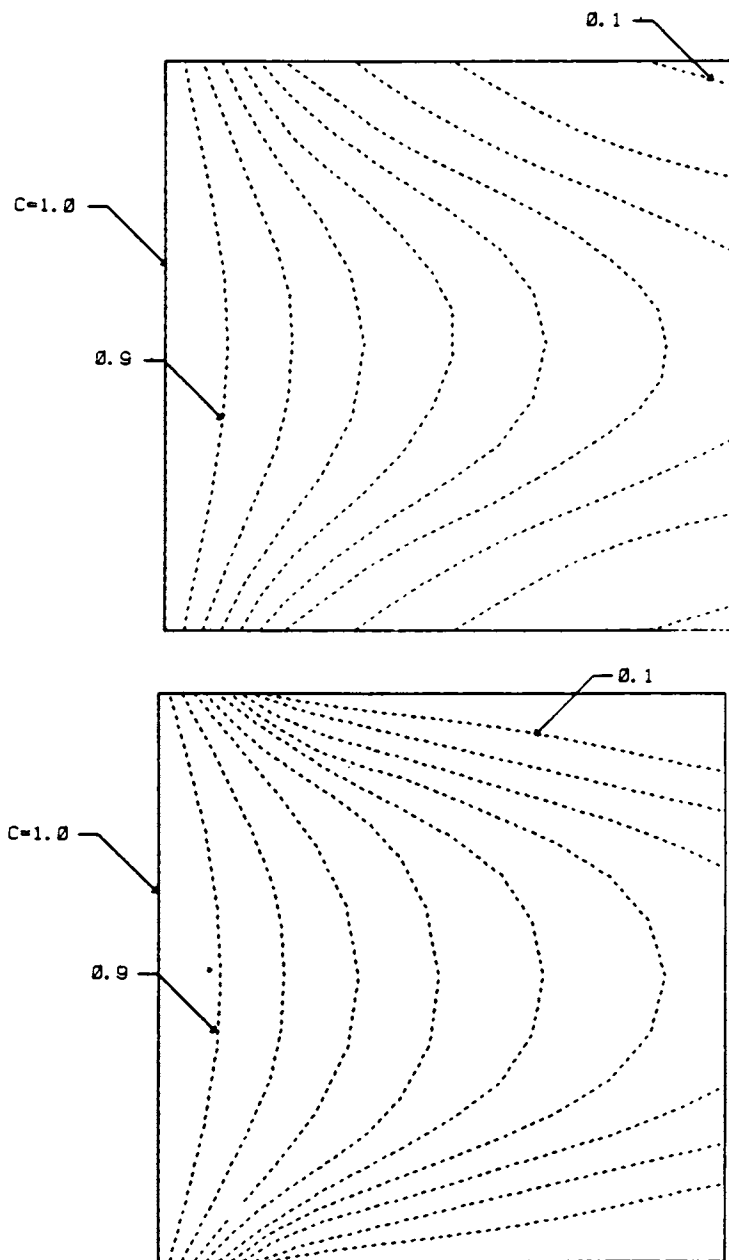


Figure 5. Isoconversion contours in two-dimensional reactive flow at two different mass diffusivities, Galerkin calculations.

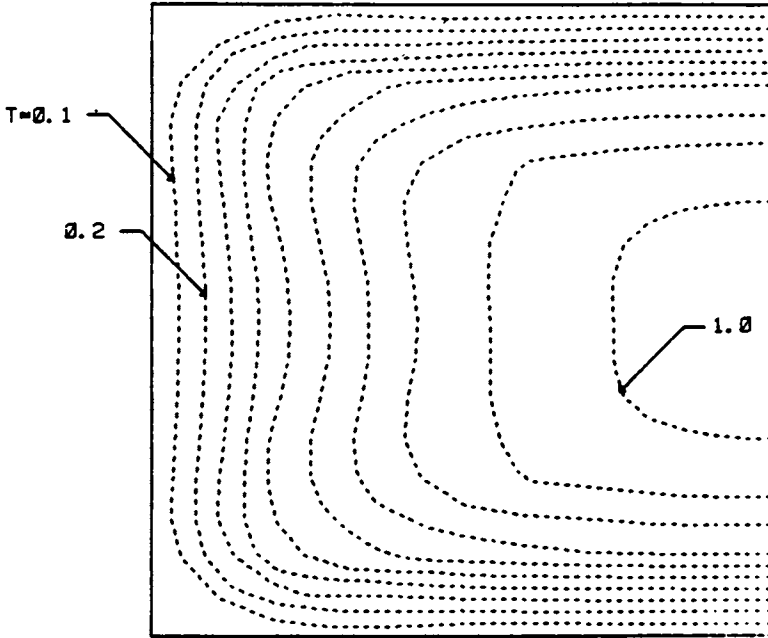


Figure 6. Isothermal contours in two-dimensional reactive flow, Galerkin calculation. Heat generation by viscous dissipation and reaction heating.

### Conclusions

The numerical model described above has a significant present ability to simulate a wide range of problems in polymer processing. At the same time, it is small enough to permit easy implementation in even rather small processing facilities, and for quick familiarization by process designers. We feel such a capability would lead to a significant advance in industry capability for process development and optimization.

### Acknowledgments

The authors gratefully acknowledge the support of this work by the Army Materials and Mechanics Research Center, the National Aeronautics and Space Administration through MIT's Materials Processing Center, and the Hysol-Dexter Corporation. We also acknowledge the invaluable assistance of Colin Freese on many aspects of this work, and for his beautiful pre- and post-processing graphics routines.

### Nomenclature

c	specific heat
C	concentration of reactive species
D	diffusion coefficient
$E_1$	activation energy for viscosity
$E_2$	activation energy for reaction
k	coefficient of thermal conduction
$k_m$	reaction rate preexponential factor
K	overall reaction rate
m	reaction order
mw	molecular weight
n	power-law exponent for viscosity
p	pressure
Q	internal heat generation
R	internal species generation
$R_g$	gas constant
T	temperature
u	velocity or velocity vector
$\beta$	factor for pressure dependency
$\dot{\gamma}$	shear rate
$\eta$	viscosity
$\eta_0$	viscosity coefficient
$\rho$	density
$\Delta H$	heat of reaction
$\nabla$	gradient operator

### Literature Cited

1. Bird, R.B., W.E. Stewart, and E.N. Lightfoot: "Transport Phenomena," John Wiley & Sons, Inc., New York, 1960.

2. Middleman, S.: "Fundamentals of Polymer Processing," Mc Graw-Hill Co., New York, 1977.
3. Zienkiewicz, O.C.: "The Finite Element Method," McGraw-Hill Co., London, 1977.
4. Huebner, K.H.: "The Finite Element Method for Engineers," John Wiley & Sons, Inc., New York, 1975.
5. Collins, B.R., S.M. Thesis, MIT, Cambridge, 1981.
6. Hughes, T.R.J., W.K. Liu, and A. Brooks, J. Comp. Physics, vol. 30, pp. 1-59, 1979.
7. Gresho, P.M., and R.L. Lee, Computers and Fluids, vol. 9, pp. 223-253, 1981.

RECEIVED June 3, 1983

# Kinetic Model of Cure Reactions

## Aids to Property and Processing Predictions

H. S.-Y. HSICH, R. M. ZURN, and R. J. AMBROSE

Lord Corporation Mechanical Group, Material and Process Research and Development, Erie, PA 16514

A generalized kinetic model of cure is developed from the aspect of relaxation phenomena. The model not only can predict modulus and viscosity during the cure cycle under isothermal and non-isothermal cure conditions, but also takes into account filler effects on cure behavior. The increase of carbon black filler loading tends to accelerate the cure reaction and also broadens the relaxation spectrum. The presence of filler reduces the activation energy of viscous flow, but has little effect on the activation energy of the cure reaction.

Understanding and predicting cure kinetics of elastomeric or thermosetting materials is of practical interest both in the manufacturing process and in end-product performance/reliability. Unfortunately, in most polymeric systems, the cure reactions are quite complex; therefore, it is difficult for one to develop a kinetic model which can explain and predict changes of physical and mechanical properties of the polymer during the cure reaction. Although there have been many studies on cure kinetics, most of them are limited to the method of calorimetry [1-5], such as differential scanning calorimetry (DSC) or differential thermal analysis (DTA). In those studies, the definition of the state of cure is not directly correlated to the physical, mechanical, or rheological properties of polymers. Therefore, kinetic models which are developed from the calorimetric method are unable to predict properties, such as viscosity and dynamic modulus, which are used to determine the manufacturing operation and end-product performance of polymeric systems.

Conventionally, rules of thumb have been widely used in the industry for curing rubbers. It has been assumed that the rate of cure is doubled for every 10°C increase in cure temperature.

0097-6156/83/0227-0263\$07.00/0

© 1983 American Chemical Society

In addition, cure time is increased five minutes for every 0.25 inches of thickness of a molding [6, 7]. In general, these rules do not apply to most polymeric systems because the phenomena of heat transfer and cure kinetics have been over-simplified. The cure rate depends on the basic polymers, curatives, cure temperature, and filler loading. The prediction of cure rate will be discussed from a new model of cure kinetics which is developed from the concept of a non-equilibrium thermodynamic fluctuation theory of chemical relaxation.

### KINETIC THEORY OF THE CURE REACTION

The kinetic model for predicting viscosity and modulus during cure of elastomers or thermosets has been given by Roller [8], Craig [9], and Musatti and Macosko [10]. Unfortunately, these models can only predict a narrow range of data during cure; also these models do not include polymer-filler interactions. Because of the shortcomings of these models, a generalized kinetic model of cure was recently proposed [11].

As has been discussed by Hsich [12, 13], any chemical relaxation (reaction) or structural relaxation can be explained from irreversible thermodynamic fluctuation theory in which changes of physical and mechanical properties during the relaxation process can be interpreted and predicted from the mean square fluctuations of thermodynamic ordering parameters. Then the physical or mechanical properties at any given cure time can be written as a relaxation function:

$$P(t) = P_0 + (P_\infty - P_0) \left\{ 1 - \exp \left[ - \left( \frac{t}{\tau} \right)^\beta \right] \right\} \quad (1)$$

where  $P(t)$  is the physical or mechanical property at time,  $t$ , and  $P_0$  and  $P_\infty$  are the initial and final values of the property.  $\beta$  is a constant describing the width of the relaxation spectrum, and  $\tau$  is the relaxation time which is a function of temperature,  $T$ , and activation energy,  $H$ , of cure.  $\tau$  can be defined as:

$$\tau = \tau_0 \exp \left[ \frac{H}{RT} \right] \quad (2)$$

Where  $\tau_0$  is a constant which represents the relaxation time at  $T \rightarrow \infty$  and  $R$  is the gas constant.

The model described in Eq.(1) not only can predict the cure behavior measured by standard curometers, but also can explain filler effects on the cure reaction. The model enables one to predict scorch time and cure time of elastomers at various filler loadings and cure temperatures. In the following discussion, this kinetic model of cure will be extended to explain and predict the modulus or viscosity of elastomers/thermosets during



cure. The model for predicting the shear modulus can be rewritten as:

$$G(t) = G_0 + (G_\infty - G_0) \left\{ 1 - \exp \left[ - \left( \frac{t - t_0}{\tau} \right)^\beta \right] \right\} \quad (3)$$

Where  $G$  represents the shear modulus, and  $G_0$  and  $G_\infty$  are the minimum and maximum values of the shear modulus during cure, respectively. The induction time,  $t_0$ , has been mentioned previously [11]. This induction time is defined as the time needed for polymer systems to reach the temperature necessary for cure onset. (This is why the cure curve decreases to a minimum value before it increases.) For predicting viscosity during cure, one only needs to substitute viscosity for shear modulus in Eq. (3).

Since non-isothermal cure is of practical importance in cure control, one would like to extend the cure model to include non-isothermal cure kinetics. This modification is shown below:

$$G'(t) = G'_e \exp \left[ \frac{E}{RT(t)} \right] + [G'_\infty - G'_e \exp \left( \frac{E}{RT_c} \right)] \left\{ 1 - \exp \left[ - \left( \int_{t_0}^{t_f} \frac{d(t - t_0)}{\tau} \right)^\beta \right] \right\} \quad (4)$$

where  $G'_e$  is a constant which represents the value of the shear storage modulus at temperature,  $T_\infty$ .  $E$  is the activation energy which is ascribed to intermolecular forces [14].  $T_c$  is the equilibrium cure temperature,  $t_0$  is the induction time at  $T_c$  and  $t_f$  is the final cure time. Under isothermal conditions,  $\tau$  is a function of temperature only. However, under non-isothermal conditions as in Eq. (4),  $\tau$  is a function of temperature which in turn is a function of time. This can be expressed as:

$$T(t) = \int_0^t \frac{dT}{dt} dt \quad (5)$$

In Eq. (4),  $G'_e \exp [E/RT(t)]$  describes the effect of temperature on the property of concern in the absence of cure. The remaining part of Eq. (4) describes the effect of the curing reaction on the property being considered. In the following discussion, Eqs. (3) and (4) will be used for predicting isothermal and non-isothermal cure curves.

Since viscosity is of vital importance in material processing, one would like to predict viscosity during cure. In doing so, Eq. (3) is modified as follows:

$$\eta(t) = \eta_0 + (\eta_\infty - \eta_0) \left\{ 1 - \exp \left[ - \left( \frac{t - t_0}{\tau} \right)^\beta \right] \right\} \quad (6)$$

Here, viscosity,  $\eta$ , can be either complex viscosity or real-part viscosity. For our studies, we have used the complex viscosity. The parameters  $\eta_0$  and  $\eta_\infty$  are the minimum and maximum value of  $\eta$  on the cure curve.

For non-isothermal cure conditions, Eq. (4) can be modified as follows for predicting viscosity data:

$$\eta(t) = \eta_e \exp\left[\frac{E}{RT(t)}\right] + \left[\eta_\infty - \eta_e \exp\left(\frac{E}{RT_c}\right)\right] \left\{ 1 - \exp\left[-\int_{t_0}^{t_f} \frac{d(t - t_0)}{\tau} \right]^\beta \right\} \quad (7)$$

where  $\eta_e$  is a constant which represents the value of viscosity at temperature  $T \rightarrow \infty$

#### EXPERIMENTAL RESULTS AND DISCUSSION

The samples for the cure study were prepared from natural rubber with 10, 20, 30, 40 and 50 parts per hundred rubber (phr) of N-330 carbon black loading. Isothermal cure curves were obtained from a Rheometric Mechanical Spectrometer (RMS) operating at angular frequency,  $\omega = 1$  rad/sec for cure temperatures at 130°C and 150°C. The results are shown in Fig. 1-8. Fig. 1-5 plot shear storage modulus vs. cure time, while Fig. 6-8 plot complex viscosity vs. cure time. The theoretical predictions for the shear storage modulus during cure as obtained from Eq. (3) are also shown in Fig. 1-5 (solid line) along with the experimental data. It can be seen that there is good agreement between the experimental data and theoretical calculations. It should be noted here, when Eq. (3) is used for fitting cure curves of the shear storage modulus, the shear storage modulus  $G'$  is used in Eq. (3) instead of  $G$ . As has been discussed in the previous study [11], the activation energy of  $H=18$  Kcal/mole was used in the calculations.

In figures 6-8, complex viscosity is plotted against cure time. Eq. (6) was used to fit the cure curves for 10, 30 and 50 phr of filler loading at cure temperature of 130°C and 150°C. The results of the theoretical calculations are shown in figures 6-8 along with the experimental data. Again, there is good

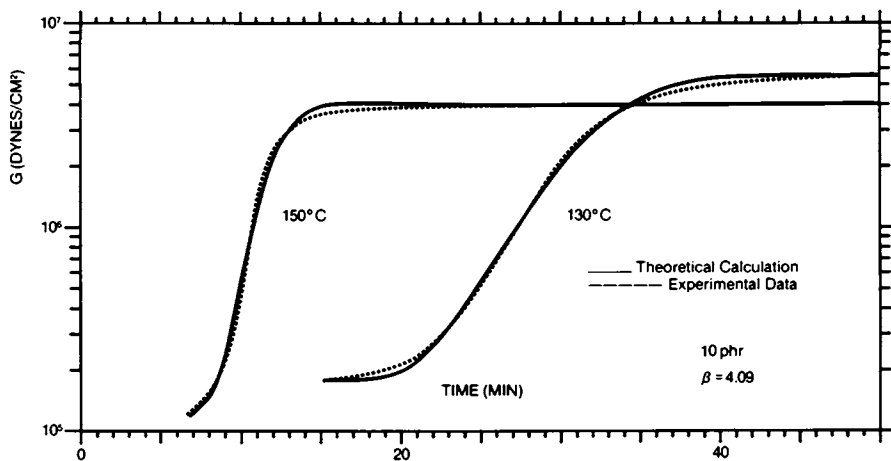


Figure 1. Shear storage modulus vs. cure time for 10 phr filler loading.

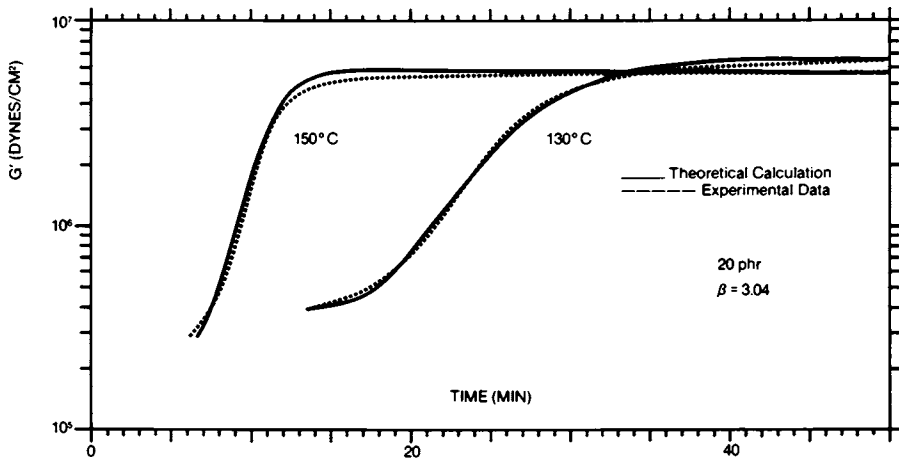


Figure 2. Shear storage modulus vs. cure time for 20 phr filler loading.

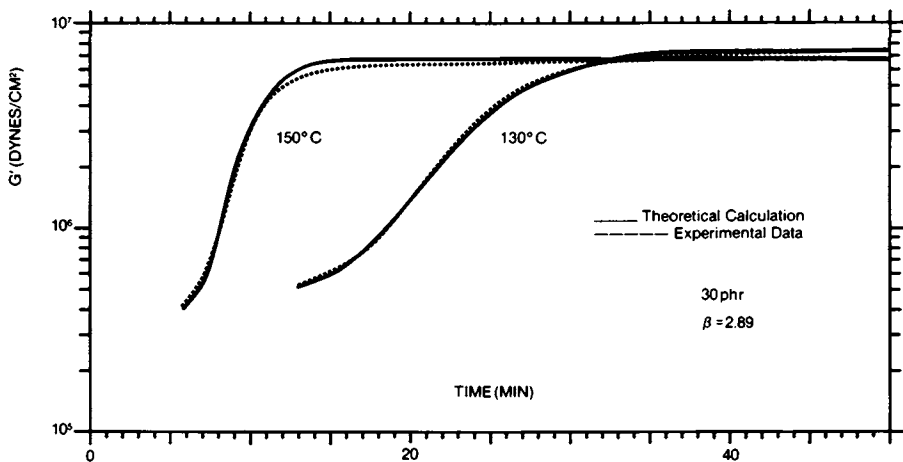


Figure 3. Shear storage modulus vs. cure time for 30 phr filler loading.

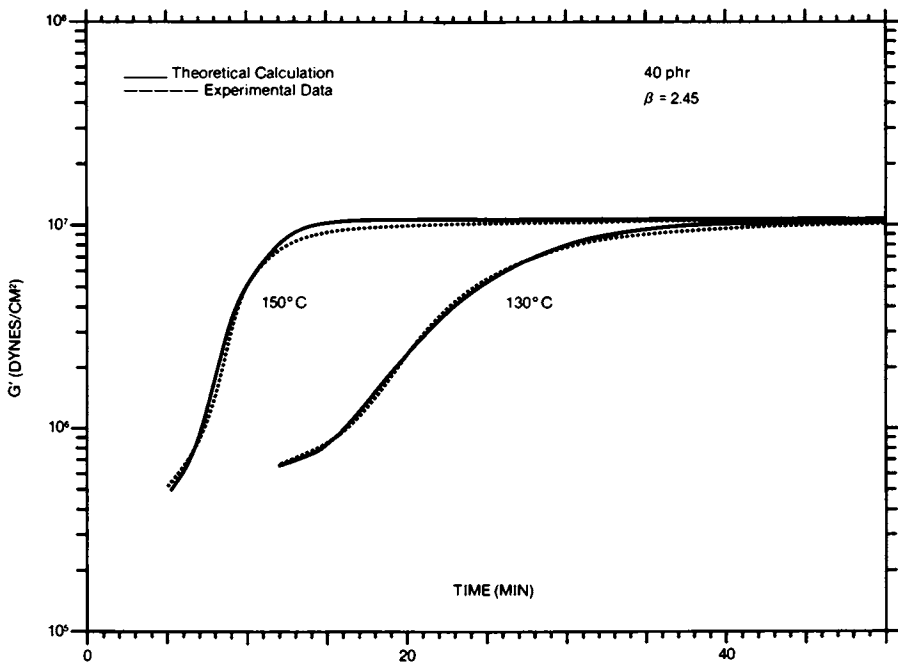


Figure 4. Shear storage modulus vs. cure time for 40 phr filler loading.

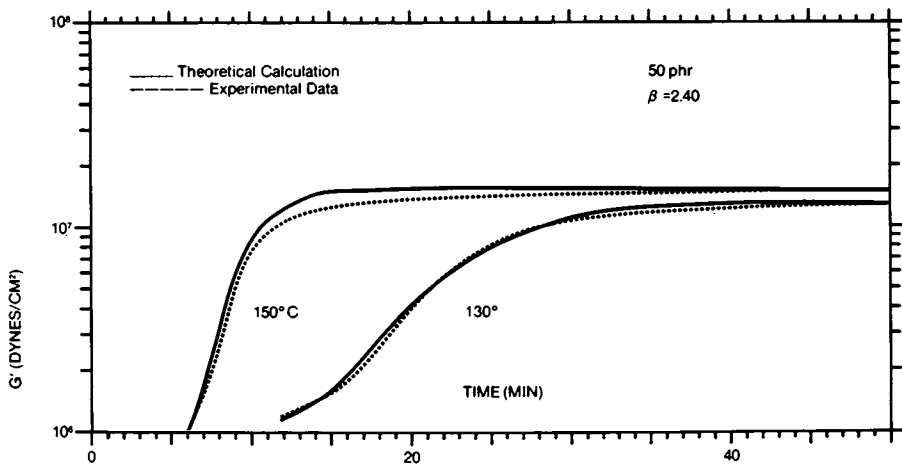


Figure 5. Shear storage modulus vs. cure time for 50 phr filler loading.

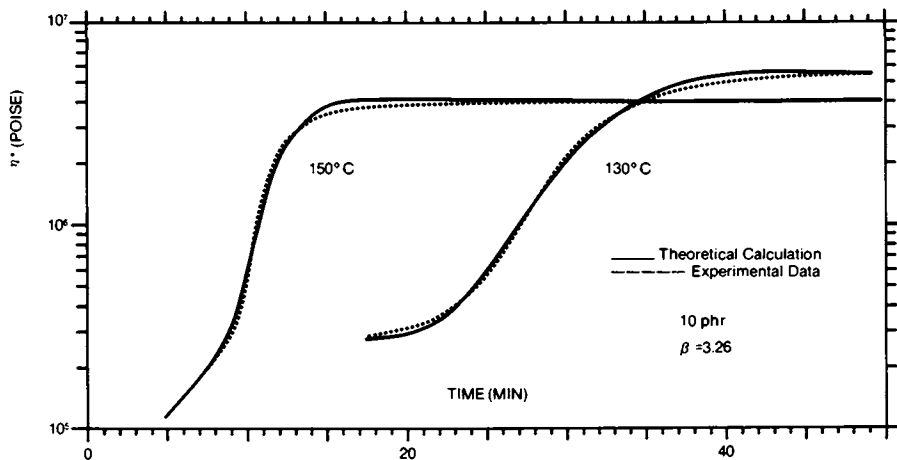


Figure 6. Complex viscosity vs. cure time for 10 phr filler loading.

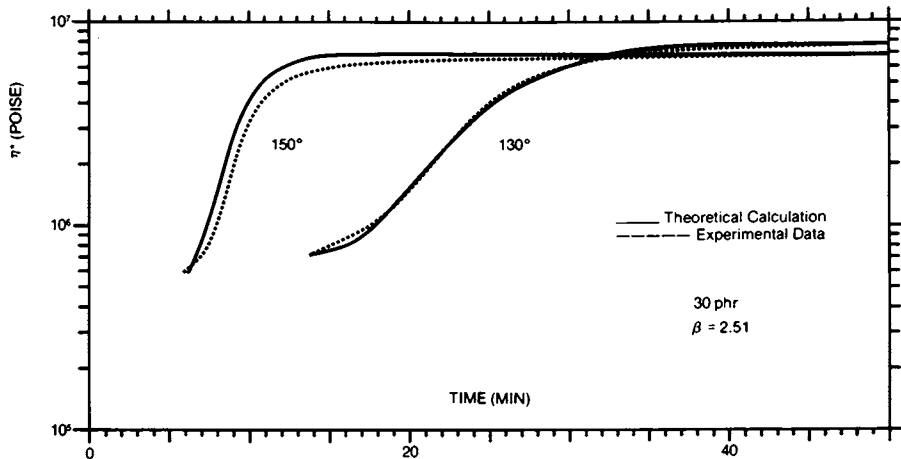


Figure 7. Complex viscosity vs. cure time for 30 phr filler loading.

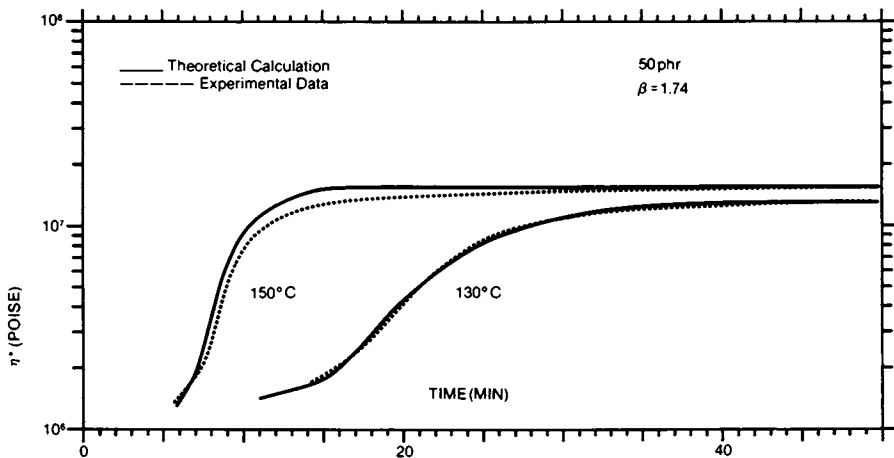


Figure 8. Complex viscosity vs. cure time for 50 phr filler loading.

agreement between theoretical predictions and experimental results. Activation energy of 18 kcal/mole was employed. In Fig. 9-11; the parameters,  $t_0$ ,  $\tau_0$  and  $\beta$ , used for curve fitting both shear modulus and viscosity are plotted. It is apparent that the parameters,  $\tau_0$  and  $\beta$  used for viscosity data are different from those values used to obtain shear modulus data. These findings are not surprising, since the relaxation spectra for different properties may have different shapes. Nevertheless, the characteristics of the relaxation spectrum should be similar for measurements of all different properties.

The activation energy of cure appears to be little affected by the filler loading. The relaxation time (or cure reaction time), however, decreases as filler loading increases. The induction time,  $t_0$  of cure also decreases with increasing filler loading. These findings support the fact that an increase in filler loading serves to accelerate the cure reaction and, therefore, reduces the cure time. It can also be seen that an increase in filler loading broadens the relaxation spectrum. This broadening of the relaxation spectrum with increasing filler loading was also observed in a previous study on viscosity/elastomer-filler interaction [14] and dynamic mechanical properties of cured rubbers [15].

It should be noted that the shape of the relaxation spectrum of the cure reaction also depends on experimental frequency. This can be seen in Fig. 12. We have found that an increase in frequency will decrease the value of  $\beta$  for natural rubber. The details of this phenomena will be discussed in an upcoming paper. Recently, Tung and Dynes [16] have used cure time at a value of  $\tan \delta = 1$  under an experimental angular frequency of  $\omega = 10$  rad/sec to define gel time. This method is very empirical, because, values of  $G'$  and  $G''$ , as obtained from cure data depend on the experimental frequency, cure temperature, and the nature of the polymer system. During the cure cycle, the structural relaxation time of the material in question increases with cure time until the cure reaction is complete. The value of the structural relaxation time after cure will depend on whether the material is in the rubbery state, glassy state or somewhere in between (transition). It is well known that materials in the glassy state will have longer structural relaxation times than those in the rubbery state. The relaxation peak of  $G''$  will occur at a cure time when the relaxation time of the material is equal or very close to the inverse of the experimental angular frequency during the cure cycle. [14,17]

In Fig. 12,  $G'$  and  $G''$  are plotted against cure time at various frequencies. For  $\omega = 10$  rad/sec, there is no relaxation peak of  $G''$  or cross-over point of  $G'$  and  $G''$ . This is due to the fact that at 140°C, the relaxation times of natural rubber at various states of cure are all longer than 0.1 sec (i.e.,  $1/\omega$ ). However, there is a relaxation peak and cross-over point of  $G'$

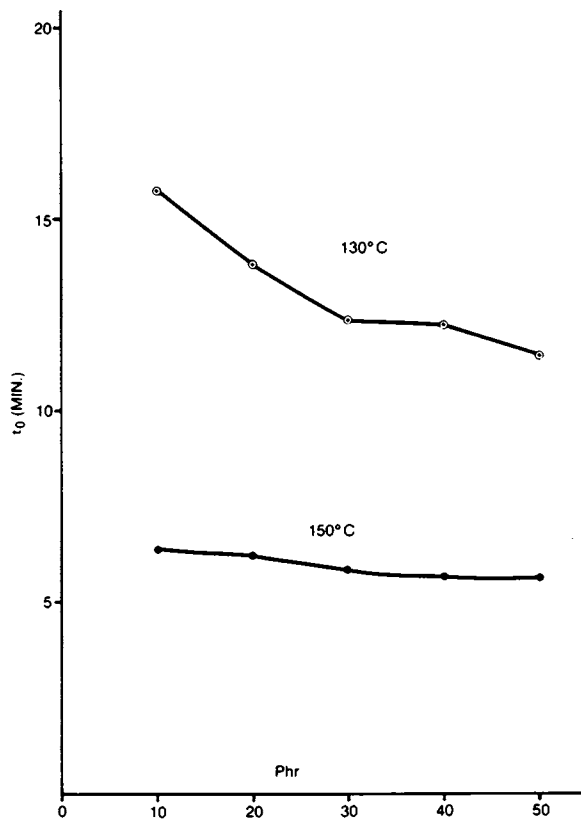
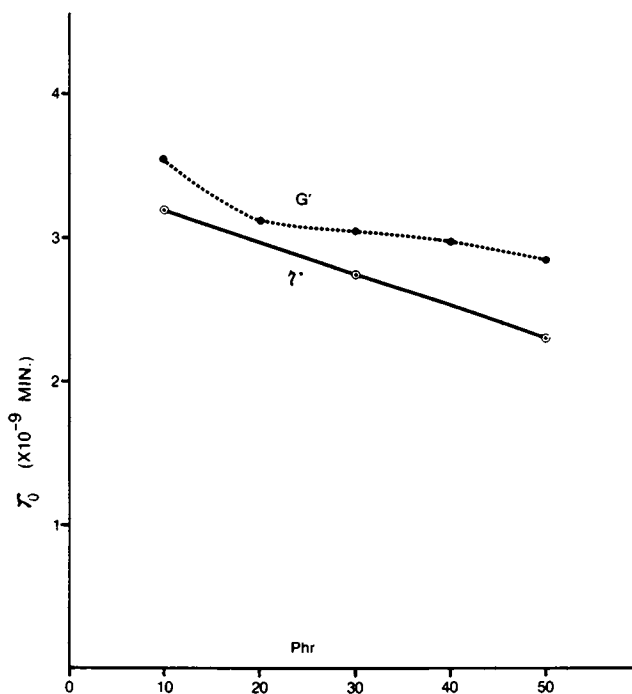


Figure 9.  $t_0$  vs. filler loading.



Figure 10.  $\tau_0$  vs. filler loading

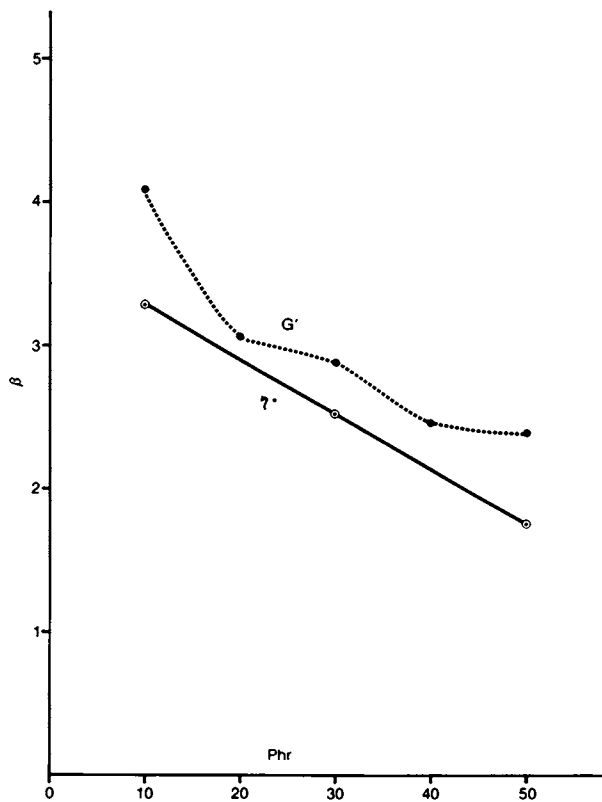


Figure 11.  $\beta$  vs. filler loading.

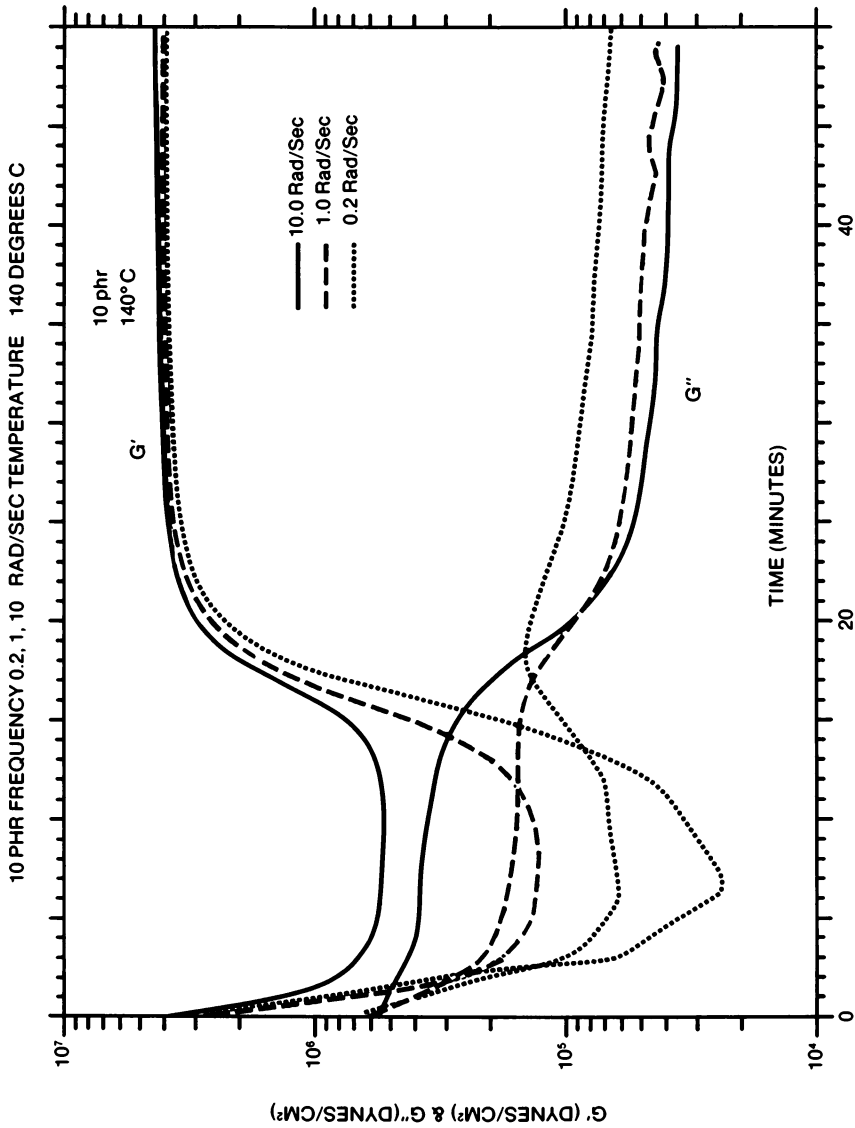


Figure 12. Cure curves vs. experimental frequency.

and  $G''$  for the angular frequency,  $\omega = 0.2$ , and 1 rad/sec. This clearly indicates that, at 140°C, the structural relaxation time of uncured natural rubber is longer than 0.1 sec but shorter than 1 sec, and the structural relaxation time of cured natural rubber is longer than 5 sec. Since the relaxation peak of  $G''$  occurs at a cure time when the structural relaxation time is equal to the inverse of the angular frequency during cure, one would expect that the relaxation peak or cross-over point of  $G'$  and  $G''$  will occur at long cure times for low experimental frequencies (Fig. 12). Therefore, one can conclude that the use of the cross-over point of  $G'$  and  $G''$  during the cure cycle for a fixed angular frequency of 10 rad/sec may be improper for determining gel points of some polymer systems.

Since non-isothermal cure is of practical importance in cure control, the non-isothermal cure curves, as shown in Fig. 13 and 14, were obtained by preprogramming heating at a heating rate of 12°C/min from room temperature to 150°C. The data in Fig. 13 represent the shear storage modulus while complex viscosity is plotted in Fig. 14. Eqs. (4) and (6) were used for fitting the data in Fig. 13 and 14 and the parameters of  $t_0$ ,  $\tau_0$  and  $\beta$  used for these calculations are taken from Fig. 9-11. The activation energies,  $E$ , for viscous flow used in Eq. (4) and (6) are 5.60, 4.00 and 2.94 kcal/mole for 10 phr, 30 phr and 50 phr of filler loading, respectively. The results of the theoretical predictions are shown in Fig. 13 and 14 along with the experimental data. Again, there is good agreement between calculated and found values. The activation energy,  $E$ , decreases with increasing filler loading. This result is not surprising, because the presence of filler tends to reduce the intermolecular forces between polymer chains and, therefore, the flow behavior and mechanical properties of the polymer system become less temperature dependent.

## CONCLUSION

A generalized kinetic model of cure has been developed from the aspect of relaxation phenomenon. The model not only can predict isothermal and non-isothermal cure curves using modulus and viscosity data, but also allows us to take into account the effect of filler on cure behavior. The prediction of viscosity and modulus values during the cure cycle allows one to preprogram cure in order to improve the material processing and end-product performance. The important findings of this study are:

- 1) Carbon black filler in natural rubber not only serves to increase the modulus of the elastomer, but also tends to accelerate the cure reaction.

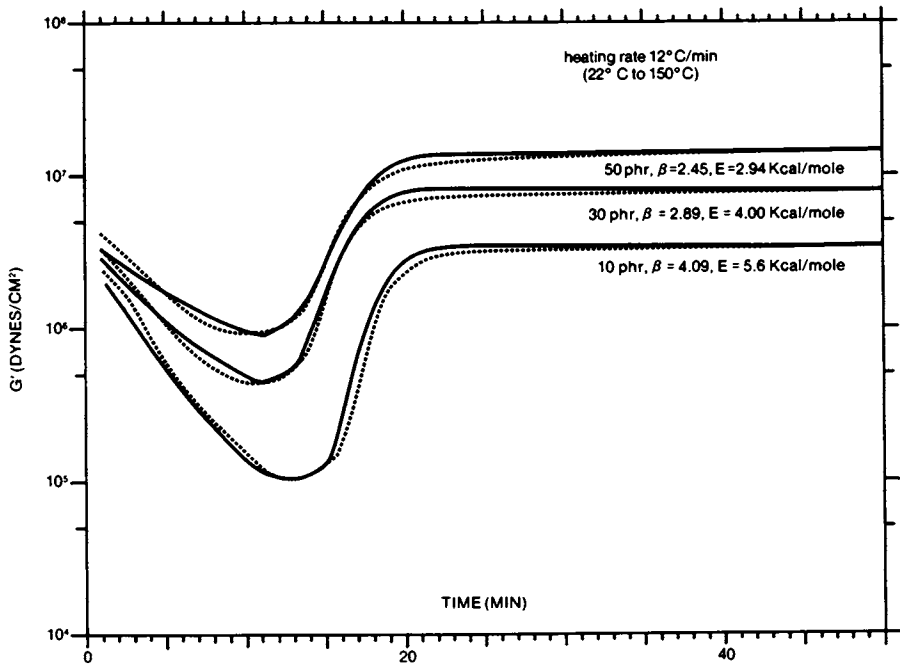


Figure 13. Shear storage modulus vs. cure time under non-isothermal cure conditions.

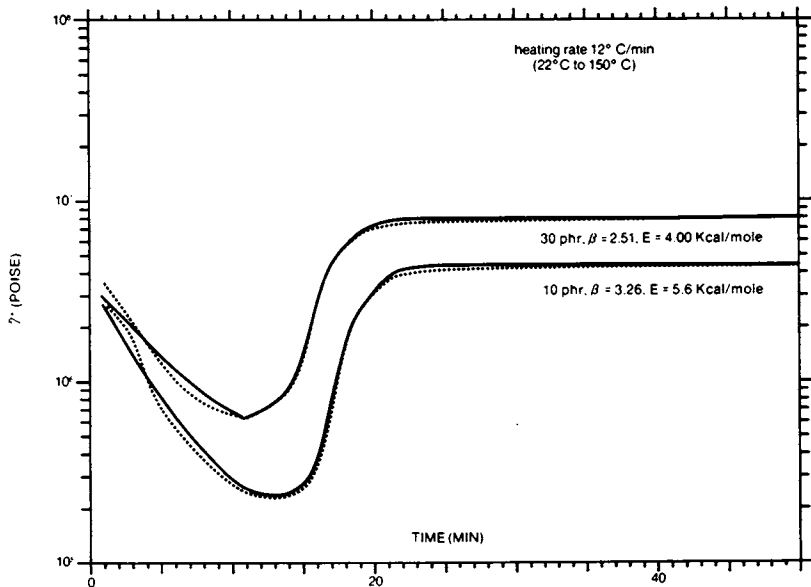


Figure 14. Complex viscosity vs. cure time under non-isothermal cure conditions.

- 2) The activation energy of viscous flow will be decreased by an increase in filler loading and, therefore, the viscosity and modulus of filled polymer systems are less temperature dependent. On the other hand, filler loading has little effect on the activation energy of cure.
- 3) Increasing filler loading broadens the relaxation spectrum of the cure reaction. Broadening the relaxation spectrum by filler loading also has been found in the mechanical spectrum of cured rubber from the glass transition region to rubbery plateau region [15].

#### Literature Cited

1. Fara, R. A., *Polymer*, 9, 137 (1968).
2. Acitelli, M. A., Prime, R. B. and Sacher, E., *Polymer*, 12, 335 (1971).
3. Prime, R. B., *Polym. Eng. and Sci.*, 13, 365 (1973).
4. Sacher, E., *Polymer*, 14, 91 (1973).
5. Kamal, M., Sourour, R. S. and Ryan, M., *Soc. Plast. Eng.*, 19, 187 (1973).
6. Wise, R. W., "Rubber Technology," Chapter 4, edited by M. Morton, Van Nostrand Reinhold Co., New York (1973).
7. Pyne, J. R., "Determination of Cure Cycles for Rubber Products," Proceedings of a RAPRA Seminar held at Shawbury (May, 1979).
8. Roller, M. B., *Polym. Eng. and Sci.*, 15 (6), 406 (1975).
9. Craig, D., *Soc. Plast. Eng.*, 18, 533 (1972).
10. Mussatti, F. G., and Macosko, C. S., *Polym. Eng. and Sci.*, 13, 236 (1973).
11. Hsich, H. S.-Y., *J. Mater. Sci.*, 13, 2560 (1978).
12. Hsich, H. S.-Y., *J. Mater. Sci.*, 15, 1194 (1980).
13. Hsich, H. S.-Y., *J. App. Polym. Sci.*, in press.
14. Hsich, H. S.-Y., *J. Mater. Sci.*, 17, 438 (1982).

15. To be published.

16. Tung, C.-Y. M, and Dynes, P. J., *J. Appl. Polym. Sci.*, 27, 569 (1982).

17. Bueche, F., "Physical Properties of Polymer", (John Wiley Interscience, New York, 1962), pp.168-221.

RECEIVED March 31, 1983

## Thermosetting Coatings—Analytical and Predictive Capability by Chemorheology

RICHARD R. ELEY

Glidden Coatings & Resins, Division of SCM Corporation, Strongsville, OH 44136

Many final film properties of a thermosetting coating will be influenced by the detailed viscosity-time path followed by the material during the cure process. These include leveling, gloss, gas release, oven sag, surface defects, particle sintering, etc. Typical industrial tests of the cure characteristics of a coating, however, are "single-point" data, and do not give any information on the actual viscosity-time profile followed during cure. Such data are often inadequate to pinpoint the cause of important performance problems. The viscosity-time curves of thermosetting coatings, prior to the gelation point (the region where flow-controlled properties are determined), have been measured on an automated Ferranti-Shirley cone and plate viscometer. Such cure curves can then be analyzed in a variety of ways to obtain data relating cure rheology, and ultimately composition variables, to performance. In particular, an empirical approach due to Roller has been used to derive physical and chemical activation parameters and predict cure performance under selected conditions simulating those of actual use.

Obviously, coatings must flow during application, film formation, and rigidification. Consequently, rheological studies are important for the proper analysis and control of coatings performance. In particular, flow-cure behavior of thermosetting coatings is expected to strongly influence film formation processes and resulting film properties such as leveling, sag, gloss, gas release, surface defects, lubricity, toughness, and particle sintering.<sup>(3)</sup> The processes involved in the formation of the crosslinked polymer network, or "cure", of a thermoset coating are not completely understood, however. Despite these considerations, studies of coatings cure by sophisticated

0097-6156/83/0227-0281\$06.00/0

© 1983 American Chemical Society



rheological methods have been very limited.(3) Rheometry is an attractive means of cure investigation because it offers several measurement quantities which are very sensitive to the changes in molecular and phase structure occurring as the cure reaction proceeds. Furthermore, analysis of rheological cure data can yield parameters related to composition,(1) thus linking flow-cure behavior with formulation variables. This gives formulators a potentially useful tool in the difficult problem of designing a system for performance. Finally, rheometry has the advantage of being able to provide direct measurement of the developing physical properties one desires from a thermosetting coating. Such information is valuable to the coatings engineer in problem solving and performance analysis.

This paper describes the methodology and some results of the study of viscosity-time profiles of thermosetting coatings by means of rotational viscometry, using an automated Ferranti-Shirley viscometer.(2) Although dynamic, or viscoelastic, characterization methods offer certain advantages over rotational methods, such as the resolution of viscous and elastic components of fluid flow and the ability to follow the cure through the gelation point, it is apparent that many important flow-controlled processes of coatings are complete at gelation. Appearance and morphological properties of thermoset films are strongly influenced by the time-integrated fluidity of the coating matrix during cure.(3-4) which essentially reaches a constant value prior to gelation. Therefore, a steady-shear instrument, such as the Ferranti-Shirley viscometer, is capable of relaying useful cure information.

### Experimental Section

The systems studied were thermosetting industrial coatings, primarily powder coatings, based on polyester and epoxy resins. The cure curve data were taken on an automated Ferranti-Shirley cone and plate viscometer, described elsewhere,(2) operating in the continuous shear stress-time mode. A truncated cone of 10mm radius and 50 micron truncation depth, having a cone angle of 1.0 degree, was used. Viscosities during cure were measured at a constant shear rate of ca. 30 sec<sup>-1</sup>, representing a compromise between measurable initial shear stress levels at cure temperature and delaying somewhat the onset of elastic failure, occurring as gelation is approached. An improved method has recently been employed in which the electronic ramp circuitry of the Ferranti-Shirley viscometer is used to cause the RPM to automatically decrease during a cure run, from an initial RPM value chosen so as to give an initial torque of at least 10% of full scale, to a pre-selected final minimum RPM value, set by using a zero-offset. By varying the "sweep time" (ramp rate), one can achieve nearly constant torque during the run, avoiding possible errors due to spring relaxation effects. This method

greatly improves the quality of experimental data, both by increasing the accuracy of the important initial portion of the viscosity-time curve, and by minimizing the problem of elastic edge-failure, allowing cure to be followed to the maximum possible fraction of conversion prior to the gel point. Mathematical analysis of the curve shapes (see below) indicates that the data obtained by the programmed decrease of shear rate method conforms better, statistically, to the Roller model(1) than typically does the constant shear rate cure data. Shear rate dependence of viscosity is not expected in the initial stages of cure,(5) nor is it evidenced in our data.

### Background

The study of rheology ordinarily restricts itself to measuring changes in flow behavior due to physical changes in a material, whereas chemorheology expands this to include the influence of chemical change on rheological properties. The term may refer either to polymerization or depolymerization processes. Tobolsky(6) originated and systematized the study of chemical degradation of polymers by rheological methods (stress relaxation), and the term chemorheology came to be applied to the field.(7)

Macosko(8), Kaelble(9), and others have used the term in reference to the study of the thermosetting process. Ono and Murakami(7) have published a recent monograph summarizing the field of polymer chemorheology, but giving only a brief treatment of the area of polymerization and crosslinking processes. A review of the field of applied rheology in the study of polymer transformation processes was recently published by Ya Malkin.(10)

Thermoset materials are inherently difficult to study because of the very properties which are also their unique advantages: insolubility, infusibility, toughness/hardness. Chiefly, methods such as reaction calorimetry, dilatometry, dielectric spectroscopy, infrared spectrophotometry, and others, have been applied to the characterization of thermoset cure processes.

Flow-cure properties of thermosetting coatings are often characterized by gel time tests, pellet flow(11) (powder coatings), and by various conventional analytical data relating to resin functionality. These are "single-point" data, however, and have often proven inadequate to highlight key variances between systems showing vital performance differences. To gain an understanding of the relationship of cure to the coatings properties mentioned above, rheological cure analysis is important, since these properties are influenced by the detailed change of viscosity and viscoelasticity with time during cure. Rheometry is well suited to the task of monitoring the process of cure, because the material functions measured, e.g., shear viscosity, dynamic viscosity, modulus of elasticity, and normal stress, are very sensitive to the changes in molecular and phase structure occurring as the cure reaction proceeds.(5)

This paper describes the general methodology and some results of the study of thermoset systems by rheological techniques, chiefly in steady rotation. Analysis of the experimental cure curve is described in detail, and the use of chemorheological data to correlate and predict product performance as well as provide guidance for formulation, is discussed.

### Cure Curve Analysis and Interpretation

Figure 1 shows typical semilogarithmic viscosity-time plots for some epoxy-based powder coatings, obtained on the Ferranti-Shirley cone/plate viscometer. Figure 2 schematically resolves the net cure curve into the competing trends in viscosity occurring during a nonisothermal cure cycle. These are (1) a decrease in viscosity as the sample initially warms, and (2) an increasing viscosity component due to advancing polymerization and crosslinking. The experimental cure curve represents the sum of these two processes. The minimum in the curve resulting from the interplay of opposing trends is the minimum cure viscosity,  $\eta_m$ , and can itself be related to final film gloss, for example. (12)

Two parameters which will be used in later kinetic treatment of cure data are the zero-time (isothermal) viscosity,  $\eta_0$  (Figure 2), and the constant  $K$ , characteristic of the rate of increase of viscosity, obtained from the linear slope of a first-order semilogarithmic cure curve plot.

Obtaining a valid viscosity-time cure curve is an important objective, especially since mathematical analysis of the curve may be intended, described later. Figure 3 illustrates different curvatures that are seen for experimental cure curves. If experimental conditions are sufficiently close to isothermal, one should see a significant linear portion of the semilog cure curve (curve B), assuming first-order kinetics. If curvature is continuously upward as in curve A, one has a problem of slow approach to temperature equilibrium, or the reaction kinetics are lower than first-order. Edge-gap instability (Weissenberg effect) produces a downward curvature or falling off of the cure curve (curve C), and is usually evident as the sample forms a "bead" around the edge of the cone, or is observed to withdraw from the edge-gap of the cone and plate. The Weissenberg effect is caused by rapidly increasing elastic character of the melt, due to crosslinked network build-up or molecular weight increase, as the system approaches gelation. The normal stresses are proportional to shear rate, and in the cone and plate geometry result in the fluid climbing out of the edge gap. This reduces the effective area being sheared and produces an artificial drop in shear stress, ending the run. The problem is minimized by monitoring the viscosity at the minimum practical shear rate. Ideally, one should have a programmable shear rate which is high

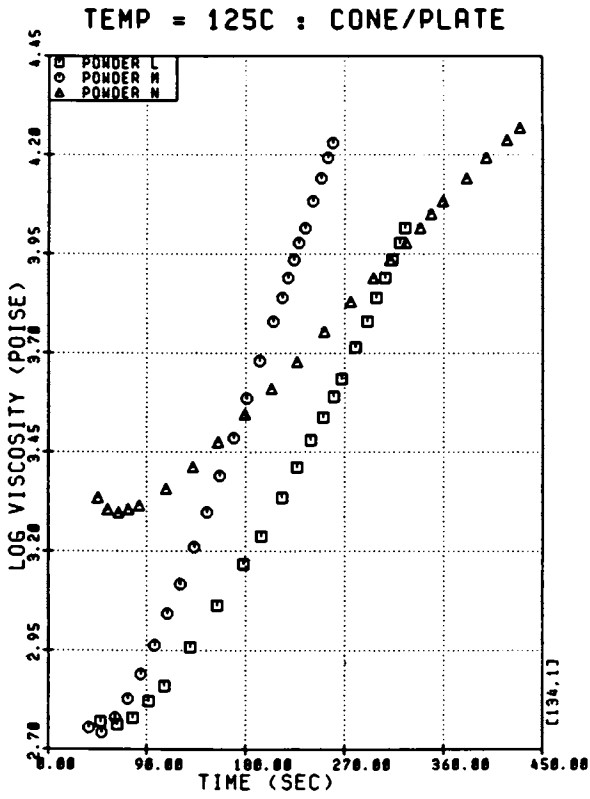


Figure 1. Viscometric cure curves for epoxy powder coatings.

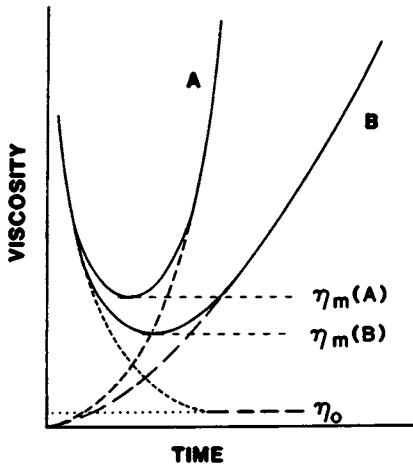


Figure 2. Resolved cure curves.

at the initiation of a run, falling to a pre-set minimum value as the torque rises during the course of a cure experiment. This would give more accurate initial viscosities (important for fluidity calculations) and also minimize the normal stress problem. (See Experimental Section.)

Falling off of the log viscosity-time cure curve can also occur due to dewetting, or wall slip, at the cone-sample interface. This occurs rarely, in our experience, and probably more with highly filled samples<sup>10</sup>, as gelation is approached. A kinetic order greater than unity could also produce a curvature similar to C, but evidence of such kinetic orders for condensation polymerization reactions has not been reported from chemorheological studies, to our knowledge. (Certain types of addition polymerization reactions may show non-first-order viscosity kinetics.)(13)

The rheological cure curve will also reflect any loss of homogeneity of the system, such as phase separation or phase inversion, occurring at a certain degree of conversion.(10) Figure 4 illustrates the characteristic drop in viscosity seen accompanying a phase separation during thermoset cure (our data). The occurrence is seen to be quite reproducible for three separate runs, and may therefore be of value in itself as a means of monitoring the progress of a cure reaction.(10)

Figure 5 offers an interesting direct comparison of steady-shear and oscillatory-shear cure studies of the same powder coating. The steady-shear viscosity data was taken on the Ferranti-Shirley viscometer, and the dynamic viscosity data on the Rheometrics Dynamic Spectrometer (courtesy Rheometrics, Inc.). Note the coincidence of the viscosity-time data, measured in two different viscometric modes, on two different instruments at the same temperature. The static shear rate was ca. 30 sec<sup>-1</sup>, the dynamic shear rate 6.3 sec<sup>-1</sup>. This suggests, in agreement with Wissbrun,<sup>(3)</sup> that the Cox-Merz rule may be valid for curing systems such as these, limited, of course, by the gelation point. The apparent rate constants of cure (slopes of the semilog viscosity-time plot) obtained by the two methods appear very similar. Hence, cure kinetic information may be equivalent whether obtained with a dynamic or a steady-shear instrument.

Wissbrun<sup>(3)</sup> and also den Otter<sup>(4)</sup> have pointed out that the leveling and gloss of a cured film can be predicted by use of a total fluidity integral, after Orchard,<sup>(14)</sup> which is

$$\Phi = \int_0^t \frac{dt}{\eta(t, T)} \quad (1)$$

if surface tension is assumed constant. The evaluation of the fluidity integral for a given cure curve gives a quantitative measure of the inherent flow of a coating, under a given set of

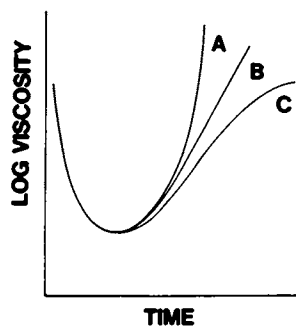


Figure 3. Curvature types seen for cure data.

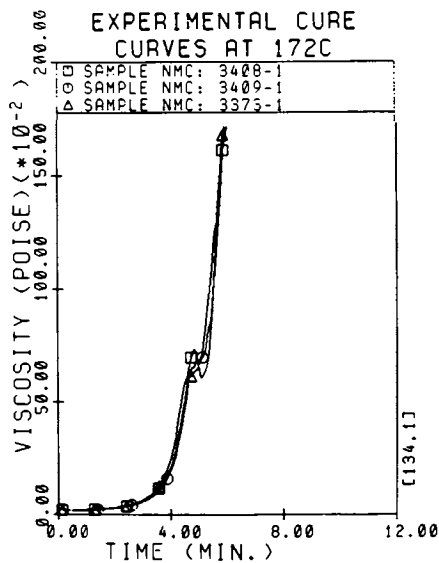


Figure 4. Cure curves showing a reproducible phase transition.

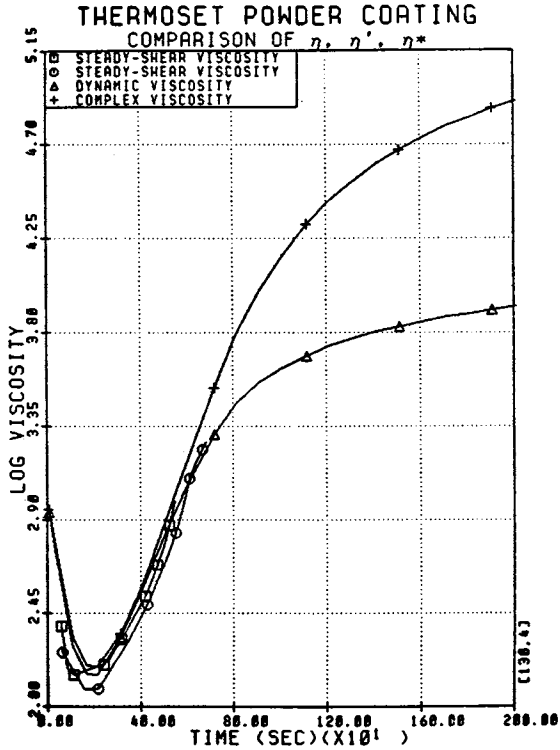


Figure 5. Comparison of cure curves obtained by dynamic and by steady-shear methods.

cure conditions. The total fluidity,  $\phi$ , should influence final film properties such as orange peel, gloss, sag, air release, cratering tendency, etc. It also offers the possibility of optimizing the system for flow, by use of predictive analytical expressions relating viscosity to temperature history and time, described below.

### Cure Modeling

There is not complete agreement on how to mathematically describe the mode of change of shear viscosity with time for thermosets. However, an expression which is basic to the approach of a number of authors is (1,3,15-17)

$$\eta = \eta_0 e^{kt} \quad (2)$$

where  $\eta$  is the viscosity at time  $t$ ,  $\eta_0$  is the zero-time viscosity, and  $k$  a constant (slope of the semi-log viscosity-time plot). This expression has the virtue of conforming to the rational model of Fig. 2. Equation 2 is a reasonable model for an isothermally curing system, but is not predictive if temperature varies, or for non-isothermal conditions. If the fact that the melt viscosity,  $\eta_0$ , and the constant  $k$  are temperature dependent is realized, then Eq. 2 can be recast in Arrhenius form, to obtain an expression which can predict viscosity-time behavior at other temperatures. If temperature is allowed to be a function of time (nonisothermal cure), Eq. 3 results, due to Roller.(1)

$$\eta(t,T) = \eta_{\infty} e^{(\Delta E_{\eta}/RT)} e^{-k_{\infty} \int_0^t \exp(\Delta E_k/R) dt} \quad (3)$$

$$T = T(t)$$

The parameters of the model are the activation energies for viscous flow ( $\Delta E_{\eta}$ ) and reaction rate ( $\Delta E_k$ ), and their respective pre-exponential  $\eta_{\infty}$  terms. This equation provides a predictive, analytical expression with which one can model nonisothermal cure using any appropriate time-temperature function  $[T(t)]$  one chooses, appropriate to the curing process of interest. For example, the baking of a coated substrate in an oven may be modeled by a relaxation-type heating function, with time constant ( $\tau$ ) to take account of the thermal inertia of the substrate. (Eq. 4)

$$T = \Delta T(1 - e^{-t/\tau}) + T_0 \quad (4)$$

In Eq. 4,  $T_0$  is the initial temperature,  $\Delta T$  the difference between initial and final temperature, and  $t$ , the time.

An important point to consider in the study of thermosetting systems is that because of the complex, nonlinear way that flow



behavior depends on the thermal history of a system during cure, rheological testing of a product should be done under conditions approximating as closely as possible the actual end-use conditions under which the product must perform. (This is also true of rheological testing in general.) It is possible to be misled by cure information obtained under test conditions representing bake schedules different from those of actual use of the product. (See below) Often, however, it is not possible or practical to duplicate actual-use conditions in the laboratory, as with heating rates or temperatures beyond the range of experimental equipment. This leads us to one of the uses of Roller's equation: Prediction of a cure curve for a specified thermal cure cycle (e.g., realistic but experimentally inaccessible cure conditions). Fluidity values calculated from the predicted cure curve can then be related to coating properties.

An example of this is given in Figures 6 and 7, which show cure curves calculated from the Roller equation for four hypothetical thermosetting systems, under two different curing schedules. Figure 6 shows the cure behavior under "normal" baking conditions of 180C nominal temperature and a heating time constant of 30 sec ( $\tau$  in Eq. 4). Figure 7 shows the drastic changes in relative cure behavior of the materials, when calculated for inductive heating-type cure conditions, such as a nominal cure temperature of 300C and a time constant of 1 sec. The calculated fluidity values for the four systems under the two different bake schedules show dramatic order reversals (See Table I). This illustrates the dangers of drawing conclusions from inappropriate data, and also shows the use of the Roller model to extend data beyond the limits of experimental equipment. The caveat associated with this is that if the reaction mechanism changes with temperature, reaction energetics may change sufficiently to cause the model to make wrong predictions.

A second valuable application of Roller's model would be as an aid to coatings formulation. With knowledge of the dependence of reaction energetics on formulation variables, e.g., the relationship of catalyst level to cure activation energy, the model could be used to derive predictive formulating information, to hit a desired performance target. This would reduce the laborious trial-and-error often a feature of formulation problems. The following illustrates the use of the Roller model to obtain data relating formulation to performance. In Fig. 8, the model was fitted to the cure data for a series of coatings representing a catalyst ladder, and the cure activation energies obtained are plotted against catalyst level. The usefulness of relationships such as this depends on the establishment of a connection between the parameters and the predictions of the model and the performance of the product, through the formulation variables. Figure 9 shows that the catalyst level for the same set of coatings is correlated to the total fluidity values,

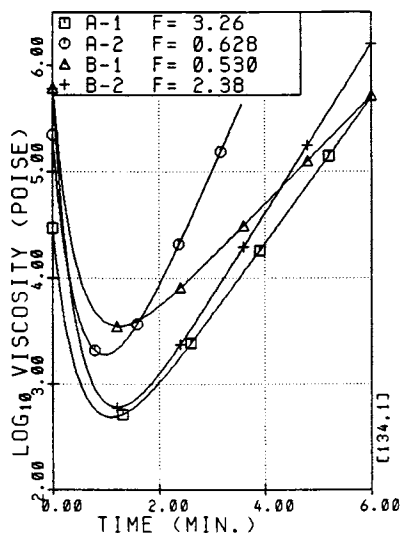


Figure 6. Cure curves calculated with roller model for four systems, under "normal" bake schedule. Nominal temperature 180 °C, heating time constant 30 sec.

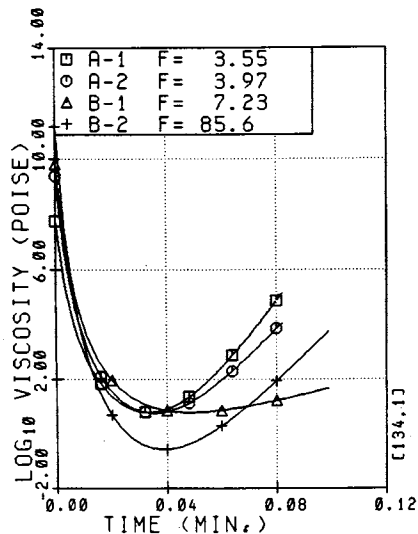


Figure 7. Calculated cure curves for systems of Figure 6, for inductive cure. Nominal temperature 300 °C, time constant 1 sec.

Table I. Comparative Fluidity Values for "Normal" vs. Inductive Cure Conditions.

'NORMAL" BAKE		INDUCTIVE BAKE	
A-1	3.26	B-2	85.6
B-2	2.38	B-1	7.23
A-2	0.63	A-2	3.97
B-1	0.53	A-1	3.55
$T_{\text{NOM}} = 175\text{C}$		$T_{\text{NOM}} = 300\text{C}$	
$\tau = 30 \text{ sec.}$		$\tau = 1 \text{ sec}$	

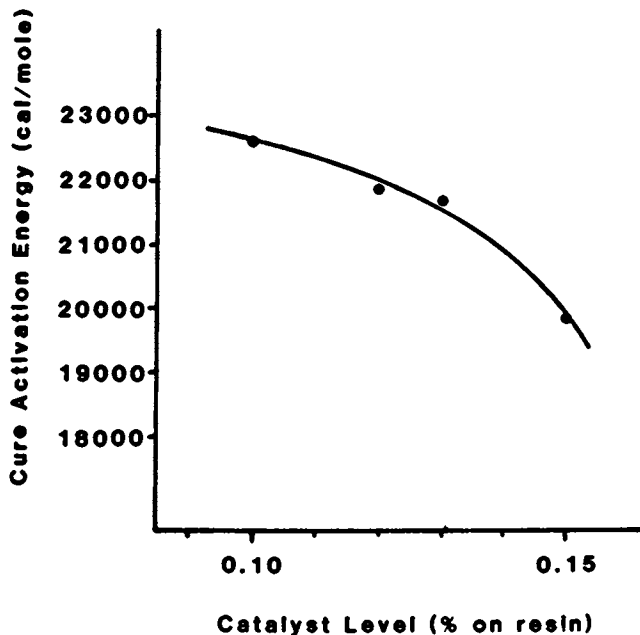


Figure 8. Cure activation energy (from roller equation) vs. catalyst level for catalyst ladder series.

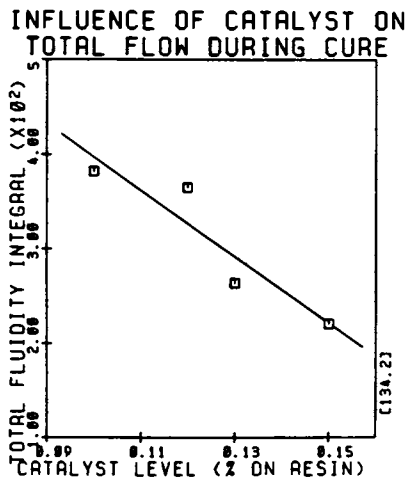


Figure 9. Experimental fluidity values vs. catalyst level for catalyst ladder series.

calculated from the experimental cure curves, according to Eq. 1. The dependence of leveling behavior ("orange peel") on the calculated fluidity of the cured film, for a series of thermosetting coatings, is illustrated in Fig. 10. The correlation of leveling and fluidity is significant at greater than 99% confidence level.

From such relationships as the above, one could have a rational basis on which to choose initial recipes, aiming to match a desired cure curve or performance. Figure 11 diagrams the approach to analysis and prediction of cure behavior using the Roller model. The experimental cure curve is the starting point from which the model parameters are obtained. From there, the double arrows signify an iterative procedure whereby the effects of resin composition or formulation variables on the model constants are learned, and in turn a relationship between acceptable end-use performance and cure rheology is established. The necessary model parameters to achieve the target rheology are then determined, and adjustments made to composition variables to achieve targeted performance. The end result would be an analytical approach to the problem of formulation, reducing significantly the labor and cost of trial-and-error methods.

To use the Roller model requires the measurement of cure curves at several different temperatures so that Arrhenius plots may be made for the rate constant,  $k$ , and the isothermal melt viscosity,  $\eta_0$ . The four model constants are then obtained from the Arrhenius plots. This entails considerable experimental work, especially for a method one would like to use in a more or less routine fashion. In addition, it is invalid in principle to estimate the isothermal melt viscosity,  $\eta_0$ , from the nonisothermal cure curve. We have instead implemented a method of obtaining the model constants from a single cure curve by use of a nonlinear sequential function minimization (Simplex) routine.<sup>(18)</sup> This program requires the input of reasonable estimates for the Roller model constants, which are then adjusted by the routine, avoiding local minima by using a strict convergence criterion. (See Fig. 12) The output of a successful convergence is a set of model constants representing the best fit of the Roller model to the experimental data. Figure 13 shows the overlay of experimental and calculated curves obtained by the Simplex method for a coating cured at 155C. In Figure 14, the model constants obtained for the data at 155C were used to predict the cure curve at a plate temperature of 165C, and the experimentally measured curve at 165C is shown for comparison. The calculated fit improves if increasingly larger heating time constants are allowed. Although the rate of heating of the

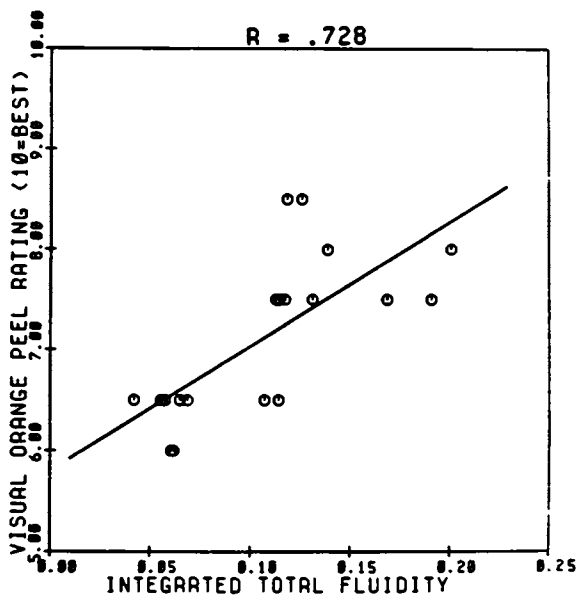


Figure 10. Leveling vs. fluidity for series of thermosetting coatings.

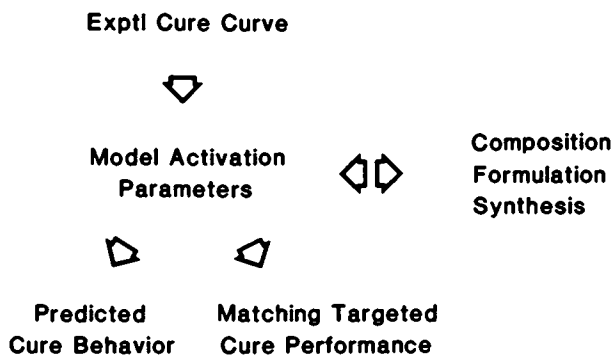


Figure 11. Use of roller model in analysis of thermoset materials.

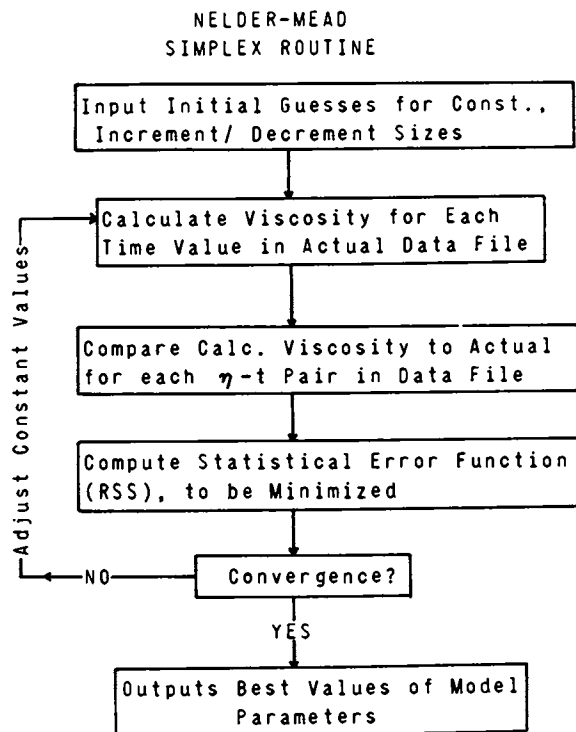


Figure 12. Sequential minimization routine.

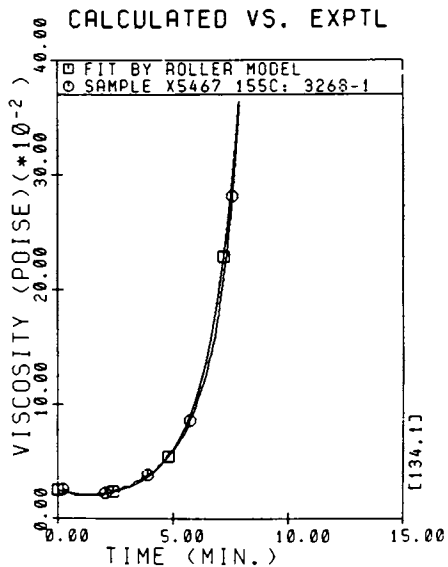


Figure 13. Cure curve at 155 °C vs. simplex fit by roller model.

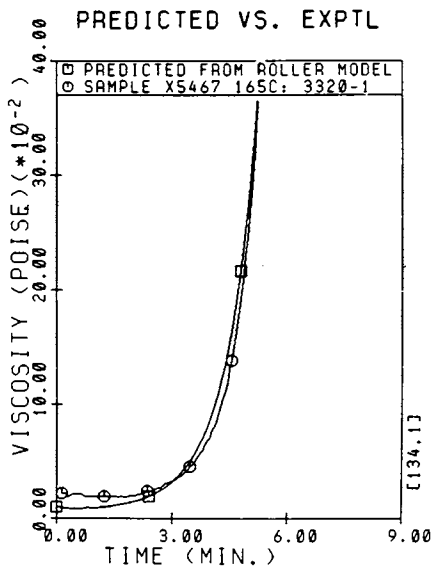


Figure 14. Cure curve at 165 °C vs. curve predicted from model constants of Figure 13.



Table II. Comparison of Roller Model Constants Obtained by Simplex Curve-Fitting Method and by Arrhenius Method.

TEMP (C)	$\eta_{\infty}$ (poise)	$\Delta E_{\eta}$ (cal/mole)	$k_{\infty}$ (min <sup>-1</sup> )	$\Delta E_k$ (cal/mole)	RSS*	
165	1.902E-15	32840	1.559E12	-29600	0.0195	
177	8.741E-15	31470	4.792E12	-30583	.1116	
190	7.208E-14	29537	6.891E12	-31110	.630	
Arrhen.						r ‡
Data	1.29E-13	29300	3.42E12	-27700	.9965	
	(E-10 - E-17)	+/- 6000	(3E10 - 4E14)	+/- 4300	.9890	

$$*\text{residual sum of squares} = \sum_i \left[ \frac{\eta_i(\text{calc}) - \eta_i(\text{obs})}{\eta_i(\text{calc})} \right]^2$$

‡ correlation coefficients of Arrhenius plots

coating melt will not be as rapid as that indicated by the plate-embedded thermocouple,\* the apparent tendency toward such slow heating rates is probably unrealistic and may be an indication that the viscosity kinetics are possibly lower than first-order. The data in Table II compare the values for the Roller model constants obtained by the Simplex curve-fitting procedure with those derived by the usual Arrhenius method. For the latter, correlation coefficients and 95% confidence intervals are given. The RSS value is the residual sum of squares difference of the experimental and calculated curves, a measure of the goodness of fit. (See Table II.) It is seen that, although there is a slight trend in the Simplex values as temperature increases, all the values are within the 95% confidence limits for the Arrhenius data.

### Conclusions

Chemorheological cure analysis yields data which can be correlated to the composition and performance of thermosetting industrial coatings. The Roller mathematical model for nonisothermal cure has been adapted to the study, analysis, and prediction of the cure of such coatings. The constants of the Roller model are derivable either by the usual Arrhenius method or by the quick method of nonlinear curve fitting. The activation parameters derived from the model have been related to composition variables, such as the catalyst level, illustrating the potential cure analytical ability of the Roller model. Furthermore, the Roller model can be used in a predictive manner, to estimate cure performance under unmeasured or unmeasurable conditions. Therefore, the methods described in this paper offer help to the coatings engineer or resin chemist in solving formulating or performance problems of coatings.

\* The accuracy of the fit obtained by the Simplex method depends on an input temperature-time function that reflects as accurately as possible the temperature of the sample during cure. We have used both the plate thermocouple output of the viscometer, corrected for heat flow as recommended by the manufacturer, and also the temperature of the melt itself, measured using a foil thermocouple inserted between cone and plate.

Literature Cited

1. Roller, M. B. Polym. Eng. Sci. 1975, 15, 406.
2. Kah, A. F.; Koehler, M. E.; Niemann, T. F.; Provder, T.; Eley, R. R. in "Computer Applications in Applied Polymer Science", Provder, T., Ed.; ACS SYMPOSIUM SERIES No. 197, ACS:Washington, D.C., 1982; p. 223.
3. Hannon, M. J.; Rhum, D.; Wissbrun, K. F. J. Coat. Technol. 1976, 48(621), 42.
4. Den Otter, J. L.; de Groot, J. L. B. TNO Report, 1974.
5. Lipshitz, S. D.; Macosko, C. W. Polym. Eng. Sci. 1976, 16, 803.
6. Andrews, R. D.; Tobolsky, A. V.; Hauson, E. E., J. Appl. Phys. 1946, 17, 352.
7. Murakami, K.; Ono, K. "Chemorheology of Polymers"; Elsevier: New York, 1979, Polymer Sci. Library, Vol. I.
8. Mussatti, F. G.; Macosko, C. W. Rheol. Acta 1973, 12, 189.
9. Kaelble, D. A.; Cirlin, J. J. Polym. Sci. Part C Polym. Symposia No. 35, Shen, M. S., Ed.; Interscience:New York, 1971.
10. Malkin, A. Y. Russ. Chem. Reviews, 1981, 50(1), 137.
11. ASTM Method D 3451-75 Section 17.
12. Eley, R. R.; Guthrie, W. H.; Kah, A. F. ACS Organic Coatings and Plastics Preprints, 1980, 42, 417.
13. Eley, R. R., unpublished data.
14. Orchard, S. E. Appl. Sci. Res., Sect. A, 1962, 11, 451.
15. White, R. P., Jr. Polym. Eng. Sci. 1974, 14, 50.
16. Kuwano, K., J. Jpn. Soc. Colour. Mater. 1977, 50, 547.
17. Hollands, K. M., Kalnin, I. L. ACS ADVANCES IN CHEMISTRY SERIES No. 92, ACS:Washington, D. C., 1970, p. 60.
18. Nelder, J. A.; Mead, R. A. The Computer Journal 1965, 7, 308.

RECEIVED March 31, 1983

## Predictive Models as Aids to Thermoset Resin Processing

M. R. DUSI and C. A. MAY

Lockheed Missiles and Space Company, Inc., Sunnyvale, CA 94086

J. C. SEFERIS

Department of Chemical Engineering, University of Washington,  
Seattle, WA 98195

Past experience has shown that processes for the fabrication of hardware from thermosetting polymers are most often derived by qualitative, empirical approaches. Process development could, however, be accomplished in a more orderly, quantitative manner if the chemorheological behavior of the resin system during the polymerization is thoroughly understood. This understanding may well evolve through the use of a mathematical model(s) which predicts the viscosity of a curing thermoset at any point in its time-temperature heat history. Additionally, mathematical modeling should be useful for quality control applications, as a tool design aid and/or as a viscosity predictor with the "closed-loop" cure cycle control.

Several researchers have described changes in the isothermal viscosity behavior during the cure of thermosetting resin systems with respect to time by the following expression:

$$[1] \quad \eta = \eta_0 \exp(kt)$$

where  $\eta$  is the time dependant viscosity,  $\eta_0$  is the zero-time viscosity,  $k$  is the apparent kinetic factor and  $t$  is the time (1,2) Roller (3) extended the model to the temperature domain by assuming Arrhenius type expressions,

$$[2] \quad \eta_0 = \eta_x \exp(\Delta E_\eta/RT)$$

and

$$[3] \quad k = k_x \exp(\Delta E_k/RT)$$

to describe the temperature dependence for the zero-time viscosity and kinetic terms of equation [1]. The terms are defined as

$\eta_x$  and  $k_x$  are Arrhenius pre-exponential frequency factors;  $\Delta E_\eta$  and  $\Delta E_k$  are the activation energies of viscous flow and the apparent kinetics, respectively;  $R$  is the gas constant and  $T$  is the temperature in degrees Kelvin. Roller models the dynamic viscosity,  $\eta(T,t)$ , by combining equations [1-3] in the following manner:

$$[4] \ln \eta(T,t) = \ln \eta_x + \Delta E_\eta/RT + k_x \int \exp(\Delta E_k/RT) dt.$$

Keenan (4) has modified equation [4] to study crosslinked systems by introducing a proportionality factor,  $\phi$ , which he relates to the amount of chain entanglement, thus

$$[5] \ln \eta(T,t) = \ln \eta_x + \Delta E_\eta/RT + \phi k_x \int \exp(\Delta E_k/RT) dt.$$

Equation [5] is subsequently used by the authors to model changes in the shear viscosity during the cure of a particular system as a function of the five material parameters and time and temperature.

As discussed herein, the model could not adequately describe the particular resin system studied and the use of an expanded six-parameter model is described.

## EXPERIMENTAL

The resin systems employed in the study are the 4,4' - diaminodiphenylsulfone (DDS) amine cured tetraglycidyl - 4,4' diaminodiphenylmethane (TGDDM) epoxy resins with and without the use of a boron trifluoride monoethylamine ( $\text{BF}_3 \cdot \text{MEA}$ ) accelerator. The dynamic shear viscosity profiles were measured on a Rheometrics Mechanical Spectrometer, RMS Model 605, employing a parallel-plate geometry. The resin samples were conditioned for approximately sixteen hours at 22°C and 2 mm Hg to remove any volatiles, e.g., moisture and residual solvents. A series of viscosity profiles were obtained for the neat resins by preheating the sample chamber to 75°C, introducing the sample and using a ramping temperature profile of 10°C/min. to reach the isothermal cure temperatures. This procedure eliminated any temperature overshoot on achieving the isothermal temperature while minimizing the extent of curing reactions during the upheat. The viscosity profiles are shown in Figure 1 for cures with isothermal holds at 95, 115, 135, 155 and 170 degrees centigrade. The chemorheological behavior for the curves can be qualitatively described by an initial decrease in viscosity due to the temperature dependence of the viscous flow term where upon reaching the isothermal temperature (approximately the point of minimum viscosity) an increase in viscosity occurs as the polymerization reactions proceed.

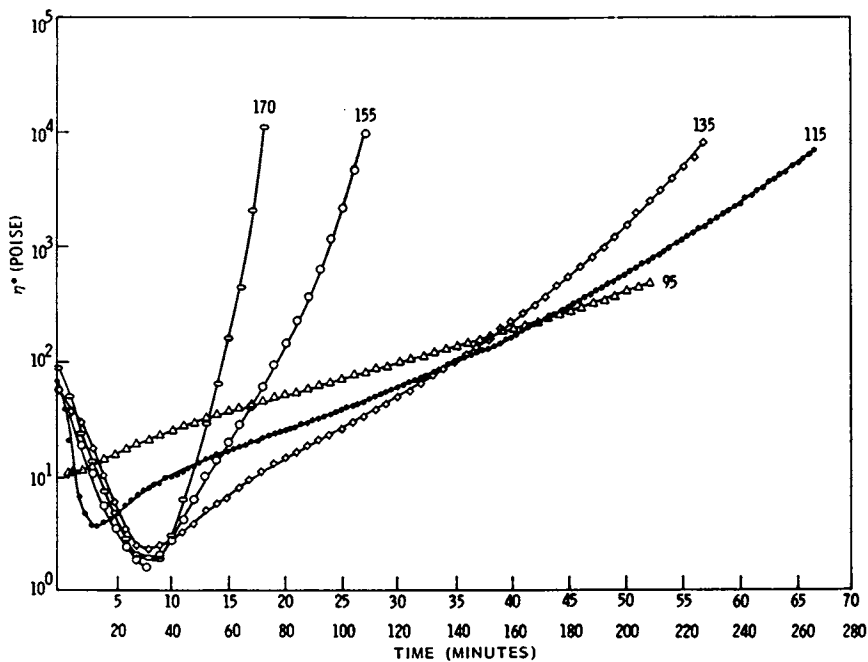


Figure 1. Viscosity profiles for the  $\text{BF}_3\text{MEA}$  accelerated TGDDM/DDS neat resin. The value above the curve indicates the isothermal hold temperature (95° profile—refer to the lower time scale).

## RESULTS AND DISCUSSION

The "five-parameter" model as described in equation [5] relates the viscosity of a particular resin system to five material parameters and time and temperature. It should be noted that the model assumes an overall reaction order of unity.

The material parameters for a resin system are determined from a series of viscosity profiles as displayed in Figure 1. It is observed that upon reaching the isothermal temperature, the viscosity profiles exhibit two relatively linear regions as demonstrated by the 115 and 135°C isothermal profiles. The viscosity corresponding to  $t=0$  at each isothermal temperature is calculated using a linear least squares analysis on the linear viscosity region directly after the point of minimum viscosity. An Arrhenius plot of the values versus  $1/T$  is constructed to obtain the viscous flow material parameters  $E_\eta$  and  $\eta_\infty$ . The values are 15.6 kcal/mole and  $5.75 \times 10^{-9}$  minutes<sup>-1</sup>, respectively, where only the data points for the 95°C and 115°C cures were used as the chemical reaction had begun prior to the isothermal temperature for the higher temperature cures. The profiles exhibit a second linear region after a few minutes into the isothermal hold which relates to the reaction kinetics of the system during the cure. The individual slopes are calculated and plotted versus  $1/T$  to yield the kinetic parameters  $E_k$  and  $k_\infty$ . The values for the kinetic parameters are 16.1 kcal/mole and  $5.70 \times 10^7$  minutes<sup>-1</sup>, respectively. Figure 2 shows the Arrhenius plots used to determine the parameters.

Predictions employing the material parameters were compared to the experimental viscosity profiles. Figure 3 displays the correlation of the predicted and the experimental viscosities with a ramping temperature profile from 35-200°C at 4°C/minute. The excellent correlation at the higher temperatures suggests that the kinetic parameters are correct since they dominate equation [5] at high temperatures. The inferior correlation of the initial portion of the prediction is attributed to the dissolution of the solid DDS into the epoxy resin, thereby contributing a so-called "filler effect" which has been substantiated with Fourier transform infrared (FTIR) studies. Figure 4 shows the correlation of the experimental and predicted viscosity profiles for the dynamic/isothermal cure using the method previously described to reach the isothermal temperature. The prediction displays an inferior correlation at the two main areas of interest on a viscosity profile: that related to the minimum viscosity and where the viscosity approaches the gel point (taken as  $10^4$  poise). Since the particular resin system may involve a variety of reactions, e.g., both primary and secondary amine/epoxy reactions as well as the  $\text{BF}_3$  catalyzed epoxy etherification or

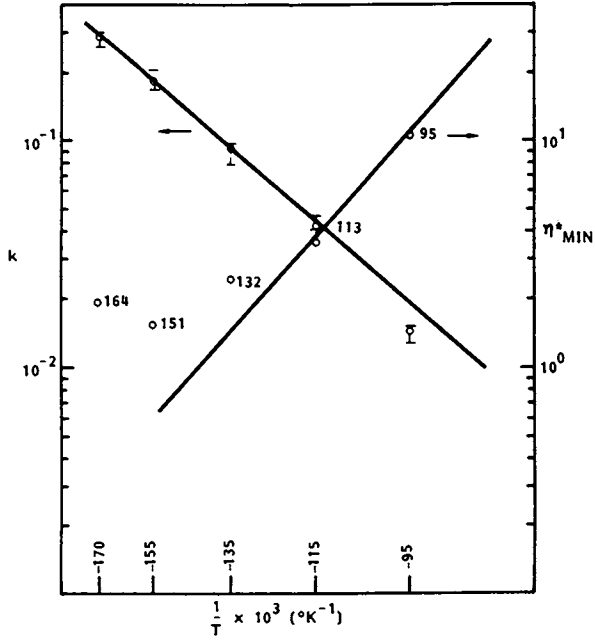


Figure 2. Arrhenius plots used to determine the material parameters.



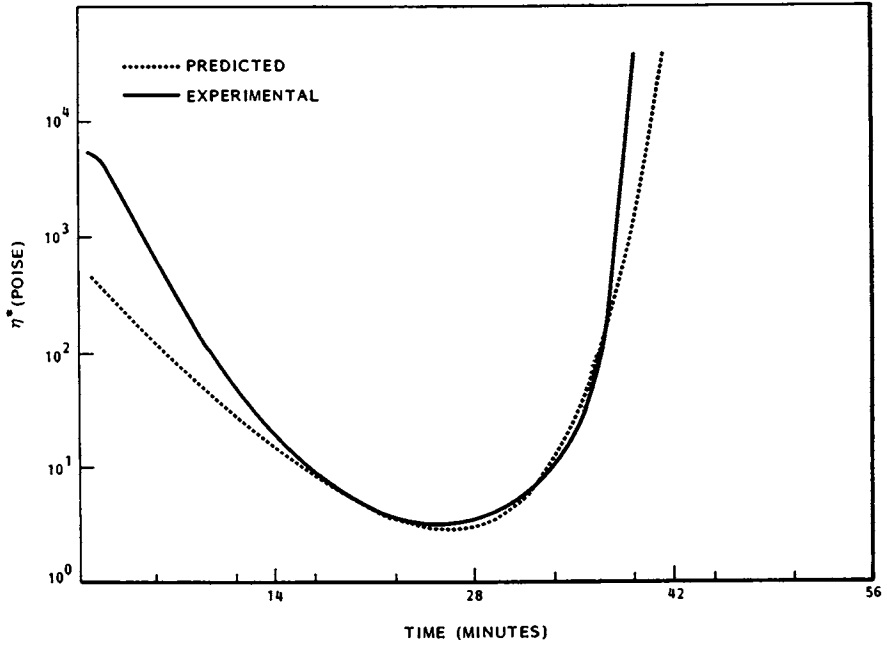


Figure 3. Correlation of the predicted and experimental viscosity profiles for a ramping temperature cure.

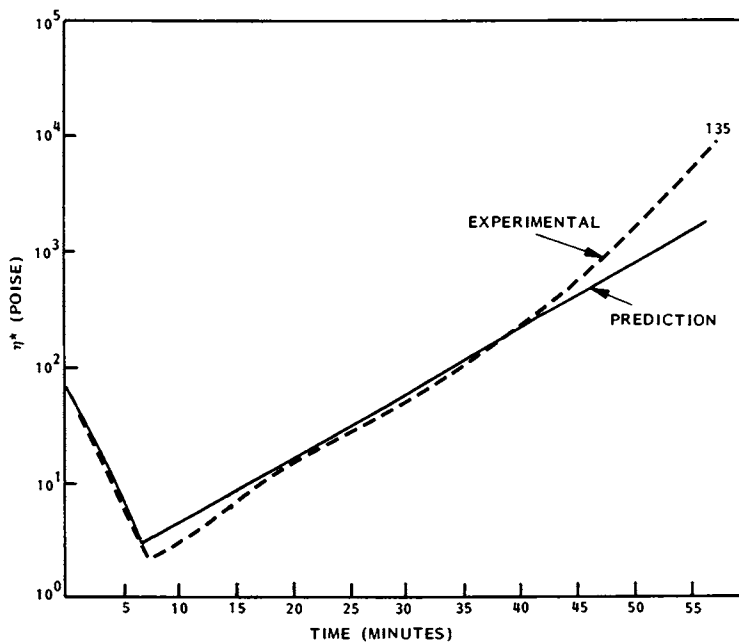


Figure 4. Correlation of the predicted and experimental viscosity profiles for a dynamic cure including a 135 °C isothermal region.

homopolymerization reaction, the assumption that the reaction order is unity throughout the course of the reaction may be invalid. The 135° isothermal cure was also monitored via Differential Scanning Calorimetry (DSC) and a plot of the conversion ( $\alpha$ ) versus time is displayed in Figure 5. The plot suggests an nth order kinetic process (6) as the slope of the curve,  $d\alpha/dt$  or the rate of polymerization, is a maximum at the initial portion of the cure. The plot displays a rapid conversion upon reaching the isothermal temperature with a change in the slope occurring approximately 15 minutes into the cure. This same change is observed in the experimental viscosity profile (Figure 1). The isothermal DSC data was analyzed by the method described by Peyser and Bascom (7) to determine the overall reaction order,  $n$ . A plot of  $\ln(dH/dt)$  versus  $\ln(1-\alpha)$  is constructed where  $dH/dt$  is the heat flow in milliwatts. The plot is displayed in Figure 6 where the slope represents the overall reaction order as initially  $n \leq 3$  and after 15 minutes into the cure  $n \leq 1$ .

The limitation of the five parameter model necessitated the development of a model that treats the overall reaction order as a separate, independent parameter. Through the relationship of the general equations for the first order ( $n = 1$ ) kinetics:

$$[7] \quad \ln C_{A_0} / C_A = k t$$

and nth order ( $n \neq 1$ ) kinetics

$$[8] \quad \frac{C_A}{C_{A_0}} = [1 + (n - 1)k t]^{1/1-n}$$

a six-parameter model including the reaction order and chain entanglement as independent parameters was derived:

$$[9] \quad \ln \eta(T, t) = \ln \eta_x + E_n/RT + \phi / (n-1) \cdot \ln [1 + (n-1) \cdot k_x \int \exp(-E_k/RT) \cdot dt]$$

where the various terms have previously been defined.

It is important to know how changes in the various parameters affect viscosity predictions using the six-parameter model. Figures 7-12 show the results of changing  $E_k$ ,  $k_x$ ,  $E_n$ ,  $\eta_x$ ,  $\phi$  and  $n$  on the predicted viscosity profiles for a hypothetical 135°C isothermal cure. The influence of the various parameters for an isothermal cure is demonstrated since a production cure often employs a 110-130°C isothermal hold to adequately advance or stage the material prior to the consolidation pressure application. The activation energy and the pre-exponential factor for both the kinetic (Figures 7 and 8) and flow (Figures 9 and 10) terms display

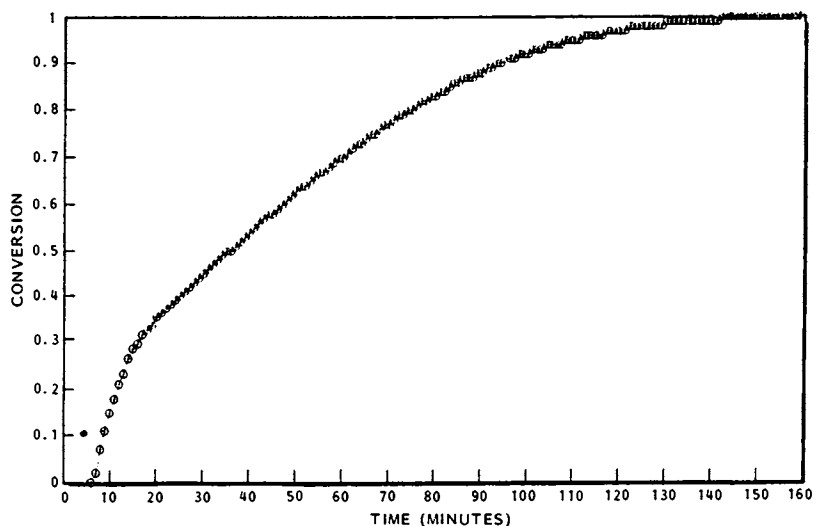


Figure 5. A conversion versus time plot for a 135 °C isothermal cure via differential scanning calorimetry (DSC).

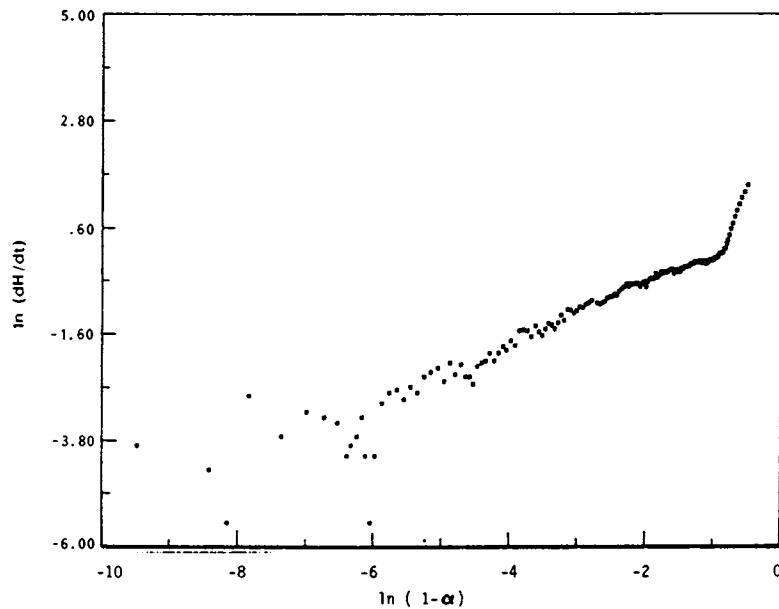


Figure 6. Determination of the reaction order from the 135 °C isothermal DSC experiment.

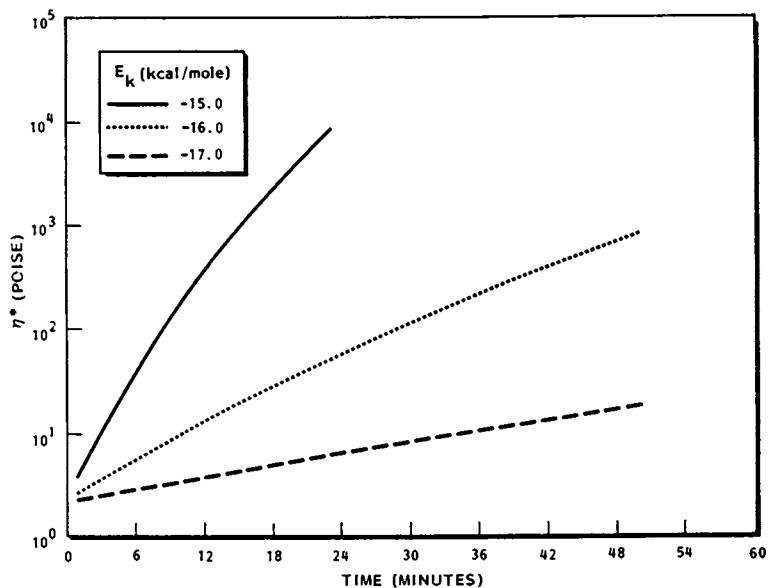


Figure 7. Influence of the kinetic activation energy,  $E_k$ , on the predicted viscosity.

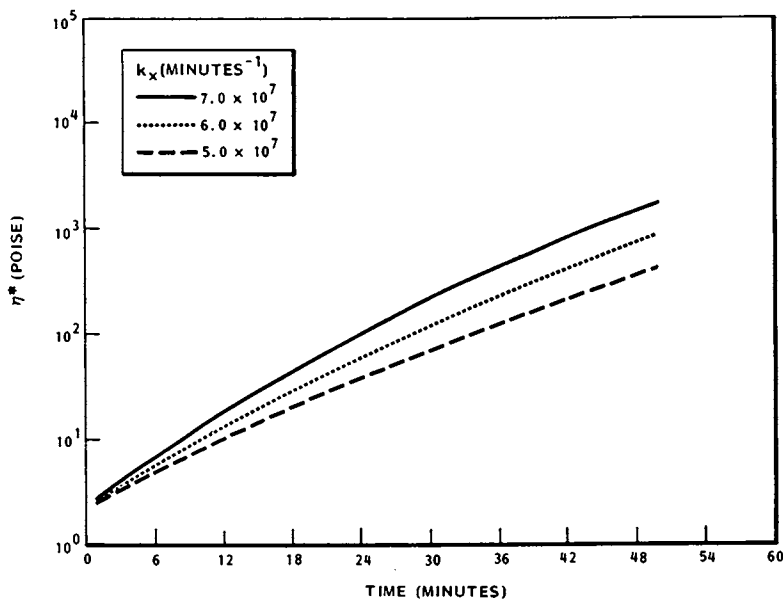


Figure 8. Influence of the pre-exponential kinetic parameter,  $k_x$ , on the predicted viscosity.

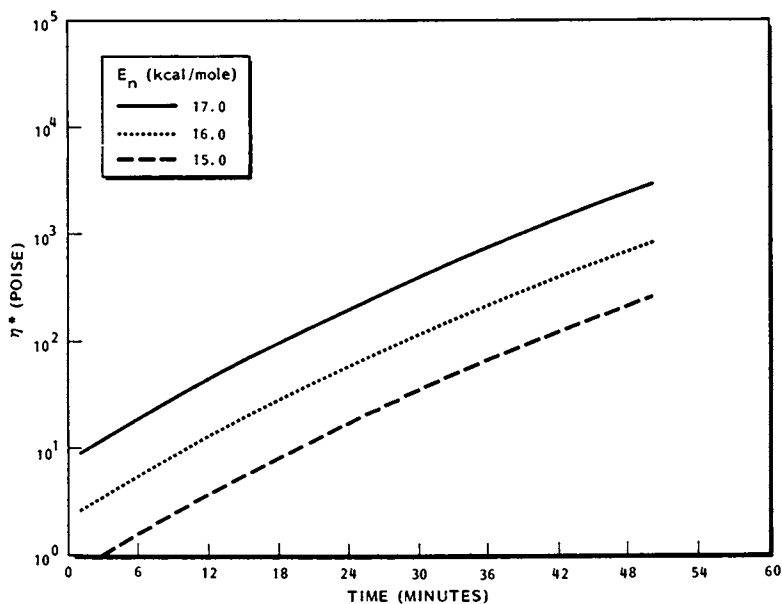


Figure 9. Influence of the flow activation energy,  $E_n$ , on the predicted viscosity.

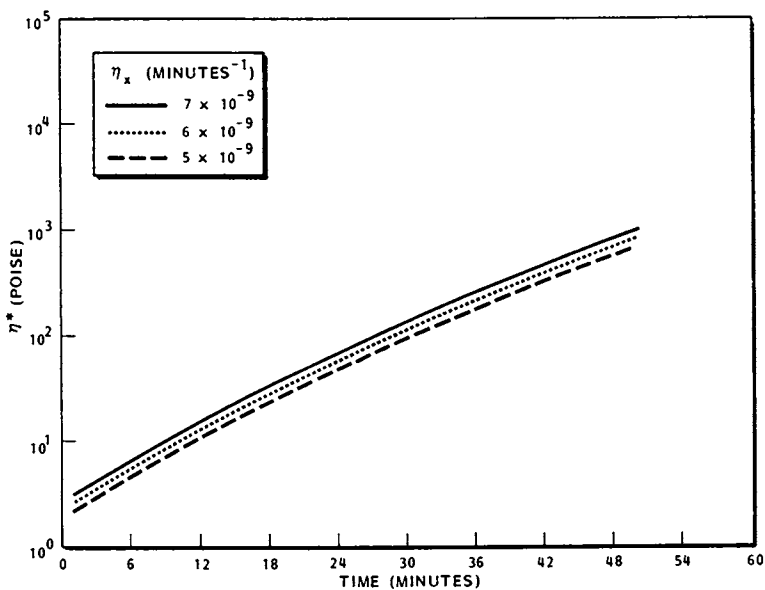


Figure 10. Influence of the pre-exponential flow parameter,  $n_x$ , on the predicted viscosity.

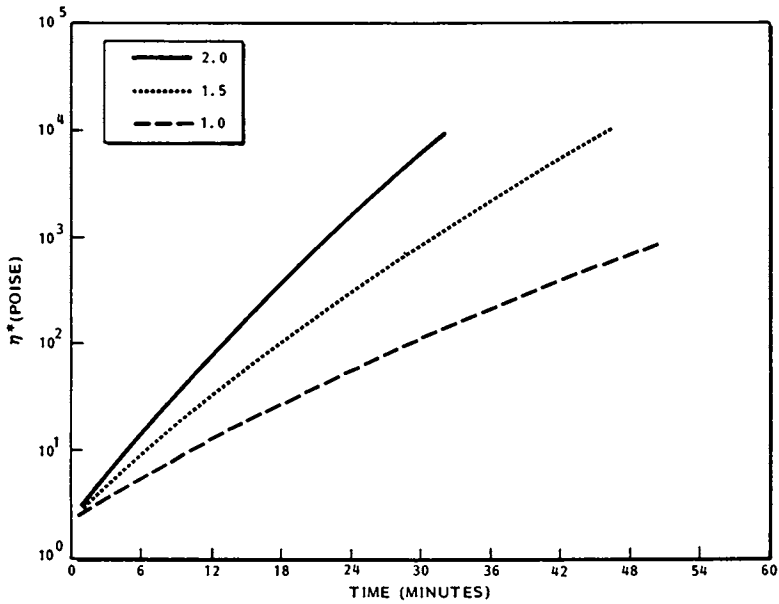


Figure 11. Influence of the chain entanglement parameter,  $\phi$ , on the predicted viscosity.

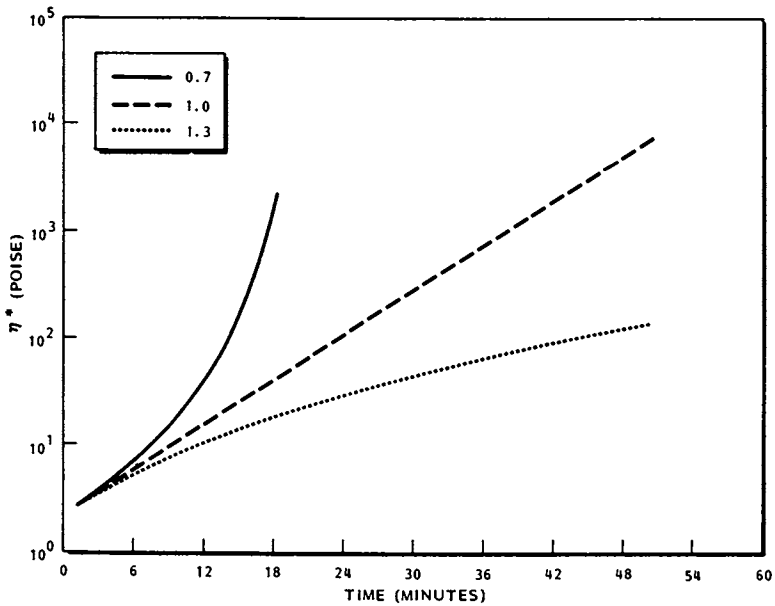


Figure 12. Influence of the reaction order,  $n$ , on the predicted viscosity.

similar trends with respect to their influence on the predicted viscosity profiles; however, changes in the activation energy terms have a more pronounced effect than similar changes for the pre-exponential parameters. It should, however, be noted that the activation energy terms will vary as a function of temperature. Increases in the chain entanglement parameter (Figure 11) serve to increase the profiles by a constant value as expected from equation [9]. Changes of the overall reaction order enables one to vary the slope of the predicted viscosity profiles are shown in Figure 12. For values of  $n < 1$  a concave slope is observed, when  $n = 1$  a linear profile is observed as predicted using the five-parameter model, and for values of  $n > 1$  a convex slope is demonstrated. With this information it was possible to estimate the direction and magnitude of changes in the parameters required to maximize the correlation between predicted and experimental viscosities.

Predictions employing the six-parameter model have been compared to the experimental viscosity profiles of the  $\text{BF}_3 \cdot \text{MEA}$  accelerated TGDDM/DDS system for a variety of curing conditions. The material parameters were previously described. Minor changes were made in the kinetic and flow pre-exponential parameters to  $5.8 \times 10^7$  and  $6.0 \times 10^{-9}$  minutes<sup>-1</sup>, respectively. In order to obtain the best correlation between the experimental and predicted viscosities, the experimental time-temperature profile was used in the calculations. To better understand the effect of reaction order on the prediction calculation, the chain entanglement factor was held equal to one. Figure 13 shows the profiles for a dynamic/135°C isothermal cure using a 10°C/minute ramping temperature profile from 75°C. A reaction order of 0.94 provided good agreement between the experimental and predicted profiles.

Figure 14 shows a dynamic/155°C isothermal cure using the same ramping temperature profile and model parameters, and again good agreement is observed. There was concern as to the effect of the ramping temperature on the agreement of the profiles. Figure 15 shows a dynamic/133°C isothermal cure employing a 3°C/minute ramping temperature profile from 50°C. Again, good agreement between the predicted and experimental profiles is observed after the solid DDS goes completely into solution. The reaction begins before the isothermal temperature is reached and the model responds quite well. Figure 16 displays the viscosity profiles for a production cure using a 2°C/minute ramping temperature profile from 50°C, holding at 121°C for 40 minutes, with a second 2°C/minute temperature profile to the gel point. The reaction order was set equal to one and the agreement was quite satisfactory. It is quite interesting that for  $\text{BF}_3 \cdot \text{MEA}$  accelerated system, the reaction order ( $n$ ) equal to one best describes the cure when isothermal holds below -130°C are used while a reaction order equal to 0.9 produces the best agreement with isothermal holds greater than 130°C. This is an excellent illustration that the cure mechanism



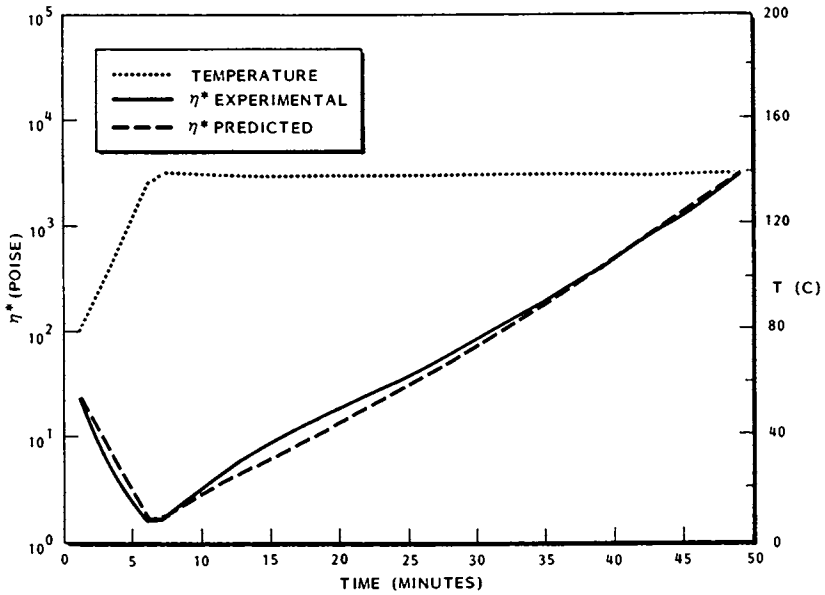


Figure 13. Viscosity profiles for a dynamic/135 °C isothermal cure.

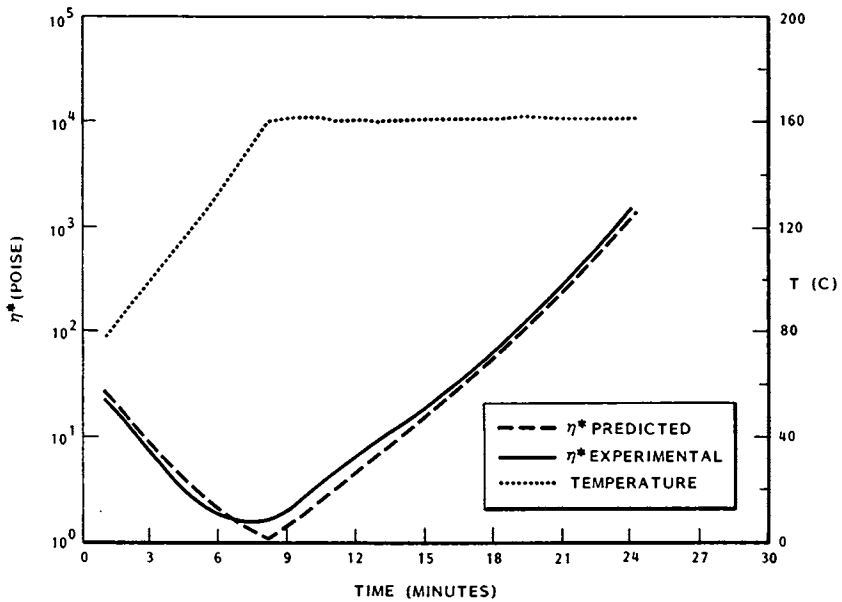


Figure 14. Viscosity profiles for a dynamic/155 °C isothermal cure.

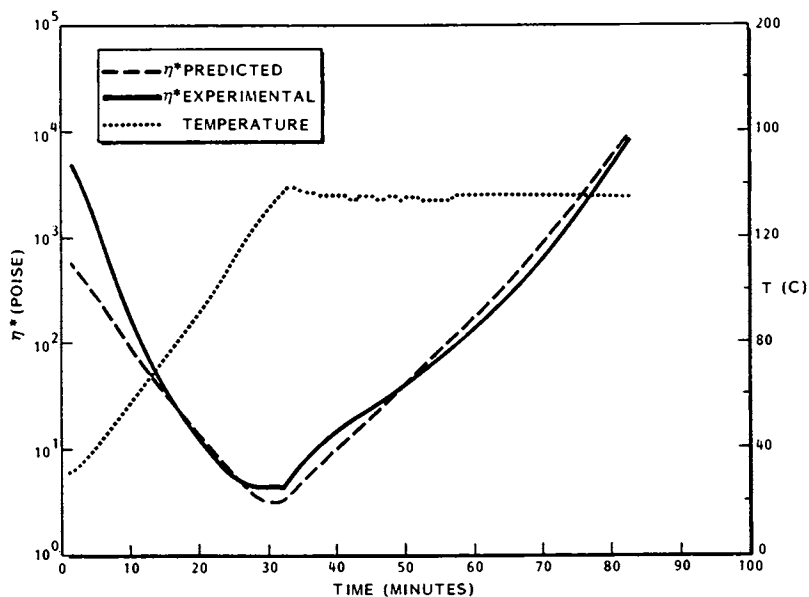


Figure 15. Viscosity profiles for a dynamic/133 °C isothermal cure.

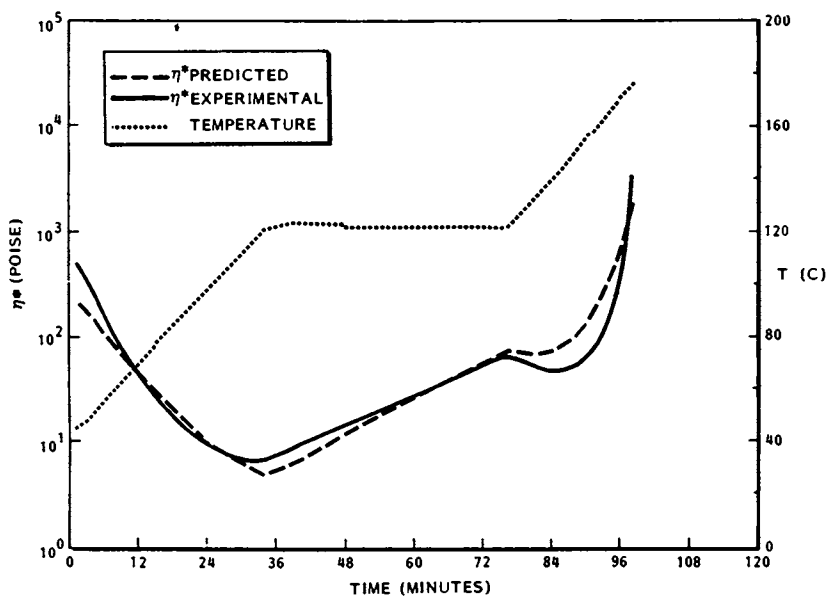


Figure 16. Viscosity profiles for a production cure.

for this system is highly complex. More than one curing reaction is indicated and the ratio between them changes with temperature.

Similar dynamic/isothermal experiments were also performed on the non-accelerated TGDDM/DDS epoxy resin system. A series of dynamic cures which include isothermal holds at 115, 135, 155 and 170°C were obtained on the neat resins as shown in Figure 17. The profiles do not display linear regions similar to the  $\text{BF}_3 \cdot \text{MEA}$  accelerated system making determination of accurate material parameters virtually impossible using the Arrhenius graphical method. The parameters were determined via a computer program based on a "best fit" iterative approach. The flow parameters were quite similar as one might expect; however, the kinetic activation energy was 17.5 kcal/mole. A prediction for the dynamic/135°C isothermal cure using a 10°C/minute ramp from 75°C is displayed in Figure 18 using a reaction order,  $n$ , equal to 0.65. The correlation is satisfactory during the early portion of the cure, however, during the latter portions of the cure the correlation could be improved. Perhaps the use of the chain entanglement parameter,  $\phi$ , other than one might be necessary. It is also plausible that the resin system may follow an autocatalytic kinetic process instead of a  $n$ th order process in which case further refinements to the six-parameter model will be necessary to adequately describe the cure.

### CONCLUSION

The most significant observations resulting from this investigation can be summarized as follows:

- 1) The inclusion of an overall reaction order parameter greatly increases the correlation of the predicted and experimental viscosity profiles for highly crosslinked epoxy resin systems.
- 2) The kinetic activation energy,  $E_k$ , is determined to be 16.1 kcal/mole for the  $\text{BF}_3 \cdot \text{MEA}$  accelerated system versus ~ 17.5 kcal/mole for the non-accelerated TGDDM/DDS system.
- 3) The change in the reaction order of the  $\text{BF}_3$  accelerated system above and below 130°C indicates the complexity of the cure mechanism.

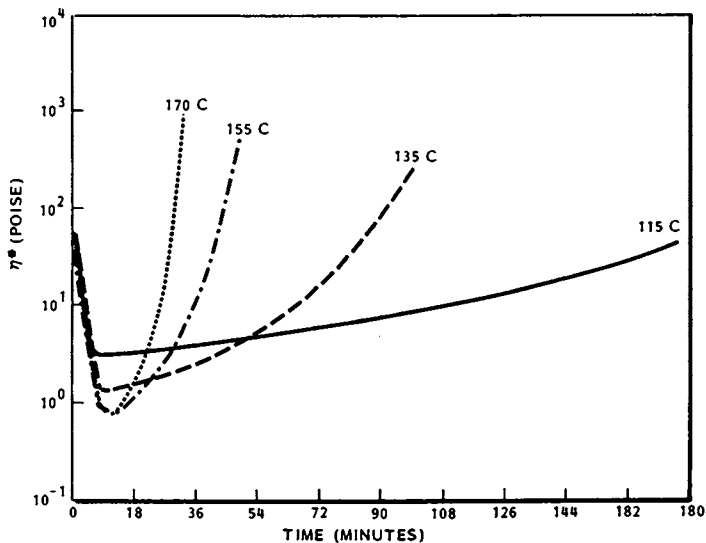


Figure 17. Dynamic viscosity profiles for the TGDDM/DDS neat resin including isothermal holds at 115, 135, 155, and 170 °C.

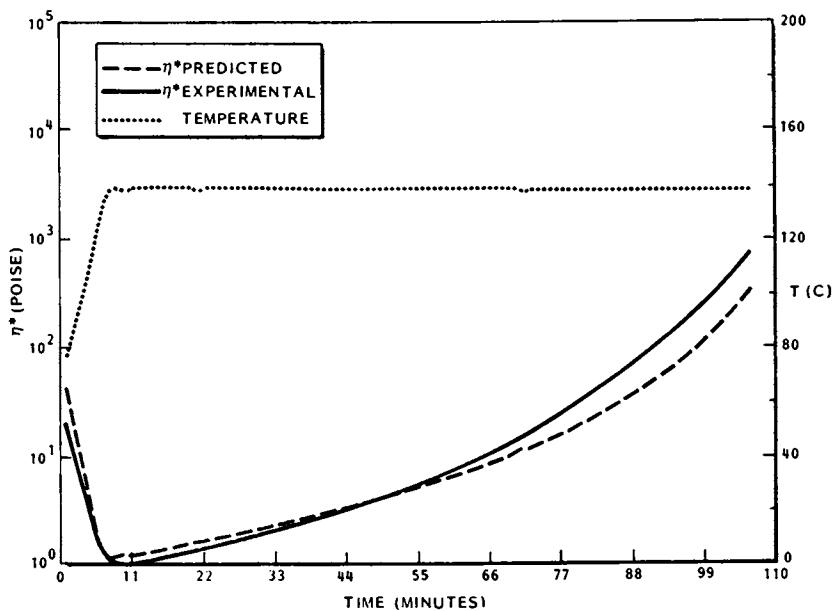


Figure 18. Viscosity profile for a dynamic/135 °C isothermal cure.

Literature Cited

- 1) Mussatti, F.G. and Macosko, C.W., Polymer Engineering and Science, 13, 236 (1973).
- 2) White, R.P., ibid, 14, 1, 50 (1974).
- 3) Roller, M.B., ibid, 15, 6, 406 (1975).
- 4) Keenan, J.D., SAMPE Educational Workshop, Sunnyvale, CA, June 1980.
- 5) Wereta, A., Dusi, M.R., and Hadad, D.K., ACS Chemical and Industrial Engineering Symposium, N.Y. August 1981.
- 6) Prime, R.B., "Thermal Characterization of Polymeric Materials" 1981, P. 480, E. Turi ed., Academic Press, N.Y.
- 7) Peyser, P., and Bascom, W., Journal of Applied Polymer Science, 21, 2359 (1977).

RECEIVED May 23, 1983

# INDEX

- A**
- AA/BMA—*See* Poly(butyl methacrylate/co-acrylic acid) films
- Accelerated aging tests ..... 122
- Accelerated epoxy system, isothermal kinetic behavior ..... 192*f*
- Acetylene-terminated quinoxaline—*See* Quinoxaline resin
- Acetylene-terminated resins
- air and nitrogen effects ..... 61–82
- dynamic mechanical properties .. 49–60
- kinetics ..... 49–60
- structure ..... 50
- torsion impregnated cloth analysis ..... 50, 54, 57
- Acetylene-terminated sulfone ..... 49
- See also* Sulfone resin
- cure kinetics ..... 51
- degree of cure vs. temperature ..... 58*f*
- glass transition temperature ..... 53–54
- vs. conversion ..... 53*r*
- vs. cure in nitrogen ..... 55*f*
- isothermal curing curves ..... 52*f*
- temperature effects ..... 58*f*
- time-temperature-transformation diagram ..... 55*f*
- torsion impregnated cloth analysis ..... 56*f*
- Acrylic acid copolymer
- adhesive failure ..... 143
- wetting results ..... 147
- Acrylic ester
- adhesive failure ..... 143
- hydrogen bonding ..... 143
- Activation energies ..... 271
- dielectric, Narmco 5208 ..... 238*r*
- for Narmco 5208 ..... 232*r*
- Activation energy terms ..... 313
- Actual-use conditions, duplicating .... 290
- Adhesive
- opaque, dynamic mechanical behavior ..... 179
- transparent, dynamic mechanical behavior ..... 179
- Aerospace industry, epoxy formulations ..... 2
- Aged prepreg
- differential scanning calorimetry ... 14*f*
- high pressure liquid chromatography ..... 11
- rheological properties ..... 14*f*
- Aged resin
- activation energies, chemiluminescence ..... 132*r*
- Aged resin—*Continued*
- vaporization gas chromatography/mass spectrometry ... 134–37
- Aging ..... 13
- moisture effects ..... 131
- Aging tests, accelerated ..... 122
- Air, curing
- quinoxaline resin ..... 75*f*
- sulfone resin ..... 72*f*
- Aliphatic diamines ..... 179
- Alkyd resins ..... 201
- Arrhenius plots, kinetic parameters .. 305*f*
- ATS—*See* Acetylene-terminated sulfone
- B**
- Benzoyl peroxide ..... 204
- 4,4'-Bis(3-ethynylphenoxy) diphenyl sulfone ..... 50
- Blocking effect ..... 108*f*
- in epoxy polymers ..... 105
- Butanedial, structure ..... 170
- C**
- Charge transport, in viscous medium 241
- Chemical events, dielectric property relationship ..... 2
- Chemiluminescence
- activation energies of aged resins .. 132*r*
- data reproducibility ..... 126
- least-squares fit ..... 128
- of thermosetting resins ..... 121–40
- variables ..... 123
- Chemiluminescence data, epoxy resin ..... 128*r*
- Chemiluminescence data, TGDDM... 129*r*
- Chemiluminescence intensity-temperature-time profiles
- epoxy resins under stress ..... 133*f*
- for epoxy resins ..... 123*f*, 129*f*
- Chemiluminescence system ..... 123*f*
- Classical polymer phase states ..... 191
- Coatings, thermosetting ..... 281–300
- leveling vs. fluidity ..... 295*f*
- Conductivity ..... 241
- Convectionless entry flow, contours
- constant temperature ..... 256*f*
- Conversion vs. curing time, TGDDM/DDS resin ..... 87*f*
- Cross-linking, epoxy resin ..... 113–20
- Cross-linking effect, glass transition temperature ..... 54
- Cure analysis ..... 162



- Epoxy polymers—*Continued*  
 moisture-temperature effects .....95–112  
 polar sites ..... 99  
 transient dynamic mechanical  
 data .....101–11  
 Epoxy powder coatings, viscometric  
 cure curves ..... 285*f*  
 Epoxy resin  
 casting ..... 123  
 chemiluminescence data ..... 128*t*  
 chemiluminescence intensity-tem-  
 perature-time ..... 123*f*  
 chemiluminescence intensity-tem-  
 perature-time profiles ..... 129*f*  
 cross-linking ..... 113–20  
 with phthalic anhydride—*See*  
 Epoxy/phthalic anhydride  
 curing  
 cured, chemiluminescence  
 observed ..... 126  
 dynamic mechanical and dielec-  
 tric properties during cure .. 223–50  
 plasticizing and blocking ..... 108*f*  
 vaporization gas-chromatography/  
 mass-spectrometry .....125–26  
 vaporization gas chromatograms ... 135*f*  
 volatiles released ..... 137*f*  
 Epoxy system, isothermal kinetic  
 phase diagram ..... 193*f*  
 Equilibrium dynamic mechanical  
 data  
 of DGEBA/TETA resins ..... 96  
 of epoxy polymers ..... 96  
 Ester groups, C–O stretching bands.. 116  
 3(2-Ethyl-4-methylimidazolyl)  
 propanenitrile ..... 114  
*See also* Curezol catalyst  
 Extent of reaction  
 calculation ..... 32  
 defined ..... 40
- F**
- Ferric acetylacetonate, structure ..... 170  
 Fiber-reinforced composite hard-  
 ware, fabrication .....21, 22*f*  
 Filler effect ..... 304  
 Filler loading effects  
 on induction time ..... 272*f*  
 on relaxation spectrum width ..... 274*f*  
 on relaxation times ..... 273*f*  
 Fingerprinting ..... 7  
 Finite element analysis ..... 251–62  
 computer model ..... 253–54  
 nonreactive entry flow .....255–57  
 one-dimensional reactive flow ...255–57  
 streamlines for nonreactive entry  
 flow ..... 256*f*  
 two-dimensional nonisother-  
 mal reactive flow ..... 257
- Finite element method, theoretical  
 background .....252–53  
 First-order kinetic analysis,  
 TGDDM/DDS resin ..... 92*f*  
 First-order kinetics ..... 308  
 Five-parameter model, limitation ..... 308  
 Flow-cure properties,  
 characterization ..... 283  
 Fluidity values vs. catalyst levels ..... 293*f*  
 Force-voltage analogy ..... 11  
 Fourier-transform IR spectroscopy,  
 TGDDM/DDS resin .....88, 89*f*, 90*f*  
 Free volume ..... 99
- G**
- Gel content determination ..... 31  
 Gel permeation chromatography  
 rate constants for TGMDDA/DDS  
 resins ..... 33*t*  
 of TGMDDA/DDS resins .....28–32, 29*f*  
 Gelation, tan delta ..... 191  
 Glass transition temperature  
 of acetylene terminated sulfone ...53–54  
 hard segment ..... 176  
 rates of change ..... 62  
 "two part theory" ..... 54
- H**
- Halhanes ..... 169  
*See also* Polyurethane adhesives ... 169  
 aromatic-cycloaliphatic polyurea  
 hard segments .....179  
 cure chemorheology ..... 175*f*  
 dynamic viscosity ..... 174*f*  
 isothermal viscosity-time curves ... 173  
 loss tangent isotherm ..... 178*f*  
 MDI-butenediol hard segments ..... 173  
 polyether soft segments ..... 173  
 viscosity vs. time ..... 180*f*  
 viscosity-temperature effects ..... 177*f*  
 with HMDI-aromatic diamine  
 chains ..... 181*f*  
 Hard segment glass transition  
 temperature ..... 176  
 Hardware fabrication ..... 1–2  
 Heat of curing  
 equation ..... 209  
 total, equation ..... 209  
 Heat of reaction, residual ..... 31  
 High performance liquid  
 chromatography ..... 7  
 chromatographs ..... 9  
 High pressure liquid chromatog-  
 raphy, of aged prepreps ..... 11  
 Humidity exposure ..... 195  
 Hydrogen bonding ..... 146  
 interference ..... 99  
 Hylene W, structure ..... 170



I	M
Impurities	Mark-Houwink-Sakurada equation .. 142
effect on TGMDA/DDS resins ....25-48	Material parameters, determination .. 304
effects in TGMDA resins	MDI— <i>See also</i> Methylene
Induction time, filler loading effects.. 272f	bis(phenylisocyanate)
Initial viscosity, equation for	MDI—butanediol hard segments,
determination ..... 173	vitrification ..... 176
Ink behavior ..... 153	Mechanical testing, of TGMDA/DDS
Intaglio printing inks	resins ..... 32
behavior ..... 153	Methyl ethyl ketone ..... 136
composition ..... 152f	Methylene bis(phenylisocyanate),
cure parameters ..... 165f	structure ..... 170
excessive drying..... 165f	Moisture sorption ..... 99
measure vs. calculated stress..... 158f	Molecular weight, determination,
oscillatory behavior ..... 156	calibration curve ..... 30f
steady flow viscosity	MY720, primary constituents..... 225
vs. cure time ..... 164f	
vs. Shear rate ..... 155f, 161f	N
steady shear flow studies ..... 152f	Narmco 5208
stress curves ..... 157f, 158f, 163f	Arrhenius plots, dielectric peaks ... 240f
stress vs. steady shear flow ..... 154f	composite loss tangent ..... 226-36
viscosity vs. steady shear flow .... 154f	dielectric composite tan delta ..... 237f
IR spectroscopy ..... 7	dielectric measurements ..... 236-42
Isothermal cure	dynamic spring
predicted vs. experimental	analysis ..... 226-36, 228f, 233f, 235f
viscosity ..... 307f	primary constituents ..... 225
torsion impregnated cloth analysis 66	thin-film tan delta ..... 243f
Isothermal curve, generation ..... 51	torsion braid analysis ..... 235f
Isothermal dielectric response,	vitrification ..... 229
measurement ..... 226	Nitrogen, curing
Isothermal kinetic diagram, phase	quinoxaline resin ..... 74f
precipitation effects ..... 194f	sulfone resin ..... 70f, 71f
Isothermal moisture transients ..... 103	Nonisothermal cure
Isothermal rheological data, applica-	cure model ..... 265
tion to production cure ..... 16	modeling ..... 289
Isothermal viscosity behavior,	Nonisothermal cure conditions
equation ..... 301	complex viscosity vs. cure time .... 277f
Izod impact energy, epoxy/amine	shear storage modulus vs. cure
ratio effects ..... 44	time ..... 277f
K	Nonisothermal cure kinetics ..... 265
Kinetic data, from viscosity mea-	Normal vs. inductive cure condi-
surements, problems ..... 171	tions, fluidity values ..... 292f
Kinetic modeling ..... 263-80	O
complex viscosity	One-dimensional reactive flow, de-
vs. cure time ..... 269f, 270f	gree of conversion ..... 258f
shear storage modulus vs. cure	Opaque adhesive, dynamic mechan-
time ..... 267f, 268f, 269f	ical behavior ..... 179
Kinetic parameters, from Arrhenius	Oscillatory behavior ..... 156
plots ..... 305f	Oxidative cross-linking, glass transi-
Kinetic terms ..... 15	tion temperature effects ..... 78
Kinetic theory ..... 264-66	P
Kinetics	PBMA— <i>See</i> Poly( <i>n</i> -butyl methacry-
first order ..... 308	late) films
nonisothermal cure ..... 265	Phase meter, use in dielectric
<i>n</i> th order ..... 308	monitoring ..... 18
L	Phase states, classical polymer ..... 191
Loss modular, relationship to phase	
angle ..... 189	

- Phthalic anhydride, cross-linked with epoxy resin ..... 113-20  
*See also* Epoxy/phthalic anhydride curing
- Physical changes on dielectric properties ..... 3*f*
- Plasticization, mechanical property changes ..... 103, 105
- Plasticizing ..... 108*f*
- Polar groups, in epoxy polymers ..... 99
- Polyallyl esters  
 preparation ..... 201  
 uses ..... 201
- Poly(*n*-butyl methacrylate) films .. 141-48  
 drying, humidity effects ..... 144*f*
- Poly(butyl methacrylate/co-acrylic acid) films ..... 141-48  
 drying, humidity effects ..... 145*f*
- Polyester resin  
 heat generated vs. isothermal cure temperature ..... 211*f*  
 reaction heat generated ..... 210*f*  
 reactivity ..... 216  
 viscosity vs. cure time ..... 206*f*
- Polyimide  
 curing, dielectric rheological response ..... 12*f*  
 dielectric dissipation factors ..... 12  
 viscosity ..... 12
- Polymer cure dynamics, evaluating ..... 187-200
- Polymer and solvent interactions ..... 146
- Polyol oligomers ..... 171
- Poly(tetramethylene oxide) ..... 170
- Poly(urea-urethane) adhesives  
 inverse temperature dependence of initial viscosity ..... 182*f*  
 loss tangent data ..... 184*f*
- Polyurea hard segment adhesives  
 curing agents ..... 172*t*  
 prepolymers ..... 172*t*
- Polyurethane adhesives  
*See also* Halthanes  
 segmented, curing behavior ..... 169-86
- Post-curing, TGMDA resins ..... 44
- Pre-cured resins, torsion impregnated cloth analysis ..... 68-78
- Pre-curing, glass transition temperature effects ..... 73
- Predictive models, aids in thermoset resin processing ..... 301-18
- Prepreg, aged, differential scanning calorimetry ..... 14*f*
- Prepreg aging, influence of dielectric properties ..... 13, 16
- Process automation ..... 1-24
- Process control ..... 7  
 and documentation, dielectric signals ..... 15
- Propanol ..... 136
- Propenal, activation energies for release ..... 136
- Q**
- Quadrol  
 effects on viscosity ..... 176  
 structure ..... 170
- Quinoxaline, vitrification time ..... 68
- Quinoxaline resin  
 air-cured ..... 75*f*, 80*f*  
 glass transition temperature vs. cure time ..... 79*f*  
 nitrogen cured ..... 74*f*  
 nitrogen post-curing ..... 80*f*  
 structure ..... 62  
 time to vitrification vs. temperature ..... 69*f*  
 torsion impregnated cloth analysis ..... 64*f*  
 vitrification ..... 66
- R**
- Rate of reaction  
 definition ..... 32, 40  
 effects of stoichiometry ..... 37  
 quenching by vitrification ..... 73
- Reactive flows, advantages ..... 251
- Reactive systems ..... 251-62
- Relaxation function ..... 264
- Relaxation spectrum width, filler loading effects ..... 274*f*
- Relaxation time  
 filler loading effects ..... 271, 273*f*  
 glassy vs. rubbery state ..... 271  
 nonisothermal cure ..... 265
- Residual heat of reaction ..... 31
- Rheological characterization, instrument calibration ..... 190
- Rheological cure, varying heat rates ..... 196*f*
- Rheological cure curve ..... 286
- Rheological cure transformation diagrams ..... 187-200  
 sample handling ..... 189  
 objectives ..... 188
- Rheological events, dielectric property relationship ..... 2
- Rheological flow terms ..... 15
- Rheometry, advantages ..... 282
- Roller's equation ..... 289  
 application ..... 290  
 comparison of constants ..... 298*t*  
 cure activation energy ..... 293*f*  
 cure curves ..... 291*f*  
 for inductive cure ..... 291*f*  
 use ..... 294
- S**
- Segmental chain mobility ..... 96
- Segmented polyurethane adhesives, curing behavior ..... 169-86
- Shrinkage ..... 208
- Six-parameter model ..... 313  
 derivation ..... 308
- Softening ..... 63

- Solvent and polymer interactions ..... 146  
 Sorption-desorption process ..... 101, 103  
 Steady-shear methods, cure curves... 288*f*  
 Stoichiometry  
   effect on TGMDA/DDS resins ..... 25-48  
   effects, rate of reaction ..... 37  
 Storage modules, relationship to  
   phase angle ..... 189  
 Structopendant ..... 202  
 Structoterminal ..... 204  
 Subtractive Fourier-transform IR ..... 10  
 Sulfone resin  
   air-cured ..... 71*f*, 72*f*  
   curing nitrogen ..... 70*f*, 71*f*  
   isothermal cure results ..... 67*f*  
   structure ..... 62  
   thermal stability ..... 66  
   time to vitrification vs.  
     temperature ..... 70*f*  
   torsion impregnated cloth analysis ..... 65*f*  
   vitrification temperature ..... 66  
   vitrification time ..... 69
- T**
- Tan delta ..... 191  
   curve ..... 195  
   moisture effects ..... 197*f*  
 Temperature scans, stages ..... 62  
 Tetraglycidyl-diaminodiphenyl  
   methane/diaminodiphenyl sul-  
   fone resin, curing process ..... 83-94  
   *See also* TGDDM/DDS resin  
 Tetraglycidyl-diaminodiphenyl  
   methane, purification ..... 125  
   *See also* TGDDM  
 Tetraglycidylmethylenedianiline,  
   structure ..... 2, 225  
   *see also* TGMDA  
 N,N' tetramethyldiphenyl sulfone,  
   synthesis ..... 84  
 TGDDM  
   *See also* Tetraglycidyl-diaminodi-  
   phenyl methane  
   chemiluminescence data ..... 128*t*  
 TGDDM/DDS resin  
   *See also* Tetraglycidyl-diaminodi-  
   phenyl methane/diaminodi-  
   phenyl sulfone  
   conversion vs. curing time ..... 87*f*  
   differential scanning  
     calorimetry ..... 85*t*, 86*t*, 87*f*, 88*t*  
     first-order kinetic analysis ..... 92*f*  
   Fourier-transform IR  
     spectroscopy ..... 88, 89*f*, 90*f*  
     viscosity curves ..... 302  
     viscosity profiles ..... 303*f*  
 TGMDA, hydrolysis ..... 26  
 TGMDA/DDS reactions  
   cure time effects ..... 34*f*  
   increasing epoxy/amine ratio ..... 46
- TGMDA/DDS resins  
   concentrations vs. cure time ..... 35*f*  
 DSC parameters for iso-  
   thermal cure ..... 44  
 effects of impurities ..... 25-48  
 gel permeation  
   chromatography ..... 28-32, 29*f*  
   mechanical testing ..... 323  
   molecular weight parameters ..... 36*f*  
   percent gel vs. cure time ..... 36*f*  
   rate constants ..... 33*t*  
   rate vs. extent of reaction ..... 38*f*  
   reaction rate determination by  
     DSC ..... 31
- TGMDA resins  
   by-products effects ..... 40  
   characteristics ..... 27*t*  
   impurities ..... 40  
   post-curing ..... 44  
 Thermal cure profile ..... 187  
 Thermal scans, in air/nitrogen ..... 63-77  
 Thermogram, of catalyzed epoxy/  
   phthalic anhydride cure ..... 115  
 Thermoset resin processing,  
   predictive models ..... 301-18  
 Thermosetting coatings ..... 281-300  
   leveling vs. fluidity ..... 295*f*  
 Thermosetting resins,  
   chemiluminescence ..... 121-40  
 TICA—*See* Torsion impregnated  
   cloth analysis  
 Time average shear rate, equation .... 159  
 Time-temperature-transformation  
   diagram, of acetylene-terminated  
   sulfone ..... 55*f*  
 Torsion braid analysis  
   advantages ..... 247  
   kinetic effects ..... 236  
   Narmco 5208 ..... 235*f*  
 Torsion impregnated cloth analysis  
   of acetylene terminated  
     resins ..... 50, 54, 57  
     acetylene-terminated sulfone ..... 56*f*  
     isothermal cure ..... 66  
     pre-cured resins ..... 68-78  
     quinoxaline resin ..... 64*f*  
     softening ..... 63  
     sulfone resin ..... 65*f*  
 Transparent adhesive, dynamic me-  
   chanical behavior ..... 179  
 Transient dynamic mechanical data,  
   epoxy polymers ..... 101-11  
 Transition, in glassy polymers ..... 96  
 Two-dimensional reactive flow  
   isoconversion contours ..... 259*f*  
   isothermal contours ..... 260*f*
- U**
- Uncured inks  
   oscillatory shear ..... 156-59  
   steady shear ..... 153, 156

Uncured resin, temperature scanning .....	63	Viscoelastic relaxation, loss peak .....	242
Unsaturated polyester resins		Viscometric cure curves, for epoxy	
chemorheology and curing		powder coatings .....	285 <i>f</i>
kinetics .....	201-21	Viscosities, predicted vs.	
uses .....	201	experimental .....	306 <i>f</i>
V			
Vaporization gas chromatograms, of		Viscosity	
epoxy resins .....	135 <i>f</i>	initial, equation for determination..	173
Vaporization gas chromatography/		moisture effects .....	197 <i>f</i>
mass spectrometry		polyimide .....	12
aged resin .....	134-37	predicted .....	15
of epoxy resins .....	125-26	predicting .....	266
Vinyl ester resin .....	202	Viscosity measurements, interpreta-	
heat generated vs. isothermal cure		tion problems .....	171
temperature .....	211 <i>f</i>	Vitrification	
reaction heat generated .....	210 <i>f</i>	effect on reaction rates .....	57
reactivity .....	216	quenching of reaction rate .....	73
viscosity vs. cure time .....	206 <i>f</i>	Volatiles	
		in torsion impregnated cloth	
		analysis .....	63
		released from epoxy resin .....	137 <i>f</i>